Aspects of Bond Graph Modelling in Control

A DISSERTATION

SUBMITTED TO THE DEPARTMENT OF MECHANICAL ENGINEERING

OF THE UNIVERSITY OF GLASOW

IN FULFILLMENT OF THE REQUIREMENTS

FOR THE DEGREE OF

DOCTOR OF PHILOSOPHY

By

Dustin Vink

January 2005

Abstract

This thesis presents new aspects of bond graph modelling in control, where established control theory is used for *closed loop* bond graph representations. In particular, the physical model based framework of bond graph modelling addresses Backstepping Control, Model Matching Control and Energy Shaping in Stabilisation Control. Even though these control design methodologies are quite different on analytical levels, it is shown that the feedback designs allow for closed loop bond graph models. Concepts of passivity and the port–Hamiltonian structure of bond graphs play a leading role throughout the thesis. Various detailed examples impart the essential results.

Summary

The bond graph modelling language has proven to offer a systematic framework for the modelling of lumped parameter multidisciplinary physical systems. Bond graph research and applications have witnessed tremendous advancement in *open loop* modelling ever since the inception of this graphical modelling technique by Professor Henry Paynter in 1968. On the other hand, bond graphs in control, or *closed loop* bond graph models, have not received the same level of research commitment compared to aspects of open loop systems modelling.

This thesis contributes new aspects of bond graphs in control design by focusing on closed loop representations, where the idea of applying bond graphs for closed loop modelling is novel and virtually non–existent in the current bond graph literature. The thesis does *not* present new control theoretical results in any way but applies well–known control concepts to find closed loop bond graph representations for stabilisation problems. The physical model based character of general bond graph models is shown to be suitable for the control strategies of Backstepping Control, Model Matching Control and Energy Shaping in Stabilisation Control.

Backstepping control within the bond graph framework is shown to be a case of *exact* backstepping by which the closed loop dynamics is put into port–Hamiltonian form through a suitable choice of variables. Consequently, a bond graph representation of the closed loop dynamics can be expected to exist. The physical modelling arguments come into play by means of additive bond graph elements to specify the stabilising function, where the overall additive bond graph is referred to as the *virtual actuator*. It is known that backstepping control is a recursive design technique to obtain a closed loop Lyapunov function; however, the geometric structure of the closed loop itself is generally not an immediate design goal. This thesis, on the other hand, aims at closed loop bond graph representations by having closed loop port–Hamiltonian dynamics as an explicit backstepping design goal. As a result, the well–known Lyapunov arguments are implicitly contained in the procedure and depend on the original plant energy function.

Model matching control addresses the (asymptotic) tracking of prescribed trajectories of some desired dynamic model. This thesis shows that such prescribed models can be chosen as bond graph models that are structurally "close" to the plant to satisfy certain solvability requirements of the Model Matching Problem (MMP). Tracking control through (bi)causal bond graph inversion has previously been reported in the bond graph literature, but the underlying mechanism of such feedback designs has not appeared in the current literature. This thesis argues that the bond graph based MMP is linked with various ideas of center manifold theory and output regulation problems. For certain cases, the MMP is shown to yield tracking error dynamics that "inherit" the plant dynamics. The conclusion drawn from this is that the closed loop error dynamics can be described by the plant bond graph such that additive bond graph elements can be used for closed loop stabilisation.

Energy shaping in stabilisation control, as considered in this thesis, addresses feedback designs that modify the energy function and possibly the junction structure and resistive elements of the plant. It is shown that bond graphs can be used to find the closed loop energy function that attains feedback passivation with respect to the natural output. Most importantly, the closed loop energy function need not be known beforehand but follows from a "power balance" of some suitable bond graph subsystem. Furthermore, instead of modifying the energy by means of the power balancing method alone, the Interconnection and Damping Assignment Passivity Based Control (IDA–PBC) is considered from a bond graph viewpoint. The interconnection and damping assignment is shown to allow for bond graph representations by modifying the junction structure and the dissipative elements of the plant bond graph. The desired closed loop interconnection and damping structures are therefore guided by bond graph topological considerations. Since IDA–PBC designs generally require the solution of first order partial differential equations, the solution to such designs must be dealt with analytically.

Preface

When I learned about bond graphs, in the year 1998, someone once said to me that bond graph modelling looked like a "black art": A collection of arcane, unpublished, and mostly ad–hoc techniques developed for a particular application or systems area.[1] At that moment, I was quite surprised by this remark; but now, in the year 2005, I do not believe this description of bond graph modelling is completely unjustified...

Bond graphs look intriguing when seen for the first time, because the graphical topology is radically different from the ubiquitous block diagrams used in academia and industry. The graphical causal assignment procedures to derive the dynamic equations is devilishly clever, for it reinforces ones confidence in the modelling process, where aspects of constraint dynamics and algebraic loops have virtually no obscurities. Furthermore, bond graphs are based on energy concepts to specifically accommodate the systematic modelling of multidisciplinary physical systems. However, even though bond graph modelling is well–known by the systems modelling community, it is safe to say that bond graphs are used by a relatively small group of professionals only. Also, instead of being a collection of ad–hoc techniques, the bond graph language is highly structured and rich in literature.

Now that my three years of graduate research have come to an end, I can say that bond graphs do embody certain elements of a "black art" after all: The graphical topology of bond graph models appears mystical at first, but a closer look reveals a spellbinding structure and cleverness. By writing this thesis, I have tried to uncover some new secrets of bond graph modelling in control design, hoping that what captivated my thoughts has been put in clear writing for everyone to read.

Dustin Vink — Groningen, The Netherlands.

[1] Free On–Line Dictionary of Computing

Acknowledgments

Research takes time and funding, so I hereby thank Dr. D. Ballance and Professor P. Gawthrop for the opportunity and financial support to enjoy three years of Ph.D. research.

Unfortunately, the three years of graduate research were sufficient to produce the required results, but I failed to finalise the thesis within this time frame. Needless to say, I wish to thank the Dutch government for its financial support while writing this thesis.

Finally, my family and friends have been extremely supportive during my days as a graduate student. Thank you all.

Contents

List of Figures

Part I.

Preliminaries on Bond Graphs and Control

1. The Art of Bond Graph Modelling

1.1. Introduction

In 1959, Henry Paynter introduced bond graph modelling at the Massachusetts Institute of Technology (MIT) in Cambridge, Massachusetts, USA, and this lead to the first book [Pay61] published on bond graphs. In addition to Henry Paynter's own work, his former Ph.D. students D. C. Karnopp, D. L. Margolis and R. C. Rosenberg subsequently accelerated bond graph research and have greatly contributed to bond graph fundamentals [Kar00]. But others, too, picked up bond graph modelling and published a wide variety of textbooks [Blu82], [Bor00], [Bor04], [Bre92b], [Cel91], [Dix74], [Gaw96], [Tho99] that describe both bond graph theory and various applications. In parallel to the ongoing bond graph research, it became clear that the systematic modelling approach offered by bond graphs rendered software implementation possible, where bond graph simulation packages [Ros74] started to emerge that were capable of numerical simulation by adhering to the strict bond graph topological rules. Today, a variety of software solutions are available that offer graphical design environments with advanced symbolical and numerical simulation engines for complex multidisciplinary systems [Dyn04], [MTT04], [BV04].

It is safe to say that the art of bond graph modelling has been subjected to extensive research on a wide variety of topics over the last four decades. However, it is relatively difficult to compile a compact list of bond graph references that provide an adequate overview of bond graph theory and its applications. This can be partially attributed to the fact that bond graph research is somewhat scattered throughout the journals, conference proceedings and communications on systems modelling and simulation. Nevertheless, the reader may wish to consult the International Conference proceedings on Bond Graph Modelling and Simulation (ICBGM) for contemporary views and bundled research topics [ICB03]. Furthermore, special issues [Bre91], [Gaw02] on bond graphs have appeared that present various states of affairs. Regardless of the topic, the reader is simply referred to the above literature and references therein on past and current research pertaining to the bond graph language.

This chapter is organised as follows. First, fundamental notions on bond graph modelling are briefly recalled and can be found in the standard literature [Gaw96], where the author seizes the opportunity to present some small modifications with respect to standard bond graph notations and conventions. It has been attempted to keep the bond graph reproductions to a minimum.

Second, there has been a relatively recent interest in port–Hamiltonian systems [Dal97] and their connection with bond graph models [Gol02], [Gol03]. These developments cannot be called standard by any means and the identification of bond graph models as a class of port–Hamiltonian systems has not made it to university textbooks at this time of writing. Because the notion of port–Hamiltonian systems will prove to be instrumental for various considerations in this thesis, some important results on bond graphs and port–Hamiltonian systems will be recalled to provide a more self–contained exposition of bond graph induced dynamics.

Finally, having presented the various modelling aspects of bond graphs, the thesis rationale and objective can be outlined constructively. It can be argued, for example, that certain aspects of physical model based control can be assisted by means of the closed loop bond graph representation, where further unification of modelling and control methods in the physical domain with a systematic modelling framework may lead to an improved understanding of physical model based control problems.

1.2. Bond Graphs and Block Diagrams

In a nutshell, block diagrams graphically depict signals connected to summation blocks, multiplication blocks, integrator blocks and other specialised blocks that operate on signals. This modelling framework can be argued to be the standard graphical modelling tool for systems and control in both academia and industry.

For example, consider the block diagram in Figure 1.1 with states x_1, x_2 and x_3, some constants a, C, m_1, m_2 and r to be multiplied, and where $\int$ integrates the ingoing signal. Even though block diagrams are straightforward, it is required that causal relations are known before the block diagram can be drawn. Hence block diagrams do not provide additional causal information, showing that the modeller must actively derive all causal relations for block diagram modelling to be applicable.

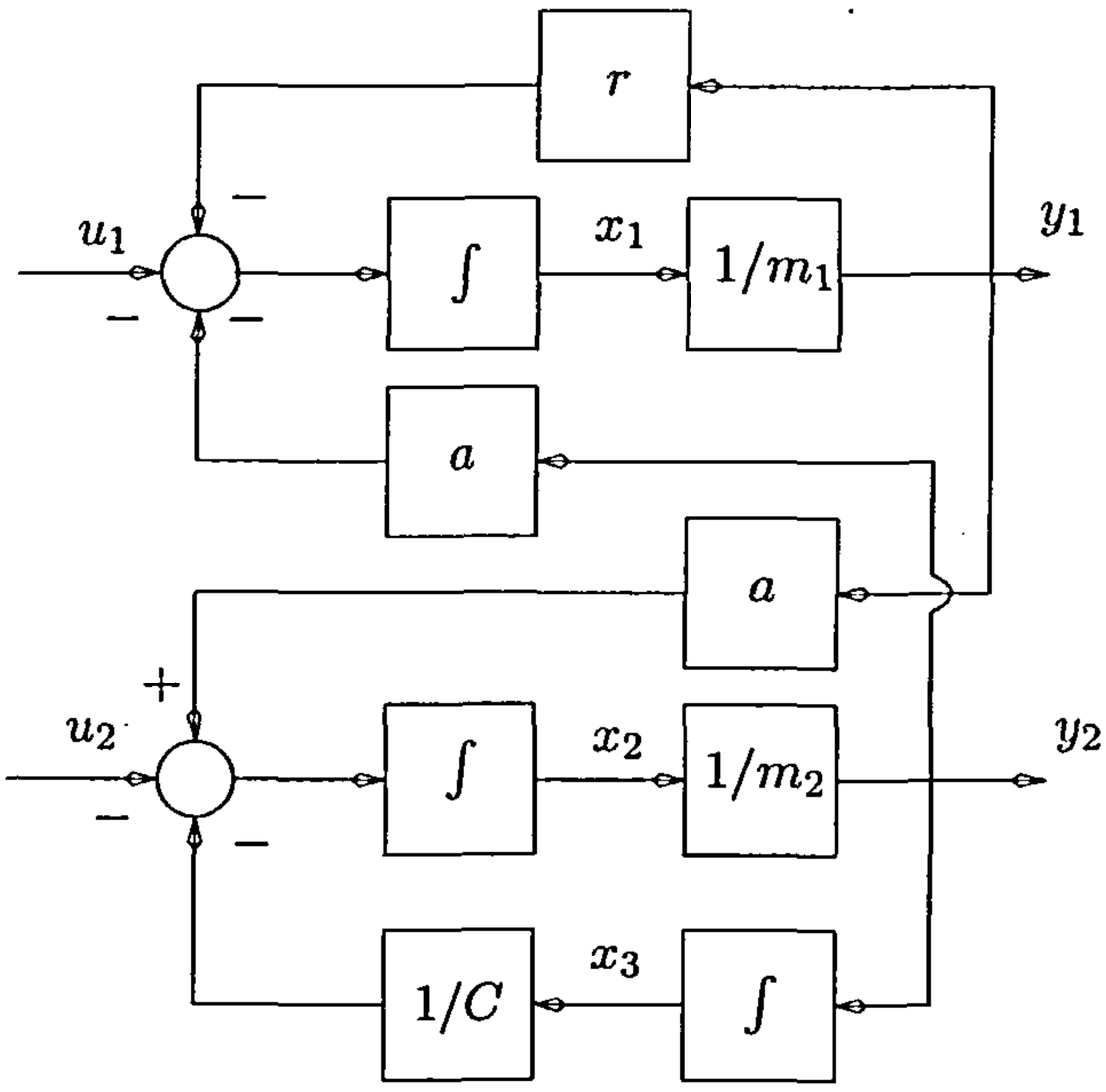

Figure 1.1.: Block diagram of electrical–mechanical system.

1.2.1. Non–Causal Bond Graphs

The bond graph language, on the other hand, is a graphical representation that does not identify system signals as completely separate entities but uses generalised energy and power considerations instead. More precisely, the bond graph identifies a natural pairing of two signals denoted as e and f, called the "effort" and "flow" respectively, such that $P = ef$ yields generalised power. Therefore, bond graph modelling focuses on systems for which notions of energy and power are meaningful, such as multidisciplinary engineering systems. Furthermore, and this is important, bond graphs incorporate the notion of computational causality, which is absent in the block diagram framework. More precisely, bond graphs make a clear distinction between $a := b$ and $b := a$, which are referred to as causal assignment statements. Moreover, the causal assignment is graphically depicted and subjected to strict rules that provide information on variable dependencies without actively putting such knowledge into the model.

To elaborate the most basic aspects of bond graphs in more detail, consider the non–causal bond graph in Figure 1.2 that represents the same electrical–mechanical system of Figure 1.1. The efforts and flows of a bond graph, e_j and flows f_j, are always associated with a "bond" that is drawn as a harpoon shaped arrow, hence the name bond graph. When $e_j f_j > 0$, the power flow is in the direction of the bond arrow.

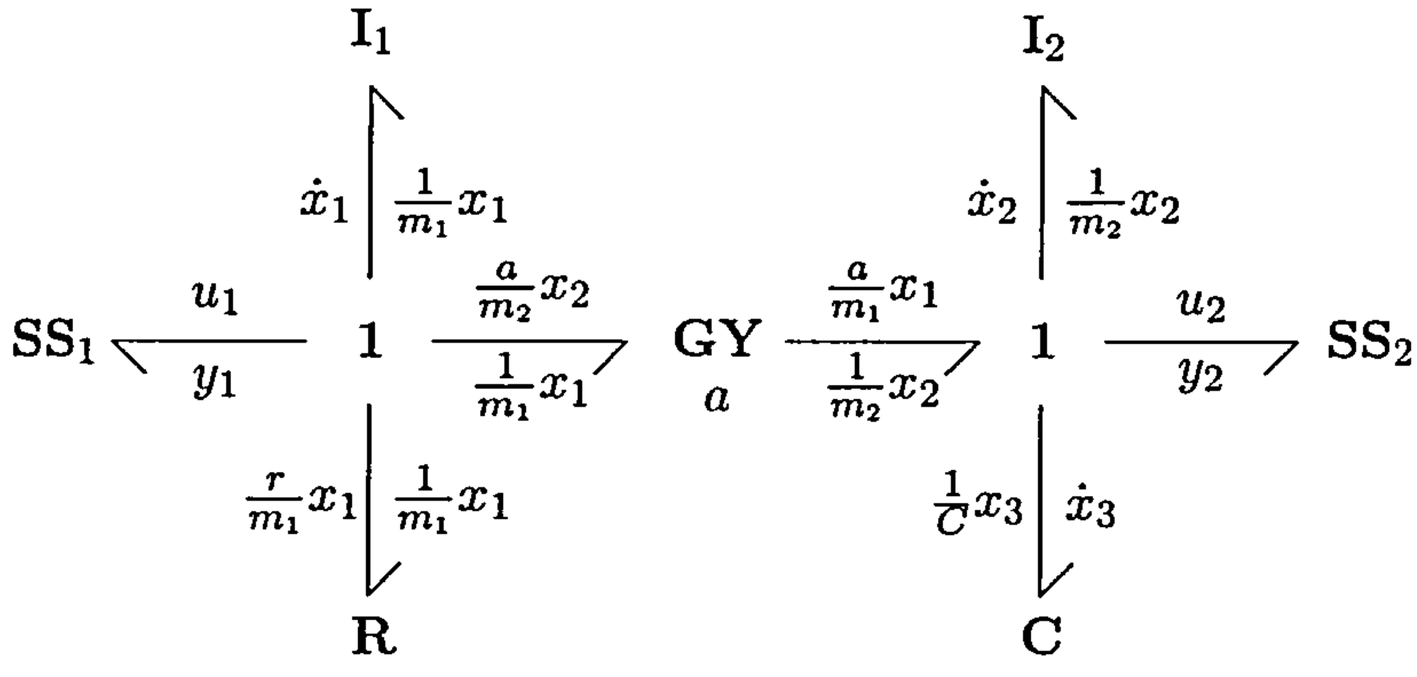

Figure 1.2.: Non–causal bond graph of electrical–mechanical system.

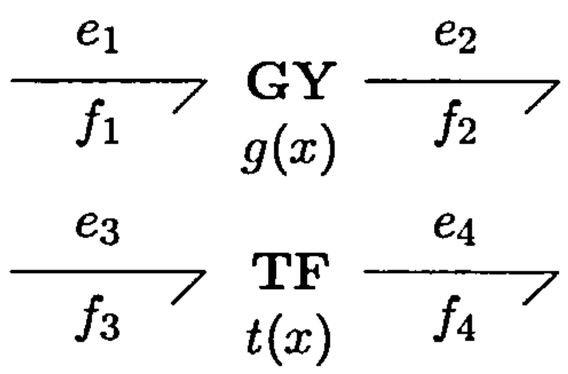

Figure 1.3.: Power continuous elements.

In this thesis, efforts are drawn to the left or above the vertical and horizontal bonds respectively, whereas flows are drawn to the right or below the bonds.

The power variables e_j and f_j of each bond can be collected into the pair (e_j, f_j) and are readily derived from Figure 1.2 as (u_1, y_1), $(\dot{x}_1, x_1/m_1)$, $(\dot{x}_2, x_2/m_2)$ and so forth. Efforts and flows contained in such pairs are referred to as conjugate power variables. Now, suppose that all bonds connected to a **1** or **0** element point outward or inward, then the power balance associated with these 0–junctions and 1–junctions is defined as

$$\sum_j e_j f_j = 0. \tag{1.1}$$

The relation (1.1) expresses power continuity of 0–junctions and 1–junctions, but correct signs must be accounted for when subsets of bonds have alternate directions. That is to say that either the inward or outward bond direction must be designated as being positive when evaluating the power balance (1.1).

In addition to 0–junctions and 1–junctions, the power continuous gyrator, **GY**, and the power continuous transformer, **TF**, as depicted in Figure 1.3 are frequently encountered in bond graph models. The gyrator maps efforts into flows and flows into efforts, whereas the transformer is defined as mapping efforts into efforts and flows into flows. These elements allow for various important relationships in multidisciplinary engineering systems.

Contrary to standard bond graph notation found in the literature [Kar00], this thesis does not use the notation of the modulated gyrator, **MGY**, and modulated transformer, **MTF**. Nonetheless, the standard non–causal definitions for gyrators and transformers in Figure 1.3 are adopted and given by

$$\begin{aligned} e_2 - g(x)f_1 = 0, \qquad e_1 - g(x)f_2 = 0, \\ e_4 - t(x)e_3 = 0, \qquad f_3 - t(x)f_4 = 0, \end{aligned} \tag{1.2}$$

where the modulations $g(x)$ and $t(x)$ may depend on state space coordinates $x \in X \subseteq \mathbb{R}^n$. Hence, the notation in Figure 1.3 is sufficient for (non)–constant gyrators and transformers, because a graphical distinction between such modulations is not strictly necessary and does not induce a loss of generality in any way. Power continuity of the **GY** and **TF** elements is indeed guaranteed, regardless of the modulation, since by (1.2) it follows that

$$\begin{aligned} e_1 f_1 = g(x) f_2 f_1 = e_2 f_2 \\ e_3 f_3 = e_3 t(x) f_4 = e_4 f_4. \end{aligned} \tag{1.3}$$

Now, standard bond graph literature shows that the power balance (1.1) not only holds for single junctions, but the power balance is likewise satisfied for *all* outer bond pairs of a junction structure, which represents an arbitrary network interconnection of bonds, junctions, gyrators and transformers.

The 0–junctions and 1–junctions do not only induce the power balance (1.1) with respect to all those bonds connected to them, but these junctions have some additional rules. For instance, by taking (1.1) into account, a single 1–junction is defined to induce the relations

$$\mathbf{1} \quad \Longrightarrow \quad f_j = f_i \quad \Longrightarrow \quad \sum_j e_j = 0, \tag{1.4}$$

whereas a single 0–junction induces

$$\mathbf{0} \quad \Longrightarrow \quad e_j = e_i \quad \Longrightarrow \quad \sum_j f_j = 0. \tag{1.5}$$

Therefore, the bond graph in Figure 1.2 shows that

$$\begin{aligned} u_1 + \dot{x}_1 + \frac{a}{m_2} x_2 + \frac{r}{m_1} x_1 = 0 \\ u_2 + \dot{x}_2 - \frac{a}{m_1} x_1 + \frac{1}{C} x_3 = 0, \end{aligned} \tag{1.6}$$

which are non–causal relationships from which the equations of motion can be derived. It is readily observed that the minus sign in the second relation of (1.6) is the result of an alternate bond direction.

It can be argued that the relations (1.1), (1.5) and (1.6) are corner stones of bond graph modelling, since they incorporate power continuity and generalised Kirchoff's laws that play crucial roles in many physical models [Bus98].

Now that basic notions of bonds, 0–junctions, 1–junctions, **TF** and **GY** components have been briefly recalled, the definitions of the **SS**, **C**, **I** and **R** components that are to terminate the outer bonds of bond graphs are given as follows. First, the source sensor, **SS**, component as described in [Gaw96] represents an element that is associated with power supply; however, the reader should note that the conventional effort source, **Se**, and flow source, **Sf**, often found in the literature will not be used in this thesis. Instead, the **Se** and **Sf** source elements are collected into the single **SS** element without losing generality of bond graph modelling features.

Second, the **C** and **I** elements are storage elements and represent the storage of physical energy, such as kinetic and potential in the mechanical domain. These elements are usually associated with real–valued functions defined on some state space manifold X, so that one defines the maps $\mathbf{C}\colon X \to \mathbb{R}$ and $\mathbf{I}\colon X \to \mathbb{R}$. The bond graph framework uses these energy functions to define the states of the system, where the bonds terminated with such **C** or **I** elements have constitutive relationships for their effort and flow pairs. Now, the non–causal constitutive relationships for efforts and flows associated with storage elements are typically defined as

$$\begin{aligned} \mathbf{C} \quad &\Longrightarrow \quad e(t) - e(0) - \int_0^t f(s)\,ds = 0 \\ \mathbf{I} \quad &\Longrightarrow \quad f(t) - f(0) - \int_0^t e(s)\,ds = 0. \end{aligned} \tag{1.7}$$

The bond graph in Figure 1.2, for example, shows that one could write $e_j(t) = \dot{x}_j(t)/m_j$ with $j \in \{1, 2\}$, so that the constitutive relations of the **I** elements take the form

$$f_j(t) - f_j(0) - x_j(t)/m_j + x_j(0)/m_j = 0. \tag{1.8}$$

But instead of defining constitutive relations as in (1.7), one often defines an energy function for the storage elements from which the constitutive relations are derived. For example, in Figure 1.2 one would define the functions $\mathbf{I}_j(x) = x_j^2/(2m_j)$ with $f_j = d\mathbf{I}_j(x)/dx_j = x_j/m_j$. Therefore, the constitutive relationships of bond graph storage elements are typically defined through the derivative of the overall energy function.

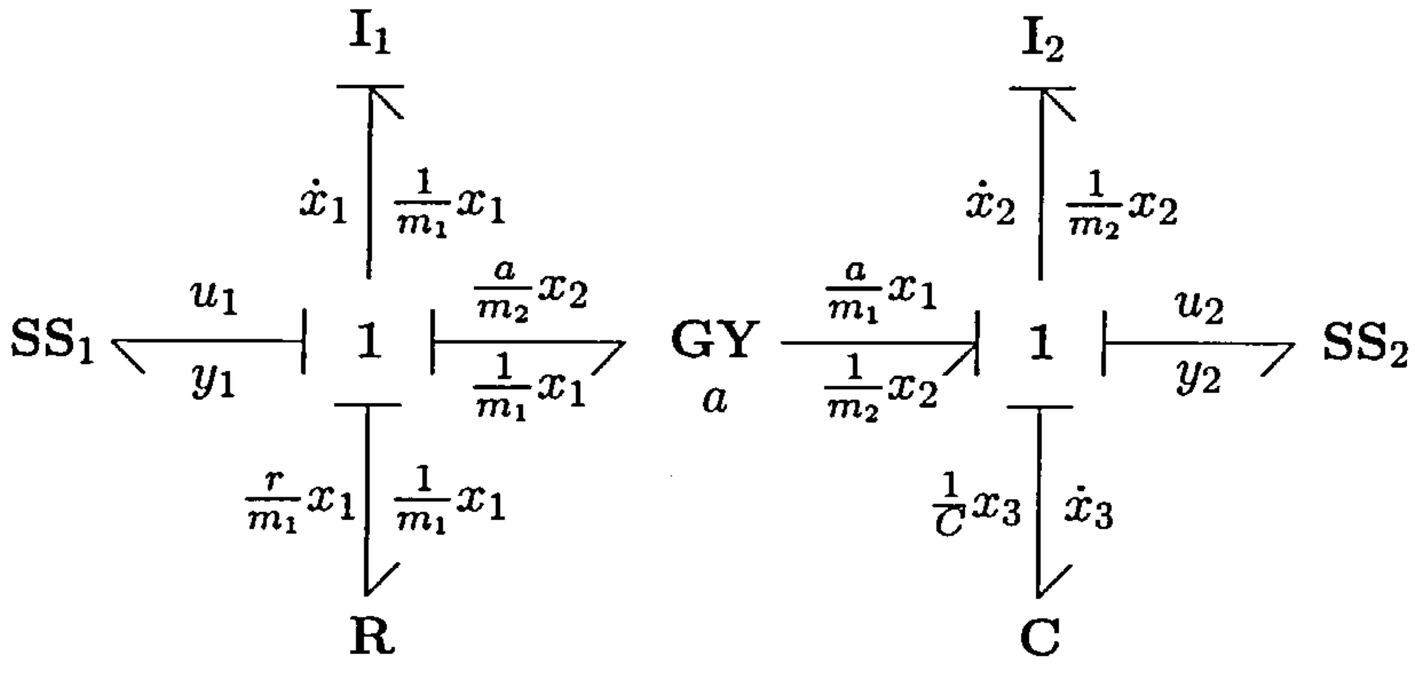

Figure 1.4.: Causal bond graph

Finally, energy dissipation phenomena are implemented through **R** elements that represent various resistive effects, where the associated signal pairs (e_j, f_j) have constitutive relationships that are to satisfy $e_j(t)f_j(t) \geq 0$ for all $t \geq 0$, thereby ensuring that energy is extracted since the power flow is positive and outgoing. Dissipative **R** elements are therefore typically associated with asymptotic stabilising effects, and this will prove to be quite valuable for stabilisation control purposes.

1.2.2. Causal Bond Graphs

The block diagram in Figure 1.1 shows the causality of variables by means of ingoing and outgoing arrows, where the causality had already been established before the block diagram was drawn. However, modelling may require alternative causal patterns with respect to system inputs, thereby rendering the block diagram of limited interest for causal analysis.

Now, the bond graph in Figure 1.2 offers a non–causal representation of the system from which the causal dynamics can be derived. In order to turn the various non–causal relationships into assignment statements, the bond graph uses causal strokes and their junction causality to propagate computational causality of all power variables throughout the bond graph. To that end, consider the system in Figure 1.4 of which each bond has been augmented with a small perpendicular stroke, which induce assignment statements that lead to the equations of motion; see Figure 1.5 for the graphical rules of these strokes in terms of strong causality on 0–junctions and 1–junctions. It should be noted that the small arrows indicate the computational direction of the efforts and flows: The flow is always directed away from the stroke whereas the effort is always directed towards the stroke, thereby offering a systematic, graphical mechanism for causal computation.

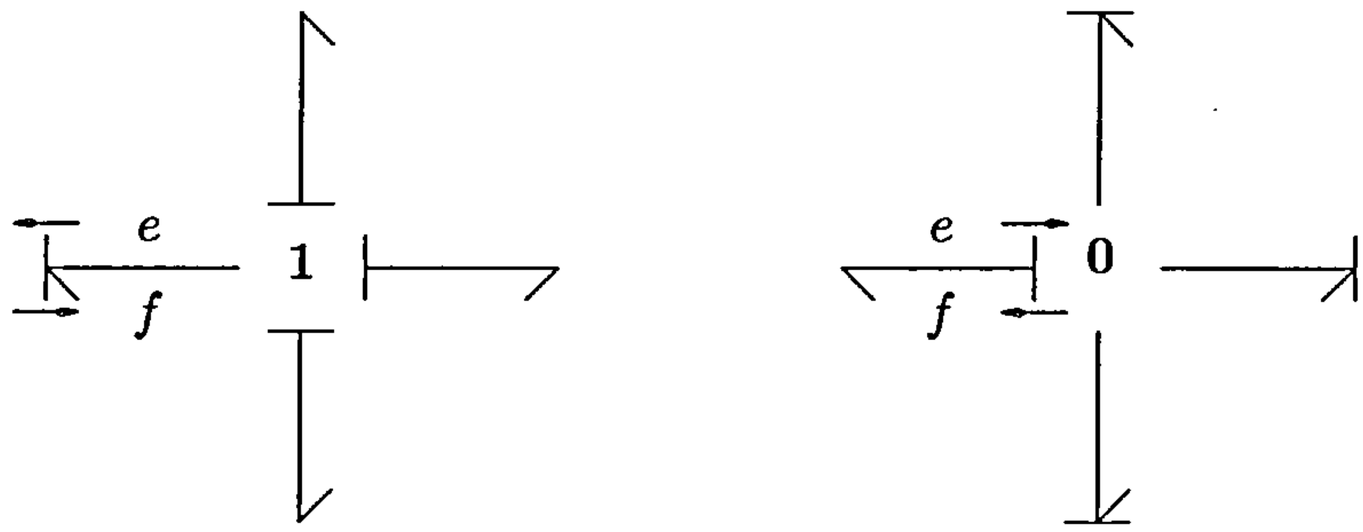

Figure 1.5.: Basic causal propagation through causal strokes.

Figure 1.6.: Integral causality for storage elements

To arrive at the equations of motion, the non–causal bond graph is first assigned the causality of source elements for which the causality is propagated using the rules depicted in Figure 1.5. Subsequently, the preferred integral causality as depicted in Figure 1.6 is imposed and propagated, where the relations (1.7) evidently become

$$\begin{aligned} \mathbf{C} \quad &\Longrightarrow \quad e(t) = e(0) + \int_0^t f(s)\,ds \\ \mathbf{I} \quad &\Longrightarrow \quad f(t) = f(0) + \int_0^t e(s)\,ds. \end{aligned} \tag{1.9}$$

The opposite of integral causality is referred to as derivative causality and is associated with the reversal of causal strokes in Figure 1.6, leading to $f(t) = \dot{e}(t)$ for $\mathbf{C}$ components and $e(t) = \dot{f}(t)$ for $\mathbf{I}$ components. So by taking the above considerations into account, it is seen that the bond graph in Figure 1.5 yields the equations of motion

$$\begin{aligned} \dot{x}_1 &= -\frac{a}{m_2}x_2 - \frac{r}{m_1}x_1 - u_1 \\ \dot{x}_2 &= \frac{a}{m_1}x_1 - \frac{1}{C}x_3 - u_2 \\ \dot{x}_3 &= \frac{1}{m_2}x_2, \end{aligned} \tag{1.10}$$

which are indeed identical to the dynamics derived from the block diagram in Figure 1.1.

Causal assignment is systematic but may require additional attention in some cases, since causal propagation need not terminate for all bonds in case of algebraic loops [Gaw92]. Also, structural properties of the bond graph may induce derivative causalities of storage elements [Kar92]. The reader is referred to the literature for further details.

The causality assignment as briefly described is sometimes referred to as the Sequential Causality Assignment Procedure (SCAP) [Ros87], [van94]. This procedure implies that **SS** elements are given their preferred causality and where a largest set of **C** and **I** elements are to have the preferred integral causality. It must be remembered that the standard bond graph language imposes state variables defined by **C** and **I** elements, but these states may not yield efficient models in certain cases. Indeed, alternative causal assignment procedures, such as the Lagrangian Causality Assignment Procedure (LCAP), have shown to be capable of offering additional freedom to manipulate the structure of bond graph induced dynamics [Kar83], [Mar02]. Detailed accounts on causality can be found in [Bir90], [Dij91], [Gaw95a], [Gaw92], [Hog87], [Jos74], [Lam97] and references therein.

Bicausal Bond Graphs

The concept of a single causal stroke to propagate the computational direction of effort and flows associated with bonds has proven to be unnecessarily restrictive in some cases [Gaw95a]. This can be attributed to the fact that propagation of causality with the single causal stroke mechanism implies opposite conjugate effort and flow directions. So by setting the causality of one bond signal fixes the propagation direction of the conjugate bond variable. On the other hand, power continuity of bond graphs is independent of causality, which implies that the causal stroke mechanism can be generalised to the cases where the conjugate effort and flow have identical computational directions.

Causality of efforts on 0–junctions and flows on 1–junctions need not be compromised when the single causal stroke is abandoned and where the conjugate efforts and flows attain individual causal strokes instead. Doing so increases the number of causal configurations for bond graph models and has shown to offer an additional tool for causal analysis and modelling purposes [Gaw00], [Gaw03]. In particular, the notion of (bi)causality has proven to be quite useful for "causal inversion" problems [Ngw96] whereby the input/output dynamics are inverted through the (bi)causal stroke mechanism, if possible.

Figure 1.7 shows the possible bicausal propagation of conjugate effort and flow pairs, where it is seen that the computational direction of both the effort and flows are rendered independent in a bicausal context. The rules for causal assignment with respect to junctions remains unchanged, and Figure 1.8 shows that efforts retain strong causality on 0–junctions and that flows retain strong causality on 1–junctions.

Figure 1.7.: Bicausal propagation of effort and flow.

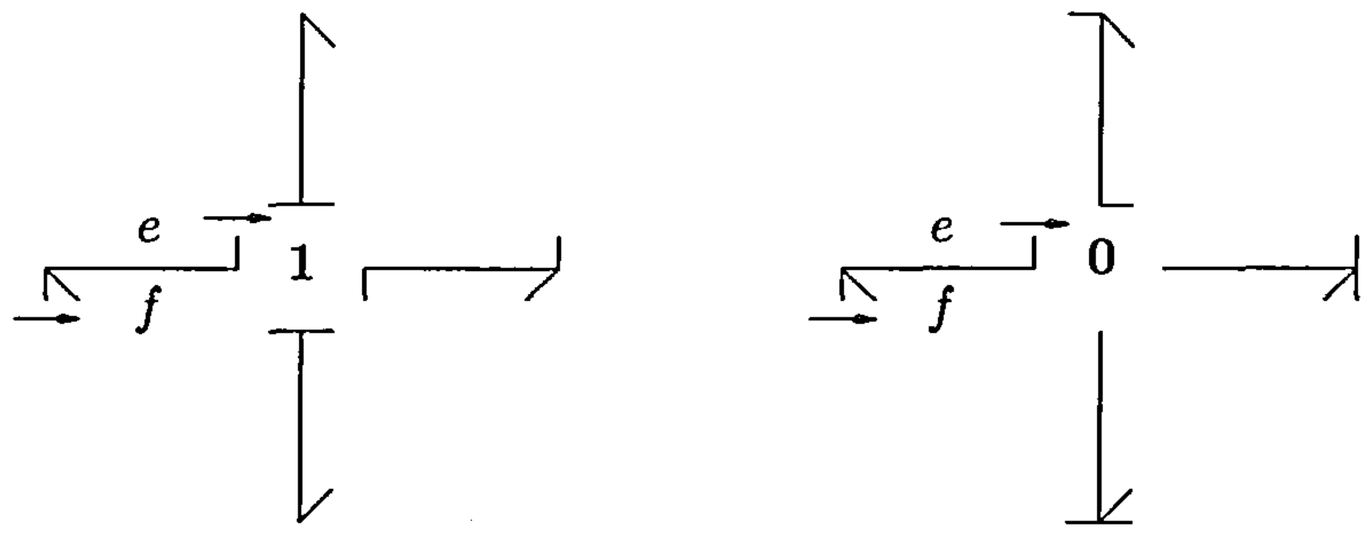

Figure 1.8.: Examples of bicausal propagation on junctions.

Bicausality for causal inversion problems is particularly instructive when bond graph input and output variables are chosen as non–conjugate pairs. To elaborate this point, from Figure 1.4 it is seen that the single causal stroke mechanism selects the bond signal y_j as the output of **SS** elements. Now, provided no causal conflict occurs, causal inversion is then achieved by moving some or all causal strokes to the other end of the bond. On the other hand, such input/output inversion is not suitable for non–conjugate input/output pairs. To see this, consider Figure 1.4 once again and suppose one defines the input/output pair (u_1, y_2) by setting $u_2 = 0$ and by ignoring the output y_1, but it is readily understood that the single stroke mechanism cannot be used to causally invert the pair (u_1, y_2) in such a scenario. The reader is referred to [Ngw99a], [Ngw01a], [Ngw01b] for further accounts on causal inversion in physical systems modelling.

1.3. Bond Graphs as Port–Hamiltonian Systems

Even though the bond graph language offers a structured framework to derive equations of motion, the underlying mathematical structure of bond graph induced dynamics are relatively non–trivial. In [Ros71], the mathematical representation of a class of bond graph models is addressed from a generic state space standpoint, whereas notions of Hamiltonian dynamics [Mar94] of bond graphs was recognised at a later stage later [Mas92], [Mas95]. Also, the port–Hamiltonian framework presented in [Dal97], [Sch96] offers a detailed geometric framework for bond graph induced dynamics [Gol02], [Gol03].

1.3.1. Basic Facts on Port–Hamiltonian Systems

In [Dal97], [Sch96], concepts of port–Hamiltonian systems are introduced in the context of energy conserving physical systems that have input and output ports by which they connect to the external environment. The authors then show that the coordinate representation of an important subclass of port–Hamiltonian systems takes the form

$$\begin{aligned} \dot{x} &= [J(x) - R(x)]K(x) - g(x)u \\ y &= g^T(x)K(x), \end{aligned} \tag{1.11}$$

where $x = (x_1, \ldots, x_n) \in X$ are independent coordinates and where $K^T(x) = \mathbf{D}H(x)$ is the row vector of partial derivatives of the smooth energy function $H\colon X \to \mathbb{R}$. The function $H(x)$ is called the Hamiltonian and represents the physical energy stored by the system. The matrix $J(x) = -J^T(x)$ is the structure matrix and defines power continuous network interconnections, whereas the positive (semi)–definite matrix $R(x) = R^T(x)$ is the dissipation structure that incorporates resistive effects. The port space of the system is represented by the matrix $g(x)$ and where $u \in \mathbb{R}^m$ are inputs and where $y \in \mathbb{R}^m$ are outputs. Clearly, the port–Hamiltonian system (1.11) satisfies

$$\frac{d}{dt}H(x) = -K^T(x)R(x)K(x) - y^T u \leq -y^T u, \tag{1.12}$$

which shows that the product $y^T u$ expresses the power injected into or extracted from the system (1.11).

As argued in [Dal97], the system (1.11) is called port–Hamiltonian by considering the following. It is possible to define a bilinear, anti–symmetric bracket operation on real–valued functions defined as

$$\{F, G\}(x) = J_{ij}(x)\frac{\partial F}{\partial x_i}(x)\frac{\partial G}{\partial x_j}(x), \tag{1.13}$$

with $F, G\colon X \to \mathbb{R}$. This bracket operation is recognised to be a Poisson bracket when Jacobi's identity is satisfied [Mar94], but this is not required. Then by following the arguments of [Mar94], one can use the structure matrix $J(x)$ of (1.11) to define the "classical" Hamiltonian system

$$\dot{x} = J(x)K(x). \tag{1.14}$$

Therefore, the port–Hamiltonian system (1.11) can be said to generalise the system (1.14) by including the dissipation matrix $R(x)$ and the input/output port interaction by means of the input matrix $g(x)$.

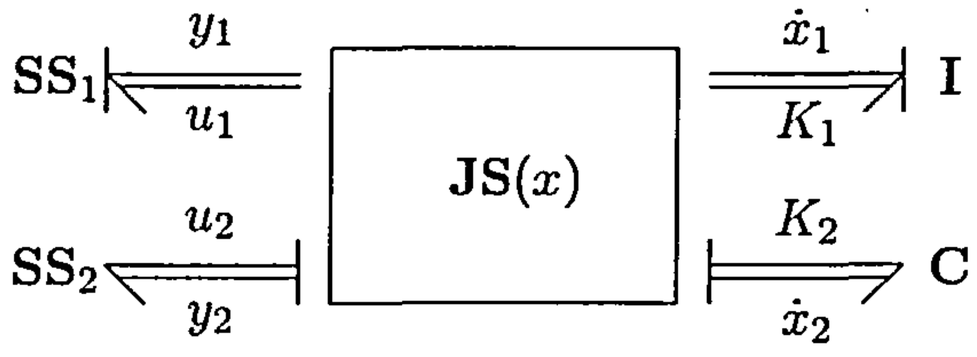

Figure 1.9.: Vector bond graph without dissipation.

1.3.2. Network Interconnections, Dissipation and Ports

The link between bond graph models and the port–Hamiltonian framework as presented in [Dal97], [Sch96], [Sch00b], [Gol02] is achieved by briefly considering the following. Figure 1.9 shows the vector bond notation [Bre92a], [Bre95] of a system without dissipative elements, where it is seen that systems inputs can be any combination of efforts and flows. Define the respective inputs and outputs $u = (u_1, u_2)$ and $y = (y_1, y_2)$, the state space coordinates $x = (x_1, x_2)$, the tangent vector $\dot{x} = (\dot{x}_1, \dot{x}_2)$, and the derivative $K(x) = (K_1(x), K_2(x))$ of the Hamiltonian $H(x)$. Note that $K_1(x)$ and $K_2(x)$ are column vectors of partial derivatives with respect to x_1 and x_2 respectively.

It can be shown that the network interconnections of power continuous bond graph elements, denoted as $\mathbf{JS}(x)$, is itself power continuous [Kar00]. Furthermore, in [Ros71] it was recognised that a junction structure $\mathbf{JS}(x)$ represents a linear map. These considerations then imply that the causal assigned bond graph in Figure 1.9 leads to the relation

$$\begin{bmatrix} \dot{x} \\ y \end{bmatrix} = B(x) \begin{bmatrix} K(x) \\ u \end{bmatrix} = \begin{bmatrix} J(x) & -g(x) \\ g^T(x) & D(x) \end{bmatrix} \begin{bmatrix} K(x) \\ u \end{bmatrix}, \tag{1.15}$$

for some matrices $J(x)$, $D(x)$ and some input matrix $g(x)$ of suitable dimensions. Next observe that power continuity of $\mathbf{JS}(x)$ implies that

$$K^T(x)\dot{x} + u^T y = \begin{bmatrix} K^T(x) & u^T \end{bmatrix} B(x) \begin{bmatrix} K(x) \\ u \end{bmatrix} = 0. \tag{1.16}$$

Since power continuity holds for all energy functions $H(x)$ and all system inputs u, it follows that (1.16) must satisfy $B(x) = -B^T(x)$, hence $J(x) = -J^T(x)$ and $D(x) = -D^T(x)$. Note that by (1.16) an arbitrary function $H(x)$ remains constant along system trajectories compatible with the constraints $u = 0$ or $y = 0$.

The system (1.15) represents an energy conserving port–Hamiltonian system, where for a relatively large class of systems it will be the case that $D(x) = 0$.

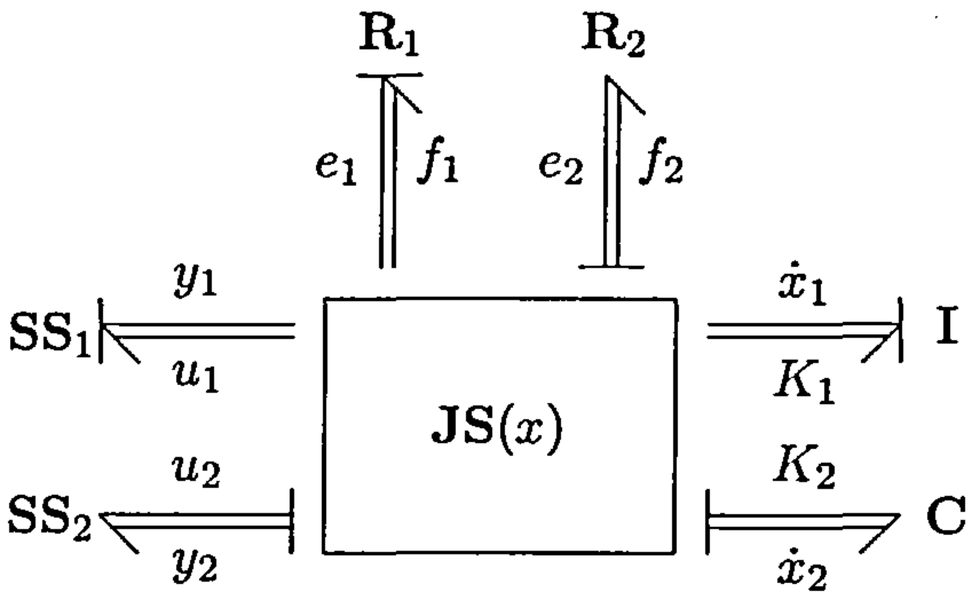

Figure 1.10.: Vector bond graph with dissipation.

To include dissipation phenomena to arrive at a larger class of bond graph induced port–Hamiltonian dynamics requires the following considerations. Define the vectors of inputs and outputs associated with the $\mathbf{R}_1$ and $\mathbf{R}_2$ elements as $u_r = (f_1, e_2)$ and $y_r = (e_1, f_2)$. Then suppose the vector bond graph in Figure 1.10 yields the dynamics

$$\begin{bmatrix} \dot{x} \\ y \\ y_r \end{bmatrix} = \begin{bmatrix} J(x) & -g(x) & -g_r(x) \\ g^T(x) & D(x) & -b(x) \\ g_r^T(x) & b^T(x) & 0 \end{bmatrix} \begin{bmatrix} K(x) \\ u \\ u_r \end{bmatrix}, \tag{1.17}$$

which defines an anti–symmetric mapping associated with the power continuous junction structure.

In many practical cases it is possible to model dissipation phenomena by considering the simple linear relation $u_r = Sy_r$ with $S = S^T \geq 0$; this implies that $y_r^T u_r \geq 0$ and energy is therefore extracted from the system. From (1.17) it follows that the port–Hamiltonian dynamics (1.17) can be rewritten as

$$\begin{bmatrix} \dot{x} \\ y \end{bmatrix} = \begin{bmatrix} J(x) - R(x) & -g(x) - A(x) \\ g^T(x) - A^T(x) & D(x) - U(x) \end{bmatrix} \begin{bmatrix} K(x) \\ u \end{bmatrix}, \tag{1.18}$$

with $A(x) = g_r(x)Sb^T(x)$, $R(x) = g_r(x)Sg_r^T(x)$ and $U(x) = b(x)Sb^T(x)$, and observe that $R(x) = R^T(x) \geq 0$ and $U(x) = U^T(x) \geq 0$.

The port–Hamiltonian dynamics (1.11) are seen to be contained in the bond graph induced dynamics (1.18), where it should be noted that a relatively large class of multidisciplinary engineering system can be adequately modelled with $A(x) = 0$, $D(x) = 0$ and $U(x) = 0$. As will be seen in the thesis, models of the form (1.11) allow for a relatively new physical model based control framework [Ort02b].

Now, the general bond graph induced dynamics (1.18) can be written in a more compact form, being

$$\begin{aligned}\begin{bmatrix} \dot{x} \\ y \end{bmatrix} &= \left(\begin{bmatrix} J(x) & -g(x)) \\ g^T(x) & D(x) \end{bmatrix} - \begin{bmatrix} R(x) & A(x)) \\ A^T(x) & U(x) \end{bmatrix} \right) \begin{bmatrix} K(x) \\ u \end{bmatrix}, \\ &:= \left[\widehat{J}(x) - \widehat{R}(x) \right] \begin{bmatrix} K(x) \\ u \end{bmatrix},\end{aligned} \tag{1.19}$$

where the junction structure $\mathbf{JS}(x)$ induces the structure matrix $\widehat{J}(x) = -\widehat{J}^T(x)$ and where the resistive elements induce the dissipation matrix $\widehat{R}(x) = \widehat{R}^T(x) \geq 0$. Then by equating the power flow of all bonds in Figure 1.10 one finally obtains

$$\frac{d}{dt}H(x) = -\begin{bmatrix} K^T(x) & u^T \end{bmatrix} \widehat{R}(x) \begin{bmatrix} K(x) \\ u \end{bmatrix} - y^T u \leq -y^T u, \tag{1.20}$$

which clearly shows that the stored energy depends on the supply rate $y^T u$.

The following final remark is in order. Section 1.2.2 pointed out that it may not be possible to have all **C** and **I** elements in the preferred integral causality without inducing causal conflicts in the junction structure $\mathbf{JS}(x)$. To overcome such causal problems, it is always possible to insert additional **SS** elements to remove any causal conflicts from occurring; however, doing so implies that the outputs of such source element are to be zero [Mar02]. In the case where such additional **SS** elements are necessary, the bond graph can be shown to induce *implicit* port–Hamiltonian dynamics [Sch00a]. This will not be further elaborated.

1.4. Thesis Rationale and Objective

It is safe to say that the *open loop* modelling capabilities of bond graphs are well–understood. Indeed, as briefly presented in Section 1.2, the graphical aspects of bond graphs have been subjected to significant research efforts, where the more geometric port–Hamiltonian description of Section 1.3 can be argued to have contributed to a further understanding of the network modelling of physical systems.

On the other hand, bond graph modelling in control cannot claim to have reached the level of research commitment and sophistication comparable to the modelling aspects of bond graphs. Nonetheless, a wide variety of compelling bond graph considerations in various control designs have appeared over the years [Kar79], [Bar77], [Gaw95b], [Hog85], [Jun01], [Rob95], [Yeh99].

Modern (robust) control theory (e.g. [Zho98]) is analytical in nature and can be argued to be quite successful in addressing a myriad of control problems. But in contrast to a sole analytic approach, there are valuable notions of "Control in the Physical Domain" [Sha91] that attempt to use certain properties of the physical system to aid the controller design. For example, the property of physical stored energy can often be used to derive certain feedback laws [Ort01].

Therefore, instead of analytical approaches, the objective of this thesis is to use established control methods for *closed loop* bond graphs. More precisely, this thesis is primarily concerned with closed loop bond graph representations to facilitate physical model arguments for control purposes. Most importantly, the port–Hamiltonian dynamics associated with bond graphs will prove to be an important fact for the various feedback designs. The reader should note, however, that the application of bond graphs in control is certainly not new [Gaw95b], [Ngw01a], but this thesis "rebundles" established control theory for the modelling of closed loop dynamics.

The main control methods considered in this thesis are (1) Backstepping Control, (2) Model Matching Control and (3) Energy Shaping in Stabilisation Control. Each of these topics are described in separate chapters that present new views and developments. The following paragraphs summarise the rationale behind these feedback designs in further detail.

Backstepping Control The backstepping method uses *virtual control* variables and recursive Lyapunov functions for stabilisation purposes and is thoroughly documented in the nonlinear control literature [Kri95], [Isi99], [Kha92]. In [Yeh99] it is recognised that bond graphs can be used to design backstepping controllers by defining additive elements that impose the virtual control law. Furthermore, in [Gaw01] it is even recognised that certain *exact* backstepping designs can be achieved through the sole application of (bi)causal inversion as outlined in Section 1.2.2.

In contrast to the existing works on bond graph based backstepping, this thesis shows that backstepping can be used to design a closed loop port–Hamiltonian system that is "close" to the plant port–Hamiltonian system. As a result, the feedback design has an intrinsic physical model interpretation.

Model Matching Control The concept that system outputs are to follow a prescribed trajectory of some desired model or exosystem can be said to have a long history in the control literature, where the reader is referred to [Hui94] for a summary of the topic. Two important characteristics of model matching are (1) the application of input/output inversion, and (2) concepts of dynamic disturbance decoupling. As argued in Section 1.2.2, the bond graph language can be used to invert the input/output map by means of the (bi)causal assignment mechanism [Gaw95a], such that the application of a causal bond graph tool is available for certain Model Matching Problems (MMP).

This thesis explores the bond graph based MMP by prescribing closed loop input/output dynamics with a bond graph model. In particular, ideas of center manifold theory [Nij90], [Isi95] will be shown to allow for additional closed loop bond graph representations in certain cases. This result offers a more fundamental understanding of what the underlying principles are of the MMP as considered in this thesis. Such developments have been absent in the current bond graph literature.

Energy Shaping in Stabilisation Control Feedback passivation is a control strategy that concerns itself with feedback laws that induce closed loop passivity with respect to some energy function and supply rate [Byr91]. It can be of interest to see whether the bond graph language provides any tools that render the passive feedback design constructive to some degree. This thesis shows that the junction structure can indeed be used to derive closed loop energy functions that induce feedback passivity with respect to the natural output. The relevance of this result can be attributed to the fact that the energy function need not be "guessed" but that it follows from power continuity considerations.

The port–Hamiltonian framework allows for a control methodology generally referred to as Interconnection and Damping Assignment Passivity Based Control (IDA–PBC) as presented in [Ort02a], [Ort02b]. This control method addresses feedback designs that can be associated with the shaping of the Hamiltonian and the modification of structure and damping matrices. The solvability of an IDA–PBC design, however, is dependent on first order partial differential equations. It is shown that the closed loop representation of basic IDA–PBC designs can be depicted with the bond graph language, where the modification of the structure matrices is prescribed by the desired junction structure and resistive components.

Concluding Remarks The above control methods may initially seem unrelated, but they have the common goal of using the closed loop bond graph for stabilisation purposes. Put differently, the presented control strategies are certainly different on the analytical level, but the closed loop dynamics obtained with those methods will allow for bond graph models.

It must be noted that aspects of bond graphs in control as presented in the thesis are not meant to define rigid procedures. Instead, the (non)linear systems framework and the various control methods render generalisations difficult, so that flexibility should be retained to facilitate unforeseen problems. In conclusion, this thesis shows that the above three control strategies have proven to allow for valuable physical interpretations that can aid the control design of multidisciplinary systems modelled with bond graphs.

2. Fundamentals on Physical Model Based Control

2.1. Introduction

Various generic control strategies exist, such as H_∞ control [Zho98] for example, that do not have explicit design goals in terms of physical interpretations of controlled dynamics. That is to say that generic feedback strategies generally apply signal theoretic techniques through considerable collections of abstract mathematical methods without concerning itself with physical interpretations of controlled dynamics. Even though such analytic control designs can be very effective and systematic for a wide variety of (robust) control problems, in order to explore bond graph representations for closed loop dynamics it can be argued that more structural approaches are to be addressed first.

By focusing on closed loop bond graph representations, it is intuitively plausible that feedback designs should impose closed loop dynamics that allows for an associated bond graph model. For example, as outlined in Section 1.3, in case the closed loop is to be represented by means of a bond graph, this would imply that closed loop port–Hamiltonian dynamics should be an explicit design goal. Therefore, the aim of this chapter is to address feedback design methods that allow for structural and physical considerations in order to attain closed loop dynamics with an associated bond graph model for stabilisation purposes.

The chapter is organised as follows. Backstepping control [Kri95] is recalled and shown to be able to impose closed loop port–Hamiltonian dynamics by judiciously chosen virtual control laws; consequently, closed loop bond graph representations are possible. Second, model matching control as presented in [Hui94] is shown to allow for closed loop bond graph models by borrowing certain ideas of center manifold theory in output regulation problems. Finally, stabilisation control through energy shaping is presented in terms of feedback passivation control [Byr91] and the interconnection and damping assignment procedure [Ort02b], which explicitly defines the closed loop interconnection and damping structures and hence closed loop port–Hamiltonian dynamics.

2.2. Backstepping Control

Physical systems modelling is often managed through an object–oriented approach by which smaller subsystems, the objects, are connected to obtain larger, complex models. In view of such decomposition into subsystems, suppose that some particular subsystem can be stabilised by placing a *virtual actuator* at some desired location but for which no regular control is available. Then, intuitively, one could try to find suitable feedback control that imposes the virtual actuator dynamics and further stabilises the subsystems "between" the actual control input and the virtually actuated subsystem.

The above conceptual control problem can be addressed by means of a systematic backstepping design, where a suitable variable is designated as the *virtual control* that represents the physical location at which the virtual actuator is to be connected. By imposing a suitable feedback law for the virtual control variable, backstepping is then applied to "step back" through the subsystem dynamics that connects the virtual control and the regular control. Most importantly, each recursive design step uses Lyapunov arguments to guarantee (global) stability and asymptotic convergence of trajectories. Interested readers are referred to the works [Kri95], [Isi99], [Kha92], [Sep97] and references therein for a comprehensive treatment on backstepping control designs.

2.2.1. Recursive Lyapunov Design

The backstepping methodology is readily explained by means of the following lemma that can be found in [Isi95] and which will be referenced in the sequel.

Lemma 2.1. ([Isi95]) *Consider a system of the form*

$$\begin{aligned} \dot{x} &= f(x,\xi) \\ \dot{\xi} &= u \end{aligned} \tag{2.1}$$

where $(x,\xi) \in \mathbb{R}^n \times \mathbb{R}$ *and* $f(0,0) = 0$. *Let* $V(x)$ *be a smooth real–valued function, which is positive definite and proper, and suppose there exists a static feedback law* $\xi = v^\star(x)$, *with* $v^\star(0) = 0$, *such that*

$$\|x\| > 0 \quad \Longrightarrow \quad \mathbf{D}V(x)f(x,v^\star(x)) < 0. \tag{2.2}$$

Then there exists a smooth feedback $u(x,\xi)$, *with* $u(0,0) = 0$, *and a smooth real-valued function* $W(x,\xi)$, *which is positive definite and proper, such that*

$$\|x\| + |\xi| > 0 \quad \Longrightarrow \quad \frac{d}{dt}W(x,\xi) = \mathbf{D}_x W(x,\xi) f(x,\xi) + \mathbf{D}_\xi W(x,\xi) u(x,\xi) < 0. \tag{2.3}$$

Proof. The point of departure is to recognise that ξ can be viewed as a *virtual control* for which a stabilising function $v^\star(x)$ exists such that (2.2) is satisfied. Then to "step back" through $\dot{\xi}$ towards u, define the global change of variable $z = \xi - v^\star(x)$, giving

$$\dot{x} = f(x, v^\star(x) + z) \tag{2.4}$$

$$\dot{z} = u - \dot{v}^\star(x). \tag{2.5}$$

Observe that the feedback $u = \dot{v}^\star(x) + \mu$ yields the system

$$\begin{aligned} \dot{x} &= f(x, v^\star(x) + z) \\ \dot{z} &= \mu, \end{aligned} \tag{2.6}$$

implying that passive stabilisation can now be used to stabilise the z–dynamics. To this end, system (2.6) can be rewritten in the form

$$\begin{aligned} \dot{x} &= f(x, v^\star(x)) + p(x,z)z \\ \dot{z} &= \mu, \end{aligned} \tag{2.7}$$

where $p(x,z)$ is a smooth function. Then take the positive definite and proper Lyapunov function

$$W(x,z) = V(x) + \frac{1}{2}z^2 = V(x) + \frac{1}{2}[\xi - v^\star(x)]^2, \tag{2.8}$$

and observe that

$$\frac{d}{dt}W(x,z) = \mathbf{D}V(x) f(x, v^\star(x)) + \mathbf{D}V(x) p(x,z) z + z\mu. \tag{2.9}$$

Thus, by taking the control

$$\mu = -cz - \mathbf{D}V(x) p(x,z), \tag{2.10}$$

for some $c > 0$, it follows that

$$\|x\| + |z| > 0 \quad \Longrightarrow \quad \frac{d}{dt}W(x,z) = \mathbf{D}V(x) f(x, v^\star(x)) - cz^2 < 0. \tag{2.11}$$

The control that globally asymptotically stabilises (2.1) is therefore given as

$$u = \dot{v}^\star(x) - c(\xi - v^\star(x)) - \mathbf{D}V(x) p(x, \xi - v^\star(x)). \tag{2.12}$$

□

The recursive application of Lemma 2.1 is briefly explained by considering a system in the *lower–triangular* form

$$\begin{aligned} \dot{x} &= f_0(x, \xi_1) \\ \dot{\xi}_1 &= f_1(x, \xi_1) + g_1(x, \xi_1)\xi_2 \\ \dot{\xi}_2 &= f_2(x, \xi_1, \xi_2) + g_2(x, \xi_1, \xi_2)\xi_3 \\ &\vdots \\ \dot{\xi}_n &= f_n(x, \xi_1, \ldots, \xi_n) + g_n(x, \xi_1, \ldots, \xi_n)u \end{aligned} \tag{2.13}$$

where $x \in \mathbb{R}^n$ and $\xi_i \in \mathbb{R}$ for $1 \leq i \leq n$ [Isi99]. The triangular structure shows that Lemma 2.1 can be applied to the upper two systems by viewing ξ_1 as the virtual control and by identifying ξ_2 as a regular control. Note that both $f_1(x, \xi_1)$ and $g_1(x, \xi_1)$ can be eliminated by feedback provided $g_1(x, \xi_1)$ is nonzero on the domain of interest. Define for each step i the change of variables

$$z_i = \xi_i - v_{i-1}^{\star}(x, \xi_1, \ldots, \xi_{i-1}) \tag{2.14}$$

and observe that the recursive application of Lemma 2.1 terminates when the control u is reached. At step i the closed loop Lyapunov function is given by

$$W_i(x, z_1, \ldots, z_i) = V(x) + \frac{1}{2}\sum_{k=1}^{i} z_k^2. \tag{2.15}$$

Note that the control (2.12) is based on exact cancellations to render (2.11) fulfilled, so that Lemma 2.1 is commonly referred to as *exact backstepping* [Isi95]. However, when model parameters are not precisely known, but known to exist within certain bounds, it is readily seen that exact backstepping cannot be applied. In case of parameter uncertainties, the control problem is then to be addressed from an alternative standpoint, where one can use notions of *input–to–state stability* and *small–gain* theorems [Isi99]. Further details on parameter uncertainties will not be elaborated and all developments in the thesis are in the context of *exact* backstepping designs.

2.2.2. Closed Loop Port–Hamiltonian Dynamics

This section shows that closed loop port–Hamiltonian dynamics is attainable through a backstepping design, and this will proof to be quite valuable for bond graph based backstepping as presented in the thesis. It is interesting to note that [Kri95] mentions the possible anti–symmetry of the closed loop in backstepping designs, but the author has not found references that explicitly refer to port–Hamiltonian dynamics.

Example 2.1. Consider the system

$$\begin{aligned} \dot{x} &= -\sin(x+\xi) \\ \dot{\xi} &= u. \end{aligned} \tag{2.16}$$

Suppose the equilibrium $(x,\xi) = (0,0)$ is to be globally asymptotically stabilised. Towards that end, define the change of variables

$$z = \xi - v^{\star}(x) = \xi - \arctan(x) + x, \tag{2.17}$$

and observe that (2.16) can be written as

$$\begin{aligned} \dot{x} &= -\frac{x}{\sqrt{x^2+1}} + \left[\frac{x - x\cos(z) - \sin(z)}{z\sqrt{x^2+1}}\right] z \\ \dot{z} &= u - \dot{v}^{\star}(x). \end{aligned} \tag{2.18}$$

Choose the Lyapunov function (2.8) as $W(x,z) = (1/2)(x^2+z^2)$ and write

$$\frac{d}{dt}W(x,z) = -\frac{x^2}{\sqrt{x^2+1}} + z\left[\frac{x^2 - x^2\cos(z) - x\sin(z)}{z\sqrt{x^2+1}} + u - \dot{v}^{\star}(x)\right], \tag{2.19}$$

which implies the control

$$u = \dot{v}^{\star}(x) - cz - \frac{x^2 - x^2\cos(z) - x\sin(z)}{z\sqrt{x^2+1}} + v, \tag{2.20}$$

for some $c > 1/2$ and where v is the new control. Set $d = \min\{1, c-(1/2)\}$ and write

$$\begin{aligned} \frac{d}{dt}W(x,z) = -\frac{x^2}{\sqrt{x^2+1}} - cz^2 + zv &\leq -\frac{x^2}{\sqrt{x^2+1}} - (c-\frac{1}{2})z^2 + \frac{1}{2}v^2 \\ &\leq -\alpha(\|(x,z)\|) + \sigma(|v|), \end{aligned} \tag{2.21}$$

where $\alpha(r) = -dr^2/\sqrt{r^2+1}$ and $\sigma(r) = (1/2)r^2$ are class $\mathcal{K}_\infty$ functions [Isi99]. Thus, the controller (2.20) yields input–to–state closed loop stability [Son95], which implies that for $v = 0$ the equilibrium $(x,\xi) = (0,0)$ is globally asymptotically stable.

The following is of great importance for bond graph based backstepping: apply control (2.20) to (2.18) and conclude that the closed loop system can be written as

$$\begin{bmatrix} \dot{x} \\ \\ \dot{z} \end{bmatrix} = \begin{bmatrix} -\dfrac{1}{\sqrt{x^2+1}} & \dfrac{x - x\cos(z) - \sin(z)}{z\sqrt{x^2+1}} \\ \\ -\dfrac{x - x\cos(z) - \sin(z)}{z\sqrt{x^2+1}} & -c \end{bmatrix} \begin{bmatrix} x \\ \\ z \end{bmatrix} + \begin{bmatrix} 0 \\ \\ 1 \end{bmatrix} v, \tag{2.22}$$

which is of port–Hamiltonian form.

In view of *robust* control, it is generally preferred to majorise nonlinearities in (2.19), which implies that the control (2.20) is to be robustified by avoiding exact cancellations in (2.19) as much as possible [Kri95], [Kha92]. To that end, write

$$\begin{aligned}\frac{d}{dt}W(x,\xi) &\leq -\frac{x^2}{\sqrt{x^2+1}} + |z|\left|\frac{x^2 - x^2\cos(z)}{z\sqrt{x^2+1}}\right| + |z||\dot{v}^\star(x)| + z\left[u - \frac{x\sin(z)}{z\sqrt{x^2+1}}\right] \\ &\leq -\left[\frac{1}{\sqrt{x^2+1}} - \frac{1}{2\delta(x)}\right]x^2 + \frac{3+\delta(x)}{2}z^2 + z\left[u - \frac{x\sin(z)}{z\sqrt{x^2+1}}\right],\end{aligned} \tag{2.23}$$

for some function $\delta(x) > (1/2)\sqrt{x^2+1}$ for all x. Take $\delta(x) = \sqrt{x^2+1}$ to obtain the *smooth* control

$$u = -\left[\frac{3}{2} + \frac{1}{2}\sqrt{x^2+1} + c\right]z + \frac{x\sin(z)}{z\sqrt{x^2+1}} + v. \tag{2.24}$$

Global asymptotic stability of the equilibrium $(x,\xi) = (0,0)$ is immediate from the inequality

$$\frac{d}{dt}W(x,z) \leq -\frac{x^2}{2\sqrt{x^2+1}} - (c - \frac{1}{2})z^2 + \frac{1}{2}v^2, \tag{2.25}$$

where $c > 1/2$. ◊

The important point of the above example is that backstepping designs offer flexibility to render (2.9) negative, such that robustness can be addressed quite systematically for systems of the form (2.1). However, this flexibility will not be used in the thesis since the closed loop is required to have a specific structure. More precisely, the following corollary shows that *exact* backstepping can be used to yield port–Hamiltonian dynamics.

Corollary 2.2. *Consider the system* (2.1) *and suppose the virtual control* $v^\star(x)$ *yields the relation*

$$f(x, v^\star(x)) = [J(x) - R(x)]K(x), \tag{2.26}$$

with $K^T(x) = \mathbf{D}V(x)$ *for some real–valued, positive and proper function* $V(x)$*, and where* $J(x) = -J^T(x)$ *and* $R(x) = R^T(x) \geq 0$ *are* $n \times n$ *matrices. Then in view of Lemma 2.1 there exists a control* $u(x,\xi)$*, with* $u(0,0)$*, such that the closed loop takes the port–Hamiltonian form*

$$\begin{bmatrix} \dot{x} \\ \dot{z} \end{bmatrix} = \begin{bmatrix} J(x) - R(x) & p(x,z) \\ -p^T(x,z) & -c \end{bmatrix} S(x,z), \tag{2.27}$$

where $W(x,z) = V(x) + (1/2)z^2$*,* $S^T(x,z) = \mathbf{D}W(x,z)$ *and* $z = \xi - v^\star(x)$*.*

Proof. In view of (2.7), take the control

$$u = \dot{v}^\star(x) - p^T(x,z)K(x) - cz, \tag{2.28}$$

and observe that the closed loop dynamics takes the form (2.27). Note that (2.2) does not hold, since

$$\|x\| > 0 \quad \Longrightarrow \quad K^T(x)f(x, v^\star(x)) = -K^T(x)R(x)K(x) \leq 0, \tag{2.29}$$

which is merely non–positive. □

Thus, going back to the system (2.18) of Example 2.1, observe that the interconnection structure $J(x) = 0$ and the damping structure $R(x) = 1/\sqrt{x^2+1}$ yields

$$\|x\| \quad \Longrightarrow \quad \mathbf{D}V(x)f(x, v^\star(x)) = -\frac{1}{\sqrt{x^2+1}}\left(\frac{\partial V}{\partial x}\right)^2 = -\frac{x^2}{\sqrt{x^2+1}} < 0. \tag{2.30}$$

Therefore, the fact that port–Hamiltonian dynamics can be obtained through an exact back-steppping design would seem to have favorable consequences for bond graph considerations. In particular, bond graphs have been shown to represent a class of port–Hamiltonian systems [Gol02], [Gol03], so that closed loop dynamics attained through exact backstepping can indeed be given an associated bond graph model.

2.3. Model Matching Control

This section recalls relevant facts on the (non)linear Model Matching Problem (MMP). In addition to the existing MMP theory of [Hui94], this section shows that various concepts of center manifold considerations in output regulation [Isi95] are valuable for an understanding of closed loop dynamics in the MMP. For example, if the *tracking error* is asymptotically regulated to zero then this implies the existence of a maximal (locally) controlled invariant submanifold on which output matching is fulfilled. This invariant manifold provides the basic characterisation of the underlying mechanism with regards to the physical model based MMP as considered in the thesis, where this mechanism has not been explicitly addressed in the current bond graph literature.

2.3.1. Some Facts on Model Matching Problems

The following developments can be found in the works [Hui94], [Hui92]. Consider the plant P of the form

$$P : \begin{cases} \dot{x} &= f(x) + g_j(x)u_j \\ y &= h(x). \end{cases} \tag{2.31}$$

Here $x \in \mathbb{R}^n$, $u \in \mathbb{R}^m$ and $y \in \mathbb{R}^p$. The vector fields $f(x)$ and $g_j(x)$ and the function $h(x)$ are assumed to be real analytic. Then consider the model M of the form

$$M : \begin{cases} \dot{\bar{x}} &= \bar{f}(\bar{x}) + \bar{g}_k(\bar{x})\bar{u}_k \\ \bar{y} &= \bar{h}(\bar{x}), \end{cases} \tag{2.32}$$

where $\bar{x} \in \mathbb{R}^{\bar{n}}$, $\bar{u} \in \mathbb{R}^{\bar{m}}$ and $\bar{y} \in \mathbb{R}^p$. Likewise, the vector fields $\bar{f}(\bar{x})$ and $\bar{g}_k(\bar{x})$, and the function $\bar{h}(\bar{x})$ are assumed to be real analytic. Notice, in particular, that $\bar{m} \leq m$ and that both y and $\bar{y}$ are of equal dimension.

Then consider the controller Q described by

$$Q : \begin{cases} \dot{z} &= \alpha(x,z) + \beta(x,z)\bar{u} \\ u &= \gamma(x,z) + \delta(x,z)\bar{u}, \end{cases} \tag{2.33}$$

where $z \in \mathbb{R}^\nu$ and where α, β, γ, δ are real analytic. Having defined the plant P, model M and the controller Q, the nonlinear MMP can now be described as follows.

Definition 2.1 (Model Matching Problem). ([Hui92]) Consider the plant P, model M and a point $(x_0, \bar{x}_0) \in \mathbb{R}^n \times \mathbb{R}^{\bar{n}}$. Find neighborhoods X of x_0 and $\bar{X}$ of $\bar{x}_0$, an integer ν, an open subset V of $\mathbb{R}^\nu$, and a map $F\colon X \times \bar{X} \to V$, such that the compensator Q, defined on $V \times U$, renders the difference

$$y(x, F(x,\bar{x}), t) - \bar{y}(\bar{x}, t) \tag{2.34}$$

independent of $\bar{u}$ for all $t \geq 0$ and all $(x, \bar{x}) \in X \times \bar{X}$. The output $y(x, F(x,\bar{x}), t)$ denotes the trajectory of $y(t)$ initialised at $(x, F(x,\bar{x}))$ and where $\bar{y}(\bar{x}, t)$ is the trajectory of $\bar{y}(t)$ initialised at $\bar{x}$. ◊

In view of (2.34), define the extended system E of the form

$$E : \begin{cases} \begin{bmatrix} \dot{x} \\ \dot{\bar{x}} \end{bmatrix} = \begin{bmatrix} f(x) \\ \bar{f}(\bar{x}) \end{bmatrix} + \begin{bmatrix} g_j(x) \\ 0 \end{bmatrix} u_j + \begin{bmatrix} 0 \\ \bar{g}_k(\bar{x}) \end{bmatrix} \bar{u}_k \\ e = h(x) - \bar{h}(\bar{x}). \end{cases} \tag{2.35}$$

The extended output e will be referred to as the *tracking error* and is to be asymptotically regulated to zero. Now, if the model inputs $\bar{u}$ are now seen as *measurable disturbances* then solvability of the MMP is readily formulated.

Theorem 2.3. ([Hui92]) *The MMP is solvable for (M, P) if and only if the nonregular dynamic disturbance decoupling problem with measurable disturbances is solvable for E.*

The proof of this theorem is omitted here, but its implications will become clear through the upcoming developments. In short, the nonregular Dynamic Disturbance Decoupling Problem (DDDP) with disturbance measurement has the property that the compensator Q with input $\bar{u}$ and output u need not be invertible, whereas the regular DDDP with disturbance measurement implies invertibility of the compensator [Hui92].

Let $M > 0$ and observe that output matching would imply $\|h(x(t)) - \bar{h}(\bar{x}(t))\| < M$ for all $t > N$ and for some $N > 0$. As a result, the MMP can be addressed by applying a constrained dynamics algorithm to $h(x) - \bar{h}(\bar{x}) = 0$ that, in loose sense, yields a maximal (locally) controlled invariant submanifold on which the output matching is fulfilled.

Even though the solvability of the MMP is expressed in terms of a nonregular DDDP with disturbance measurement, the following lemma summarises a relative degree condition that characterises a class of systems that can be encountered in the MMP.

Lemma 2.4. [Hui94] *Consider a square plant P and a square model M. Let $x_0 \in X$ and $\bar{x}_0 \in \bar{X}$ be given. If the decouplings matrix $A(x)$ of P has full rank for $x = x_0$, then the MMP is solvable around $(x_0, \bar{x}_0)$ if and only if $r_i \leq \bar{r}_i$ $(i = 1, \ldots, m)$.*

The relevance of this lemma can be explained by the following. In [Hui92], the nonregular DDDP with disturbance measurement is addressed through an algorithm that is capable of handling cases where an intrinsic disturbance dependence exists. In terms of the MMP, this intrinsic $\bar{u}$–dependence can be described by the appearance of model inputs "before" the plant inputs in the time derivative

$$\frac{d^r}{dt^r}[h(x) - \bar{h}(\bar{x})] = 0 \tag{2.36}$$

for some $r > 0$. Such an intrinsic $\bar{u}$–dependence is generally remedied by the expense of certain controls, meaning that some controls are set to zero in order for this intrinsic $\bar{u}$–dependence to be removed. However, this chapter addresses MMPs that have a physical model based character of which the prescribed models will be structurally "close" to the plant. As a result, the relative degree condition $r_i \leq \bar{r}_i$, where r_i and $\bar{r}_i$ are the relative degrees of the plant and model respectively, is readily satisfied. Furthermore, and this is important, the thesis does not explicitly assume that both the plant and model are square as per Lemma 2.4. Nonetheless, the relative degree condition $r_i \leq \bar{r}_i$ will be in effect for all physical systems considered in the thesis.

Since bond graph representations are the main theme, the affine plant (2.31) is now specialised to the system

$$\begin{aligned} \dot{x} &= [J(x) - R(x)]K(x) + g_j(x)u_j \\ y_j &= h_j(x), \end{aligned} \tag{2.37}$$

which is *not* port–Hamiltonian due to the output definition $h_j(x)$. The reason for choosing more general outputs, and not the collocated outputs $y_j = g_j^T(x)K(x)$, allows a larger class of systems to be considered. This will become clear later in the thesis.

There are some key aspects of the MMP and its associated nonregular DDDP that are of significant importance. First, the constrained dynamics algorithm found in [Nij90] and [Isi95] can be used to solve the nonregular DDDP [Hui92], where it must be noted that disturbance decoupling does not address stability of possible internal dynamics. Second, if output matching is to be achieved then the controller imposes attractivity of the submanifold on which output matching is fulfilled. These aspects of an MMP design are readily clarified through the following example.

Example 2.2. Consider the linear plant P of the form

$$\begin{bmatrix} \dot{x}_1 \\ \dot{x}_2 \\ \dot{x}_3 \\ \dot{x}_4 \end{bmatrix} = \begin{bmatrix} 0 & 0 & 1 & 0 \\ 0 & 0 & -1 & 1 \\ -1 & 1 & -1 & 0 \\ 0 & -1 & 0 & 0 \end{bmatrix} \begin{bmatrix} (1+\mu_1)x_1 \\ (1+\mu_2)x_2 \\ (1+\mu_3)x_3 \\ (1+\mu_4)x_4 \end{bmatrix} + \begin{bmatrix} -1 \\ 0 \\ 1 \\ 0 \end{bmatrix} u_1 + \begin{bmatrix} 0 \\ -1 \\ 0 \\ 0 \end{bmatrix} u_2 \tag{2.38}$$

$$\begin{bmatrix} y_1 \\ y_2 \end{bmatrix} = \begin{bmatrix} x_3 \\ x_4 \end{bmatrix}.$$

Observe that P is *not* port–Hamiltonian due to the non–collocated output $y = (x_3, x_4)$. The vector $\mu = (\mu_1, \ldots, \mu_4)$ represents small physical parameters with nominal value $\mu = 0$. Next consider the model M described by the Brunovsky canonical form

$$\begin{bmatrix} \dot{\bar{x}}_1^j \\ \dot{\bar{x}}_2^j \\ \dot{\bar{x}}_3^j \\ \dot{\bar{x}}_4^j \end{bmatrix} = \begin{bmatrix} \bar{x}_2^j \\ \bar{x}_3^j \\ \bar{x}_4^j \\ 0 \end{bmatrix} + \begin{bmatrix} 0 \\ 0 \\ 0 \\ 1 \end{bmatrix} \bar{u}_j \tag{2.39}$$

$$\bar{y}_j = \bar{x}_1^j,$$

where $1 \leq j \leq 2$ and $\bar{x} = (\bar{x}_1^1, \ldots, \bar{x}_4^1, \bar{x}_1^2, \ldots, \bar{x}_4^2)$.

The definition of M is seen to address a conventional tracking design, because the input $\bar{u}_j$ can be used to generate "any" desired trajectories for $\bar{y}_j$ [Nij90]. Let r_i and $\bar{r}_i$ denote the relative degrees of y_i and $\bar{y}_i$ respectively, so that a dimensionality argument yields $r_i \leq \bar{r}_i$ for $1 \leq i \leq 2$. The appearance of model inputs can therefore be "intercepted" by plant inputs.

The MMP for the extended system (2.35) can now be constructively addressed by means of the *constrained dynamics* algorithm of [Nij90] and/or the *zero dynamics* algorithm presented in [Isi95]. Towards this end, write the output matching constraint

$$h(x) - \bar{h}(\bar{x}) := S_0(x, \bar{x}) = \begin{bmatrix} x_3 - \bar{x}_1^1 \\ x_4 - \bar{x}_1^2 \end{bmatrix} = 0, \tag{2.40}$$

where $S_0(x, \bar{x})$ has constant rank $s_0 = 2$ for all $(x, \bar{x})$. Define the submanifold

$$Z_0 = \{(x, \bar{x}) \in \mathbb{R}^4 \times \mathbb{R}^8 : S_0(x, \bar{x}) = 0\}, \tag{2.41}$$

so that

$$\frac{d}{dt} S_0(x, \bar{x}) = B_0(x, \bar{x}) + A_0(x, \bar{x}) \begin{bmatrix} u \\ \bar{u} \end{bmatrix} = 0 \tag{2.42}$$

for all $(x, \bar{x}) \in Z_0$. This yields

$$B_0(x, \bar{x}) = \begin{bmatrix} -x_1 + x_2 - \bar{x}_1^1 - \bar{x}_2^1 \\ -x_2 - \bar{x}_2^2 \end{bmatrix}, \quad A_0(x, \bar{x}) = \begin{bmatrix} 1 & 0 & 0 & 0 \\ 0 & 0 & 0 & 0 \end{bmatrix}. \tag{2.43}$$

It is seen that $A_0(x, \bar{x})$ has constant rank $r_0 = 1$ on Z_0, which implies the existence of a $(s_0 - r_0) \times s_0$ matrix $R_0(x, \bar{x})$ satisfying $R_0(x, \bar{x}) A_0(x, \bar{x}) = 0$. From (2.43) write

$$R_0(x, \bar{x}) = \begin{bmatrix} 0 & 1 \end{bmatrix}, \tag{2.44}$$

giving

$$\Phi_0(x, \bar{x}) = R_0(x, \bar{x}) B_0(x, \bar{x}) = -x_2 - \bar{x}_2^2 = 0. \tag{2.45}$$

Now use $\Phi_0(x, \bar{x})$ to extend the constraint (2.40) as

$$S_1(x, \bar{x}) = \begin{bmatrix} S_0(x, \bar{x}) \\ \Phi_0(x, \bar{x}) \end{bmatrix} = \begin{bmatrix} x_3 - \bar{x}_1^1 \\ x_4 - \bar{x}_1^2 \\ x_2 + \bar{x}_2^2 \end{bmatrix}. \tag{2.46}$$

Observe that $S_1(x, \bar{x})$ has constant rank $s_0 + s_1 = 3$ with $s_1 = s_0 - r_0 = 1$. Define the new constraint submanifold

$$Z_1 = \{(x, \bar{x}) \in \mathbb{R}^4 \times \mathbb{R}^8 : S_1(x, \bar{x}) = 0\}. \tag{2.47}$$

This yields

$$\frac{d}{dt}S_1(x,\bar{x}) = B_1(x,\bar{x}) + A_1(x,\bar{x})\begin{bmatrix} u \\ \bar{u} \end{bmatrix} = 0 \tag{2.48}$$

for $(x,\bar{x}) \in Z_1$, and write

$$B_1(x,\bar{x}) = \begin{bmatrix} -x_1 - \bar{x}_1^1 - \bar{x}_2^1 - \bar{x}_2^2 \\ 0 \\ -\bar{x}_1^1 + \bar{x}_1^2 + \bar{x}_3^2 \end{bmatrix}, \quad A_1(x,\bar{x}) = \begin{bmatrix} 1 & 0 & 0 & 0 \\ 0 & 0 & 0 & 0 \\ 0 & -1 & 0 & 0 \end{bmatrix}. \tag{2.49}$$

The constrained dynamics algorithm terminates since rank $A_1(x,\bar{x}) = m = 2$, hence $Z^\star = Z_1$ and the feedback

$$\begin{aligned} u_1 &= x_1 + \bar{x}_1^1 + \bar{x}_2^1 + \bar{x}_2^2 \\ u_2 &= -\bar{x}_1^1 + \bar{x}_1^2 + \bar{x}_3^2 \end{aligned} \tag{2.50}$$

solves the nonregular DDDP with disturbance measurement. Therefore, as per Theorem 2.3, the MMP is solvable and (2.50) renders $Z^\star$ controlled invariant for $(x(0),\bar{x}(0)) \in Z^\star$.

Looking back on the steps taken, it is clear that the decoupling process does not address the behavior for $(x(0),\bar{x}(0)) \notin Z^\star$, so that the attractivity of $Z^\star$ is to be further analysed. Doing so leads to the conclusion that the decoupling control (2.50) does in fact regulate the difference $h(x) - \bar{h}(\bar{x})$ to zero. To see this, define the "error" variables

$$e_2 = x_2 + \bar{x}_2^2, \quad e_3 = x_3 - \bar{x}_1^1, \quad e_4 = x_4 - \bar{x}_1^2, \tag{2.51}$$

and conclude that attractivity of $Z^\star$ is confirmed by writing the dynamics

$$\begin{aligned} \dot{x}_1 &= -x_1 + e_3 - \bar{x}_2^1 - \bar{x}_2^2 \\ \begin{bmatrix} \dot{e}_2 \\ \dot{e}_3 \\ \dot{e}_4 \end{bmatrix} &= \begin{bmatrix} 0 & -1 & 1 \\ 1 & -1 & 0 \\ -1 & 0 & 0 \end{bmatrix}\begin{bmatrix} e_2 \\ e_3 \\ e_4 \end{bmatrix}. \end{aligned} \tag{2.52}$$

On $Z^\star$ there exists the dynamics

$$\dot{x}_1 = -x_1 - \bar{x}_2^1 - \bar{x}_2^2, \tag{2.53}$$

which is seen to be input–to–state stable [Son95] with respect to $\bar{x}_2^1$ and $\bar{x}_2^2$. Let $w = (w_1, w_2)$ be new control inputs, then the feedback (2.50) can now be written as

$$\begin{aligned} \dot{\eta} &= -\eta - \bar{x}_2^1 - \bar{x}_2^2 \\ u_1 &= \eta + \bar{x}_1^1 + \bar{x}_2^1 + \bar{x}_2^2 + w_1 \\ u_2 &= -\bar{x}_1^1 + \bar{x}_1^2 + \bar{x}_3^2 + w_2. \end{aligned} \tag{2.54}$$

Next defining the error variable $e_1 = x_1 - \eta$, so that by applying (2.54) one obtains the closed loop port–Hamiltonian dynamics

$$\begin{bmatrix} \dot{e}_1 \\ \dot{e}_2 \\ \dot{e}_3 \\ \dot{e}_4 \end{bmatrix} = \begin{bmatrix} 0 & 0 & 1 & 0 \\ 0 & 0 & -1 & 1 \\ -1 & 1 & -1 & 0 \\ 0 & -1 & 0 & 0 \end{bmatrix} \begin{bmatrix} e_1 \\ e_2 \\ e_3 \\ e_4 \end{bmatrix} + \begin{bmatrix} -1 \\ 0 \\ 1 \\ 0 \end{bmatrix} w_1 + \begin{bmatrix} 0 \\ -1 \\ 0 \\ 0 \end{bmatrix} w_2 \tag{2.55}$$

$$\begin{bmatrix} \psi_1 \\ \psi_2 \end{bmatrix} = \begin{bmatrix} e_3 - e_1 \\ -e_2 \end{bmatrix}.$$

where $H(e) = (1/2)||e||_2^2$ and where $\psi = (\psi_1, \psi_2)$ are new collocated outputs for feedback purposes. Observe that the closed loop interconnection and damping structures as well as the input vector fields are identical to those of the plant.

Finally, note that the stability of the closed loop is *not* compromised by small parameter perturbations in some ball $||\mu|| < \delta$, since by continuity it follows that the nominal stabilising controller is stabilising in a neighborhood of the nominal system [Mai03]. However, the convergence property $\lim_{t\to\infty} e(t) = 0$ will generally not hold in such case and the tracking objective will therefore not be attained. ◊

Stability of the zero–dynamics is an important requirement for the MMP considered here. Indeed, it is readily seen that (2.53) is asymptotically stable, but it is certainly not obvious whether systems of the form (2.37) have intrinsic stable internal dynamics that is compatible with the constraint $h_j(x) = 0$. The following proposition shows that internal stability for such systems is not implied.

Proposition 2.5. *Consider the system*

$$\begin{aligned} \dot{x} &= [J(x) - R(x)]K(x) + g_j(x)u_j \\ y_j &= h_j(x), \end{aligned} \tag{2.56}$$

where $\mathbf{D}^T H(x) = K(x)$ *for some smooth, positive definite function* $H(x)$. *Let* $J(x)$ *be anti–symmetric and let* $R(x)$ *be positive (semi)–definite, then the dynamics compatible with* $h_j(x) = 0$ *need not be stable.*

Proof. First consider the collocated output $y_j = g_j^T(x)K(x)$ such that

$$\frac{d}{dt}H(x) \leq y_j u_j. \tag{2.57}$$

This implies that the dynamics compatible with $y_j(x) = 0$ is stable since $\dot{H}(x) \leq 0$. On the other hand, in case the output functions $h_j(x)$ are not collocated, it follows that

$$\frac{d}{dt}H(x) \leq K(x)^T g_j(x) u_j. \tag{2.58}$$

Hence, stability of the dynamics compatible with $h_j(x) = 0$ cannot be inferred. Indeed, consider the linear system

$$\begin{bmatrix} \dot{x}_1 \\ \dot{x}_2 \end{bmatrix} = \begin{bmatrix} 0 & -I_m \\ I_m & 0 \end{bmatrix} \begin{bmatrix} Q_1 x_1 \\ Q_2 x_2 \end{bmatrix} + \begin{bmatrix} -I_m \\ I_m \end{bmatrix} u \tag{2.59}$$

$$y = x_2,$$

where $x_1, x_2 \in \mathbb{R}^m$, and where Q_1 and Q_2 are symmetric positive definite. The system is of the form (2.56) but does not have collocated outputs. It is readily checked that the control $u = -Q_1 x_1$ renders the submanifold $x_2 = 0$ controlled invariant. The internal dynamics is given by $\dot{x}_1 = Q_1 x_1$ and the Hamiltonian $H^\star(x) = (1/2) x_1^T Q_1 x_1$ satisfies

$$\frac{d}{dt}H^\star(x) = x_1^T Q_1 Q_1 x_1 > 0 \tag{2.60}$$

for all nonzero x_1. Instability is thus immediate. □

The above proposition on unstable zero–dynamics with non–collocated outputs is not unimportant: Collocated outputs of port–Hamiltonian systems are often not the quantities to be controlled, so that output redefinition is justifiable from a control point of view. For example, in the mechanical domain it is often the case that positions are to be controlled, whereas *velocities* are the collocated outputs in the port–Hamiltonian framework. It is therefore logical to define positions as the outputs for control purposes. In bond graph modelling, for example, such non–collocated outputs are typically associated with **SS** elements of which the input variables are identically zero.

Model Inversion

Instead of going through the constrained dynamics algorithm to find the feedback (2.54), consider the *nominal* plant inverse of (2.38) given as

$$\begin{aligned} \dot{\eta} &= y_1 - u_1 \\ u_1 &= \eta + y_1 + \dot{y}_1 + \dot{y}_2 + v_1 \\ u_2 &= -y_1 + y_2 + \ddot{y}_2 + v_2. \end{aligned} \tag{2.61}$$

Next observe that the feedback (2.54) can be obtained by enforcing the relations $y_1 = \bar{x}_1^1$ and $y_2 = \bar{x}_1^2$. Therefore, in terms of bond graphs, if the (bi)causal plant inverse exists and the relative degree condition $r_i \leq \bar{r}_i$ is fulfilled, then the disturbance decoupling feedback can be found by enforcing the relation $h(x) = \bar{h}(\bar{x})$. However, such (bi)causal inversion mechanism will *not* compute $Z^\star$, so that the constrained dynamics algorithm remains an important tool in the search for this constrained manifold.

2.3.2. Remarks on Output Regulation and Center Manifold Theory

The MMP is closely linked with the *output regulation* problem as presented in [Isi90], where regulation is achieved when trajectories converge to a *center manifold* containing the origin. More precisely, consider the system

$$\begin{aligned} \dot{x} &= f(x, \bar{x}, u) \\ \dot{\bar{x}} &= s(\bar{x}) \\ e &= h(x, \bar{x}), \end{aligned} \tag{2.62}$$

where $x \in X$, $\bar{x} \in \bar{X}$, $u \in \mathbb{R}^m$ and $f(0,0,0) = 0$, $s(0) = 0$ and $h(0,0) = 0$. The model $\dot{\bar{x}} = s(\bar{x})$ is assumed to be neutrally stable in the sense that the Jacobian $\mathbf{D}s(0)$ merely has eigenvalues on the imaginary axis. In [Isi95], the "Full Information Output Regulation Problem" is formulated as follows.

Definition 2.2 (Full Information Output Regulation). ([Isi95]) Given the nonlinear system (2.62), find, if possible, a mapping $\alpha(x, \bar{x})$ such that

1. the equilibrium $x = 0$ of

$$\dot{x} = f(x, 0, \alpha(x, 0)) \tag{2.63}$$

   is asymptotically stable in the first approximation.

2. there exists a neighborhood $V \subset X \times \bar{X}$ of $(0,0)$ such that for each initial condition $(x(0), \bar{x}(0)) \in V$ the solution of (2.62) with $u = \alpha(x, \bar{x})$ satisfies

$$\lim_{t \to \infty} h(x(t), \bar{x}(t)) = 0. \tag{2.64}$$

◊

Define $A = \mathbf{D}_x f(0,0,0)$ and $B = \mathbf{D}_u f(0,0,0)$, then the solvability requirement of the above regulation problem is given by the following theorem.

Theorem 2.6. ([Isi95]) *The Full Information Output Regulation Problem is solvable if and only if the pair* (A, B) *is stabilisable and there exists mappings* $x = \varphi(\bar{x})$ *and* $u = c(\bar{x})$, *with* $\varphi(0) = 0$ *and* $c(0) = 0$, *both defined in a neighborhood* $\bar{X}$ *of the origin, satisfying the conditions*

$$\begin{aligned} \frac{d}{dt}\varphi(\bar{x}) &= f(\varphi(\bar{x}), \bar{x}, c(\bar{x})) \\ 0 &= h(\varphi(\bar{x}), \bar{x}) \end{aligned} \tag{2.65}$$

for all $\bar{x} \in \bar{X}$.

The feedback that solves the regulation problem is then given as

$$u = \alpha(x, \bar{x}) = c(\bar{x}) + K[x - \varphi(\bar{x})], \tag{2.66}$$

where K is a suitable gain. Indeed, the gain K renders the origin of (2.63) asymptotically stable in the first approximation, thereby guaranteeing the existence of a center manifold since $\mathbf{D}s(0)$ merely has eigenvalues on the imaginary axis. Thus, on the center manifold, $x = \varphi(\bar{x})$ and the relation (2.65) is satisfied since $u = \alpha(\varphi(\bar{x}), \bar{x}) = c(\bar{x})$.

Now, to demonstrate the similarities between MMP objectives and the condition (2.65), consider Example 2.2 and observe that from (2.54) and (2.55) one can define

$$x = \varphi(\eta, \bar{x}) = \begin{bmatrix} \varphi_1(\eta, \bar{x}) \\ \varphi_2(\eta, \bar{x}) \\ \varphi_3(\eta, \bar{x}) \\ \varphi_4(\eta, \bar{x}) \end{bmatrix} = \begin{bmatrix} \eta \\ -\bar{x}_2^2 \\ \bar{x}_1^1 \\ \bar{x}_1^2 \end{bmatrix} \tag{2.67}$$

and

$$u = c(\eta, \bar{x}) = \begin{bmatrix} c_1(\eta, \bar{x}) \\ c_2(\eta, \bar{x}) \end{bmatrix} = \begin{bmatrix} \eta + \bar{x}_1^1 + \bar{x}_2^1 + \bar{x}_2^2 \\ -\bar{x}_1^1 + \bar{x}_1^2 + \bar{x}_3^2 \end{bmatrix}. \tag{2.68}$$

Then, evidently, the *nominal* system (2.38) satisfies

$$\frac{d}{dt}\varphi(\eta, \bar{x}) = \begin{bmatrix} 0 & 0 & 1 & 0 \\ 0 & 0 & -1 & 1 \\ -1 & 1 & -1 & 0 \\ 0 & -1 & 0 & 0 \end{bmatrix} \begin{bmatrix} \varphi_1(\eta, \bar{x}) \\ \varphi_2(\eta, \bar{x}) \\ \varphi_3(\eta, \bar{x}) \\ \varphi_4(\eta, \bar{x}) \end{bmatrix} + \begin{bmatrix} -1 \\ 0 \\ 1 \\ 0 \end{bmatrix} c_1(\eta, \bar{x}) + \begin{bmatrix} 0 \\ -1 \\ 0 \\ 0 \end{bmatrix} c_2(\eta, \bar{x}). \tag{2.69}$$

From (2.67), define the "error" $e = x - \varphi(\eta, \bar{x})$ and observe that (2.55) can be stabilised with the feedback $w_1 = -d_1(e_3 - e_1)$ and $w_2 = d_2 e_2$, with $d_1 > 0$ and $d_2 > 0$, giving the control

$$u = c(\eta, \bar{x}) + \begin{bmatrix} d_1 & 0 & -d_1 & 0 \\ 0 & d_2 & 0 & 0 \end{bmatrix} [x - \varphi(\eta, \bar{x})]. \tag{2.70}$$

In conclusion, the MMP has been shown to be closely related to the Full Information Output Regulation Problem found in [Isi95], and this fact is used to characterise the bond graph based MMP designs.

2.4. Stabilisation Control through Energy Shaping

The concept of *passivity* can be safely argued to be a pillar of systems theory and control [Wil72], [Des75], [Byr91], where the notion of rendering the system passive through feedback has shown to be effective [Ort89], [Ort98], [Str98]. The idea that control can be associated with energy storage and dissipation phenomena possibly explains the appeal of the passivity framework to the subject of physical systems modelling.

This section recalls some basic aspects of control through *feedback passivation* that will subsequently be explored in the second part of the thesis. Feedback passivation requires the knowledge of some suitable closed loop storage function, where this thesis shows that the bond graph junction structure can be used to select such storage function in certain cases. In addition, port–Hamiltonian systems in control have received significant attention [Ort00c], [Bla02], [Ort02b], and this type of feedback is generally referred to as Interconnection and Damping Assignment Passivity Based Control (IDA–PBC). Fundamental facts on IDA–PBC are recalled, showing that this feedback methodology is based on structural considerations of closed loop port–Hamiltonian dynamics.

2.5. Feedback Passivation

Consider the affine control system

$$\begin{aligned} \dot{x} &= f(x) + g(x)u \\ y &= h(x), \end{aligned} \tag{2.71}$$

where $x \in X$ and $u, y \in \mathbb{R}^m$, and where $f(0) = 0$ and $h(0) = 0$.

Definition 2.3 ([Sch00b]). The system (2.71) is said to be *passive* if there exists a function $V : X \to \mathbb{R}$, referred to as the *storage function*, such that

$$V(x(t)) - V(x(0)) \leq \int_0^t y^T(s)u(s)\,ds \tag{2.72}$$

for all $x(0) \in X$, all $u(t)$ with $t \geq 0$.

There are two properties of passive systems that are of interest. Let (2.71) be passive with a smooth positive definite storage function $V(x)$, then

1. for $u = 0$ the point $x = 0$ is stable by $\dot{V}(x) = \mathbf{D}V(x)f(x) \leq 0$,
2. for $y(x) = 0$ the point $x = 0$ is stable by $\dot{V}(x) = \mathbf{D}V(x)[f(x) + g(x)u^\star] \leq 0$ for $u^\star(x)$ compatible with $y(x) = 0$.

Therefore, passivity with respect to a positive definite storage function implies zero–input and zero–dynamics stability of the system (2.71).

Since stability of the zero–input system is somewhat restrictive, it can be of interest to establish what the conditions are to render an unstable system (2.71) passive by means of feedback, hence feedback passivation. Towards that end, consider the smooth feedback $u = \alpha(x) + \beta(x)v$, with $\beta(x)$ invertible and $\alpha(0) = 0$, yielding the closed loop

$$\begin{aligned} \dot{x} &= f(x) + g(x)\alpha(x) + g(x)\beta(x)v \\ y &= h(x). \end{aligned} \tag{2.73}$$

Suppose the above closed loop system is passive with smooth positive definite $V(x)$, then from the above two properties it follows that the zero–dynamics are stable, where

$$\dot{x} = f(x) + g(x)u^\star(x) = f(x) + g(x)\alpha(x) + g(x)\beta(x)v^\star(x) \tag{2.74}$$

for $v^\star(x) = \beta^{-1}(x)[u^\star(x) - \alpha(x)]$ compatible with $y(x) = 0$ [Sch00b]. Hence, if the system (2.71) is to be rendered passive by means of feedback passivation then the zero–dynamics must be stable since it is invariant under feedback.

In case the system has been rendered passive with respect to the positive definite storage function $V(x)$, it is readily seen that with $v = -ry$, for some $r > 0$, the asymptotic stability can be achieved provided the system is zero–state detectible [Sep97].

2.6. Interconnection and Damping Assignment

The notion that an open loop port–Hamiltonian systems can be turned into a closed loop port–Hamiltonian system has been studied in various papers [Ort02b], [Ort02a], [Ort00c]. Because closed loop bond graph representations are a main theme of the thesis seems to indicate possible bond graph interpretations in IDA–PBC.

By following the exposition of [Ort02b], consider a port–Hamiltonian system of the form

$$\begin{aligned} \dot{x} &= [J(x) - R(x)]K(x) - g(x)u \\ y &= g^T(x)K(x), \end{aligned} \tag{2.75}$$

where $x \in X$ and $u, y \in \mathbb{R}^m$, and $K^T(x) = \mathrm{D}H(x)$ for some smooth Hamiltonian $H\colon X \to \mathbb{R}$. Define the *shaped* Hamiltonian

$$H_s(x) = H(x) + H_a(x), \tag{2.76}$$

where $H_a(x)$ is the *assigned* or *additive* Hamiltonian. Then define the shaped interconnection and damping matrices

$$J_s(x) = J(x) + J_a(x), \qquad R_s(x) = R(x) + R_a(x), \tag{2.77}$$

where $J_a(x) = -J_a^T(x)$ and $R_a(x) = R_a^T(x) \geq 0$ are the assigned interconnection and damping matrices. Now, let $u = \alpha(x) + w$ be a smooth feedback such that

$$[J_a(x) - R_a(x)]K(x) + [J_s(x) - R_s(x)]K_a(x) = -g(x)\alpha(x). \tag{2.78}$$

It is readily verified that the closed loop has the port–Hamiltonian form

$$\begin{aligned} \dot{x} &= [J_s(x) - R_s(x)]K_s(x) - g(x)w \\ y_s &= g^T(x)K_s(x), \end{aligned} \tag{2.79}$$

showing that the feedback $\alpha(x)$ yields a port–Hamiltonian closed loop with modified interconnection and damping structures. In order for such IDA–PBC design to be possible it must hold that

$$g^{\perp}(x)[J_a(x) - R_a(x)]K(x) + g^{\perp}(x)[J_s(x) - R_s(x)]K_a(x) = 0, \tag{2.80}$$

where $g^{\perp}(x)$ is a full rank left annihilator of $g(x)$. The relation (2.80) represents a set of first order Partial Differential Equations (PDE's) that are to be satisfied simultaneously by the function $K_a(x)$. Clearly, when (2.80) can be solved for some function $H_a(x)$ then the control is given as

$$-[g^T(x)g(x)]^{-1}g^T(x)\Big[[J_a(x) - R_a(x)]K(x) + [J_s(x) - R_s(x)]K_a(x)\Big] = u. \tag{2.81}$$

The effectiveness of IDA–PBC can be described by the fact that the closed loop energy function $H_s(x)$ need not be "guessed" but follows from (2.80). That is to say that the IDA–PBC method characterises all possible energy function $H_a(x)$ that can be assigned.

Let x_e be an admissible equilibrium of (2.75), then for this equilibrium to be assigned it must hold that

$$K_a(x_e) = -K(x_e), \tag{2.82}$$

ensuring $K_s(x_e) = 0$. In addition, one must have

$$\mathbf{D}^2 H_s(x_e) > 0, \tag{2.83}$$

so that x_e is a strict (local) minimum of the energy function $H_s(x)$. In this way it is possible to assign a non–zero equilibrium or "forced" equilibrium to the system (2.75).

Even though IDA–PBC would appear to be conceptually straightforward, this design method can be said to be difficult. For example, there are no clear guidelines in regard to the choice of interconnection matrices $J_a(x)$ and $R_a(x)$ to judge the attainability of the stabilisation objective. Furthermore, as the authors of [Ort02b] point out, no explicit conditions can be offered for the solvability of (2.80) for choices of $J_a(x)$ and $R_a(x)$. In the second part of the thesis, an instructive example of bond graph representations of IDA–PBC designs is presented, where the bond graph topology is used to represent the choices of desired interconnection and damping structures.

2.7. Concluding Remarks

Three control methods have been presented that are largely based on structural considerations to allow for closed loop bond graph considerations. However, this chapter is by no means exhaustive and other control strategies may well exist that allow for structural closed loop design goals. Furthermore, the presented theory is fully contained in the existing literature and the interested reader is referred to the various citations and references therein for further details.

It is interesting to note that backstepping, model matching and energy shaping have major differences on the analytical level, yet all three control methods allow for structural design goals, such as port–Hamiltonian dynamics for example. This has not been addressed in the bond graph literature, so that the identification of a particular set of control methods for closed loop bond graphs is an appreciable contribution to the current literature.

Part II.

Bond Graphs for Closed Loop Dynamics

3. Backstepping Control

3.1. Introduction

The concept of *virtual control* can be found in authoritative literature on backstepping control design [Kri95], [Isi99], where the fundamentals of backstepping have been recalled in Section 2.2. The main contribution of this chapter is the detailed presentation of bond graph based backstepping in relation to port–Hamiltonian dynamics. Some results on bond graphs in backstepping control have appeared in [Yeh99] and in the works of [Gaw01], [Gaw04] on virtual actuators. However, these papers do not address the port–Hamiltonian framework and do not address certain nonlinear cases. In addition, multi–input systems have not received considerable attention in the bond graph literature. As a result, it can be safely argued that a sufficient number of open questions remain on bond graph based backstepping to justify the various results in this chapter.

3.2. Backstepping Control in the Physical Domain

This section explores the application of bond graphs for physical model based backstepping control. Bond graph tools in backstepping as introduced by [Yeh99] will be addressed through detailed examples and subjected to port–Hamiltonian considerations. Furthermore, the novel (bi)causal approach to backstepping in [Gaw01] will be presented in more detail and offers a "shortcut" method to a backstepping design in certain cases. See [Yeh01] and [Yeh02] for further developments on backstepping control in the physical domain.

The explicit association of port–Hamiltonian dynamics with the closed loop through a backstepping design is an important contribution of the chapter. Backstepping theory of Section 2.2 is self–contained and forms the basis for the all developments, showing the clear parallels between existing theory and the closed loop bond graph considerations.

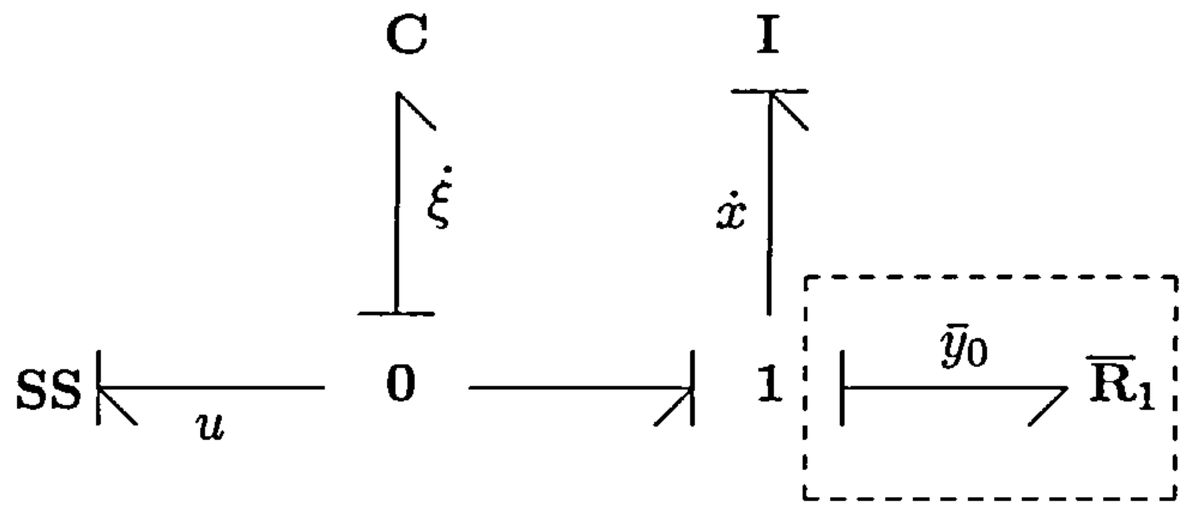

Figure 3.1.: Virtual resistive $\overline{\mathbf{R}}_1$ element of Example 3.1.

3.2.1. Single–Input Systems: Examples

To build a foundation for further generalisations and formalisations, three instructive examples are used to introduce fundamental bond graph arguments in the context of physical model based backstepping. The first example shows a simplest backstepping design conceivable, laying out key ideas of virtual actuators and stabilising functions in a bond graph context. The second example can be found in [Gaw01], which addresses a set–point control problem that is can be addressed with bicausal bond graphs; the actual bicausal bond graph approach will not be addressed until later sections. Now, because the first two examples are one–step designs, the third example addresses a multiple–step design taken from [Yeh99], which will be presented in considerable detail here.

Example 3.1. Consider the bond graph of a mass–spring system in Figure 3.1 with the element definitions

$$\mathbf{I}(x) = \frac{1}{m}(\sqrt{x^2+1}-1), \qquad \mathbf{C}(\xi) = \frac{1}{2}k\xi^2. \tag{3.1}$$

Then consider the smooth function $\bar{y}_0(x)$ as the output of the virtual actuator defined as a resistive $\overline{\mathbf{R}}_1$ element.

The control objective is to impose the effect of $\bar{y}_0(x)$ on the 1–junction through a backstepping control design. By ignoring the dashed region in Figure 3.1, causal analysis of the bond graph yields the system

$$\begin{aligned} \dot{x} &= k\xi \\ \dot{\xi} &= -\frac{x}{m\sqrt{x^2+1}} - u. \end{aligned} \tag{3.2}$$

Next introduce the change of variable

$$k\xi = -\bar{y}_0(x) + kz, \tag{3.3}$$

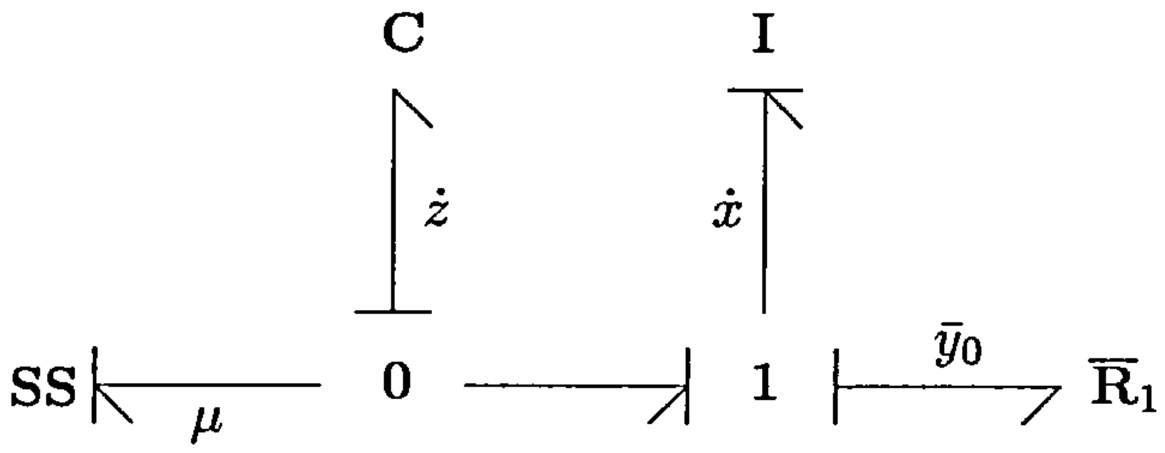

Figure 3.2.: Dynamics (3.7) of Example 3.1.

yielding the x–dynamics

$$\dot{x} = f(x,\xi) = f(x, -\frac{1}{k}\bar{y}_0(x) + z) = -\bar{y}_0(x) + kz. \tag{3.4}$$

Hence the desired effect of the virtual $\overline{\mathbf{R}}_1$ element is now imposed. Then choose the smooth and proper Lyapunov function

$$V(x) = \frac{1}{m}(\sqrt{x^2+1} - 1), \tag{3.5}$$

such that

$$\frac{d}{dt}V(x) = -\frac{x\bar{y}_0(x)}{m\sqrt{x^2+1}} + \frac{x}{m\sqrt{x^2+1}}kz. \tag{3.6}$$

Since $\overline{\mathbf{R}}_1$ is assumed to be globally resistive implies that $x\bar{y}_0(x) > 0$ for all $x \neq 0$, rendering the x–dynamics globally asymptotically stable for $z = 0$. To stabilise the z–dynamics, choose the control $u = (1/k)\dot{\bar{y}}_0(x) + \mu$ such that (3.2) takes the form

$$\begin{aligned} \dot{x} &= -\bar{y}_0(x) + kz \\ \dot{z} &= -\frac{x}{m\sqrt{x^2+1}} - \mu. \end{aligned} \tag{3.7}$$

Now, the following conveys a key aspect of the ideas of this chapter: Observe that (3.7) has the bond graph representation depicted in Figure 3.2, which is seen to be identical to the plant bond graph with the virtual resistive element, where u and ξ are to be interchanged with μ and z respectively.

Further stabilisation of (3.7) is readily achieved by replacing the **SS** element with a linear resistive $\overline{\mathbf{R}}_2$ element, where one can choose the control $\mu = (k/\bar{r})z$ for some positive damping constant r, for example. Doing so yields the closed loop bond graph in Figure 3.3 of which the elements are defined as

$$\mathrm{I}(x) = \frac{1}{m}(\sqrt{x^2+1} - 1), \quad \mathrm{C}(z) = \frac{1}{2}kz^2. \tag{3.8}$$

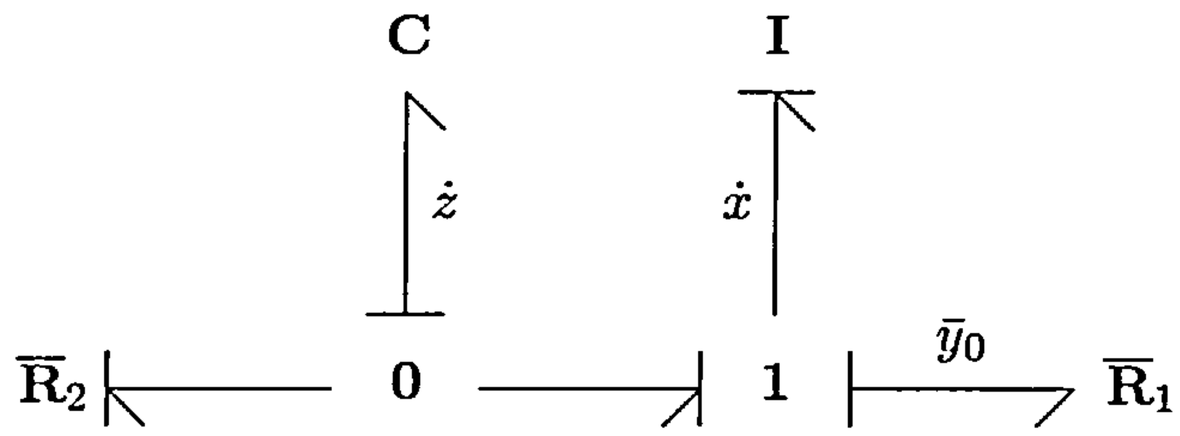

Figure 3.3.: Closed loop bond graph of Example 3.1.

Finally, take $W(x,z) = V(x) + (1/2)kz^2$ and conclude that

$$|x| + |z| > 0 \quad \Longrightarrow \quad \frac{d}{dt}W(x,z) = -\frac{x\bar{y}_0(x)}{m\sqrt{x^2+1}} - \frac{k^2}{\bar{r}}z < 0, \tag{3.9}$$

which shows that the origin $(x,z) = (0,0)$ is globally asymptotically stable because $W(x,z)$ is positive definite and proper. ◊

Some important observations on behalf of Example 3.1 can now be made. First, the bond graph in Figure 3.1 has the required interlaced structure as mentioned in [Yeh99], which is a consequence of the fact that systems need to be in a lower–triangular form if backstepping is to be possible. Second, the **C** element is *linear*, which is one of the requirements expressed in [Yeh99] for the backstepping design. Third, the change of variable (3.3) is not written in the conventional form as defined in Lemma 2.1, but it can be derived naturally from the bond graph in Figure 3.1 by considering that $\bar{y}_0$ cannot be placed at the 1–junction by means of the control variable u. So, it is intuitively plausible that $k\xi$ should "carry" the term $-\bar{y}_0 + kz$ and where kz is to replicate $k\xi$, which is the virtual control. Finally, observe that the closed loop is structurally identical to the plant with the added resistive $\overline{\mathbf{R}}_1$ and $\overline{\mathbf{R}}_2$ components. This emphasises the idea that the controller should induce physical, closed loop dynamics by emulating plant interaction with another physical system [Sha91].

Remark 3.1. From now on, all bond graph elements that are part of the backstepping design are *overlined* as demonstrated in Figure 3.3. This should separate and clarify those parts of the bond graph that belong to the open loop plant.

The main point so far is that backstepping in the physical domain can be facilitated by viewing the stabilising control as the output of another physical system connected at some desired location, where it should be noted that single bond graph components are the simplest virtual actuators that can be defined. However, there is no reason to restrict the virtual actuator solely to single bond graph components, so that the stabilising function may depend on controller states and controller inputs.

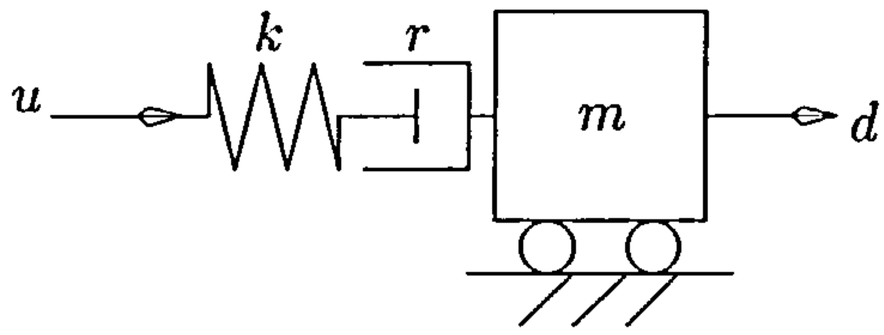

Figure 3.4.: Simple mass–spring–damper system of Example 3.2.

In [Gaw01], the authors address a set–point control problem by specifying a virtual actuator with a single control input. As a result, the backstepping design is shown to yield a dynamic compensator through relatively simple modelling arguments.

Example 3.2. ([Gaw01]) Consider the physical system depicted in Figure 3.4 and its bond graph representation in Figure 3.5. The element definitions are given by

$$\mathbf{C}(\xi) = \frac{1}{2}k\xi^2, \quad \mathbf{I}(x) = \frac{1}{2m}x^2, \quad \mathbf{R} = r. \tag{3.10}$$

The control objective is to find the velocity u such that the closed loop dynamics behaves like the system depicted in Figure 3.6, where μ is a velocity input to the virtual actuator and where d is a *constant* disturbance force acting on the mass m; the velocity of mass m is the system output w conjugate to d. The dashed region in Figure 3.6 represents the virtual actuator of which the bond graph is depicted in Figure 3.7, where the virtual bond graph elements have the definitions

$$\overline{\mathbf{C}}_1(\bar{x}_1) = \frac{1}{2}\bar{k}_1\bar{x}_1^2(1 + \frac{1}{2}\bar{x}_1^2), \quad \overline{\mathbf{C}}_2(\bar{x}_2) = \frac{1}{2}\bar{k}_2\bar{x}_2^2, \quad \overline{\mathbf{R}} = \bar{r}. \tag{3.11}$$

It should be noted that the $\overline{\mathbf{C}}_1$ storage element has the characteristic of a hardening spring instead of the linear characteristic deployed in [Gaw01]; using such a hardening spring allows the restoring force to increase rapidly for larger excursions. Since the junction structure topology is independent of the bond graph element definitions [Kar00], this shows that the bond graph based virtual actuator offers some design flexibility through the use of different storage and dissipation functions.

Without any further analysis, it is plausible that the closed loop system will meet the set–point control objective, for consider a step velocity μ to the right such that the virtual actuator increases the pulling force until the step velocity is reached. Next observe that the closed loop is intended to have the physical representation of Figure 3.6, where the $\mathbf{R}$ element elongates continuously when the mass travels to the right. It is therefore possible to confirm the set–point objective through the physical closed loop representation.

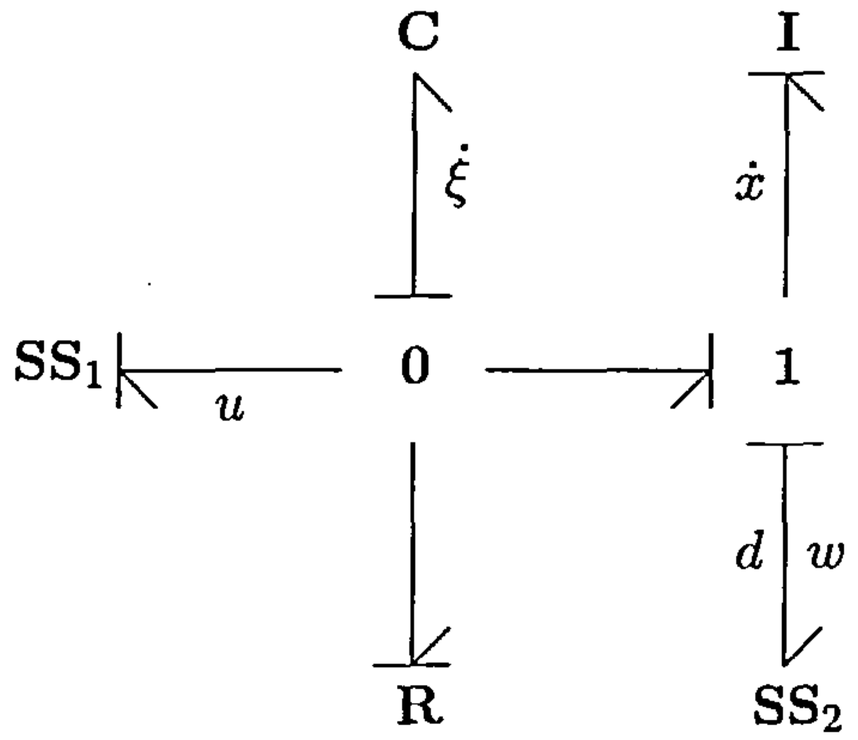

Figure 3.5.: Mass–spring–damper bond graph of Example 3.2.

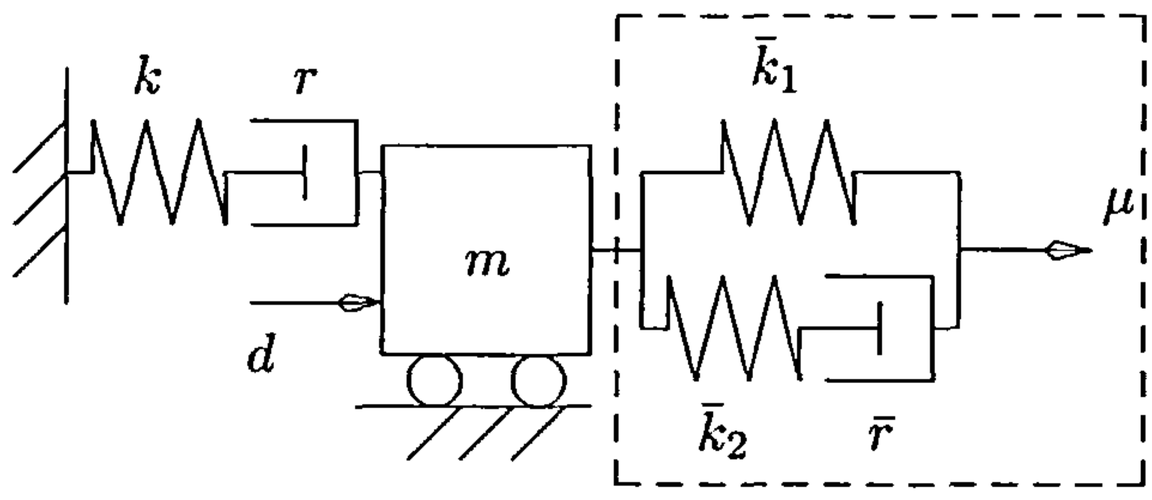

Figure 3.6.: Target closed loop system of Example 3.2.

The backstepping design starts with the simple causal analysis of Figures 3.5 and 3.7, yielding the model

$$\begin{aligned} \dot{x} &= k\xi - d \\ \dot{\xi} &= -\frac{k}{r}\xi - \frac{1}{m}x - u \\ y_0 &= \frac{1}{m}x. \end{aligned} \tag{3.12}$$

The virtual actuator dynamics is given by

$$\begin{aligned} \dot{\bar{x}}_1 &= \bar{u}_0 - \mu \\ \dot{\bar{x}}_2 &= -\frac{\bar{k}_2}{\bar{r}}\bar{x}_2 + \bar{u}_0 - \mu. \\ \bar{y}_0 &= \bar{k}_1(\bar{x}_1 + \bar{x}_1^3) + \bar{k}_2\bar{x}_2, \end{aligned} \tag{3.13}$$

where $\bar{y}_0$ can be seen as the bond graph stabilising function. Notice that the virtual control $v^\star$ as defined in Section 2.2.1 is not a function of the states x. To see this, observe that the bond graphs in Figures 3.5 and 3.7 are interconnected to satisfy the constraint $\bar{u}_0 = y_0$ such that the backstepping method gives the virtual control

$$k\xi = -\bar{y}_0 + kz \quad \Longrightarrow \quad v^\star = -\frac{1}{k}\bar{y}_0(\bar{x}_1, \bar{x}_2). \tag{3.14}$$

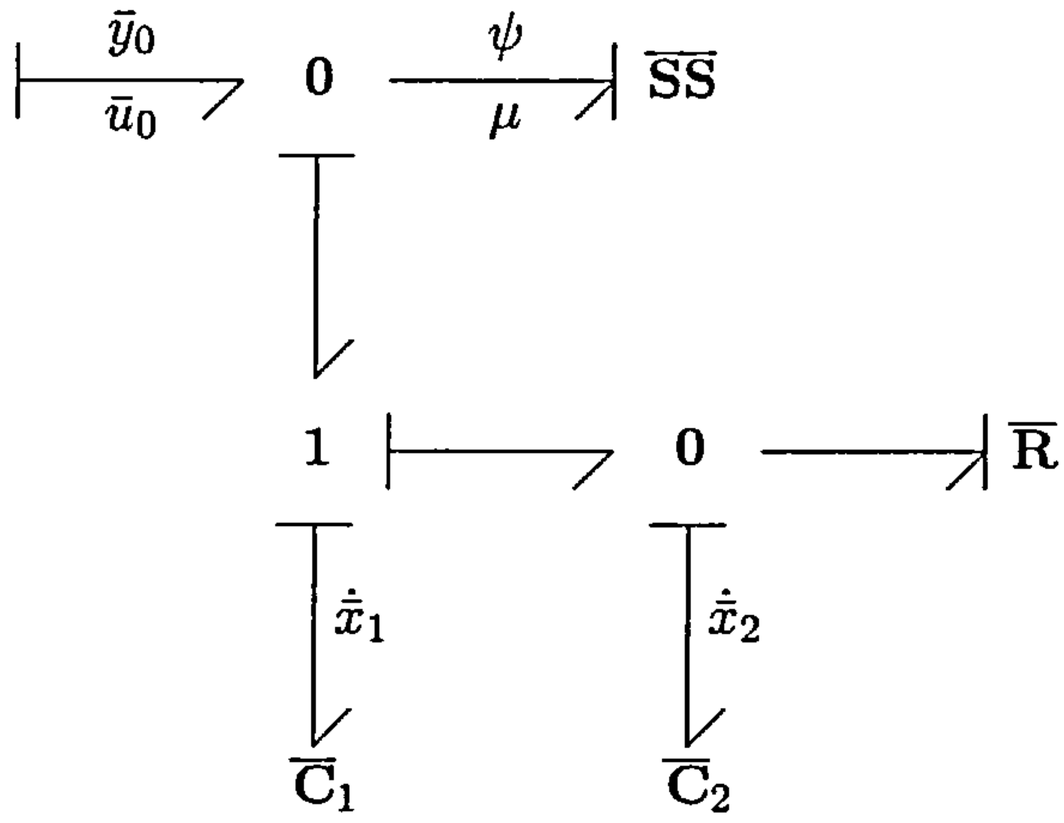

Figure 3.7.: Bond graph virtual actuator of Example 3.2.

The dynamic nature of the virtual actuator can be confusing with respect to the theory of Section 2.2.1, since the virtual control is generally taken to be a static function of the plant states, but where the backstepping design can still be applied unmodified where the appearance of controllers states $\bar{x}_1$ and $\bar{x}_2$ does not alter the backstepping procedure.

Next use (3.14), (3.12) and (3.13) to write

$$\begin{bmatrix} \dot{\bar{x}}_1 \\ \dot{\bar{x}}_2 \\ \dot{x} \\ \dot{z} \end{bmatrix} = \begin{bmatrix} 0 & 0 & 1 & 0 \\ 0 & -1/\bar{r} & 1 & 0 \\ -1 & -1 & 0 & 1 \\ 0 & 0 & -1 & 0 \end{bmatrix} \begin{bmatrix} \bar{k}_1(\bar{x}_1 + \bar{x}_1^3) \\ \bar{k}_2\bar{x}_2 \\ x/m \\ kz \end{bmatrix} + \begin{bmatrix} 0 \\ 0 \\ 0 \\ -k\xi/r + \dot{\bar{y}}_0/k \end{bmatrix} - \begin{bmatrix} 1 & 0 & 0 \\ 1 & 0 & 0 \\ 0 & 0 & 1 \\ 0 & 1 & 0 \end{bmatrix} \begin{bmatrix} \mu \\ u \\ d \end{bmatrix}. \tag{3.15}$$

By considering the damper r in the target system of Figure 3.6, choose the feedback

$$u = -\frac{k}{r}\xi + \frac{1}{k}\dot{\bar{y}}_0 + \frac{k}{r}z, \tag{3.16}$$

which induces the closed loop

$$\begin{bmatrix} \dot{\bar{x}}_1 \\ \dot{\bar{x}}_2 \\ \dot{x} \\ \dot{z} \end{bmatrix} = \begin{bmatrix} 0 & 0 & 1 & 0 \\ 0 & -1/\bar{r} & 1 & 0 \\ -1 & -1 & 0 & 1 \\ 0 & 0 & -1 & -1/r \end{bmatrix} \begin{bmatrix} \bar{k}_1(\bar{x}_1 + \bar{x}_1^3) \\ \bar{k}_2\bar{x}_2 \\ x/m \\ kz \end{bmatrix} - \begin{bmatrix} 1 & 0 \\ 1 & 0 \\ 0 & 1 \\ 0 & 0 \end{bmatrix} \begin{bmatrix} \mu \\ d \end{bmatrix}. \tag{3.17}$$

Clearly, the closed loop dynamics allows for the bond graph representation of Figure 3.8. Take the Lyapunov function

$$W(x, z, \bar{x}) = \frac{1}{2m}x^2 + \frac{1}{2}kz^2 + \frac{1}{2}\bar{k}_1\bar{x}_1^2(1 + \frac{1}{2}\bar{x}_1^2) + \frac{1}{2}\bar{k}_2\bar{x}_2^2 \tag{3.18}$$

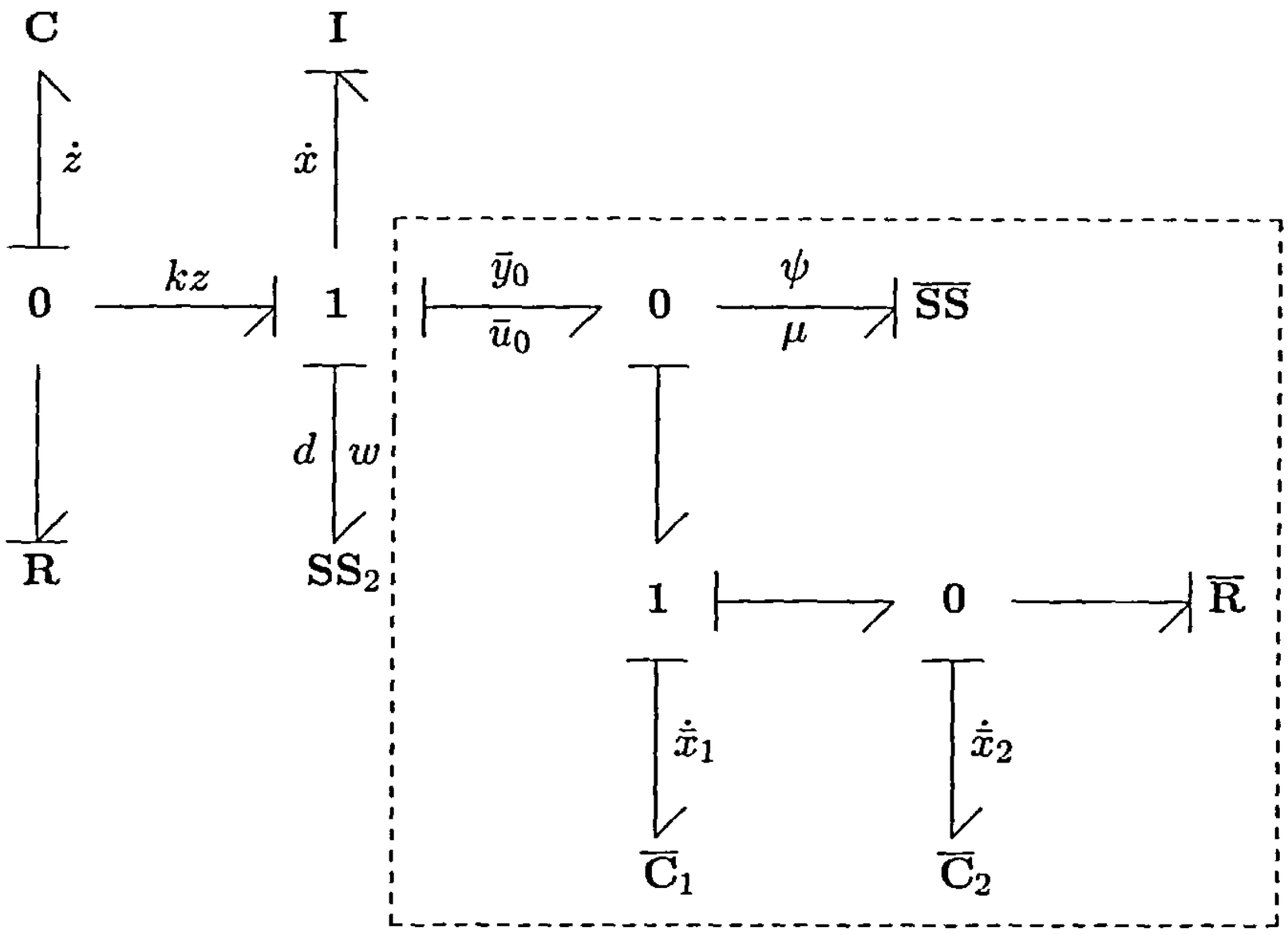

Figure 3.8.: Closed loop mass–spring–damper of Example 3.2.

and write

$$\frac{d}{dt}W(x,z,\bar{x}) = -\frac{\bar{k}_2^2}{\bar{r}}\bar{x}_2^2 - \frac{k^2}{r}z^2 - \psi\mu - wd. \tag{3.19}$$

Thus, the closed loop is *passive* with respect to the supply rates $\psi\mu$ and wd. The feedback is found by reversing the change of coordinates (3.14). ◊

It must be noted that Lyapunov arguments have not been used to obtain the control in the Examples 3.1 and 3.2. Instead, the closed loop Lyapunov function is implicitly contained in the bond graph based backstepping design by retaining the form of the Hamiltonian.

Even though Examples 3.1 and 3.2 are one–step designs, multi–step designs are realised in an analogous manner. The example found in [Yeh99] will now be presented to show a two–step design in detail, where the causal path between the virtual actuator and control readily shows the bond signals that are to be transformed.

Example 3.3. ([Yeh99], adapted) Consider the mass–spring–damper system depicted in Figure 3.9 and its bond graph representation in Figure 3.10, where the element definitions are given as

$$\begin{aligned} \mathrm{I}_1(\xi_2) &= \frac{1}{2m_1}\xi_2^2, \quad \mathrm{I}_2(x_3) = \frac{1}{2m_2}x_3^2, \quad \mathrm{I}_3(x_1) = \frac{1}{2m_3}x_1^2, \\ \mathrm{C}_1(\xi_1) &= \frac{1}{2}k_1\xi_1^2, \quad \mathrm{C}_2(x_2) = \frac{1}{2}k_2x_2^2. \qquad \mathrm{R} = r. \end{aligned} \tag{3.20}$$

It is emphasised that this examples considers the control u and disturbance d to be forces instead of velocities.

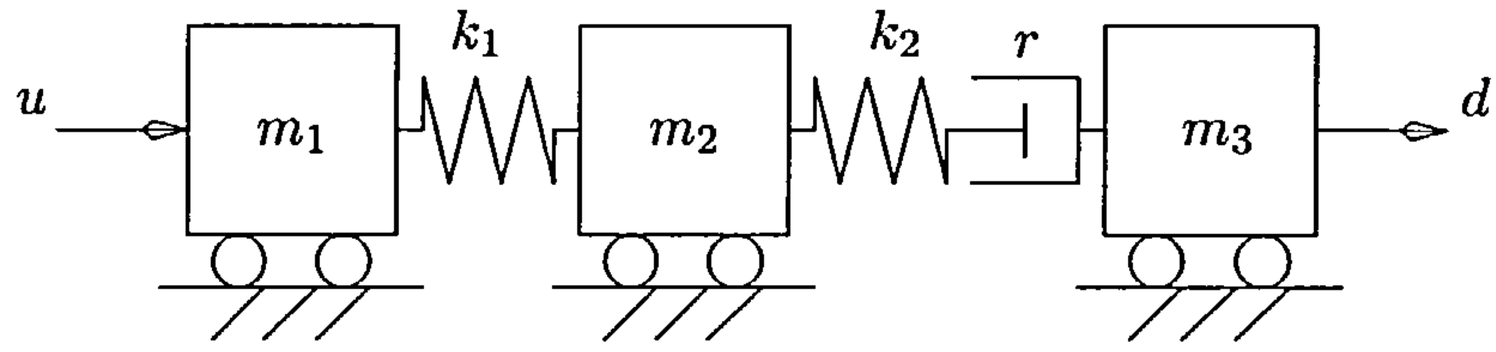

Figure 3.9.: Mass–spring–damper of Example 3.3.

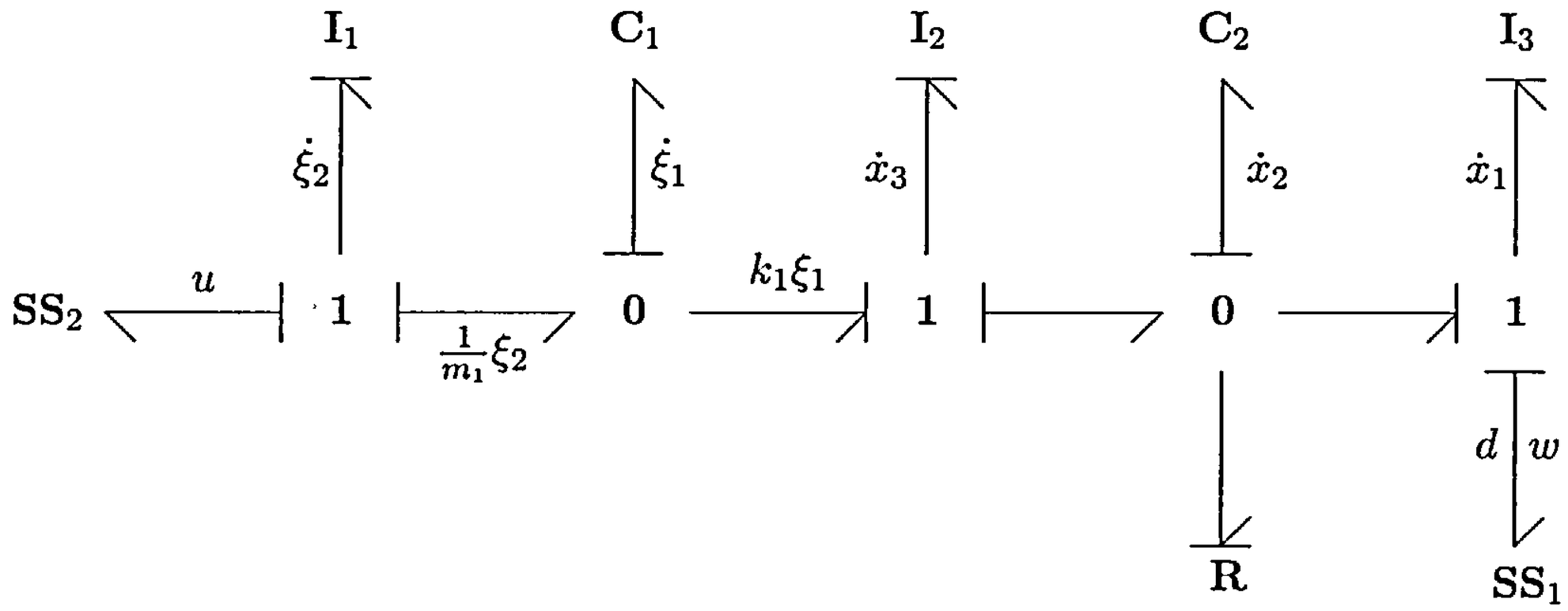

Figure 3.10.: Bond graph system of Example 3.3.

Suppose the system in Figure 3.9 is to attain a particular disturbance attenuation level through feedback on u. Instead of addressing the disturbance attenuation problem in an analytical fashion, the context of the chapter demands that the closed loop dynamics is specified in terms of some "physical equivalent" system [Sha91].

Consider the physical system in Figure 3.11, where the control objective is to find an appropriate (dynamic) feedback u such that the closed loop dynamics from d to w is associated with this system. Clearly, the controller is to induce closed loop dynamics with the bond graph representation of Figure 3.12, where the virtual elements are defined as

$$\overline{\mathrm{C}}_1(\bar{x}_1) = \frac{1}{2}\bar{k}_1\bar{x}_1^2, \quad \overline{\mathrm{C}}_2(\bar{x}_2) = \frac{1}{2}\bar{k}_2\bar{x}_2^2, \quad \overline{\mathrm{R}}_1 = \bar{r}_1, \quad \overline{\mathrm{R}}_2 = \bar{r}_2, \quad \overline{\mathrm{R}}_3 = \bar{r}_3. \tag{3.21}$$

The most characteristic step of the backstepping design considered here is the choice of virtual controls $k_1\xi_1$ and ξ_2/m_1 depicted in Figure 3.10. Thus, without any further analysis, the backstepping design requires two steps to be completed. By inspection of the target bond graph in Figure 3.12 it is readily seen that the efforts of the virtual $\overline{\mathrm{R}}_1$ and $\overline{\mathrm{C}}_1$ elements cannot be imposed by the regular control u, so that a backstepping design seems necessary. Thus, as a first step in the design, the reasoning from the first two examples would suggest that the bond signal $k_1\xi_1$ should "carry" the effort imposed by the virtual actuator composed of the $\overline{\mathrm{R}}_1$ and $\overline{\mathrm{C}}_1$ elements.

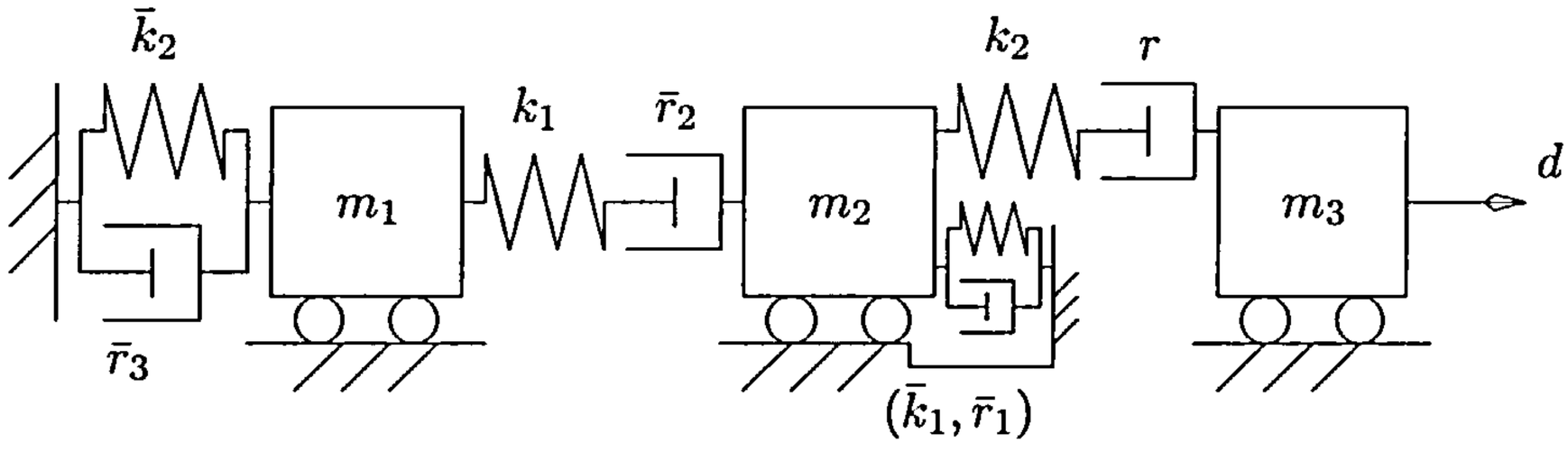

Figure 3.11.: Target closed loop of Example 3.3.

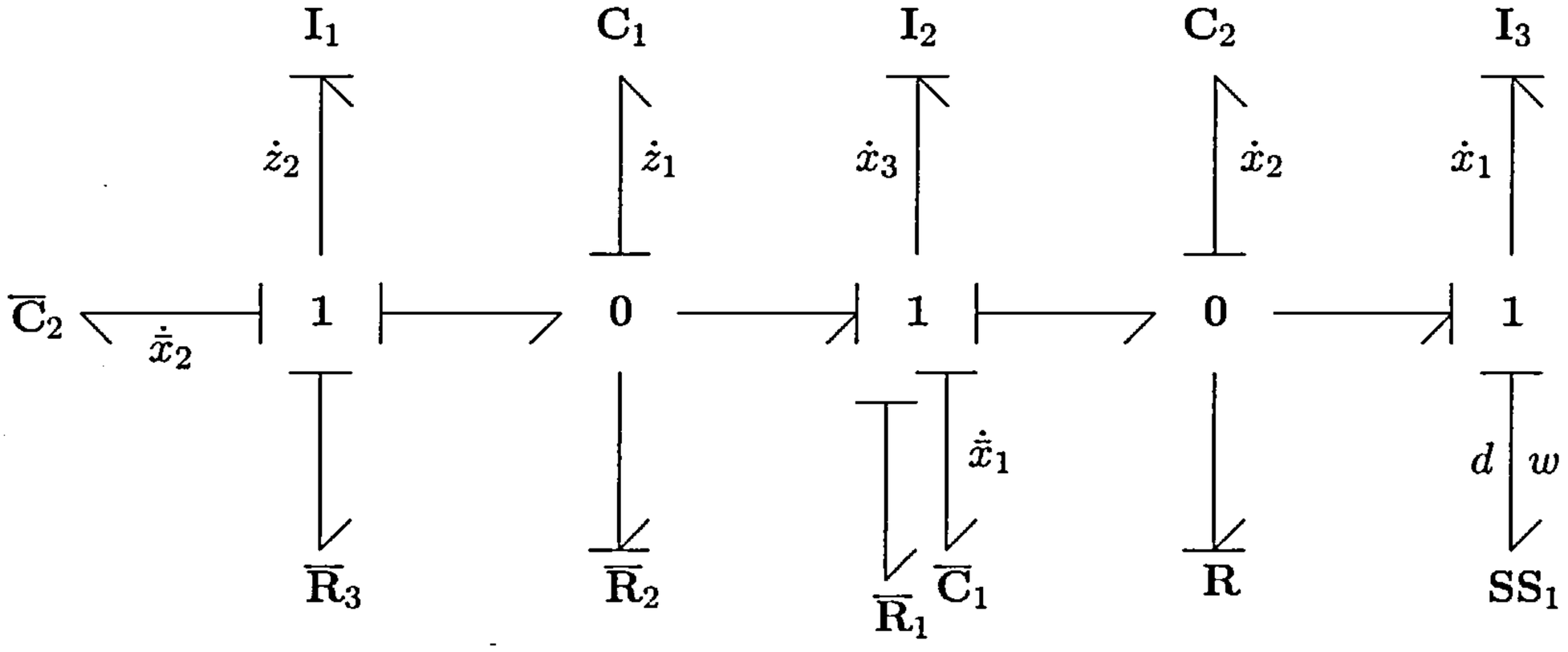

Figure 3.12.: Target closed loop bond graph of Example 3.3.

Now, the backstepping design starts with the causal analysis of Figure 3.10 to obtain the system

$$\begin{aligned}
\begin{bmatrix} \dot{x}_1 \\ \dot{x}_2 \\ \dot{x}_3 \end{bmatrix} &= \begin{bmatrix} 0 & 1 & 0 \\ -1 & -1/r & 1 \\ 0 & -1 & 0 \end{bmatrix} \begin{bmatrix} x_1/m_3 \\ k_2 x_2 \\ x_3/m_2 \end{bmatrix} + \begin{bmatrix} 0 \\ 0 \\ 1 \end{bmatrix} k_1 \xi_1 - \begin{bmatrix} 1 \\ 0 \\ 0 \end{bmatrix} d \\
\dot{\xi}_1 &= -\frac{1}{m_2} x_3 + \frac{1}{m_1} \xi_2 \\
\dot{\xi}_2 &= -k_1 \xi_1 - u.
\end{aligned} \tag{3.22}$$

Note that the x–dynamics are written in the port–Hamiltonian form, thereby making the application of Corollary 2.2 possible. Then, in accordance with Figure 3.12, the first change of variable is found to be

$$k_1 \xi_1 = -\frac{\bar{r}_1}{m_2} x_3 - \bar{k}_1 \bar{x}_1 + k_1 z_1 \quad \Longrightarrow \quad v_0^\star = -\frac{\bar{r}_1}{k_1 m_2} x_3 - \frac{\bar{k}_1}{k_1} \bar{x}_1, \tag{3.23}$$

so that the $(\bar{x}_1, x)$–dynamics is port–Hamiltonian with the dissipative $\mathbf{R}$ and $\overline{\mathbf{R}}_1$ elements. By invoking LaSalle's theorem [Kha92], the point $(\bar{x}_1, x) = (0, 0)$ is globally asymptotically stable. In view of (3.23), write

$$\dot{z}_1 = -\frac{1}{m_2} x_3 + \frac{1}{m_1} \xi_2 - \dot{v}_0^\star, \tag{3.24}$$

and define the second change of variable

$$\frac{1}{m_1}\xi_2 = -\frac{k_1}{\bar{r}_2}z_1 + \dot{v}_0^\star + \frac{1}{m_1}z_2 \quad \Longrightarrow \quad v_1^\star = -\frac{m_1 k_1}{\bar{r}_2}z_1 + m_1\dot{v}_0^\star. \tag{3.25}$$

The last step is given by

$$\dot{z}_2 = -k_1 z_1 + \frac{\bar{r}_1}{m_2}x_3 + \bar{k}_1\bar{x}_1 - u - \dot{v}_1^\star, \tag{3.26}$$

which clearly suggests the control

$$u = \bar{k}_2\bar{x}_2 + \frac{\bar{r}_3}{m_1}z_2 + \bar{k}_1\bar{x}_1 + \frac{\bar{r}_1}{m_2}x_3 - \dot{v}_1^\star. \tag{3.27}$$

The backstepping design is completed by evaluating the time derivatives $\dot{v}_0^\star$ and $\dot{v}_1^\star$ and by substituting the definitions for z_1 and z_2. Collecting the results, it is now readily verified that the closed loop takes the form

$$\begin{bmatrix} \dot{\bar{x}}_1 \\ \dot{\bar{x}}_2 \\ \dot{x}_1 \\ \dot{x}_2 \\ \dot{x}_3 \\ \dot{z}_1 \\ \dot{z}_2 \end{bmatrix} = \begin{bmatrix} 0 & 0 & 0 & 0 & 1 & 0 & 0 \\ 0 & 0 & 0 & 0 & 0 & 0 & 1 \\ 0 & 0 & 0 & 1 & 0 & 0 & 0 \\ 0 & 0 & -1 & -1/r & 1 & 0 & 0 \\ -1 & 0 & 0 & -1 & -\bar{r}_1 & 1 & 0 \\ 0 & 0 & 0 & 0 & -1 & -1/\bar{r}_2 & 1 \\ 0 & -1 & 0 & 0 & 0 & -1 & -\bar{r}_3 \end{bmatrix} \begin{bmatrix} \bar{k}_1\bar{x}_1 \\ \bar{k}_2\bar{x}_2 \\ x_1/m_3 \\ k_2 x_2 \\ x_3/m_2 \\ k_1 z_1 \\ z_2/m_1 \end{bmatrix} - \begin{bmatrix} 0 \\ 0 \\ 1 \\ 0 \\ 0 \\ 0 \\ 0 \end{bmatrix} d.$$
$$w = x_1/m_3. \tag{3.28}$$

Just as in the first two examples, the above backstepping design relies on the derivation of the virtual controls $v_0^\star$ and $v_1^\star$ through the bond signals $k_1\xi_1$ and ξ_2/m_1. One would normally choose the states ξ_1 and ξ_2 as virtual controls in view of Lemma 2.1, but these virtual controls are counter intuitive to some extent. Instead, it is more intuitive to take the bond signals $a_i\xi_i$ as virtual control, since they are to "carry" the dynamic effects of the virtual elements. Furthermore, these bond signals $a_i\xi_i$ are readily selected from the causal path connecting the control u.

The following important observation can be made on the influence of the disturbance d depicted in Figure 3.12. Even though it would seem obvious that the target closed loop can be attained through a backstepping design, the *relative degrees* of the virtual controls with respect to the disturbance d may pose problems that render the closed loop representation more difficult to address.

The relative degree problem can be loosely explained by observing that $v_0^\star$ in (3.23) depends on x_3 and $\bar{x}_1$, so that $v_1^\star$ depends on x_2, x_3 and ξ_1 by (3.25). In turn, the control u has a dependency on x_1 because of (3.27). It can now be concluded that the closed loop does take the form (3.28), but this will *not* be the case when the **R** element in Figure 3.10 is virtual as well. In such a scenario the backstepping design would require an additional step, rendering u directly dependent on d. But disturbances are generally assumed to be unknown, so that the disturbance cannot be removed by feedback. In such case, the closed loop will *not* allow for the bond graph representation of Figure 3.12 and the disturbance would feed through at the location of mass m_1.

To clarify this problem with a simple counter example, consider the system

$$\begin{aligned} \dot{x} &= \xi - d \\ \dot{\xi} &= -x - u. \end{aligned} \tag{3.29}$$

It is readily seen that for $z = \xi + x$ and $u = -x + z$ the closed loop becomes

$$\begin{aligned} \dot{x} &= -x + z - d \\ \dot{z} &= -x - d. \end{aligned} \tag{3.30}$$

Hence, the z–dynamics has an unanticipated dependency on d, which can be attributed to the relative degree of $v_0^\star$ with respect to d. The following section will address this point in further detail. ◊

3.2.2. Results on Single–Input Systems

Having seen three introductory examples on backstepping in the physical domain, this section addresses various observations and conditions for such designs to be applicable. While the material to be presented has certainly been inspired by the work of [Yeh99] and [Gaw01], the results presented here explicitly uses the port–Hamiltonian formulation to define the control objective and to give the closed loop an associated bond graph representation. One–step and multi–step designs are considered.

Proposition 3.1. *Consider the single–input system in Figure 3.13, where the dashed region represents the virtual actuator to be connected to the 1–junction. Let the real–valued functions $H(x)$ and $\bar{H}_0(\bar{x}^0)$ be smooth, positive definite and proper, where $x \in \mathbb{R}^n$ and $\bar{x}^0 \in \mathbb{R}^{\bar{n}_0}$. Define the cascaded element as $\mathbf{C}(\xi) = (1/2)a\xi^2$ for some $a > 0$.*

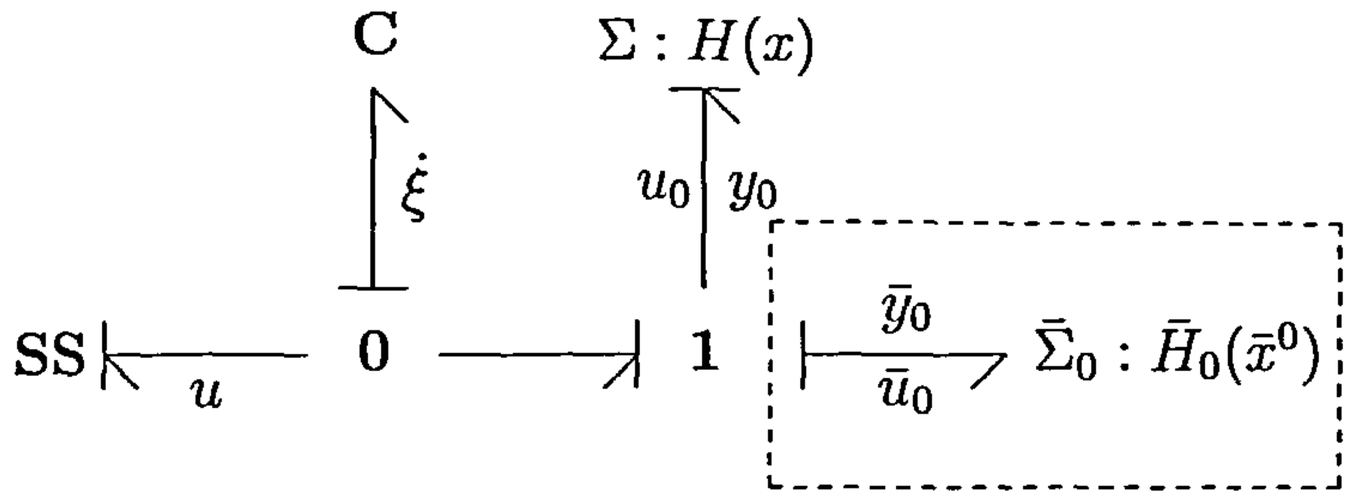

Figure 3.13.: Cascaded C element of Proposition 3.1.

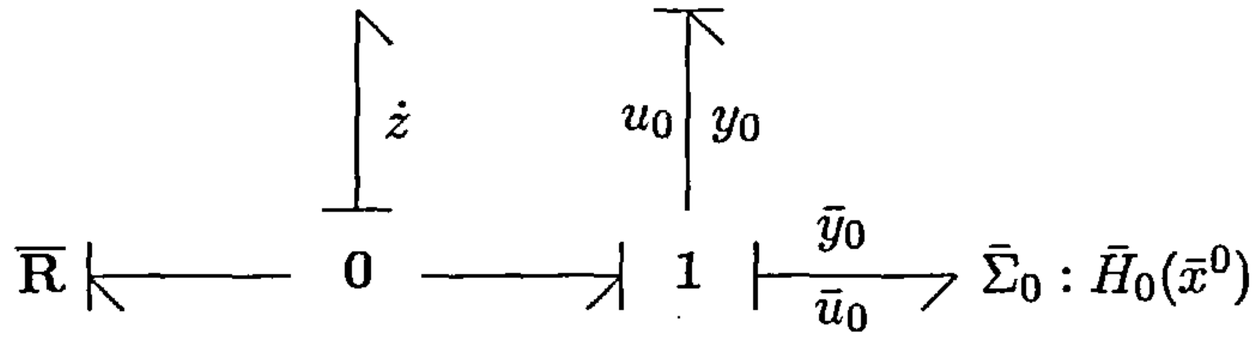

Figure 3.14.: Closed loop C–cascaded system of Proposition 3.1.

Suppose the systems Σ and $\bar{\Sigma}_0$ are explicit bond graph models with the input–output pairs $(u_0, y_0), (\bar{u}_0, \bar{y}_0) \in \mathbb{R} \times \mathbb{R}$ respectively, where $y = y(x)$ and $\bar{y}_0 = \bar{y}_0(\bar{x}^0, \bar{u}_0)$. Then there exists a smooth (dynamic) feedback law $u(x, \xi, \bar{x}^0)$ such that the closed loop allows the bond graph representation of Figure 3.14, where $\mathbf{C}(z) = (1/2)az^2$ and $\overline{\mathbf{R}} = \bar{r}$.

The closed loop Lypanov function is given as

$$W(x, z, \bar{x}^0) = H(x) + \bar{H}_0(\bar{x}^0) + \frac{1}{2}az^2 \tag{3.31}$$

and satisfies

$$\frac{d}{dt}W(x, z, \bar{x}^0) = -U(x, \bar{x}^0) - \frac{a^2}{\bar{r}}z^2 \leq 0, \tag{3.32}$$

for all nonzero $(x, z, \bar{x}^0)$ and positive (semi)-definite $U(x, \bar{x}^0)$.

Proof. Since the systems Σ and $\bar{\Sigma}_0$ are explicit bond graph systems, it follows that Σ can be given the form

$$\begin{aligned} \dot{x} &= [J(x) - R(x)]K(x) + g(x)u_0 \\ y_0 &= g^T(x)K(x), \end{aligned} \tag{3.33}$$

where $K^T(x) = \mathbf{D}H(x)$. Likewise, $\bar{\Sigma}_0$ admits the port–Hamiltonian representation

$$\begin{aligned} \dot{\bar{x}}^0 &= [\bar{J}_0(\bar{x}^0) - \bar{R}_0(\bar{x}^0)]\bar{K}_0(\bar{x}^0) + \bar{g}_0(\bar{x}^0)\bar{u}_0 \\ \bar{y}_0 &= \bar{g}_0^T(\bar{x}^0)\bar{K}_0(\bar{x}^0) + \bar{b}_0(\bar{x}^0)\bar{u}_0. \end{aligned} \tag{3.34}$$

The interconnection of Σ and $\bar{\Sigma}_0$ is then achieved by considering the change of variable of the form

$$a\xi = -\bar{y}_0(\bar{x}^0, y_0(x)) + az \quad \Longrightarrow \quad v^\star = -\frac{1}{a}\bar{y}_0(\bar{x}^0, y_0(x)). \tag{3.35}$$

The system in Figure 3.13 then becomes

$$\begin{bmatrix} \dot{x} \\ \dot{\bar{x}}^0 \end{bmatrix} = \begin{bmatrix} J(x) - R(x) - g(x)\bar{b}_0(\bar{x}^0)g^T(x) & -g(x)\bar{g}_0^T(\bar{x}^0) \\ \bar{g}_0(\bar{x}^0)g^T(x) & \bar{J}_0(\bar{x}^0) - \bar{R}_0(\bar{x}^0) \end{bmatrix} \begin{bmatrix} K(x) \\ \bar{K}_0(\bar{x}^0) \end{bmatrix} + \begin{bmatrix} g(x) \\ 0 \end{bmatrix} az$$
$$\dot{z} = -g^T(x)K(x) - u - \dot{v}^\star. \tag{3.36}$$

Hence the control

$$u = \frac{1}{\bar{r}}az - \dot{v}^\star \tag{3.37}$$

induces the closed loop of the form

$$\begin{bmatrix} \dot{x} \\ \dot{\bar{x}}^0 \\ \dot{z} \end{bmatrix} = \begin{bmatrix} J(x) - R(x) - g(x)\bar{b}_0(\bar{x}^0)g^T(x) & -g(x)\bar{g}_0^T(\bar{x}^0) & g(x) \\ \bar{g}_0(\bar{x}^0)g^T(x) & \bar{J}_0(\bar{x}^0) - \bar{R}_0(\bar{x}^0) & 0 \\ -g^T(x) & 0 & -1/\bar{r} \end{bmatrix} \begin{bmatrix} K(x) \\ \bar{K}_0(\bar{x}^0) \\ az \end{bmatrix}. \tag{3.38}$$

In view of (3.32) and (3.38), it is seen that

$$U(x, \bar{x}^0) = K^T(x)[R(x) + g(x)\bar{b}_0(\bar{x}^0)g^T(x)]K(x) + \bar{K}_0^T(\bar{x}^0)\bar{R}_0(\bar{x}^0)\bar{K}_0(\bar{x}^0). \tag{3.39}$$

Because $W(x, \xi, \bar{x}^0)$ is positive definite and proper, the origin is globally stable since $U(x, \bar{x}^0)$ is assumed to be positive (semi)–definite. To investigate the global asymptotic stability of the origin, consider the set

$$P = \{(x, z, \bar{x}^0) : U(x, \bar{x}^0) = \frac{a^2}{\bar{r}}z^2 = 0\}. \tag{3.40}$$

Let P_0 be the largest subset of P that is invariant under the dynamics (3.38), then by LaSalle's Theorem [Kha92] the origin is globally asymptotically stable if $P_0 = \{0\}$. □

It should be noted that the class of systems Σ can be enlarged by observing that both $J(x)$ and $R(x)$ in (3.33) can be smoothly modulated with ξ. Observe that the structure matrix $J(x, \xi)$ remains trivially anti–symmetric and where $U(x, \xi, \bar{x}^0)$ positive (semi)–definite. However, observe that if the change of variables (3.35) is to remain valid then it must hold that $\bar{y}_0 = \bar{y}_0(\bar{x}^0, y_0(x))$ does not depend on ξ, thus $d\bar{y}_0/d\xi = 0$, which is clearly satisfied for the relation $g(x, \xi) = g(x)$. From now it will be assumed that $J(x, \xi) = J(x)$ and $R(x, \xi) = R(x)$.

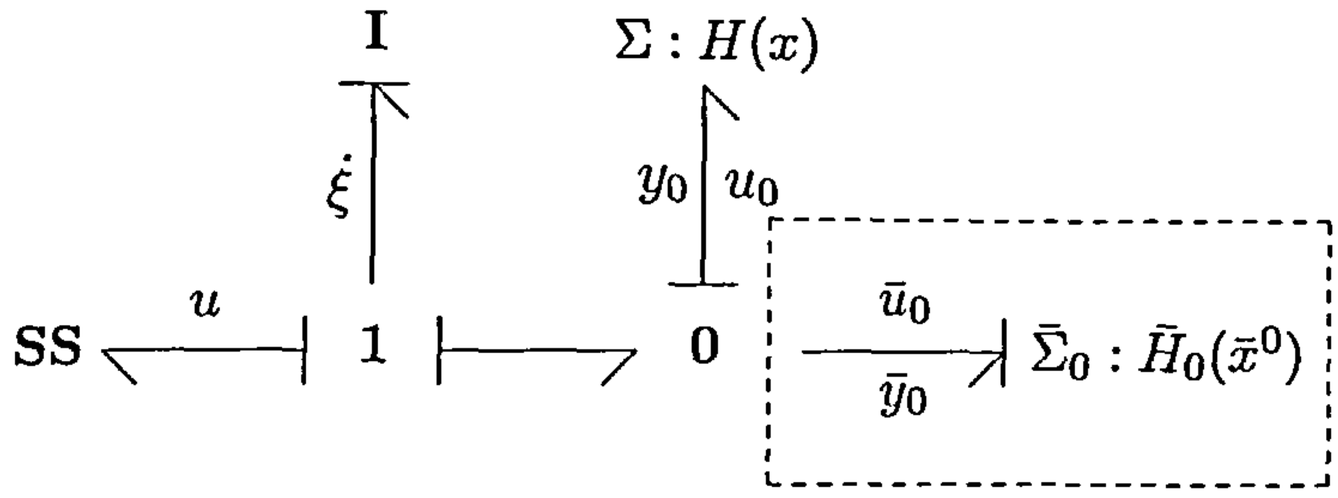

Figure 3.15.: Cascaded I element of Corollary 3.2.

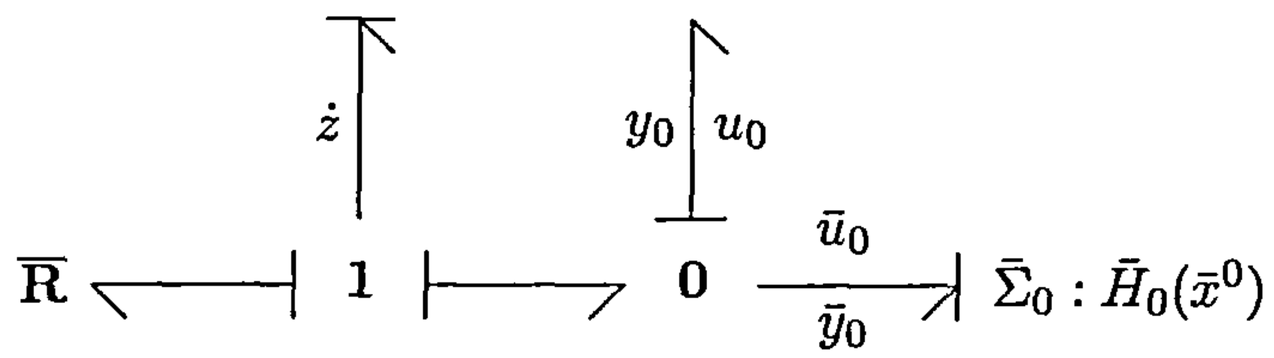

Figure 3.16.: Closed loop I–cascaded system of Corollary 3.2.

Corollary 3.2. *The* I*–cascaded system depicted in Figure 3.15 allows for the bond graph representation of Figure 3.16 by some smooth feedback* $u(x, \xi, \bar{x}^0)$.

Proof. Entirely analogues to Proposition 3.1, but (3.32) evidently reads

$$\frac{d}{dt}W(x, z, \bar{x}^0) = -U(x, \bar{x}^0) - \bar{r}a^2z^2 \leq 0, \tag{3.41}$$

for all nonzero $(x, z, \bar{x}^0)$ and positive (semi)–definite $U(x, \bar{x}^0)$. □

The following corollary recognises that for stabilisation purposes the simple $\overline{\mathbf{R}}$ elements in Figures 3.14 and 3.16 can be generalised to more complicated systems.

Corollary 3.3. *Consider the systems in Figures 3.13 and 3.15. Then there exists a smooth (dynamic) feedback* $u(x, \xi, \bar{x})$, *with* $\bar{x} = (\bar{x}^0, \bar{x}^1)$, *such that the respective closed loops in Figures 3.17 and 3.18 are attained. The explicit bond graph model* $\bar{\Sigma}_1 : \bar{H}_1(\bar{x}^1)$ *has the states* $\bar{x}^1 \in \mathbb{R}^{\bar{n}_1}$ *and the input/output pair* $(\bar{u}_1, \bar{y}_1) \in \mathbb{R} \times \mathbb{R}$ *with* $\bar{y}_1 = \bar{y}_1(\bar{x}^1, \bar{u}_1)$.

Proof. From Figures 3.17 and 3.18 define the control in (3.36) as

$$u = \bar{y}_1(\bar{x}^1, az) - \dot{v}^\star = \bar{g}_1^T(\bar{x}^1)\bar{K}_1(\bar{x}^1) + \bar{b}_1(\bar{x}^1)az - \dot{v}^\star. \tag{3.42}$$

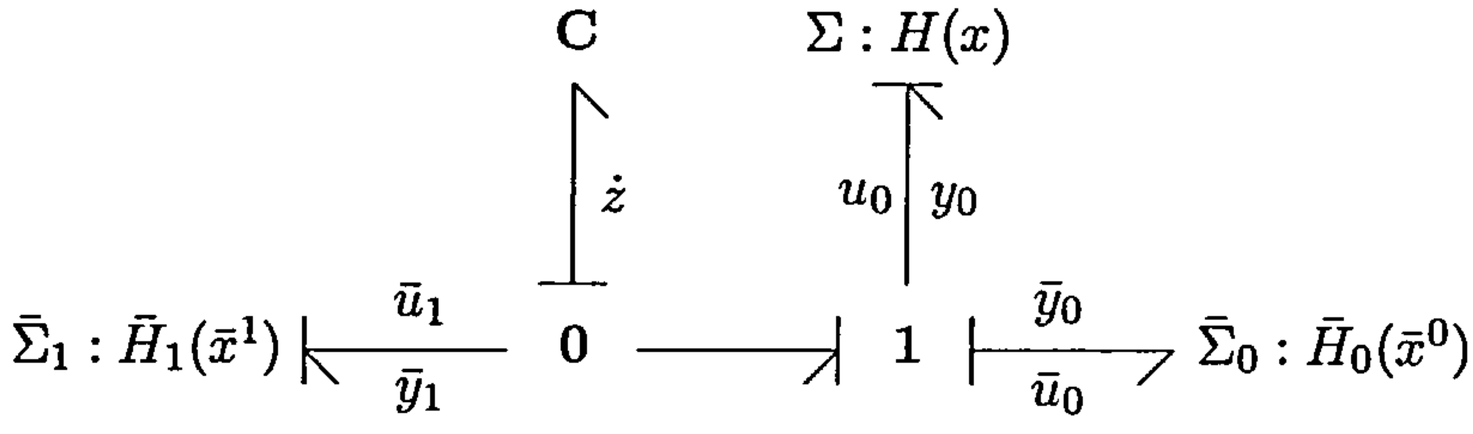

Figure 3.17.: Closed loop **C**–cascaded system of Corollary 3.3.

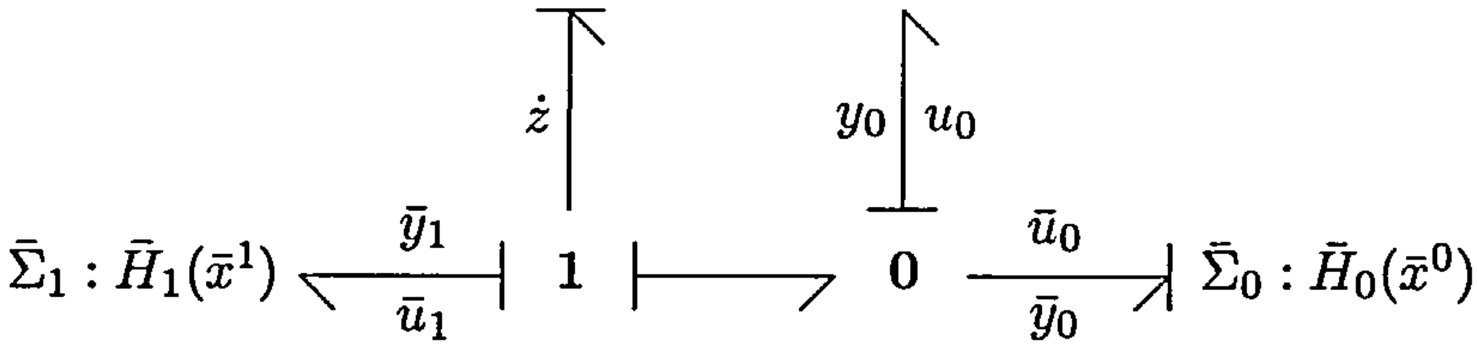

Figure 3.18.: Closed loop **I**–cascaded system of Corollary 3.3.

Then rewrite the port–Hamiltonian dynamics (3.36) as

$$\begin{bmatrix} \dot{x} \\ \dot{\bar{x}}^0 \\ \dot{\bar{x}}^1 \\ \dot{z} \end{bmatrix} = \begin{bmatrix} * & * & 0 & g(x) \\ * & * & 0 & 0 \\ 0 & 0 & \bar{J}_1(\bar{x}^1) - \bar{R}_1(\bar{x}^1) & \bar{g}_1(\bar{x}^1) \\ -g^T(x) & 0 & -\bar{g}_1^T(\bar{x}^1) & -\bar{b}_1(\bar{x}^1) \end{bmatrix} \begin{bmatrix} K(x) \\ \bar{K}_0(\bar{x}^0) \\ \bar{K}_1(\bar{x}^1) \\ az \end{bmatrix}. \tag{3.43}$$

□

So far, the **C** and **I** elements are taken as simple quadratic elements. The reason for doing so can be attributed to the fact that one–step backstepping designs as defined by Lemma 2.1 induce a closed loop Lyapunov function of the form $W(x) = V(x) + (1/2)z^2$. From this standpoint, if the plant dynamics already has the simple quadratic storage $(1/2)a\xi^2$ associated with a **C** or **I** element, then the change of variable (3.35) simply interchanges the role of ξ with z. Thus, such a backstepping design renders the closed loop Lyapunov function identical to the plant Hamiltonian; however, due to the change of variables, one must be aware that it is not possible to associate physical energy with the closed loop Hamiltonian. Furthermore, the closed loop bond graph represents a physical system in conceptual sense.

Now, it would seem that Proposition 3.1 and Corollaries 3.2 and 3.3 are restricted to the change of variable $z = \xi - v^\star$, but the following proposition shows that the relationship $z = (1/a)\lambda(\xi) - v^\star(x)$ can be used for certain nonlinear **C** or **I** elements, where $\lambda(\xi)$ is a smooth function and where $a > 0$.

Proposition 3.4. *Consider Proposition 3.1 and Corollaries 3.2 and 3.3. Suppose all conditions apply except that* $\mathbf{C}(\xi) = F(\xi)$ *or* $\mathbf{I}(\xi) = F(\xi)$ *for some smooth, positive definite function* $F(\xi)$ *satisfying* $F''(\xi) > 0$ *for all* ξ*. Then the closed loops in Figures 3.17 and 3.18 are attainable by smooth feedback* $u(x, \bar{x}, \xi)$*.*

Proof. Put $\lambda(\xi) = F'(\xi)$ and observe that the plant has the form

$$\begin{aligned} \dot{x} &= [J(x) - R(x)]K(x) + g(x)\lambda(\xi) \\ \dot{\xi} &= -g^T(x)K(x) - u. \end{aligned} \tag{3.44}$$

Now, in the same fashion as (3.35), define the change of variable

$$\lambda(\xi) = -\bar{y}_0(\bar{x}^0, y_0(x)) + az, \tag{3.45}$$

which reflects the idea that the bond signal $\lambda(\xi)$ is to "carry" the virtual actuator output $\bar{y}_0$ and where az renders the $\mathbf{C}$ element into a simple quadratic storage function. Because $F(\xi)$ is positive definite and satisfies $F''(\xi) > 0$ for all ξ, it follows that $\lambda(\xi) = 0$ implies $\xi = 0$. The change of variable (3.45) is seen to yield the system

$$\begin{aligned} \dot{x} &= [J(x) - R(x)]K(x) - g(x)\bar{y}_0(\bar{x}^0, y_0(x)) + g(x)az \\ \dot{z} &= \frac{1}{a}\lambda'(\xi)[-g^T(x)K(x) - u] + \frac{1}{a}\dot{\bar{y}}_0(\bar{x}^0, y_0(x)), \end{aligned} \tag{3.46}$$

from which to derive the control

$$u = -g^T(x)K(x) + \frac{a}{\lambda'(\xi)}\left[g^T(x)K(x) + \frac{1}{a}\dot{\bar{y}}_0(\bar{x}^0, y_0(x)) + \bar{y}_1(\bar{x}^1, az)\right]. \tag{3.47}$$

Hence (3.43) holds with $\mathbf{C}(z) = (1/2)az^2$ or $\mathbf{I}(z) = (1/2)az^2$. □

The main result at this stage is that one–step bond graph based backstepping need not be restricted to linear $\mathbf{C}$ and $\mathbf{I}$ elements as in [Yeh99]. This enlarges the class of systems suitable for Proposition 3.1 and Corollaries 3.2 and 3.3. The following example demonstrates such nonlinear case.

Example 3.4. Consider Example 3.1 but suppose the $\mathbf{C}$ element in (3.1) is defined as

$$\mathbf{C}(\xi) = F(\xi) = a\xi \arctan(\xi) - \frac{a}{2}\ln(\xi^2 + 1), \tag{3.48}$$

which is smooth, positive definite and satisfies $F''(\xi) > 0$ for all ξ and $a > 0$. The plant is readily given as

$$\begin{aligned} \dot{x} &= a \arctan(\xi) \\ \dot{\xi} &= -\frac{x}{m\sqrt{x^2 + 1}} - u. \end{aligned} \tag{3.49}$$

It is instructive to briefly consider a conventional backstepping design first, which would view the state ξ as the virtual control. In this case, observe that the change of variable $\xi = -x + z$ stabilises the x–dynamics, because the dynamics $\dot{x} = -a\arctan(x)$ is readily seen to be globally asymptotically stable. Although the system (3.49) is relatively simple, a conventional backstepping design can become quite involved since the x–dynamics must be written as

$$\begin{aligned} a\arctan(-x+z) &= -a\arctan(x) + z\int_0^1 \frac{\partial}{\partial s}\arctan(-x+s)\Big|_{s=tz} dt \\ &= -a\arctan(x) + p(x,z)z, \end{aligned} \tag{3.50}$$

where $p(x,z)$ is smooth. This procedure will induce port–Hamiltonian as per Corollary 2.2 but not with the structure of Figure 3.3. So instead of focusing on the state variable ξ as the virtual control, identify the bond signal $a\arctan(x)$ as the virtual control, where it can be argued that such a choice is somewhat unconventional. Nonetheless, the change of variable (3.45) is a logical choice within the bond graph context and yields the virtual control

$$a\arctan(\xi) = -\frac{\bar{r}_1 x}{m\sqrt{x^2+1}} + az, \tag{3.51}$$

where the resistive $\overline{\mathbf{R}}_1$ element in Figure 3.2 is chosen to be linear. Then (3.47) reads

$$u = -\frac{x}{m\sqrt{x^2+1}} + (\xi^2+1)\left[\frac{x}{m\sqrt{x^2+1}} + \frac{\bar{r}_1}{am\sqrt{x^2+1}} - \frac{\bar{r}_1 x^2}{am(x^2+1)^{3/2}} + \frac{1}{\bar{r}_2}az\right], \tag{3.52}$$

which induces the closed loop

$$\begin{bmatrix} \dot{x} \\ \dot{z} \end{bmatrix} = \begin{bmatrix} -\bar{r}_1 & 1 \\ -1 & -1/\bar{r}_2 \end{bmatrix} \begin{bmatrix} x/(m\sqrt{x^2+1}) \\ az \end{bmatrix}. \tag{3.53}$$

Global asymptotic stability follows immediately. ◊

The recursive application of Proposition 3.1 and Corollaries 3.2 and 3.3 is readily possible for systems having a cascading sequence of **C** and **I** elements. The following proposition shows the recursive application of Corollary 3.3 that encompasses Proposition 3.1 and Corollary 3.3. Just as in the one–step design, the closed loop retains the plant structure to which additional bond graph elements are added that represent stabilising dynamics. More precisely, for each step a new coordinate is introduced such that the plant bond graph topology is retained to provide arguments for stabilising elements.

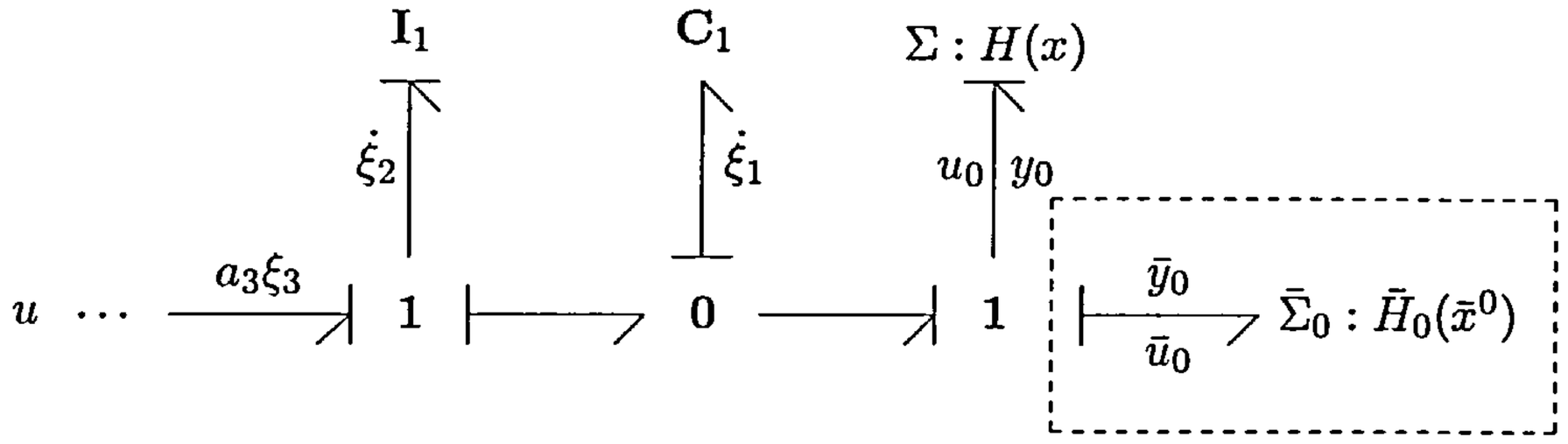

Figure 3.19.: Repeated *linear* cascaded elements of Proposition 3.5.

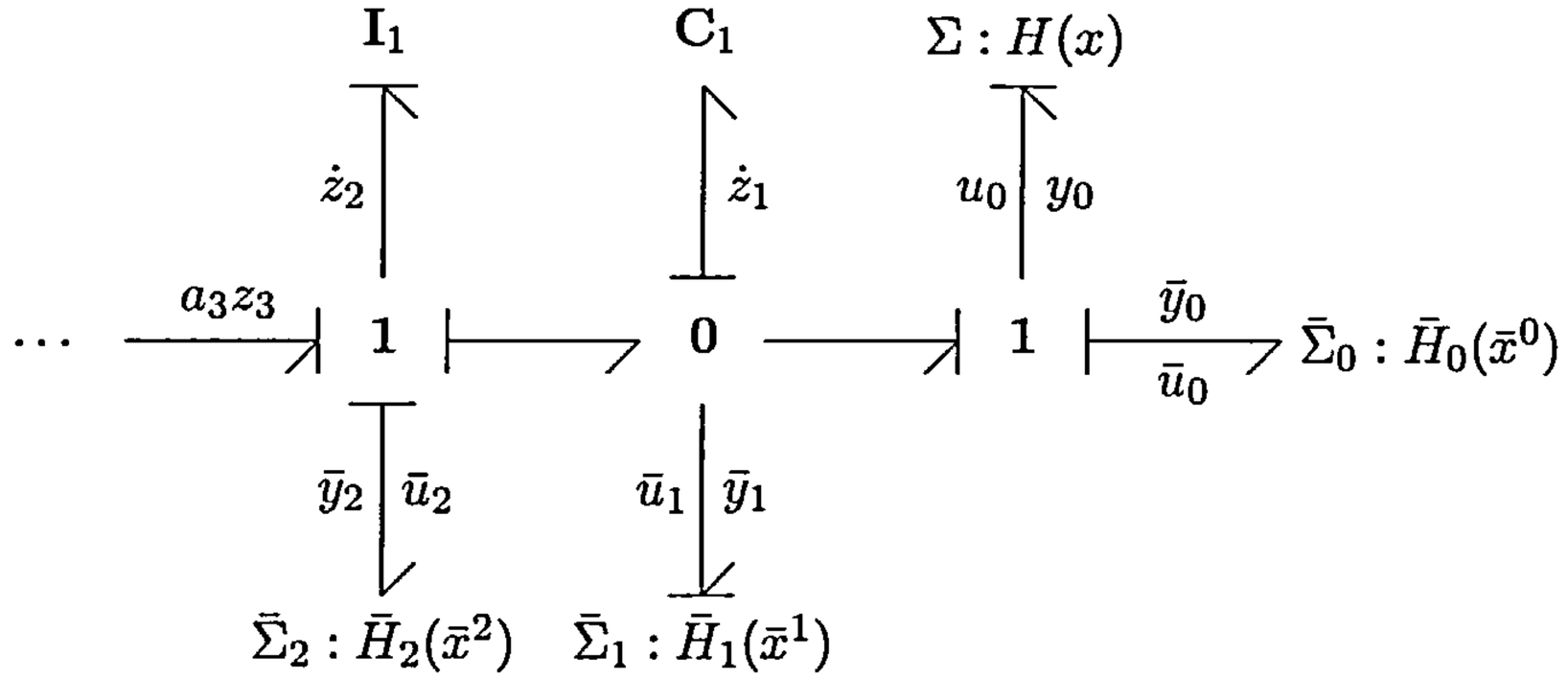

Figure 3.20.: Target cascaded closed loop of Proposition 3.5.

Proposition 3.5. *Consider the cascaded system depicted in Figure 3.19, where* Σ *and* $\bar{\Sigma}_0$ *are explicit bond graph systems defined on* $\mathbb{R}^n$ *and* $\mathbb{R}^{\bar{n}_0}$ *respectively. The input/output pairs are* (u_0, u_0),$(\bar{u}_0, \bar{y}_0) \in \mathbb{R} \times \mathbb{R}$ *with* $y_0 = y_0(x)$ *and* $\bar{y}_0 = \bar{y}_0(\bar{x}^0, \bar{u}_0)$. *Let the real-valued functions* $H(x)$ *and* $\bar{H}_0(\bar{x}^0)$ *be smooth, positive definite and define quadratic storage elements as*

$$\mathbf{C}_j(\xi_{2j-1}) = \frac{1}{2} a_{2j-1} \xi_{2j-1}^2, \quad \mathbf{I}_k(\xi_{2k}) = \frac{1}{2} a_{2k} \xi_{2k}^2, \tag{3.54}$$

for appropriate $j, k \in \mathbb{N}$, *where* $a_i > 0$ *for all* i. *Then there exists a feedback* $u(x, \bar{x}, \xi)$, *with* $\bar{x} = (\bar{x}^0, \bar{x}^1, \ldots)$ *and* $\xi = (\xi_1, \xi_2, \ldots)$, *such that the closed loop admits the bond graph representation of Figure 3.20. The explicit bond graph systems* $\bar{\Sigma}_i$ *are defined on* $\mathbb{R}^{\bar{n}_i}$, *for* $i \geq 1$, *and have the input/output pairs* $(\bar{u}_i, \bar{y}_i) \in \mathbb{R} \times \mathbb{R}$ *with* $\bar{y}_i = \bar{y}_i(\bar{x}^i, \bar{u}_i)$.

Proof. Depending upon which element terminates the sequence, the control u in Figure 3.19 is either an effort or a flow. Now, the first step of the design is analogue to Proposition 3.1 and the first change of variable is therefore defined as

$$a_1 \xi_1 = -\bar{y}_0(\bar{x}^0, y_0(x)) + a_1 z_1 \quad \Longrightarrow \quad v_0^\star = -\frac{1}{a_1} \bar{y}_0(\bar{x}^0, y_0(x)), \tag{3.55}$$

thus

$$\dot{z}_1 = -y_0(x) + a_2 \xi_2 - \dot{v}_0^\star. \tag{3.56}$$

By considering the target dynamics of Figure 3.20, it is seen that the second change of variable becomes

$$a_2\xi_2 = -\bar{y}_1(\bar{x}^1, a_1z_1) + \dot{v}_0^\star + a_2z_2 \quad \Longrightarrow \quad v_1^\star = -\frac{1}{a_2}[\bar{y}_1(\bar{x}^1, a_1z_1) - \dot{v}_0^\star]. \tag{3.57}$$

Then, for $j \geq 2$, define the recursive relation

$$\dot{z}_j = -a_{j-1}z_{j-1} - a_{j-1}v_{j-2}^\star + a_{j+1}\xi_{j+1} - \dot{v}_{j-1}^\star, \tag{3.58}$$

where

$$\begin{aligned} a_{j+1}\xi_{j+1} &= a_{j-1}v_{j-2}^\star + \dot{v}_{j-1}^\star - \bar{y}_j(\bar{x}^j, a_jz_j) + a_{j+1}z_{j+1} \\ \Longrightarrow \qquad v_j^\star &= \frac{1}{a_{j+1}}[a_{j-1}v_{j-2}^\star + \dot{v}_{j-1}^\star - \bar{y}_j(\bar{x}^j, a_jz_j)]. \end{aligned} \tag{3.59}$$

□

It is readily seen that Proposition 3.5 holds for the the cascaded pattern of elements in Figures 3.19 and 3.20 for which the C and I elements are swapped.

Corollary 3.6. *Let the elements in Proposition 3.5 be defined as*

$$\mathbf{C}_j(\xi_{2j-1}) = F_j(\xi_{2j-1}), \quad \mathbf{I}_k(\xi_{2k}) = G_k(\xi_{2k}), \tag{3.60}$$

for positive definite functions $F_j(\xi_{2j-1})$ and $G_k(\xi_{2k})$, satisfying the conditions $F_j''(\xi_{2j-1}) > 0$ and $G_k''(\xi_{2k}) > 0$ for all ξ_i. Then the closed loop in Figure 3.20 can be attained by smooth feedback.

Proof. The first step of the design starts with the relation

$$\lambda_1(\xi_1) = -\bar{y}(\bar{x}^0, y_0(x)) + a_1z_1, \tag{3.61}$$

yielding the z_1–dynamics

$$\dot{z}_1 = \frac{1}{a_1}\lambda_1'(\xi_1)[-y_0(x) + \lambda_2(\xi_2)] + \frac{1}{a_1}\dot{\bar{y}}_0(\bar{x}^0, y_0(x)). \tag{3.62}$$

To further enforce the target dynamics in Figure 3.20, define the virtual control

$$\lambda_2(\xi_2) = y_0(x) + \frac{a_1}{\lambda_1'(\xi_1)}\left[-y_0(x) - \frac{1}{a_1}\dot{\bar{y}}_0(\bar{x}^0, y_0(x)) - \bar{y}_1(\bar{x}^1, a_1z_1) + a_2z_2\right], \tag{3.63}$$

so that the z_2–dynamics becomes

$$\begin{aligned} \dot{z}_2 = \frac{1}{a_1a_2}\lambda_1'(\xi_1)[\lambda_2'(\xi_2)[-\lambda_1(\xi_1) + \lambda_3(\xi_3)] - \dot{y}_0(x)] + \frac{1}{a_1a_2}\dot{\lambda}_1'(\xi_1)[\lambda_2(\xi_2) - y_0(x)] \\ + \frac{1}{a_2}\left[\dot{y}_0(x) + \frac{1}{a_1}\ddot{\bar{y}}_0(\bar{x}^0, y_0(x)) + \dot{\bar{y}}_1(\bar{x}^1, a_1z_1)\right]. \end{aligned} \tag{3.64}$$

Select the expression for $\lambda_3(\xi_3)$ that "cancels" the right–hand side of (3.64) and that imposes the proper target dynamics. Unfortunately, the expressions become too complex for presentational purposes, but it is readily seen that the recursive process does yield the closed loop port–Hamiltonian dynamics of Figure 3.20. □

The recursive scheme for nonlinear elements can be clarified by considering Example 3.3, but assume that the $\mathbf{C}_1$ and $\mathbf{I}_1$ elements are nonlinear elements that satisfy the conditions of Proposition 3.5.

Example 3.5. Consider Figure 3.10 and define $\mathbf{C}_1(\xi_1) = F_1(\xi_1)$ and $\mathbf{I}_1(\xi_2) = G_1(\xi_2)$, where the actual definitions of $\mathbf{C}_1(\xi_1)$ and $\mathbf{I}_1(\xi_2)$ will be omitted to avoid some algebra, but observe that (3.22) now reads

$$\begin{bmatrix} \dot{x}_1 \\ \dot{x}_2 \\ \dot{x}_3 \end{bmatrix} = \begin{bmatrix} 0 & 1 & 0 \\ -1 & -1/r & 1 \\ 0 & -1 & 0 \end{bmatrix} \begin{bmatrix} x_1/m_3 \\ k_2 x_2 \\ x_3/m_2 \end{bmatrix} + \begin{bmatrix} 0 \\ 0 \\ 1 \end{bmatrix} \lambda_1(\xi_1) - \begin{bmatrix} 1 \\ 0 \\ 0 \end{bmatrix} d \tag{3.65}$$

$$\begin{aligned} \dot{\xi}_1 &= -y_0(x) + \lambda_2(\xi_2) \\ \dot{\xi}_2 &= -\lambda_1(\xi_1) - u. \end{aligned}$$

The design can now be based on (3.61) and (3.63) for which $a_1 = k_1$, $a_2 = 1/m_1$ and $\lambda(\xi_3) = -u$. ◊

As mentioned earlier, the class of systems depicted in Figure 3.19 of Proposition 3.5 are relatively small, so that the application of the presented backstepping procedure is somewhat limited. However, it is possible to enlarge this class of systems by allowing explicit bond graph systems to be connected to the junctions of the cascaded pattern of **C** and **I** elements. For simplicity, the following corollary explains this process for a single quadratic **C** element, but it is understood that the same arguments equally holds for a quadratic **I** element.

Corollary 3.7. *Let $\Sigma_\eta : H_\eta(\eta)$ be an explicit bond graph model with the input/output pair $(u_\eta, y_\eta) \in \mathbb{R} \times \mathbb{R}$ with $y_\eta = y_\eta(\eta, u_\eta)$. Suppose Σ_η is connected to a 0–junction of some quadratic C_i element as depicted in Figure 3.21. Then the recursive backstepping procedure of Proposition 3.5 can be applied if Σ_η is input–to–state stable.*

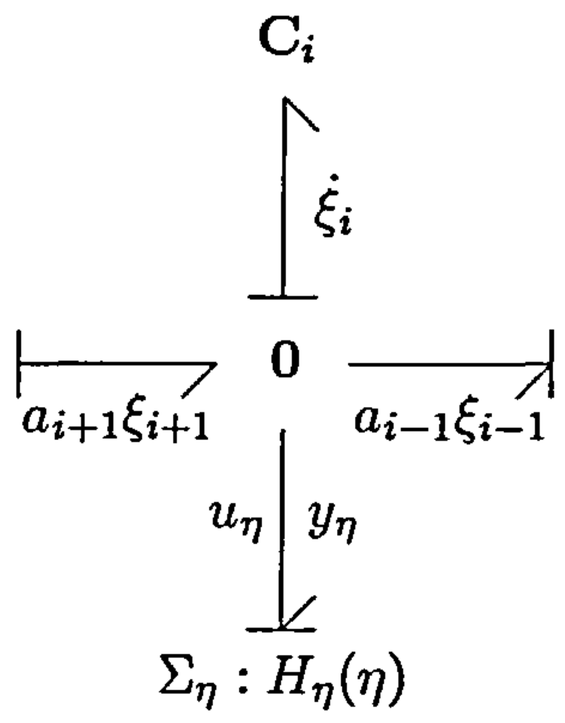

Figure 3.21.: Extended backstepping junction of Corollary 3.7.

Proof. First observe that the bond graph in Figure 3.21 yields the system

$$\begin{aligned} \dot{\xi}_i &= -a_{i-1}\xi_{i-1} + a_{i+1}\xi_{i+1} - y_\eta(\eta, a_i\xi_i) \\ \dot{\eta} &= [I_\eta(\eta) - R_\eta(\eta)]K_\eta(\eta) + g_\eta(\eta)a_i\xi_i. \\ y_\eta &= g_\eta^T(\eta)K_\eta(\eta) + b_\eta(\eta)a_i\xi_i. \end{aligned} \tag{3.66}$$

The target dynamics of Figure 3.20 are attainable by amending the relation (3.59) to

$$\begin{aligned} a_{i+1}\xi_{i+1} &= a_{i-1}v_{i-2}^\star + \dot{v}_{i-1}^\star - \bar{y}_i(\bar{x}^i, a_iz_i) + y_\eta(\eta, a_i\xi_i) + a_{i+1}z_{i+1} \\ \Longrightarrow \qquad v_i^\star &= \frac{1}{a_{i+1}}[a_{i-1}v_{i-2}^\star + \dot{v}_{i-1}^\star - \bar{y}_i(\bar{x}^i, a_iz_i) + y_\eta(\eta, a_i\xi_i)], \end{aligned} \tag{3.67}$$

thereby removing the influence of y_η from the target dynamics. However, this implies that the internal η–dynamics must remain stable for arbitrary bounded input u_η.

Take the usual change of variable $\xi_i = z_i + v_{i-1}^\star$, so that (3.66) with (3.67) reads

$$\begin{aligned} \dot{z}_i &= -a_{i-1}z_{i-1} - \bar{y}_i(\bar{x}^i, a_iz_i) + a_{i+1}z_{i+1} \\ \dot{\eta} &= [I_\eta(\eta) - R_\eta(\eta)]K_\eta(\eta) + g_\eta(\eta)a_i[v_{i-1}^\star + z_i]. \end{aligned} \tag{3.68}$$

The target dynamics are therefore attained, but the η–dynamics are driven by arbitrary, bounded inputs $v_{i-1}^\star + z_i$. To guarantee that η–trajectories remain stable, it is desirable that there exists a smooth, real–valued function $V(\eta)$, which is positive definite and proper, such that

$$\frac{d}{dt}V(\eta) \leq -\alpha(\|\eta\|) + \sigma(|u_\eta|), \tag{3.69}$$

where α and σ are class $\mathcal{K}_\infty$ functions [Son95], [Isi99]. So if the η–dynamics are input–to–state stable then the backstepping procedure can be applied. □

Example 3.6. Consider the physical system depicted in Figure 3.22 and its bond graph representation in Figure 3.23, where the various elements are defined as

$$\mathbf{I}(x) = \frac{1}{2m}x^2, \quad \mathbf{C}_1(\xi) = \frac{1}{2}k_1\xi^2, \quad \mathbf{C}_2(\eta) = \frac{1}{2}k_2\eta^2, \quad \mathbf{R} = r. \tag{3.70}$$

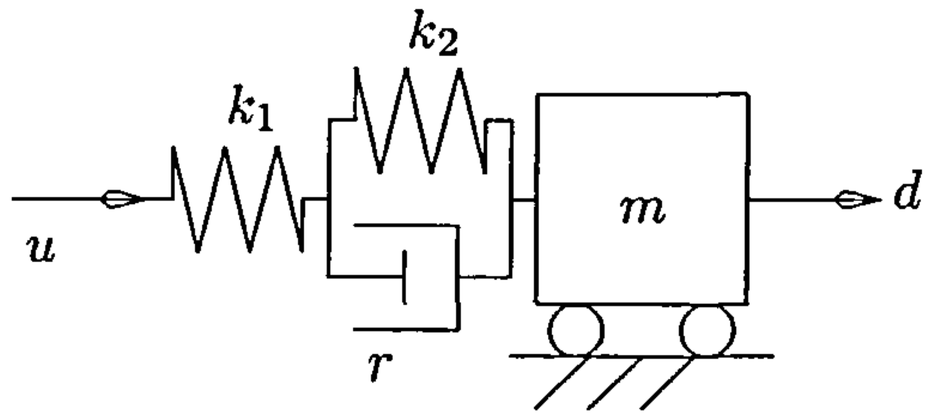

Figure 3.22.: Compound element backstepping of Example 3.6.

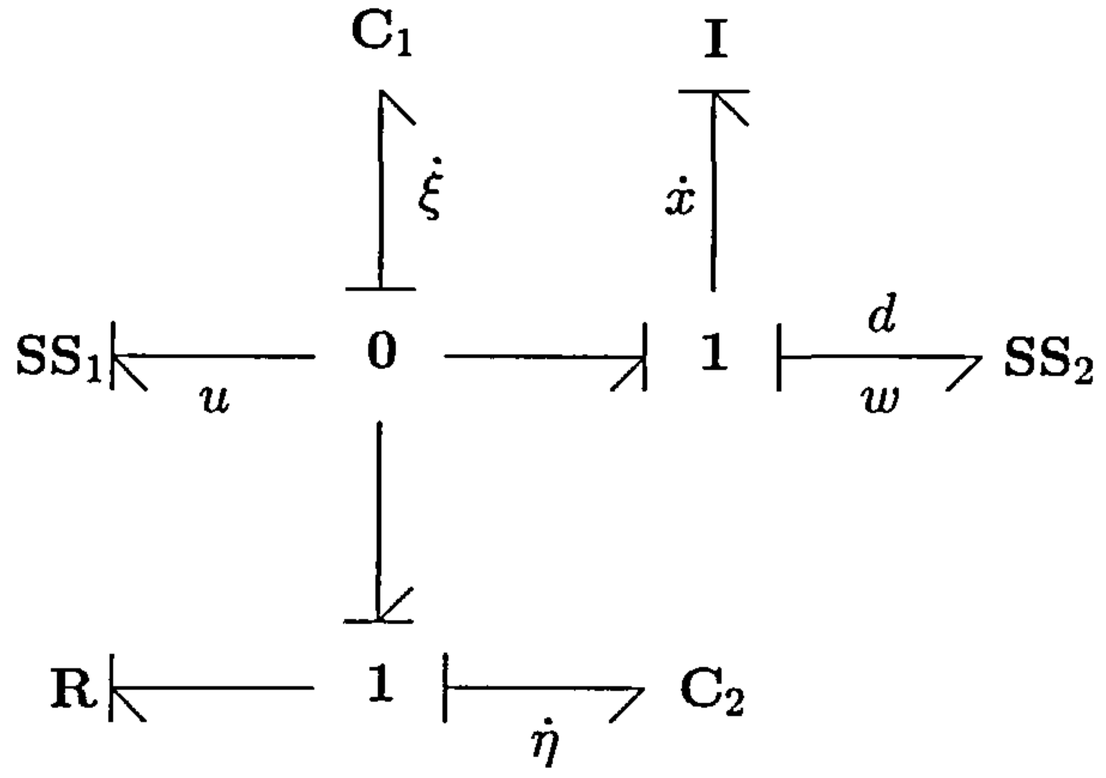

Figure 3.23.: Compound backstepping bond graph of Example 3.6.

As in example 3.2, suppose that the virtual actuator in Figure 3.7 is to be connected to the mass m with the connection constraint $\bar{u} = w$, then by Corollary 3.7 it is still possible to attain the closed loop of Figure 3.6 through a backstepping design.

The point of departure is straightforward causal analysis to obtain the system

$$\begin{aligned} \dot{x} &= k_1\xi - d \\ \dot{\xi} &= -\frac{1}{m}x - \frac{k_1}{r}\xi - u + \frac{k_2}{r}\eta \\ \dot{\eta} &= -\frac{k_2}{r}\eta + \frac{k_1}{r}\xi, \end{aligned} \tag{3.71}$$

where the dynamics (3.66) are clearly recognised. Then by recalling Example 3.2, take the change of variable

$$k_1\xi = -\bar{y}_0(\bar{x}_1^0, \bar{x}_2^0) + k_1 z \quad \Longrightarrow \quad v_0^\star = -\frac{1}{k_1}\bar{y}_0(\bar{x}_1^0, \bar{x}_2^0), \tag{3.72}$$

where $\bar{y}_0$ is the output of the virtual actuator in Figure 3.7. In view of (3.67), the closed loop in Figure 3.8 is attainable by choosing the control

$$u = -\frac{k_1}{r}\xi + \frac{k_2}{r}\eta - \dot{v}_0^\star + \frac{k_1}{r}z. \tag{3.73}$$

This yields the dynamics

$$\begin{aligned} \dot{x} &= -\bar{y}_0(\bar{x}_1^0, \bar{x}_2^0) + k_1 z - d \\ \dot{z} &= -\frac{1}{m}x - \frac{k_1}{r}z \\ \dot{\eta} &= -\frac{k_2}{r}\eta + \frac{k_1}{r}(v_0^\star + z). \end{aligned} \tag{3.74}$$

It is clearly seen that the linear η–dynamics are driven by $v_0^\star + z$, so that the input–to–state stability property it trivially fulfilled. More precisely, observe that $u_\eta = k_1(v_0^\star + z)$ and that the Lyapunov function $V(\eta) = (1/2)\eta^2$ yields

$$\begin{aligned} \frac{d}{dt}V(\eta) &\leq -\frac{k_2}{r}\eta^2 + \frac{1}{r}|\eta||u_\eta| \\ &\leq -\left(\frac{k_2}{r} - \frac{\delta}{2r}\right)\eta^2 + \frac{1}{2\delta r}u_\eta^2 \\ &= -\alpha(|\eta|) + \sigma(|u_\eta|), \end{aligned} \tag{3.75}$$

with $\delta < 2k_2$, and where α and σ are class $\mathcal{K}_\infty$ functions. Consequently, the η–dynamics remains stable if $|v_0^\star(t) + z(t)|$ remains bounded. ◊

The presented results on bond graph based backstepping did not yet address possible disturbances entering the subsystem Σ: $H(x)$; however, it has been shown by Examples 3.2 and 3.3 that backstepping can be used for disturbance attenuation problems. Now, the presented theory can "in principle" be applied unmodified, but caution must be taken if the closed loop is to have a particular desired representation. The following proposition shows that relative degrees are instrumental to address disturbances.

Proposition 3.8. *Consider the recursive procedure of Proposition 3.5, but where the system* Σ: $H(x)$ *in Figure 3.19 has an additional input/output pair* $(d, w) \in \mathbb{R} \times \mathbb{R}$. *The disturbance is denoted as* d *and the conjugate output as* w. *Suppose that the cascaded pattern of quadratic* $\boldsymbol{C}$ *and* $\boldsymbol{I}$ *elements define the state variables* $(\xi_1, \ldots, \xi_k)$. *Then the closed loop in Figure 3.20 can be attained if* $y_0(x)$ *has a relative degree* $r_0 > k$ *with respect to* d.

Proof. Recall that each system $\bar{\Sigma}_j : \bar{H}_j(\bar{x}^j)$ with $j \geq 0$ is an explicit port–Hamiltonian system of the form

$$\begin{aligned} \dot{\bar{x}}^j &= [\bar{J}_j(\bar{x}^j) - \bar{R}_j(\bar{x}^j)]\bar{K}_j(\bar{x}^j) + \bar{g}_j(\bar{x}^j)\bar{u}_j \\ \bar{y}_j &= \bar{g}_j^T(\bar{x}^j)\bar{K}_j(\bar{x}^j) + \bar{b}_j(\bar{x}^j)\bar{u}_j. \end{aligned} \tag{3.76}$$

Set $j = 0$ and $\bar{u}_0 = y_0(x)$, then it follows that

$$\frac{d^r}{dt^r}v_0^\star = -\frac{1}{a_1}\frac{d^r}{dt^r}\bar{y}_0(\bar{x}^0, y_0(x)). \tag{3.77}$$

This implies that (3.77) does not depend on d for $0 \leq r \leq k$. Now, the proposition is readily seen to be true for $k = 1$ since

$$\dot{z}_1 = -y_0(x) + a_2\xi_2 - \dot{v}_0^\star, \tag{3.78}$$

which does not depend on d by (3.77). To apply (3.59) in the following steps, set $k = 2$ and write

$$v_1^\star = \frac{1}{a_2}\left[\frac{d}{dt}v_0^\star - \bar{y}_1(\bar{x}^1, a_1 z_1)\right], \tag{3.79}$$

so that by taking $\dot{z}_2 = \dot{\xi}_2 - \dot{v}_1^\star$ it readily follows that

$$\dot{z}_2 = \dot{\xi}_2 - \frac{1}{a_2}\left[\frac{d^2}{dt^2}v_0^\star - \frac{d}{dt}\bar{y}_1(\bar{x}^1, a_1 z_1)\right]. \tag{3.80}$$

Continuing this scheme with $k = 3$ yields the virtual control

$$v_2^\star = \frac{1}{a_3}\left[a_1 v_0^\star + \frac{1}{a_2}\left[\frac{d^2}{dt^2}v_0^\star - \frac{d}{dt}\bar{y}_1(\bar{x}^1, a_1 z_1)\right] - \bar{y}_2(\bar{x}^2, a_2 z_2)\right], \tag{3.81}$$

so that with $\dot{z}_3 = \dot{\xi}_3 - \dot{v}_2^\star$ this gives

$$\dot{z}_3 = \dot{\xi}_3 - \frac{1}{a_3}\left[a_1\frac{d}{dt}v_0^\star + \frac{1}{a_2}\left[\frac{d^3}{dt^3}v_0^\star - \frac{d^2}{dt^2}\bar{y}_1(\bar{x}^1, a_1 z_1)\right] - \frac{d}{dt}\bar{y}_2(\bar{x}^2, a_2 z_2)\right]. \tag{3.82}$$

It is clear that $\dot{z}_2$ depends on at most $d^2v_0^\star/dt^2$ and that $\dot{z}_3$ depends on at most $d^3v_0^\star/dt^3$. The above procedure can be continued by back–substitution of previously defined virtual controls and their time derivatives. In addition, the various time derivatives of $\bar{y}_i(\bar{x}^i, a_i z_i)$ can be resolved through (3.76) and the relations $z_i = \xi_i - v_{i-1}^\star$. Then, by (3.77) and $r_0 > k$, it is seen that the closed loop in Figure 3.20 is attainable since $\dot{z}_k$ depends on at most $d^k v_0/dt^k$, proving that the disturbance d does not enter the z–dynamics. □

Various techniques for bond graph based backstepping have been presented, but this section is by no means exhaustive and further extensions of the various developments are readily conceivable. For example, the class of systems suitable for bond graph based backstepping can be further enlarged by certain modulations of the systems $\bar{\Sigma}_j$: $H_j(x^j)$. In any case, it is safe to say that valuable problems have been presented to allow for such extensions to be developed in the future.

Bond graph based backstepping as considered here addresses the case in which no derivative causalities are induced by the bond graph topology. It can be argued that such bond graph models belong to a relatively small subset of models, rendering the backstepping method somewhat limited. Future research could look into bond graph based backstepping in case of dependent storage elements, but this can be expected to be more complex.

3.2.3. Multi–Input Systems

This section briefly shows how the results of the previous sections can be applied to multi–input systems, but no attempt is made to develop additional results since the techniques for the single–input case readily transfer to the multi–input case.

For simplicity, consider a multi–input bond graph model as the port–Hamiltonian system

$$\begin{aligned}
\dot{x} &= [J(x) - R(x)]K(x) + g_j(x)a_1^j\xi_1^j \\
\dot{\xi}_1^j &= -g_j^T(x)K(x) + a_2^j\xi_2^j \\
\dot{\xi}_2^j &= -a_1^j\xi_1^j + a_3^j\xi_3^j \\
&\vdots \\
\dot{\xi}_{n_j}^j &= -a_{n_j-1}^j\xi_{n_j-1}^j - u_j,
\end{aligned} \tag{3.83}$$

where $x \in \mathbb{R}^n$ and $\xi^j = (\xi_1^j, \ldots, \xi_{n_j}^j)$. Observe that Proposition 3.4 can be applied to each branch $\xi^j \in \mathbb{R}^{n_j}$, where the application of Proposition 3.5 is possible also. Towards that end, the design starts with the relations

$$a_1^j\xi_1^j = -\bar{y}_{0j}(\bar{x}^{0j}, y_{0j}(x)) + a_1^j z_1^j, \tag{3.84}$$

where the recursive scheme applies to all relation (3.84) in parallel fashion. Depending on the various values n_j, the backstepping design may lead to certain controls u_j to depend on other controls u_i, hence the lowest dimensional branch ξ^j is to be resolved first.

Example 3.7. Consider the two–input system in Figure 3.24 with the element definitions

$$\mathrm{C}_1(\xi_1^1) = \frac{1}{2}k_1^1(\xi_1^1)^2, \quad \mathrm{C}_2(\xi_1^2) = \frac{1}{2}k_1^2(\xi_1^2)^2, \quad \mathrm{I}_1(\xi_2^1) = \frac{1}{2m_2^1}(\xi_2^1)^2, \quad \mathrm{I}_2(x) = \frac{1}{2m}x^2. \tag{3.85}$$

The control objective is to impose the closed dynamics with the bond graph representation of Figure 3.25. Even though it may seem that the control problem is considerably more complex than the single–input case, the backstepping design for single–input systems can be applied without modification.

From Figure 3.25 it follows that the virtual actuator is given as a single resistive $\overline{\mathrm{R}}$ element, where the causal path from this resistive element to both controls emanates from a common 1–junction. In such a scenario it is possible to fictitiously replace the $\overline{\mathrm{R}}$ element with two resistive elements and to assign the corresponding virtual actuator outputs $\bar{y}_{01}$ and $\bar{y}_{02}$

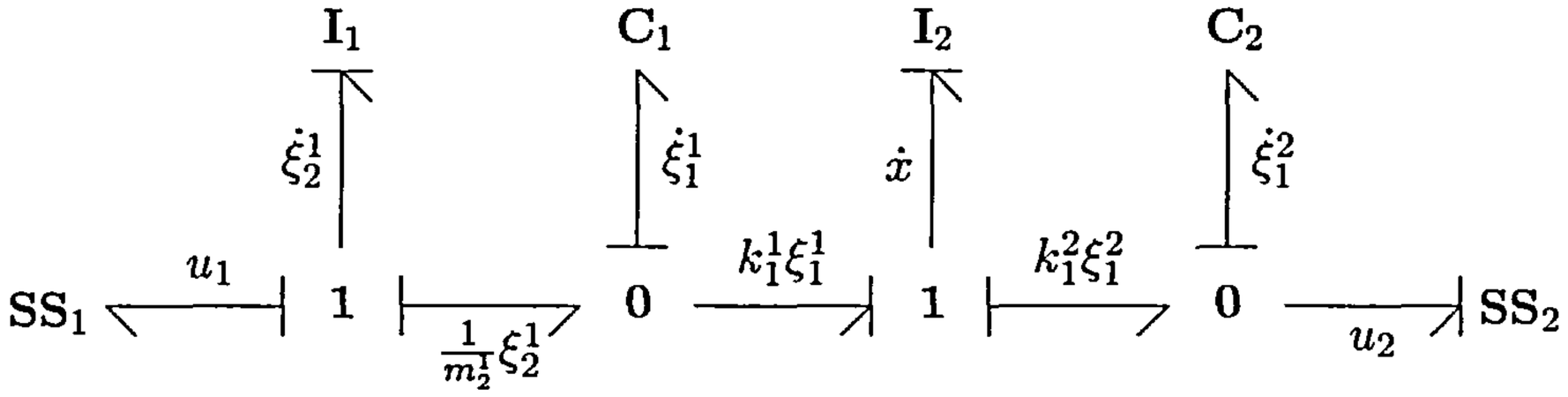

Figure 3.24.: Two–input system of Exercise 3.7.

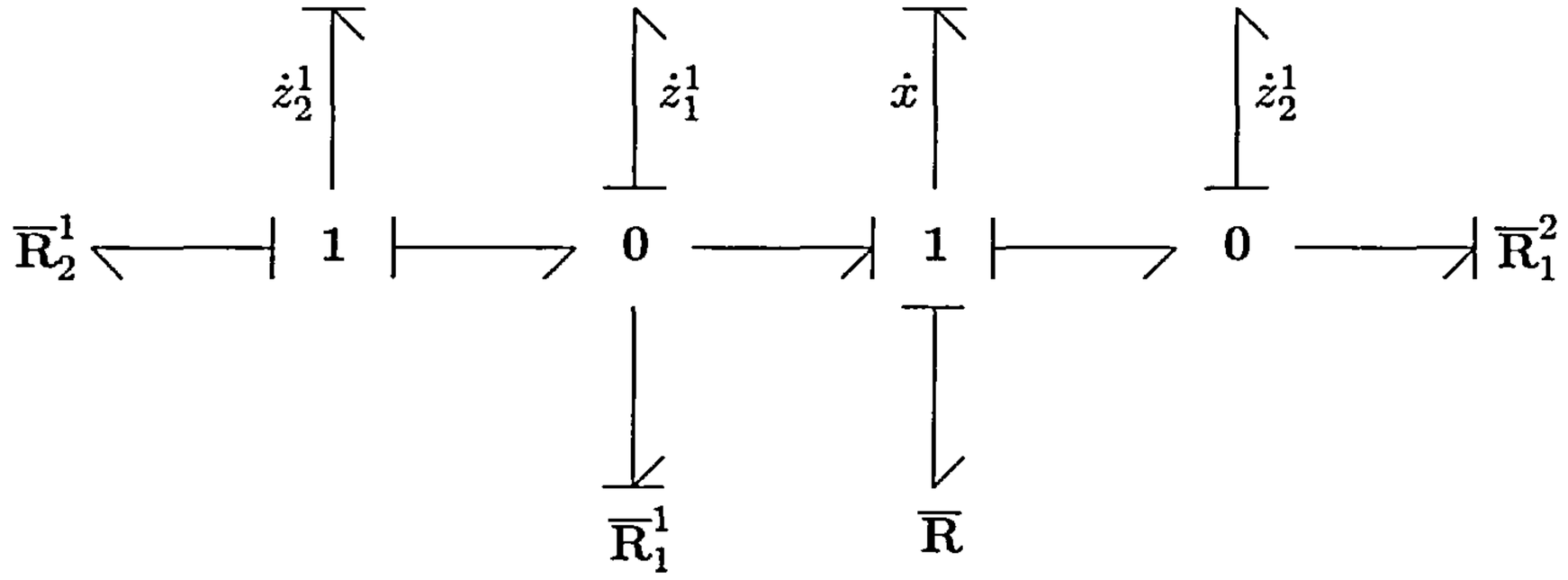

Figure 3.25.: Target closed loop of Exercise 3.7.

to the corresponding signals $k_1^1\xi_1^1$ and $k_1^2\xi_1^2$. Now, causal analysis yields the dynamics

$$\begin{aligned} \dot{x} &= k_1^1\xi_1^1 - k_1^2\xi_1^2 \\ \dot{\xi}_1^1 &= -\frac{1}{m}x + \frac{1}{m_2^1}\xi_2^1 \\ \dot{\xi}_2^1 &= -k_1^1\xi_1^1 - u_1 \\ \dot{\xi}_1^2 &= \frac{1}{m}x - u_2, \end{aligned} \tag{3.86}$$

which are of the form (3.83) with $J(x) = R(x) = 0$, $g_1(x) = 1$ and $g_2(x) = -1$. In accordance with (3.84), define the change of variables

$$\begin{aligned} k_1^1\xi_1^1 = -\frac{\bar{r}}{2m}x + k_1^1 z_1^1 \qquad &\Longrightarrow \qquad v_{01}^\star = -\frac{\bar{r}}{2k_1^1 m}x \\ k_1^2\xi_1^2 = \frac{\bar{r}}{2m}x + k_1^2 z_1^2 \qquad &\Longrightarrow \qquad v_{02}^\star = \frac{\bar{r}}{2k_1^2 m}x, \end{aligned} \tag{3.87}$$

yielding

$$\begin{aligned} \dot{z}_1^1 &= -\frac{1}{m}x + \frac{1}{m_2^1}\xi_2^1 - \dot{v}_{01}^\star \\ \dot{z}_1^2 &= \frac{1}{m}x - u_2 - \dot{v}_{02}^\star. \end{aligned} \tag{3.88}$$

As in the single–input case, the target dynamics in Figure 3.25 shows that one can choose the change of variable

$$\frac{1}{m_2^1}\xi_2^1 = -\frac{1}{\bar{r}_1^1}k_1^1 z_1^1 + \dot{v}_{01}^\star + \frac{1}{m_2^1}z_2^1 \qquad \Longrightarrow \qquad v_{11}^\star = -\frac{m_2^1}{\bar{r}_1^1}k_1^1 z_1^1 + m_2^1 \dot{v}_{01}^\star \tag{3.89}$$

and the regular control

$$u_2 = \frac{1}{\bar{r}_1^2} k_1^2 z_1^2 - \dot{v}_{02}^\star. \tag{3.90}$$

The z_2^1–dynamics takes the form

$$\dot{z}_2^1 = -k_1^1 z_1^1 + \frac{\bar{r}}{2m} x - u_1 - \dot{v}_{11}^\star, \tag{3.91}$$

from which to choose the control

$$u_1 = -k_1^1 v_{01}^\star - \dot{v}_{11}^\star + \frac{\bar{r}_2^1}{m_2^1} z_2^1. \tag{3.92}$$

The design technique considered so far is identical to the procedure for single–input systems except that two branches must considered instead. Also, it is readily checked that the expansion of the control u_1 requires the definition for u_2. This is readily explained by observing that $n_1 = 2$ and $n_2 = 1$. By applying both controls to the plant in Figure 3.24, the target closed loop allows for the port–Hamiltonian representation

$$\begin{bmatrix} \dot{x} \\ \dot{z}_1^1 \\ \dot{z}_2^1 \\ \dot{z}_1^2 \end{bmatrix} = \begin{bmatrix} -\bar{r} & 1 & 0 & -1 \\ -1 & -1/\bar{r}_1^1 & 1 & 0 \\ 0 & -1 & -\bar{r}_2^1 & 0 \\ 1 & 0 & 0 & -1/\bar{r}_1^2 \end{bmatrix} \begin{bmatrix} x/m \\ k_1^1 z_1^1 \\ z_2^1/m_2^1 \\ k_1^2 z_1^2 \end{bmatrix}, \tag{3.93}$$

which is globally asymptotically stable.

Note that simple quadratic C_1, C_2, I_1 elements have been considered so far, but the structure of the port–Hamiltonian dynamics (3.83) shows that Proposition 3.4 can be used for branches having nonlinear elements. In such cases, the relationships (3.87) read

$$\begin{aligned} \lambda_1^1(\xi_1^1) &= -\frac{\bar{r}}{2m} x + k_1^1 z_1^1 \\ \lambda_1^2(\xi_1^2) &= \frac{\bar{r}}{2m} x + k_1^2 z_1^2, \end{aligned} \tag{3.94}$$

so that

$$\begin{aligned} \dot{z}_1^1 &= \frac{1}{k_1^1} (\lambda_1^1)'(\xi_1^1) \left[-\frac{1}{m} x + \lambda_2^1(\xi_2^1) \right] + \frac{\bar{r}}{2m} \dot{x} \\ \dot{z}_1^2 &= \frac{1}{k_1^2} (\lambda_1^2)'(\xi_1^2) \left[\frac{1}{m} x - u_2 \right] - \frac{\bar{r}}{2m} \dot{x}. \end{aligned} \tag{3.95}$$

Next enforce the relation

$$\lambda_2^1(\xi_2^1) = \frac{1}{m} x + \frac{k_1^1}{(\lambda_1^1)'(\xi_1^1)} \left[-\frac{\bar{r}}{2m} \dot{x} - \frac{1}{m} x - \frac{1}{\bar{r}_1^1} k_1^1 z_1^1 + \frac{1}{m_2^1} z_2^1 \right] \tag{3.96}$$

and the control

$$u_2 = \frac{1}{m} x + \frac{k_1^2}{(\lambda_1^2)'(\xi_1^2)} \left[-\frac{\bar{r}}{2m} \dot{x} - \frac{1}{m} x + \frac{1}{\bar{r}_1^2} k_1^2 z_1^2 \right]. \tag{3.97}$$

The z_2^1–dynamics is now given as

$$\dot{z}_2^1 = \frac{m_2^1}{k_1^1}\frac{d}{dt}\left[(\lambda_1^1)'(\xi_1^1)\right]\left[\lambda_2^1(\xi_2^1) - \frac{1}{m}x\right] + \frac{m_2^1}{k_1^1}(\lambda_1^1)'(\xi_1^1)\left[(\lambda_2^1)'(\xi_2^1)[-k_1^1\xi_1^1 - u_1] - \frac{1}{m}x\right] + m_2^1\left[\frac{\bar{r}}{2m}\ddot{x} + \frac{1}{m}\dot{x} + \frac{1}{\bar{r}_1^1}k_1^1\dot{z}_1^1\right]. \quad (3.98)$$

Finally, choose the control u_1 that cancels the right–hand side of (3.98), where the desired target dynamics is imposed by further control. Note that u_2 is needed to do so. ◊

3.3. Bicausal Bond Graphs in Backstepping Control

The previous sections primarily used the bond graph to define the plant and the closed loop target dynamics, which comprised the explicit bond graph models $\bar{\Sigma}_j\colon \bar{H}_j(\bar{x}^j)$ for $j \geq 0$. In particular, the characteristic step of the backstepping procedure was shown to be a proper change of coordinates to induce a closed loop bond graph identical to the plant with additional elements. It can be shown that some of the design steps can be performed through the sole application of bicausality [Gaw01]. More precisely, instead of manually going through the various changes of variables, bicausal assignment can be used to immediately derive the backstepping controller without the explicit introduction of new variables.

Most of the material presented will use the examples of Section 3.2.1 and the various results of Section 3.2.2, thereby facilitating comparisons with the bicausal approach. It should be noted that in [Gaw01] the connection between the "Bond Graph Based Control with Virtual Actuators" and bond graph based backstepping is recognised. This section intends to complement that paper by showing a different account on bicausality in bond graph based backstepping.

In [Gaw01], it is shown that bond graph based backstepping is possible through the (bi)causal inversion mechanism, but the paper does not address these ideas in great detail other than through the motivational Example 3.2 in Section 3.2.1. The main impetus of this section is therefore to complement [Gaw01] by showing that the bicausal approach does indeed yield certain *exact* backstepping controllers for particular problems. Furthermore, it will be shown that the bicausal approach is applicable when no stabilising dynamics $\bar{\Sigma}_j\colon \bar{H}_j(\bar{x}^j)$ is to be imposed, where the **C** and **I** elements are assumed to be quadratic. The following proposition structures these ideas.

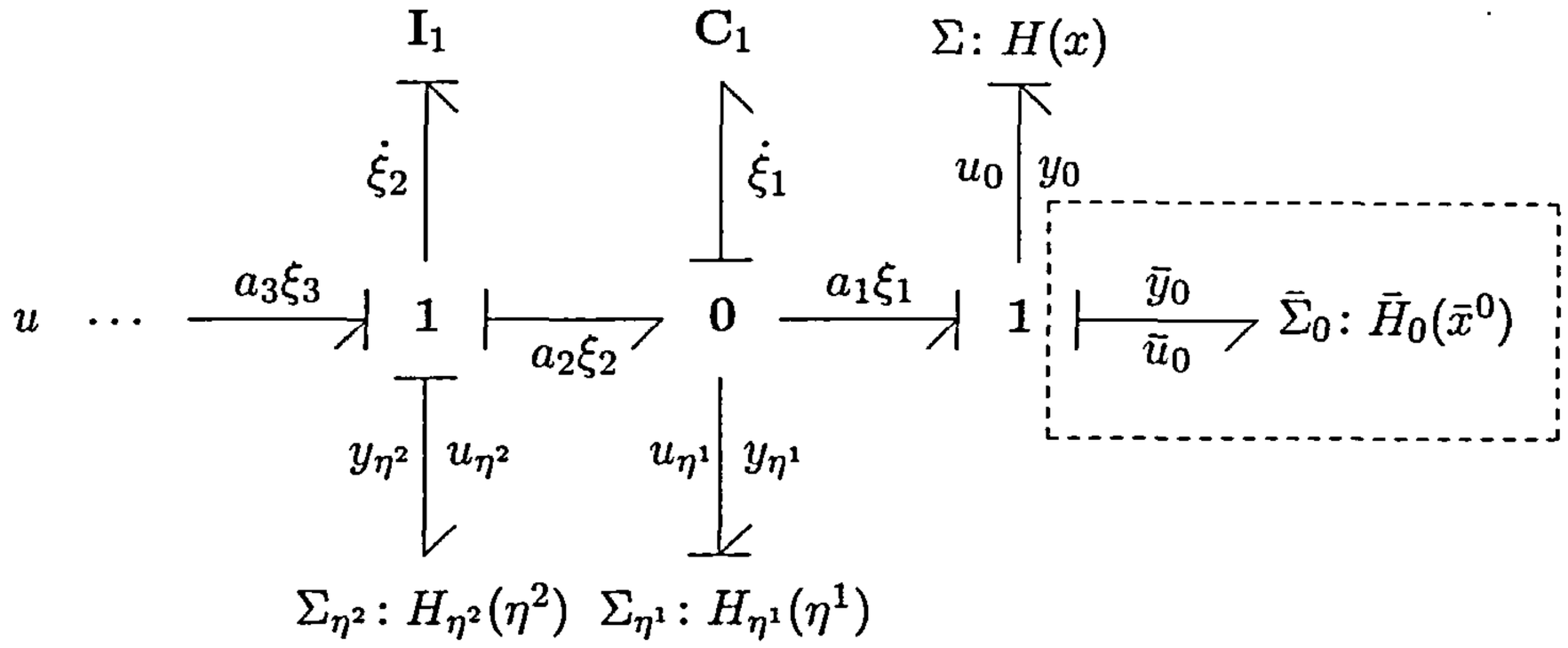

Figure 3.26.: Extended cascaded bond graph of Proposition 3.9.

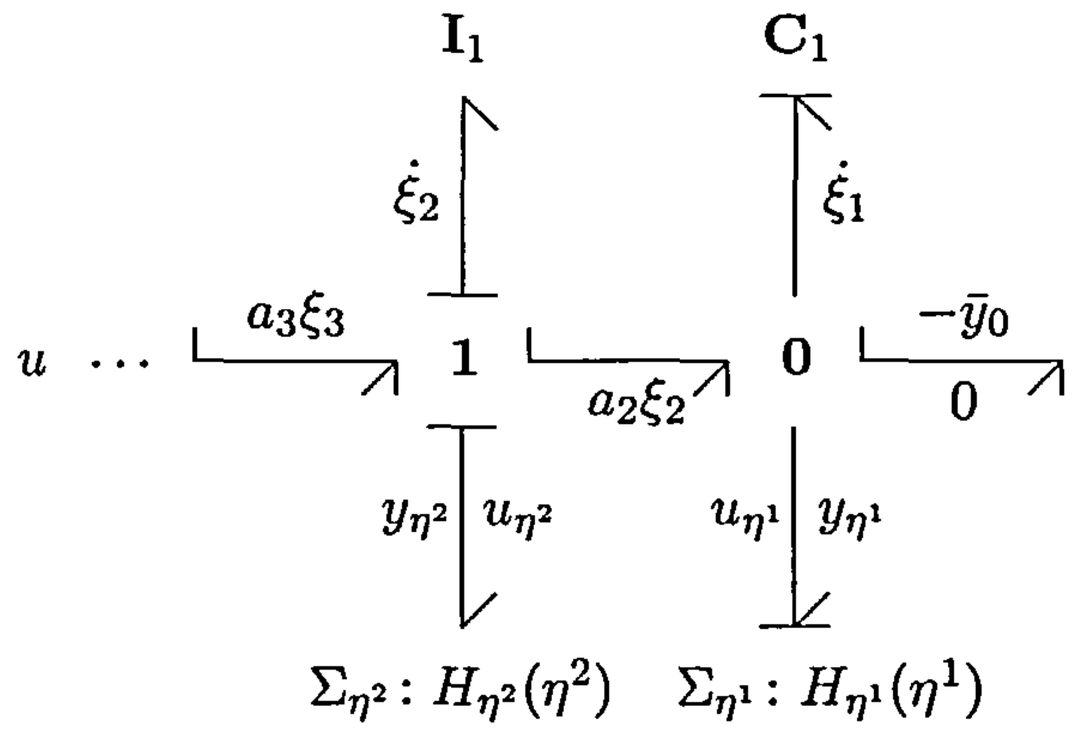

Figure 3.27.: Bicausal extended cascaded C and I pattern of Proposition 3.9.

Proposition 3.9. *Consider the bond graph in Figure 3.26 and the bicausal bond graph in Figure 3.27. Suppose that the cascaded elements have the definitions* (3.54) *and that*

$$y_{\eta^j}(\eta^j, u^1_{\eta^j} + u^2_{\eta^j}) = y_{\eta^j}(\eta^j, u^1_{\eta^j}) + y_{\eta^j}(\eta^j, u^2_{\eta^j}). \tag{3.99}$$

Then the bicausal bond graph yields a smooth feedback $u(x, \xi, \eta^j)$ *that induces the closed loop dynamics of Figure 3.28.*

Proof. Consider the change of variable

$$a_1\xi_1 = -\bar{y}_0 + a_1 z_1 = a_1 v_0^\star + a_1 z_1, \tag{3.100}$$

giving the z_1–dynamics

$$\begin{aligned} \dot{z}_1 &= -y_0 - y_{\eta^1}(\eta^1, a_1\xi_1) + a_2\xi_2 - \dot{v}_0^\star \\ &= -y_0 - y_{\eta^1}(\eta^1, a_1 z_1) + a_2\xi_2 - y_{\eta^1}(\eta^1, a_1 v_0^\star) - \dot{v}_0^\star. \end{aligned} \tag{3.101}$$

Suppose that the original port–Hamiltonian structure is to be retained and that no stabilising dynamics $\bar{\Sigma}_1 : \bar{H}_1(\bar{x}^1)$ are imposed. The virtual control $a_2\xi_2$ then becomes

$$a_2\xi_2 = \dot{v}_0^\star + y_{\eta^1}(\eta^1, a_1 v_0^\star) + a_2 z_2 = a_2 v_1^\star + a_2 z_2. \tag{3.102}$$

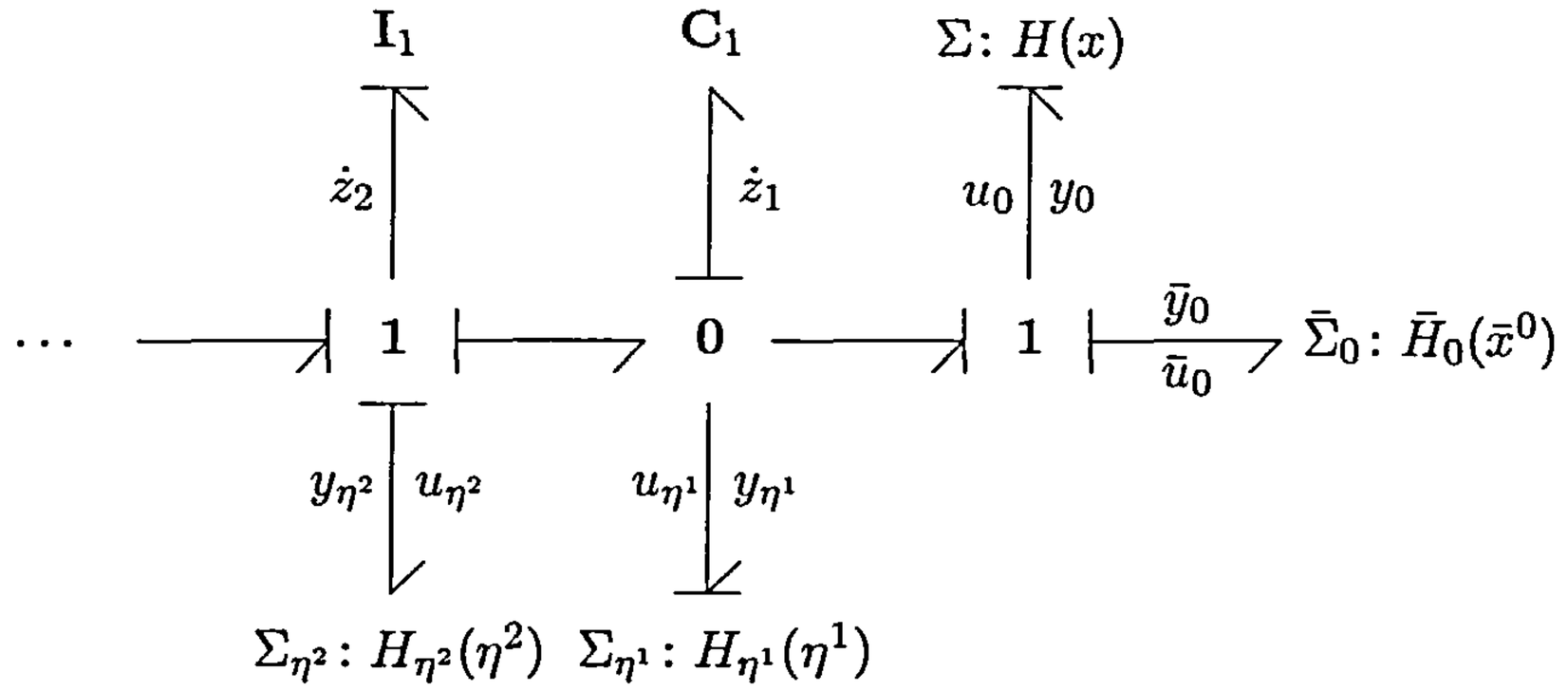

Figure 3.28.: Closed loop dynamics with bicausal approach of Proposition 3.9.

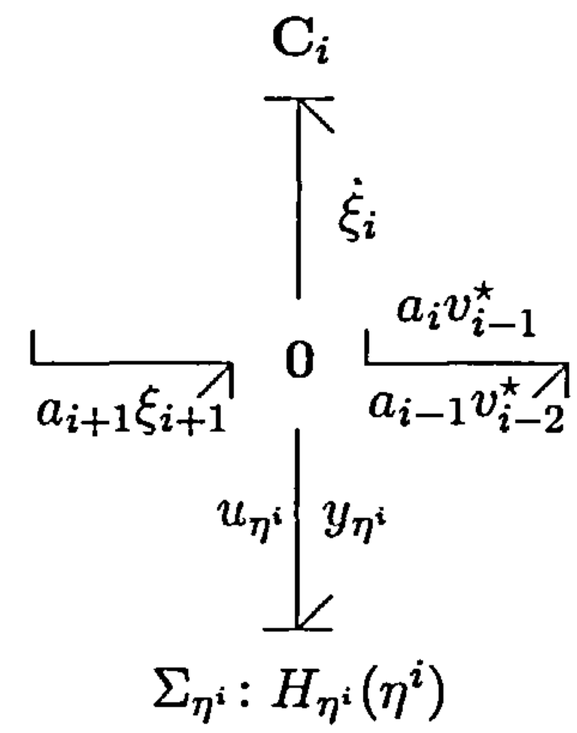

Figure 3.29.: Generic C_i backstepping junction of Proposition 3.9.

Recall that $a_1 v_0^\star = -\bar{y}_0$ and consider the bicausal bond graph in Figure 3.27. Bicausal analysis then shows that the bond signal $a_2\xi_2$ coincides with (3.102) for $z_2 = 0$. Thus, for a one–step design it follows that the bicausal approach coincides with the backstepping controller. Continuing with (3.102) yields the z_2–dynamics

$$\begin{aligned}\dot{z}_2 &= -a_1\xi_1 - y_{\eta^2}(\eta^2, a_2\xi_2) + a_3\xi_3 - \dot{v}_1^\star \\ &= -a_1 z_1 - y_{\eta^2}(\eta^2, a_2 z_2) - a_1 v_0^\star - y_{\eta^2}(\eta^2, a_2 v_1^\star) + a_3\xi_3 - \dot{v}_1^\star,\end{aligned} \tag{3.103}$$

therefore

$$a_3\xi_3 = a_1 v_0^\star + y_{\eta^2}(\eta^2, a_2 v_1^\star) + \dot{v}_1^\star + a_3 z_3. \tag{3.104}$$

Set $z_3 = 0$ and observe that bicausal analysis yields the virtual control (3.104). The recursive process continues for $j \geq 2$ as

$$\begin{aligned}\dot{z}_j &= -a_{j-1}\xi_{j-1} - y_{\eta^j}(\eta^j, a_j\xi_j) + a_3\xi_3 - \dot{v}_{j-1}^\star \\ &= -a_{j-1} z_{j-1} - y_{\eta^j}(\eta^j, a_j z_j) - a_{j-1} v_{j-2}^\star - y_{\eta^j}(\eta^j, a_j v_{j-1}^\star) + a_{j+1}\xi_{j+1} - \dot{v}_{j-1}^\star.\end{aligned} \tag{3.105}$$

The virtual controls are of the form

$$a_{j+1}\xi_{j+1} = a_{j-1} v_{j-2}^\star + y_{\eta^j}(\eta^j, a_j v_{j-1}^\star) + \dot{v}_{j-1}^\star + a_{j+1} z_{j+1}. \tag{3.106}$$

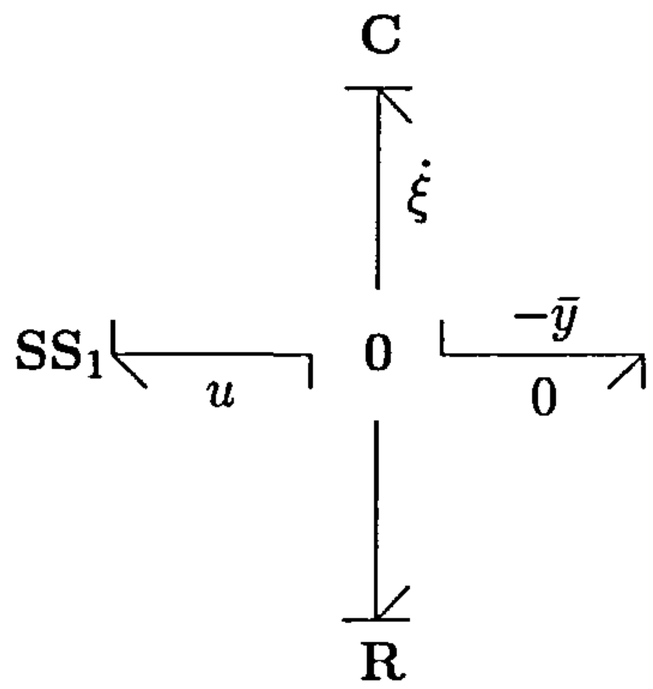

Figure 3.30.: Backstepping with bicausal assignment; Example 3.8.

Now, the bicausal bond graph does not introduce new variables, so that it follows that (3.106) must impose $z_{j+1} = 0$ if the virtual controls $a_{j+1}\xi_{j+1}$ are to coincide with the bicausal mechanism. Further causal analysis of Figure 3.27 yields the generic $\mathbf{C}_i$ backstepping junctions depicted in Figure 3.29, where it should be noted that the indexing does not conform to (3.60) but merely reflects the relationships between the various bond signals incident to the 0–junctions. Of course, the generic $\mathbf{I}_i$ has the same bond signal relationships.

Finally, the virtual control $a_{i+1}\xi_{i+1}$ is now seen to coincide with (3.106) for $z_{j+1} = 0$, but is must be noted that the obtained closed loop port–Hamiltonian dynamics by means of the bicausal approach still require the variables z_j for their definition. □

It can be concluded that the exposition in [Gaw01] does indeed produce a class of exact backstepping controllers; however, the bicausal bond graph does not introduce new variables to define the dynamics $\bar{\Sigma}_j : H_j(\bar{x}^j)$, thereby restricting the class of systems. That is to say that the bicausal inversion mechanism retains the plant structure but does not provide tools to define further stabilising dynamics without resorting to the new variables z_j.

Example 3.8. The controller (3.16) of Example 3.2 is obtained by means of the bicausal bond graph in Figure 3.30. To see this, observe that $y_\eta(\eta, u_\eta) = u_\eta/r$ and therefore the condition (3.99) is satisfied. Bicausal analysis then yields the control

$$u = \frac{1}{r}\bar{y}_0 + \frac{1}{k}\dot{\bar{y}}_0, \tag{3.107}$$

where Proposition 3.9 confirms the closed loop in Figure 3.8. It can be concluded that the bicausal bond graph provides a "shortcut" for the backstepping design but for which the closed loop bond graph representation requires the variables z_j. ◊

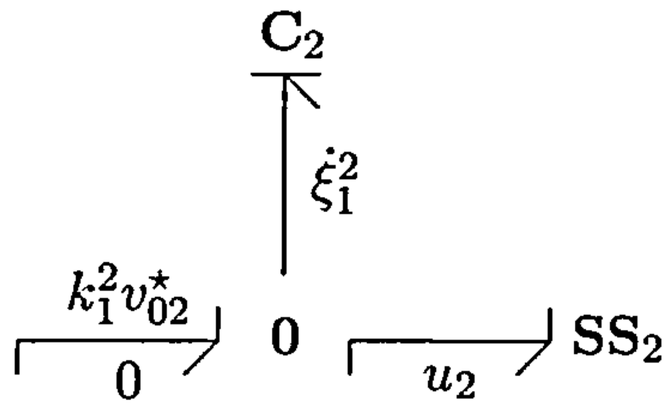

Figure 3.31.: Bicausal backstepping towards u_2; Example 3.9.

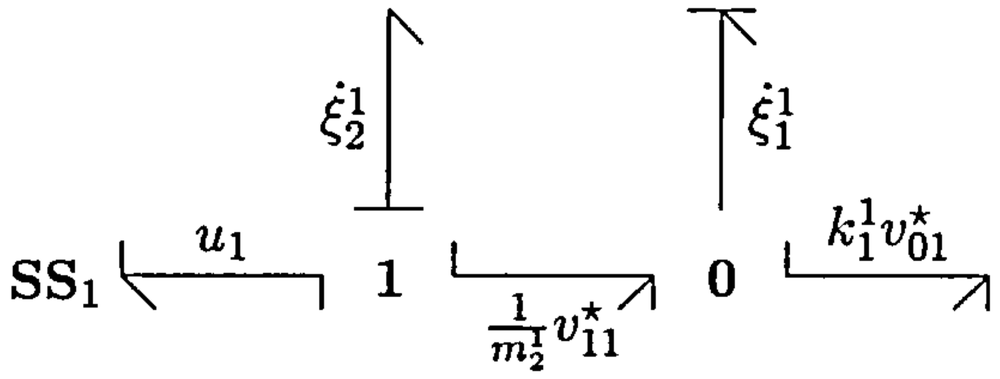

Figure 3.32.: Bicausal backstepping towards u_1; Example 3.9.

In [Gaw01], only the single–input case is considered, however, the multi–input system (3.83) shows that bicausality can be applied for such multi–input scenarios. The following example complements [Gaw01] by applying Proposition 3.9 to a multi–input case and shows that the closed loop does not comprise any stabilising dynamics, thereby retaining the original structure of the system.

Example 3.9. Consider, once again, the system in Figure 3.24 and the associated bicausal bond graphs in Figures 3.31 and 3.32. Clearly, u_2 must be found first since $\xi^1 = (\xi_1^1, \xi_2^1)$ and $\xi^2 = \xi_1^2$. The control u_2 is immediate from Figure 3.31, being

$$u_2 = -\dot{v}_{02}, \tag{3.108}$$

which coincides with (3.90) for $z_1^2 = 0$. Then, from Figure 3.32, the control u_1 becomes

$$u_1 = -k_1^1 v_{01}^\star - \dot{v}_{11}^\star, \tag{3.109}$$

so that u_1 coincides with (3.92) for $z_2^1 = 0$. ◊

3.4. Conclusions

This chapter contributes certain results on bond graph based backstepping control that were inspired by the works [Yeh99], [Yeh01], [Yeh02], [Gaw01] and references therein. The novelty of the presented results are the applications of judiciously chosen virtual control laws to allow for closed loop bond graph representations.

Crucial to all developments is that backstepping control is capable of inducing bond graph based dynamics provided that the virtually actuated subsystem has certain port–Hamiltonian properties. More precisely, the fact that bond graphs have intrinsic port–Hamiltonian properties [Gol02] clearly shows the connections between backstepping and bond graph modelling. This observation readily materialises by taking the virtually actuated system as a bond graph so that the backstepping design can be made to retain the original port–Hamiltonian structure of the dynamics through which to "step back". These ideas show that such an approach is both pragmatic and effective; however, as with all backstepping designs, new variables for the states "between" the virtual control and regular control have to be introduced. Consequently, the closed loop is port–Hamiltonian with respect to the states of the virtually actuated subsystem and the *new* coordinates. This last point is important, because the states of the virtually actuated trajectories can be made to emulate the trajectories of another physical system.

The bond graph based backstepping method shows to allow for certain disturbances to enter the virtually actuated subsystem, provided a relative degree condition is fulfilled. If such relative degree conditions are not satisfied, then the backstepping controller may depend on the disturbance and its time derivatives. This would be problematic since disturbances are generally assumed *not* to be measurable.

Multi–input systems show to be solvable by means of the single–input case, but no further results have been elaborated since the single–input case readily transfers to multi–input systems. Even though such extensions to multi–input systems are relatively straightforward, it should be observed that the regular controls are likely to have different relative degrees with respect to the virtual controls. This implies that regular controls with the lowest relative degrees have to be resolved first.

Finally, the bicausal approach does indeed yield a class of backstepping controllers, but the approach only works on a smaller class of systems since new variables are not part of the controller design. Consequently, stabilising dynamics remain somewhat difficult to define from within the bicausal approach. Like the single–input case, multi–input backstepping problems can be solved through (bi)causal assignment, but it also suffers from the lack of further stabilisation.

4. Model Matching Control

4.1. Introduction

The (non)linear Model Matching Problem (MMP) addressed in Section 2.3 applies to the affine plant (2.31) and model (2.32). However, it can be of interest to specialise these affine systems to certain physical models, where both P and M describe physical behavior such that the MMP incorporates a form of "physical equivalence" as outlined in [Sha91]. Put differently, the plant is to be controlled in way that attaches explicit physical behavior to the input/output dynamics associated with the prescribed physical model M. Such control method would represent the physical design objective by means of modelling arguments instead of a sole signal theoretic approach.

This section presents applications of the bond graph based MMP for which the control objective has a physical interpretation. The main ingredients of a typical application considered here is as follows. It is intended to specify the MMP through bond graph representations of the plant and model, so that P and M belong to a class of port–Hamiltonian systems. Then, once P and M are defined, the natural passive outputs of the bond graphs are often not to be controlled as mentioned in Section 2.3.1. Consequently, redefinition of such passive outputs may be required, where the model M will be defined to contain a copy of the plant and be "close" to the plant in structural sense. This will allow a necessary relative degree condition to be satisfied.

The key aspects of this chapter are not about strict design steps such as bond graph based backstepping. This chapter shows that the closed loop bond graph representation may be inferred, in some cases, from the plant in accordance with the MMP theory presented in Section 2.3. Furthermore, bicausal bond graphs are used whenever possible to find the decoupling controller through (bi)causal inversion, where the constrained dynamics that describes the matching of the plant and model outputs must be found in a conventional manner.

There may exist certain MMP scenarios that need not be efficiently solved through a bicausal inversion mechanism. Indeed, the problem that could hinder such application of bicausality is that the Standard Causality Assignment Procedure (SCAP) does not efficiently model the plant bond graph, or that plant outputs are difficult to define through **SS** components. More precisely, it is known that SCAP can yield unnecessary complex dynamics due to the "inefficient" selection of state variables. To remedy such problems, alternative causality assignment procedures can be used to simplify the dynamics significantly [Mar02]. For example, in the mechanical domain it is often the case that the Lagrangian Causality Assignment Procedure (LCAP) provides a more efficient method to obtain second order dynamics, which can be readily transformed into first order form. However, LCAP is difficult to use in the bicausal context, mainly because bicausal assignment is typically applied to bond graphs that are causally assigned with SCAP. Also, there are no available results on this matter in the current literature. This chapter will address the above considerations in more detail.

Even though the bicausal bond graph mechanism will be used for inversion purposes whenever possible, certain outputs may not be readily modelled with **SS** components such that the bicausal mechanism becomes problematic. This can occur when outputs appeár nonlinearly in the model or when they are functions of state variables. As a result, the **SS** component is not a suitable solution for extracting the output of the bond graph, rendering bicausal inversion not applicable due to the absence of suitable **SS** components that define the required output. These issues will be elaborated in later sections.

Bond graphs that contain nonlinear modulations often restrict the applicability of feedback linearising designs, since the dynamics need not have a well–defined relative degree on some domain of interest. To render the MMP solvable, it is quite natural to address the linearised MMP instead. The bond graphs for P and M do not change, but their induced dynamics is linearised around some point of interest. It will be shown that the closed loop bond graph is then merely associated with input/output dynamics of the prescribed model.

It must be acknowledged that the MMP considered here is nothing new in itself, but the specific application of physical considerations through bond graph modelling can be seen as a novel contribution. Furthermore, and this holds for all bond graph based MMPs, the output regulation problem addressed in Section 2.3.2 provides control theoretical foundations that were previously non–existent in the bond graph literature.

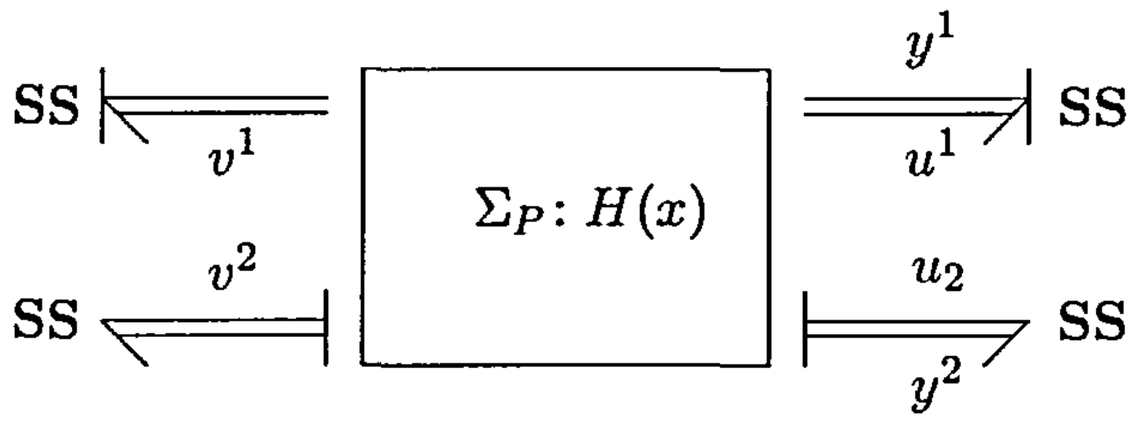

Figure 4.1.: Plant input/output configuration.

4.2. Virtual Actuation of Input/Output Dynamics

This section addresses virtual actuation in input/output sense, which is different from the virtual actuation concept in backstepping. The input/output dynamics of the plant is to be controlled in a manner that emulates the input/output dynamics of the plant with external dynamics. Such control objective can be specified with a model that comprises an *exact* copy of the plant, where additive dynamics represents the external dynamics. The plant is a bond graph model with a subset of passive outputs ignored. The model, on the other hand, is a standard bond graph model.

Consider the plant P in Figure 4.1, where $u = (u^1, u^2)$, $y = (y^1, y^2)$ and $v = (v^1, v^2)$. The input and output variables have the dimensions

$$\begin{aligned} v^1 &= (v^1_1, \ldots, v^1_{m_1}), \quad v^2 = (v^2_1, \ldots, v^2_{m_2}) \\ u^1 &= (u^1_1, \ldots, u^1_{p_1}), \quad y^1 = (y^2_1, \ldots, y^2_{p_1}) \\ u^2 &= (u^1_1, \ldots, u^1_{p_2}), \quad y^2 = (y^2_1, \ldots, y^2_{p_2}) \end{aligned} \tag{4.1}$$

with $m_1 + m_2 = m$ and $p_1 + p_2 = m$. The superscript $(\cdot)^1$ associates its variables with flow sources whereas the superscript $(\cdot)^2$ associates its variables with effort sources. The Hamiltonian is denoted as the smooth, real–valued function $H\colon X \to \mathbb{R}$. Bond graph storage and dissipative elements are contained in Σ_P.

Next consider the model M depicted in Figure 4.2, where $\bar{u} = (\bar{u}^1, \bar{u}^2)$ and $\bar{y} = (\bar{y}^1, \bar{y}^2)$. The dimensions of the model inputs and outputs are

$$\begin{aligned} \bar{u}^1 &= (\bar{u}^1_1, \ldots, \bar{u}^1_{p_1}), \quad \bar{y}^1 = (\bar{y}^2_1, \ldots, \bar{y}^2_{p_1}) \\ \bar{u}^2 &= (\bar{u}^1_1, \ldots, \bar{u}^1_{p_2}), \quad \bar{y}^2 = (\bar{y}^2_1, \ldots, \bar{y}^2_{p_2}). \end{aligned} \tag{4.2}$$

The model Hamiltonian is denoted as the smooth, real–valued function $\bar{H}\colon \bar{X} \to \mathbb{R}$. Bond graph storage and dissipative elements are contained in Σ_M.

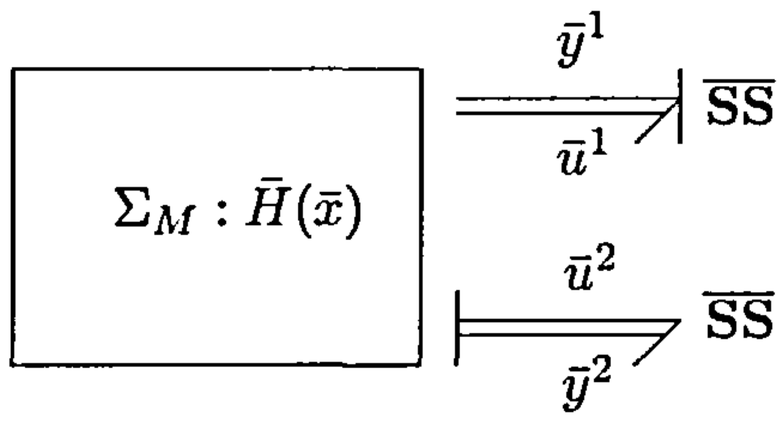

Figure 4.2.: Model input/output configuration.

The bond graph based MMP objective considered in this section can be clarified as follows. Suppose that the plant P has dynamics of the form

$$\begin{aligned} \dot{x} &= [J(x,\mu) - R(x,\mu)]K(x,\mu) - g_j(x,\mu)u_j - q_i(x,\mu)v_i \\ y_j &= g_j^T(x,\mu)K(x,\mu), \end{aligned} \tag{4.3}$$

where $x \in \mathbb{R}^n$ are the states associated with the storage elements, and where the system inputs and outputs are $u, y \in \mathbb{R}^m$ and $v \in \mathbb{R}^m$. Physical parameters of the plant are $\mu = (\mu_1, \ldots, \mu_k)$ for some k. Then consider a model M described by

$$\begin{aligned} \begin{bmatrix} \dot{\bar{x}}^1 \\ \dot{\bar{x}}^2 \end{bmatrix} &= \begin{bmatrix} J(\bar{x}^1,\mu) - R(\bar{x}^1,\mu) & -S(\bar{x}^2) \\ S^T(\bar{x}^2) & \bar{J}(\bar{x}^2) - \bar{R}(\bar{x}^2) \end{bmatrix} \begin{bmatrix} K(\bar{x}^1,\mu) \\ \bar{K}(\bar{x}^2) \end{bmatrix} - \begin{bmatrix} g_j(\bar{x}^1,\mu) \\ 0 \end{bmatrix} \bar{u}_j \\ \bar{y}_j &= g_j^T(\bar{x}^1,\mu)K(\bar{x}^1,\mu), \end{aligned} \tag{4.4}$$

where $\bar{x}^1 \in \mathbb{R}^n$, $\bar{x}^2 \in \mathbb{R}^{\bar{n}}$ and $\bar{u}, \bar{y} \in \mathbb{R}^m$.

The above definitions of P and M show that the plant $\bar{x}^1$–dynamics can be seen to be "actuated" by the $\bar{x}^2$–dynamics of the model. To implement the idea that the (u,y)–dynamics matches the $(\bar{u},\bar{y})$–dynamics should be the result of imposing the condition $u = \bar{u}$ as a partial solution to the nonregular DDDP with disturbance measurement. Note that the plant (4.3) is derivable from *explicit* port–Hamiltonian dynamics associated with the bond graphs in Figure 4.1. So, for the following developments, it is assumed that the bond graph of P yields *explicit* port–Hamiltonian dynamics that take the form (4.3) when the conjugate outputs to v are ignored. Such explicit systems are typically obtained from bond graphs that have no storage elements in derivative causality.

By definition of P and M it follows that the relative degree condition $r_i \leq \bar{r}_i$ is fulfilled. The solvability of the MMP considered here now depends on whether the bicausal bond graph in Figure 4.3 exists and that $u = \bar{u}$ is fulfilled to render the difference $y - \bar{y}$ independent of $\bar{u}$.

The following example shows the basic concept on how the bond graph based MMP can be defined to have virtual actuation in an input/output sense.

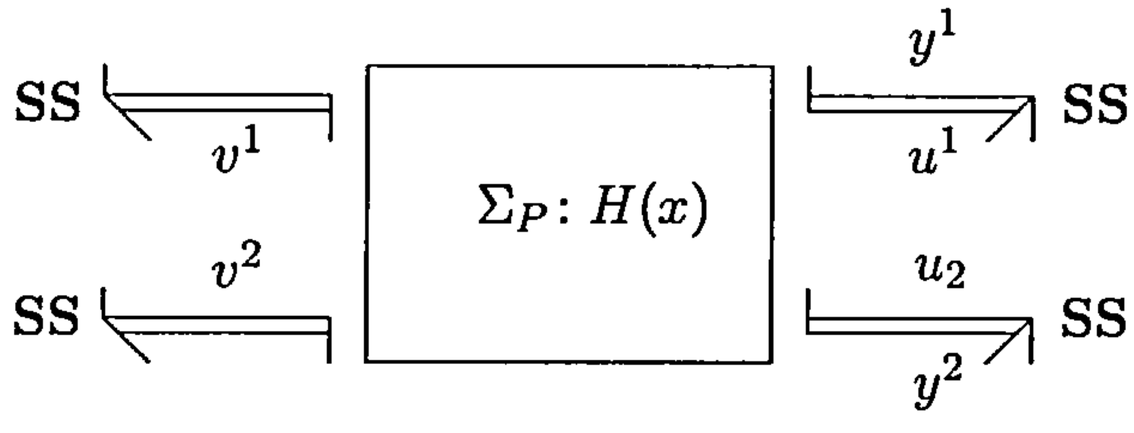

Figure 4.3.: Causal inversion of P.

Example 4.1. Consider the linear plant P, with all parameters unity, of the form

$$\begin{bmatrix} \dot{x}_1 \\ \dot{x}_2 \\ \dot{x}_3 \end{bmatrix} = \begin{bmatrix} 0 & -1 & 0 \\ 1 & 0 & -1 \\ 0 & 1 & 0 \end{bmatrix} \begin{bmatrix} x_1 \\ x_2 \\ x_3 \end{bmatrix} - \begin{bmatrix} 1 \\ 0 \\ 0 \end{bmatrix} u - \begin{bmatrix} 0 \\ 0 \\ 1 \end{bmatrix} v \tag{4.5}$$

$$y = x_1,$$

and let the model be defined as

$$\begin{bmatrix} \dot{\bar{x}}_1 \\ \dot{\bar{x}}_2 \\ \dot{\bar{x}}_3 \\ \dot{\bar{x}}_4 \end{bmatrix} = \begin{bmatrix} 0 & -1 & 0 & -a \\ 1 & 0 & -1 & 0 \\ 0 & 1 & 0 & 0 \\ a & 0 & 0 & 0 \end{bmatrix} \begin{bmatrix} \bar{x}_1 \\ \bar{x}_2 \\ \bar{x}_3 \\ b\bar{x}_4 \end{bmatrix} - \begin{bmatrix} 1 \\ 0 \\ 0 \\ 0 \end{bmatrix} \bar{u} \tag{4.6}$$

$$\bar{y} = \bar{x}_1,$$

where a and b are model parameters. It is seen that M contains an exact copy of the plant and that the x_1–dynamics is virtually actuated by the $\bar{x}_4$–dynamics.

In view of the associated disturbance decoupling problem, the difference $x_1 - \bar{x}_1$ is now to be rendered independent of $\bar{u}$. To that end, consider the plant inverse of (4.5) given by

$$v = -2y^{(1)} - y^{(3)} - u - u^{(2)} + w, \tag{4.7}$$

where $d^r y/dt^r = y^{(r)}$ and where w is a new control. By enforcing $y = \bar{y}$ it is found that the relation $u = \bar{u}$ is indeed required to attain decoupling, giving the control

$$v = c(\bar{x}, \bar{u}) + w = ab\bar{x}_4 + a^2b(-\bar{x}_2 - ab\bar{x}_4 - \bar{u}) + w. \tag{4.8}$$

To address the stabilisation of the the difference $y - \bar{y}$, the ideas of the Full Information Output Regulation Problem are used. Furthermore, the constrained dynamics algorithm yields the maximal (locally) controlled invariant submanifold Z^*, which is described by

$$Z^* = \{(x, \bar{x}) : x - \varphi(\bar{x}) = \begin{bmatrix} x_1 \\ x_2 \\ x_3 \end{bmatrix} - \begin{bmatrix} \bar{x}_1 \\ \bar{x}_2 + ab\bar{x}_4 \\ \bar{x}_3 - a^2b\bar{x}_1 \end{bmatrix} = 0\}. \tag{4.9}$$

The similarities between the MMP and Theorem 2.6 become apparent by noting that

$$\frac{d}{dt}\varphi(\bar{x}) = \mathrm{D}\varphi(\bar{x})[\bar{f}(\bar{x}) - \bar{g}\bar{u}] = f(\varphi(\bar{x})) - g\bar{u} - qc(\bar{x},\bar{u}), \tag{4.10}$$

where the plant (4.5) and model (4.6) have been written in affine form for convenience. It is now readily seen that the error $e = x - \varphi(\bar{x})$ leads to the dynamics

$$\begin{bmatrix} \dot{e}_1 \\ \dot{e}_2 \\ \dot{e}_3 \end{bmatrix} = \begin{bmatrix} 0 & -1 & 0 \\ 1 & 0 & -1 \\ 0 & 1 & 0 \end{bmatrix} \begin{bmatrix} e_1 \\ e_2 \\ e_3 \end{bmatrix} - \begin{bmatrix} 0 \\ 0 \\ 1 \end{bmatrix} w, \tag{4.11}$$

and observe that this system has the structure of the plant (4.5). Closed loop stabilisation is now achieved through the passive feedback

$$u = c(\bar{x},\bar{u}) + re_3 \tag{4.12}$$

for some damping constant $r > 0$. ◊

The general setup of the MMP considered in this section is to consider bond graphs that induce systems of the form (4.3), after which the plant bond graph is copied and extended with additional storage and dissipative elements to define the MMP objective. To solve the MMP then requires that the bicausal inverse exists and that it is well defined. If the causal inverse exists, then the virtual actuation should be achieved when $u = \bar{u}$ is imposed and the relation $y = \bar{y}$ is substituted into the plant inverse.

Decoupling $\bar{u}$ from the difference $y - \bar{y}$ is the first step in all bond graph based MMPs in this section. The second step requires the application of the constrained dynamics algorithm, which is often sufficient in finding the map $\varphi(\bar{x})$, or $\varphi(\eta,\bar{x})$ in case of internal dynamics η. These maps are used for the feedback control with the structure of (2.66) to stabilise $Z^\star$ if possible. It is interesting to note that the bicausal bond graph is *not* a requirement in the bond graph based MMP, because the constrained dynamics algorithm yields $Z^\star$, which, in turn, leads to the decoupling control.

The following example extends the basic Example 4.1 by using bond graph modelling arguments to define the MMP.

Example 4.2. Consider the simple mass–spring system in Figure 4.4 and its associated model in Figure 4.5. Note that all input variables u, v and $\bar{u}$ denote forces and that all output variables are the conjugate velocities.

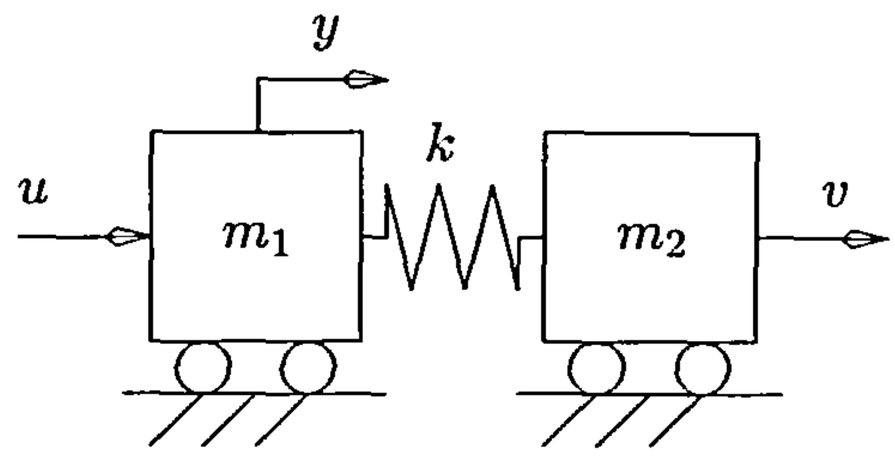

Figure 4.4.: Simple mass–spring plant of Example 4.2.

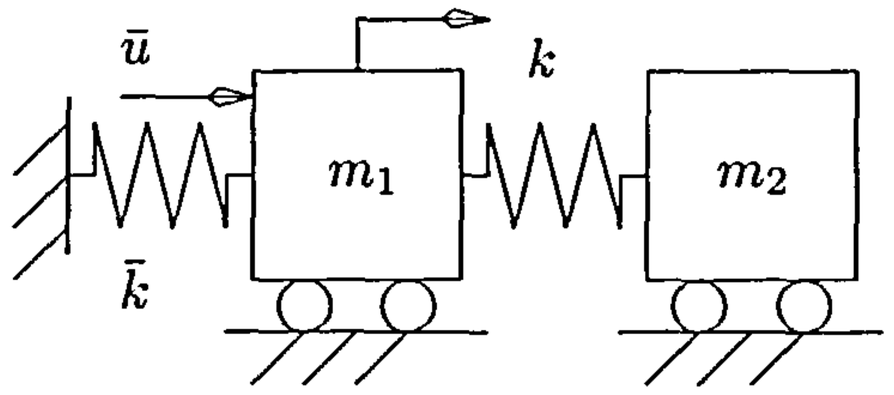

Figure 4.5.: Simple mass–spring model of Example 4.2.

The bond graphs of both system are depicted in Figure 4.6 and Figure 4.7. From causal analysis it immediately follows that the plant P has the form

$$\begin{bmatrix} \dot{x}_1 \\ \dot{x}_2 \\ \dot{x}_3 \end{bmatrix} = \begin{bmatrix} 0 & -1 & 0 \\ 1 & 0 & -1 \\ 0 & 1 & 0 \end{bmatrix} \begin{bmatrix} x_1/m_1 \\ kx_2 \\ x_3/m_2 \end{bmatrix} - \begin{bmatrix} 1 \\ 0 \\ 0 \end{bmatrix} u - \begin{bmatrix} 0 \\ 0 \\ 1 \end{bmatrix} v \tag{4.13}$$

$$y = x_1/m_1$$

and where the model M is described by

$$\begin{bmatrix} \dot{\bar{x}}_1 \\ \dot{\bar{x}}_2 \\ \dot{\bar{x}}_3 \\ \dot{\bar{x}}_4 \end{bmatrix} = \begin{bmatrix} 0 & -1 & 0 & -1 \\ 1 & 0 & -1 & 0 \\ 0 & 1 & 0 & 0 \\ 1 & 0 & 0 & 0 \end{bmatrix} \begin{bmatrix} \bar{x}_1/m_1 \\ k\bar{x}_2 \\ \bar{x}_3/m_2 \\ \bar{k}\bar{x}_4 \end{bmatrix} - \begin{bmatrix} 1 \\ 0 \\ 0 \\ 0 \end{bmatrix} \bar{u} \tag{4.14}$$

$$\bar{y} = \bar{x}_1/m_1$$

The MMP objective is now seen to have a straightforward physical interpretation: Feedback on v should impose convergence of the plant and model outputs, thus $|y(t) - \bar{y}(t)| \to 0$, and the influence of model inputs on the extended output $y - \bar{y}$ is removed by the relation $u = \bar{u}$.

Since the relative degree condition $r \leq \bar{r}$ is fulfilled by construction, the bicausal bond graph in Figure 4.8 yields the inverse plant

$$v = -u - (m_1 + m_2)y^{(1)} - \frac{m_2}{k}u^{(2)} - \frac{m_1 m_2}{k}y^{(3)}. \tag{4.15}$$

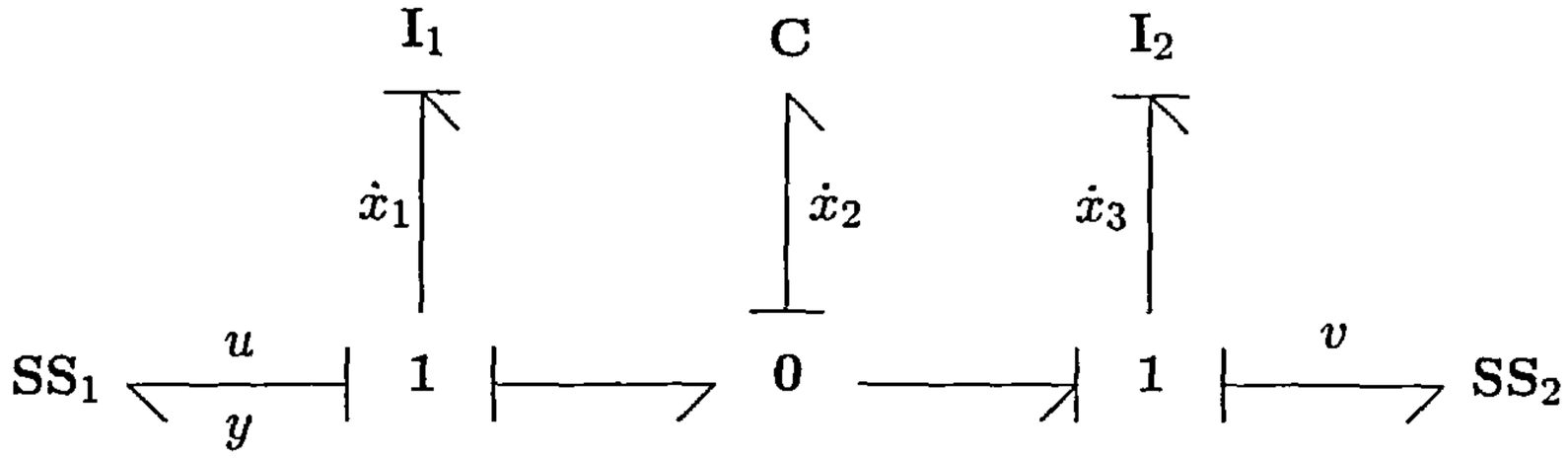

Figure 4.6.: Plant bond graph of Example 4.2.

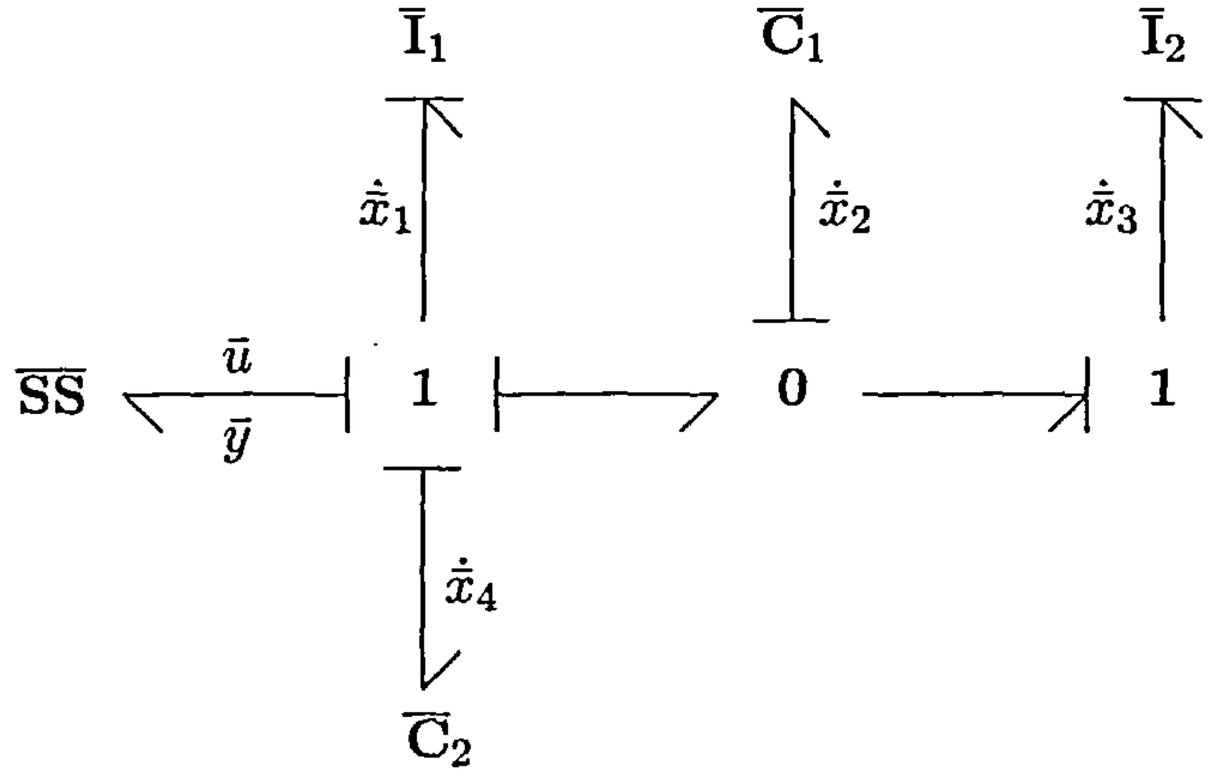

Figure 4.7.: Model bond graph of Example 4.2.

The decoupling control is found by setting $y = \bar{y}$ and $u = \bar{u}$, yielding

$$v = c(\bar{x}, \bar{u}) + w = -\frac{m_2\bar{k}}{m_1}\bar{x}_2 + \left(\bar{k} - \frac{m_2\bar{k}^2}{km_1}\right)\bar{x}_4 - \frac{m_2\bar{k}}{km_1}\bar{u} + w. \tag{4.16}$$

As mentioned in Section 2.3.1 on model inversion, the bicausal bond graph does *not* yield the output matching submanifold $Z^\star$, so that the constrained dynamics algorithm remains to be an important tool in the search for this submanifold for all MMP problems. The constrained dynamics can be found to take the form

$$Z^\star = \{\,(x, \bar{x}) : x - \varphi(\bar{x}) = \begin{bmatrix} x_1 \\ x_2 \\ x_3 \end{bmatrix} - \begin{bmatrix} \bar{x}_1 \\ \bar{x}_2 + \dfrac{\bar{k}}{k}\bar{x}_4 \\ \bar{x}_3 - \dfrac{m_2\bar{k}}{m_1 k}\bar{x}_1 \end{bmatrix} = 0\,\}, \tag{4.17}$$

so that by setting $e = x - \varphi(\bar{x})$ this allows the closed loop dynamics to be written as the port–Hamiltonian system

$$\begin{bmatrix} \dot{e}_1 \\ \dot{e}_2 \\ \dot{e}_3 \end{bmatrix} = \begin{bmatrix} 0 & -1 & 0 \\ 1 & 0 & -1 \\ 0 & 1 & 0 \end{bmatrix} \begin{bmatrix} e_1/m_1 \\ ke_2 \\ e_3/m_2 \end{bmatrix} - \begin{bmatrix} 0 \\ 0 \\ 1 \end{bmatrix} w \tag{4.18}$$

$$\psi = e_3/m_2.$$

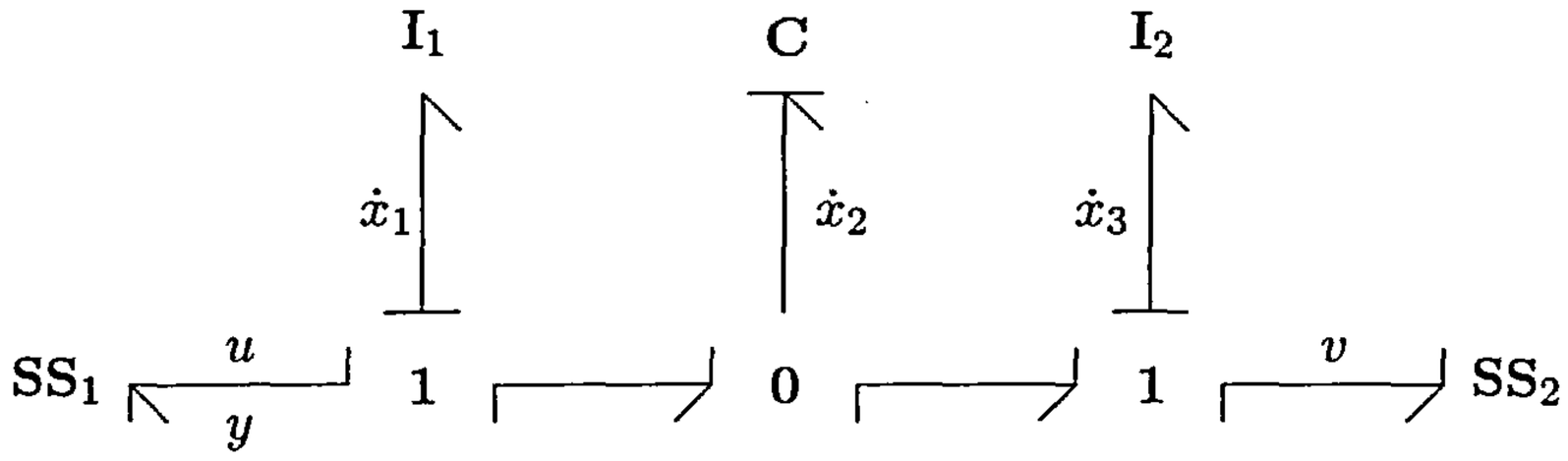

Figure 4.8.: Bicausal inversion of the plant of Example 4.2.

Observe that this systems has the bond graph topology of Figure 4.6 for which $\mathbf{SS}_1$ is removed. Passive stabilisation of the origin $e = 0$ is possible by terminating the $\mathbf{SS}_2$ with a linear resistive element that yields the control $w = re_3$ for some $r > 0$. ◊

In [Vin03], the bond graph based MMP and its virtual actuation interpretation is presented but no clear answer is given on how the attractivity of $Z^\star$ is verified and controlled. The answer to this question is readily found by the various considerations in Section 2.3.1, being that no bond graph operations exists that "automatically" yields some map $x = \varphi(\bar{x})$ or $x = \varphi(\eta, \bar{x})$, and considerable analysis remains necessary regarding the description and stabilisation of $Z^\star$.

The multi–input case is not intrinsically different from a single–input scenario and the following example taken from [Vin03] presents such a multi–input scenario. Note, in particular, that the considerations of Section 2.3.2 on the Full Information Output Regulation Problem are not mentioned in that paper.

Example 4.3. Consider the mechanical system depicted in Figure 4.9 and its associated model in Figure 4.10. The plant inputs u_1 and u_2 are forces applied to the masses m_1 and m_2 respectively, and where the controls v are velocities. By passivity, the plant outputs are the velocities of m_1 and m_2 in accordance with (4.3). In view of (4.4), the model in Figure 4.10 incorporates a copy of the plant and adds further dynamics through a nonlinear spring characteristic $\bar{k}(x)$ to be defined later. The bond graphs of the plant P and model M are depicted in Figure 4.11 and 4.12.

The control v imposes the desired dynamics whereas the inputs $\bar{u}$ are known and the condition $u = \bar{u}$ should render the difference $y - \bar{y}$ independent of $\bar{u}$. In particular, to implement virtual actuation in an input/output sense, observe that the physical plant parameters have been copied to the prescribed model in Figure 4.10.

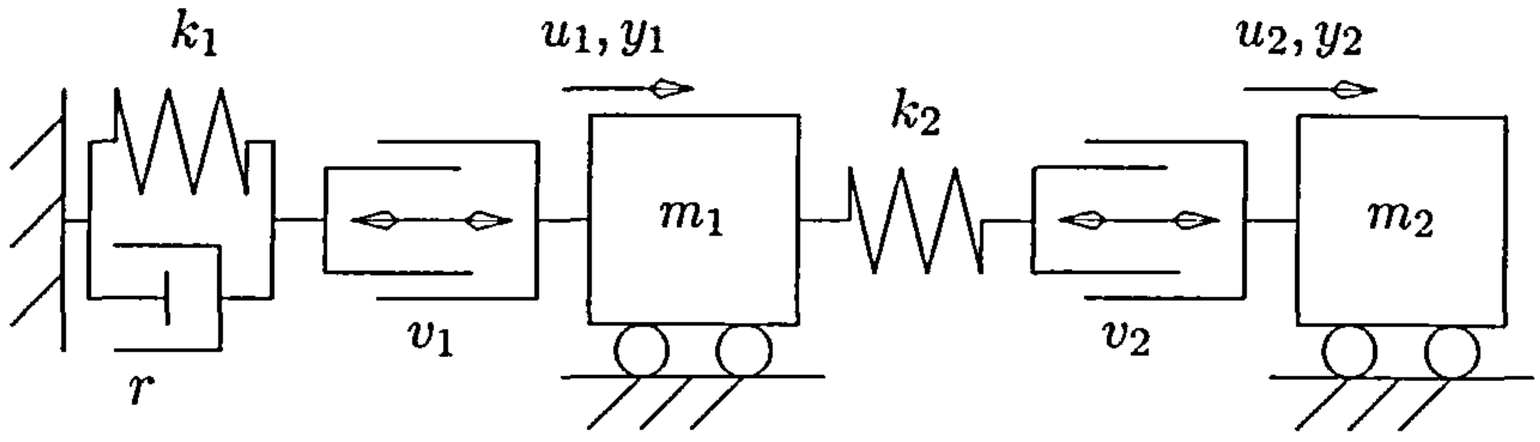

Figure 4.9.: Multi–input mechanical plant of Example 4.3.

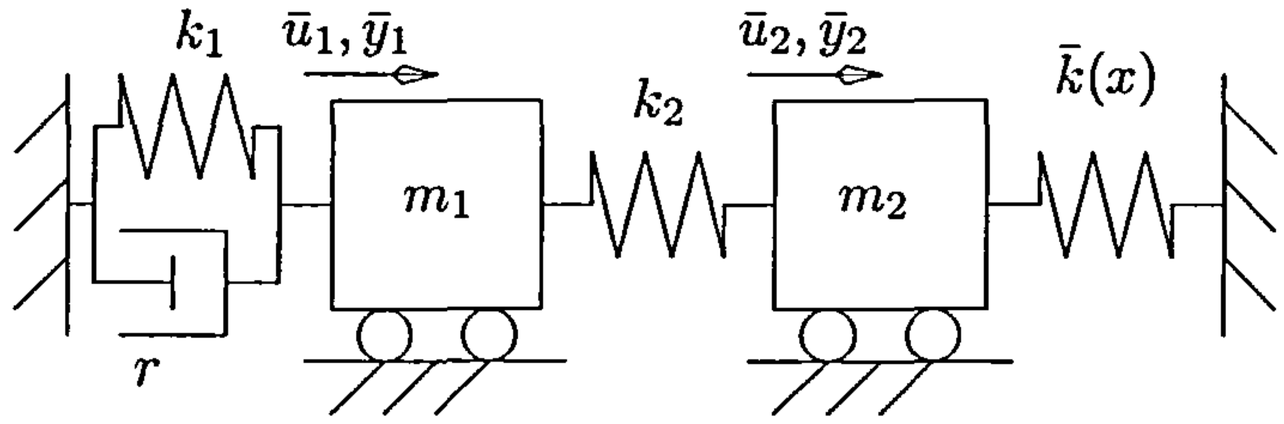

Figure 4.10.: Model with nonlinear spring element of Example 4.3.

The design proceeds with the causal analysis of the plant bond graph in Figure 4.11, giving the dynamics

$$\begin{bmatrix} \dot{x}_1 \\ \dot{x}_2 \\ \dot{x}_3 \\ \dot{x}_4 \end{bmatrix} = \begin{bmatrix} 0 & 0 & 1 & 0 \\ 0 & 0 & -1 & 1 \\ -1 & 1 & -r & 0 \\ 0 & -1 & 0 & 0 \end{bmatrix} \begin{bmatrix} k_1 x_1 \\ k_2 x_2 \\ x_3/m_1 \\ x_4/m_2 \end{bmatrix} - \begin{bmatrix} 0 & 0 \\ 0 & 0 \\ 1 & 0 \\ 0 & 1 \end{bmatrix} \begin{bmatrix} u_1 \\ u_2 \end{bmatrix} - \begin{bmatrix} 1 & 0 \\ 0 & 1 \\ -r & 0 \\ 0 & 0 \end{bmatrix} \begin{bmatrix} v_1 \\ v_2 \end{bmatrix}$$

$$\begin{bmatrix} y_1 \\ y_2 \end{bmatrix} = \begin{bmatrix} x_3/m_1 \\ x_4/m_2 \end{bmatrix}. \tag{4.19}$$

The model bond graph in Figure 4.12 then induces the system

$$\begin{bmatrix} \dot{\bar{x}}_1 \\ \dot{\bar{x}}_2 \\ \dot{\bar{x}}_3 \\ \dot{\bar{x}}_4 \\ \dot{\bar{x}}_5 \end{bmatrix} = \begin{bmatrix} 0 & 0 & 1 & 0 & 0 \\ 0 & 0 & -1 & 1 & 0 \\ -1 & 1 & -r & 0 & 0 \\ 0 & -1 & 0 & 0 & -1 \\ 0 & 0 & 0 & 1 & 0 \end{bmatrix} \begin{bmatrix} k_1 \bar{x}_1 \\ k_2 \bar{x}_2 \\ \bar{x}_3/m_1 \\ \bar{x}_4/m_2 \\ \sinh(\bar{x}_5) \end{bmatrix} - \begin{bmatrix} 0 & 0 \\ 0 & 0 \\ 1 & 0 \\ 0 & 1 \\ 0 & 0 \end{bmatrix} \begin{bmatrix} \bar{u}_1 \\ \bar{u}_2 \end{bmatrix}$$

$$\begin{bmatrix} \bar{y}_1 \\ \bar{y}_2 \end{bmatrix} = \begin{bmatrix} \bar{x}_3/m_1 \\ \bar{x}_4/m_2 \end{bmatrix}. \tag{4.20}$$

To solve the disturbance decoupling problem, observe that the relative degree condition $r_i \leq \bar{r}_i$ is satisfied and that the bicausal bond graph in Figure 4.13 shows no causal conflicts.

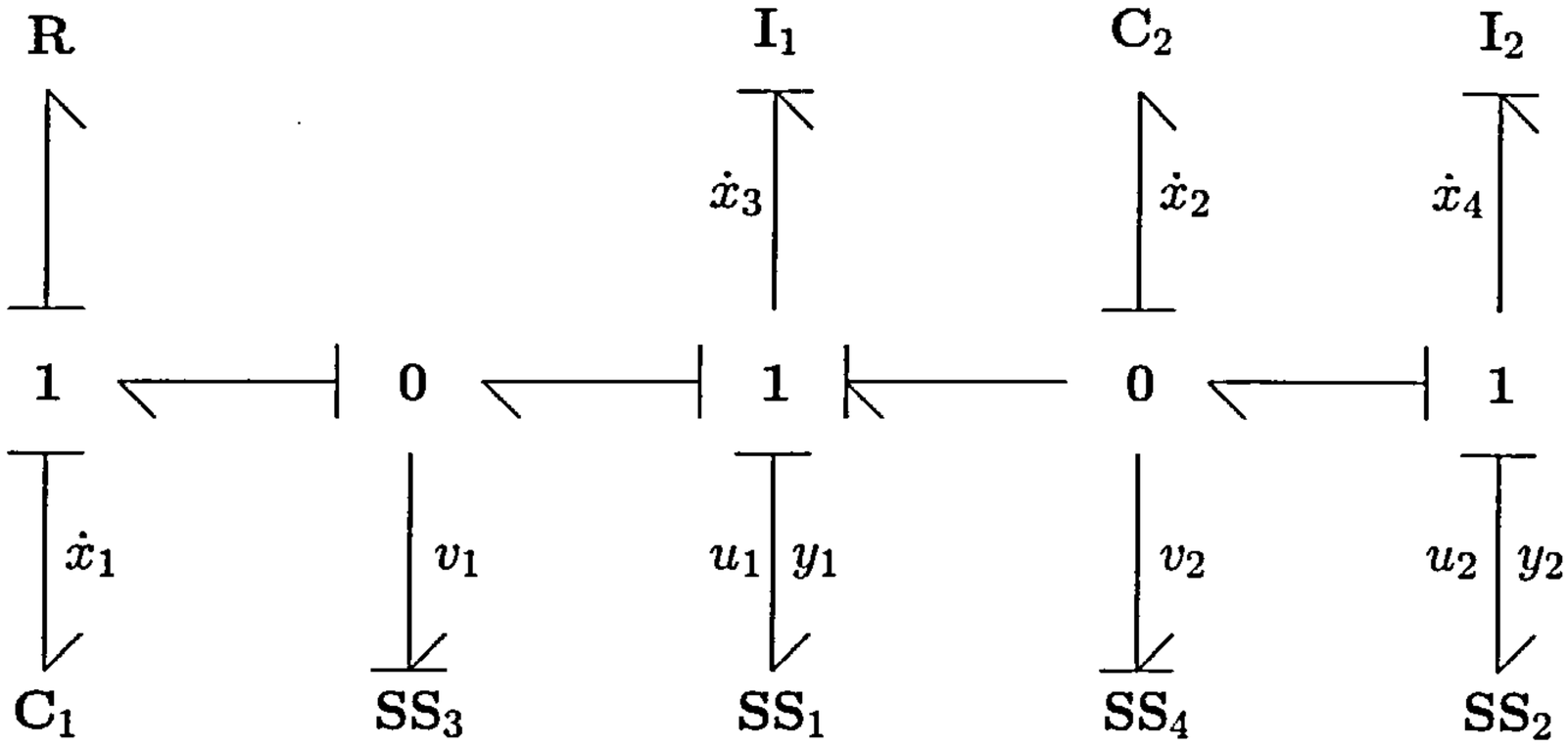

Figure 4.11.: Plant bond graph of Example 4.3.

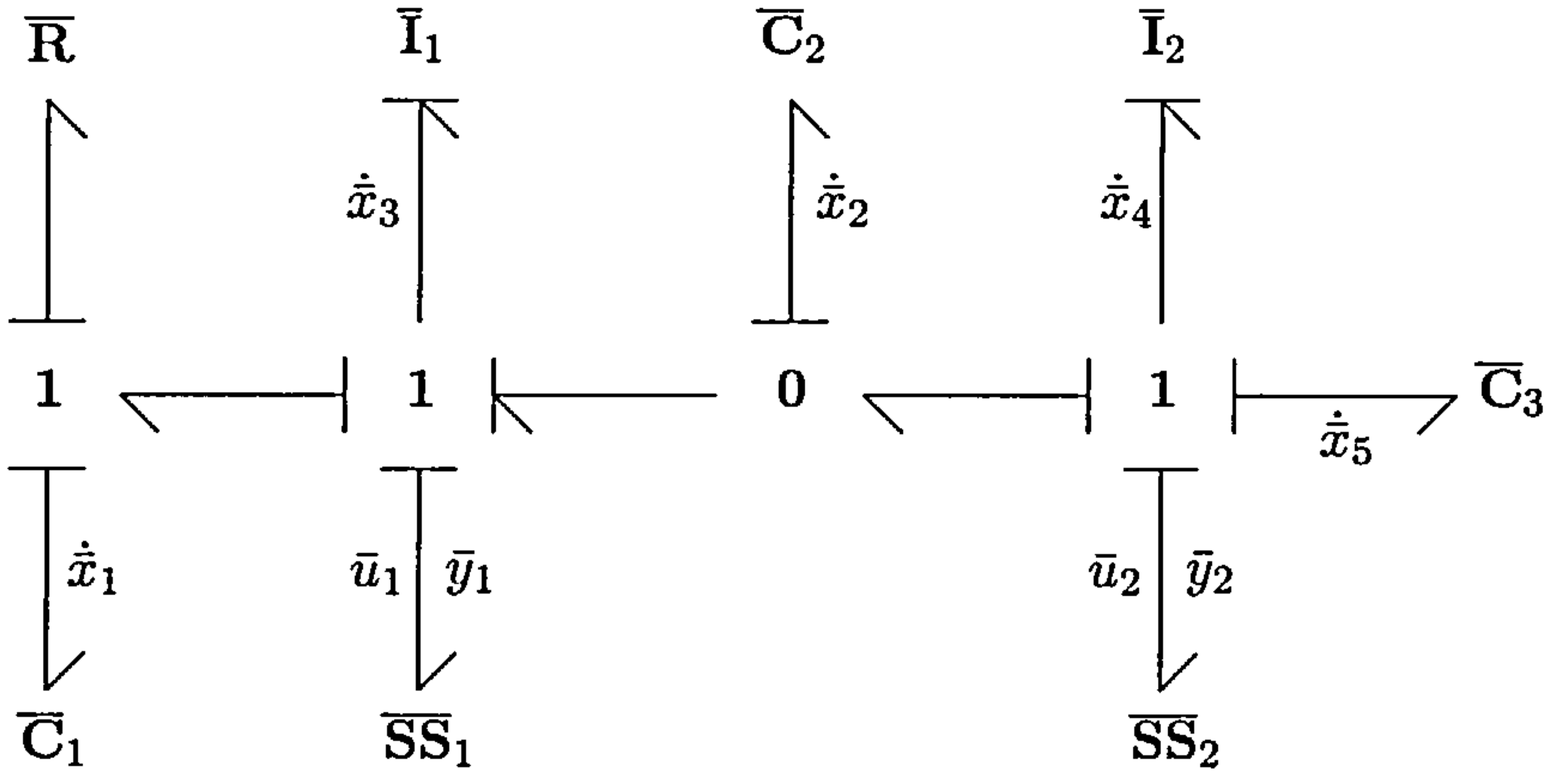

Figure 4.12.: Model bond graph of Example 4.3.

The inverse is readily found to be

$$\begin{aligned} \dot{\eta} &= -\frac{1}{r}(m_1 y_1^{(1)} + m_2 y_2^{(1)} + k_1\eta + u_1 + u_2) \\ v_1 &= y_1 + \frac{1}{r}(m_1 y_1^{(1)} + m_2 y_2^{(1)} + k_1\eta + u_1 + u_2) + w_1 \\ v_2 &= y_2 - y_1 + \frac{m_2}{k_2} y_2^{(2)} + \frac{1}{k_2} u_2^{(1)} + w_2, \end{aligned} \tag{4.21}$$

where w_1 and w_2 are new controls for stabilisation purposes. It can now be verified that the relations $y = \bar{y}$ and $u = \bar{u}$ yield the control

$$\begin{aligned} \dot{\eta} &= -\frac{k_1}{r}\eta + \frac{k_1}{r}\bar{x}_1 + \frac{1}{r}\sinh(\bar{x}_5) + \frac{1}{m_1}\bar{x}_3 \\ v_1 &= \frac{k_1}{r}\eta - \frac{k_1}{r}\bar{x}_1 - \frac{1}{r}\sinh(\bar{x}_5) + w_1 \\ v_2 &= -\frac{1}{k_2 m_2}\bar{x}_4\cos(\bar{x}_5) + w_2. \end{aligned} \tag{4.22}$$

Even though the bicausal approach gives the decoupling controller in straightforward manner, the submanifold $Z^\star$ is needed to derive the feedback of the form

$$u = c(\eta, \bar{x}, \bar{u}) + K[x - \varphi(\eta, \bar{x})]. \tag{4.23}$$

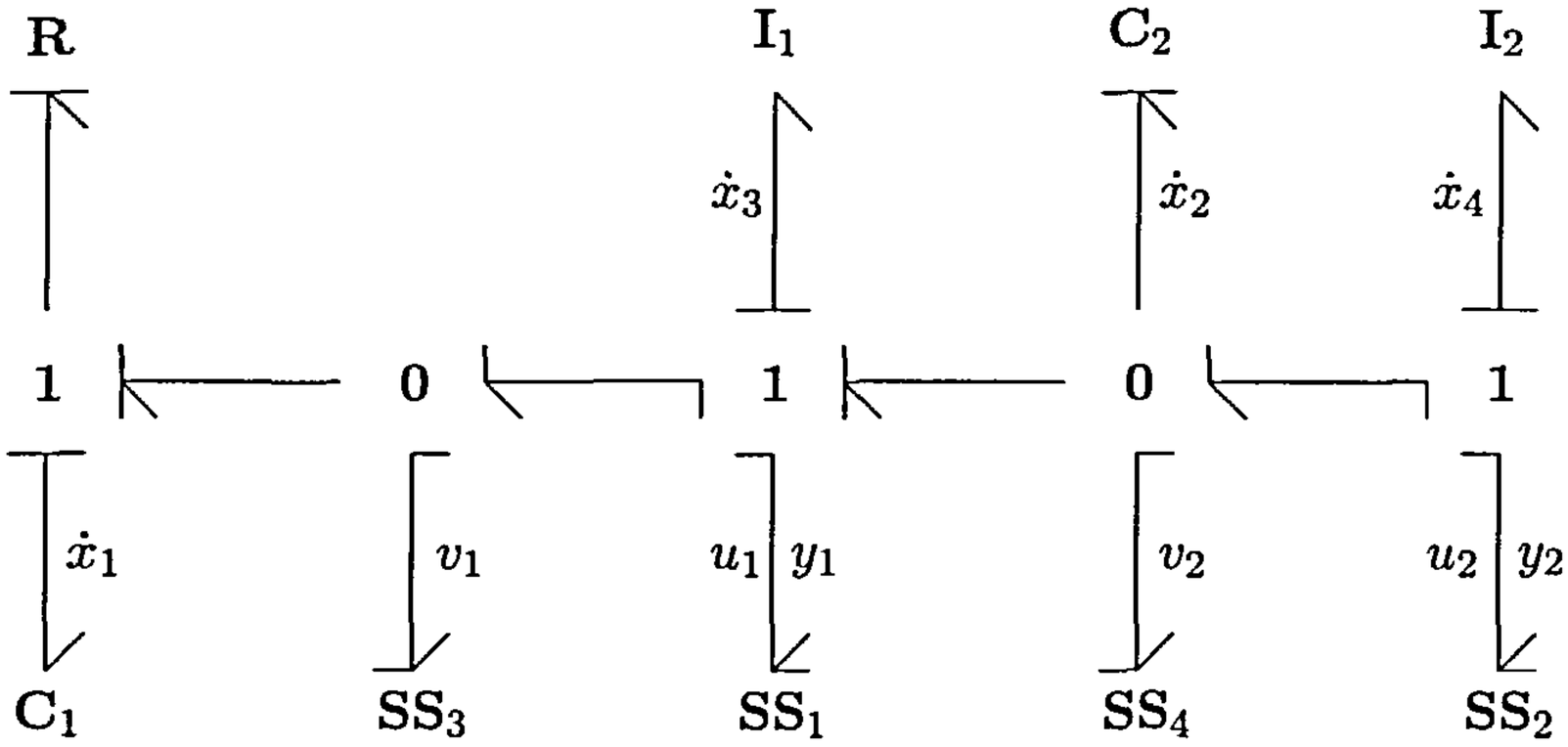

Figure 4.13.: Bicausal plant inversion of Example 4.3.

The constrained dynamics algorithm now yields

$$Z^\star = \{(\eta, x, \bar{x}) : x - \varphi(\eta, \bar{x}) = \begin{bmatrix} x_1 \\ x_2 \\ x_3 \\ x_4 \end{bmatrix} - \begin{bmatrix} \eta \\ \bar{x}_2 + \dfrac{1}{k_2}\sinh(\bar{x}_5) \\ \bar{x}_3 \\ \bar{x}_4 \end{bmatrix} = 0\}. \tag{4.24}$$

It is important to note that $Z^\star$ in (4.24) is *not* the maximal (locally) controlled invariant submanifold in the usual sense, because it has been "extended" with the internal dynamics η for convenience.

Next define the error $e = x - \varphi(\eta, \bar{x})$ and write the closed loop as the port–Hamiltonian system of the form

$$\begin{bmatrix} \dot{e}_1 \\ \dot{e}_2 \\ \dot{e}_3 \\ \dot{e}_4 \end{bmatrix} = \begin{bmatrix} 0 & 0 & 1 & 0 \\ 0 & 0 & -1 & 1 \\ -1 & 1 & -r & 0 \\ 0 & -1 & 0 & 0 \end{bmatrix} \begin{bmatrix} k_1 e_1 \\ k_2 e_2 \\ e_3/m_1 \\ e_4/m_2 \end{bmatrix} - \begin{bmatrix} 1 & 0 \\ 0 & 1 \\ -r & 0 \\ 0 & 0 \end{bmatrix} \begin{bmatrix} w_1 \\ w_2 \end{bmatrix}$$

$$\begin{bmatrix} \psi_1 \\ \psi_2 \end{bmatrix} = \begin{bmatrix} k_1 e_1 + r e_3/m_1 \\ k_2 e_2 \end{bmatrix} - \begin{bmatrix} r & 0 \\ 0 & 0 \end{bmatrix} \begin{bmatrix} w_1 \\ w_2 \end{bmatrix}. \tag{4.25}$$

Observe that the closed loop has the bond graph topology of Figure 4.14: The e–dynamics allows for a bond graph topology that is identical to the plant with $u = 0$. Furthermore, the closed loop passive outputs are those which are ignored in the plant definition but can be readily included from the bond graph in Figure 4.14. The submanifold $Z^\star$ is therefore seen to be attractive for $w = 0$ due to the dissipative element of the plant. Further stabilisation of $Z^\star$ is possible through $w = K[x - \varphi(\eta, \bar{x})]$ for some suitable gain K. ◊

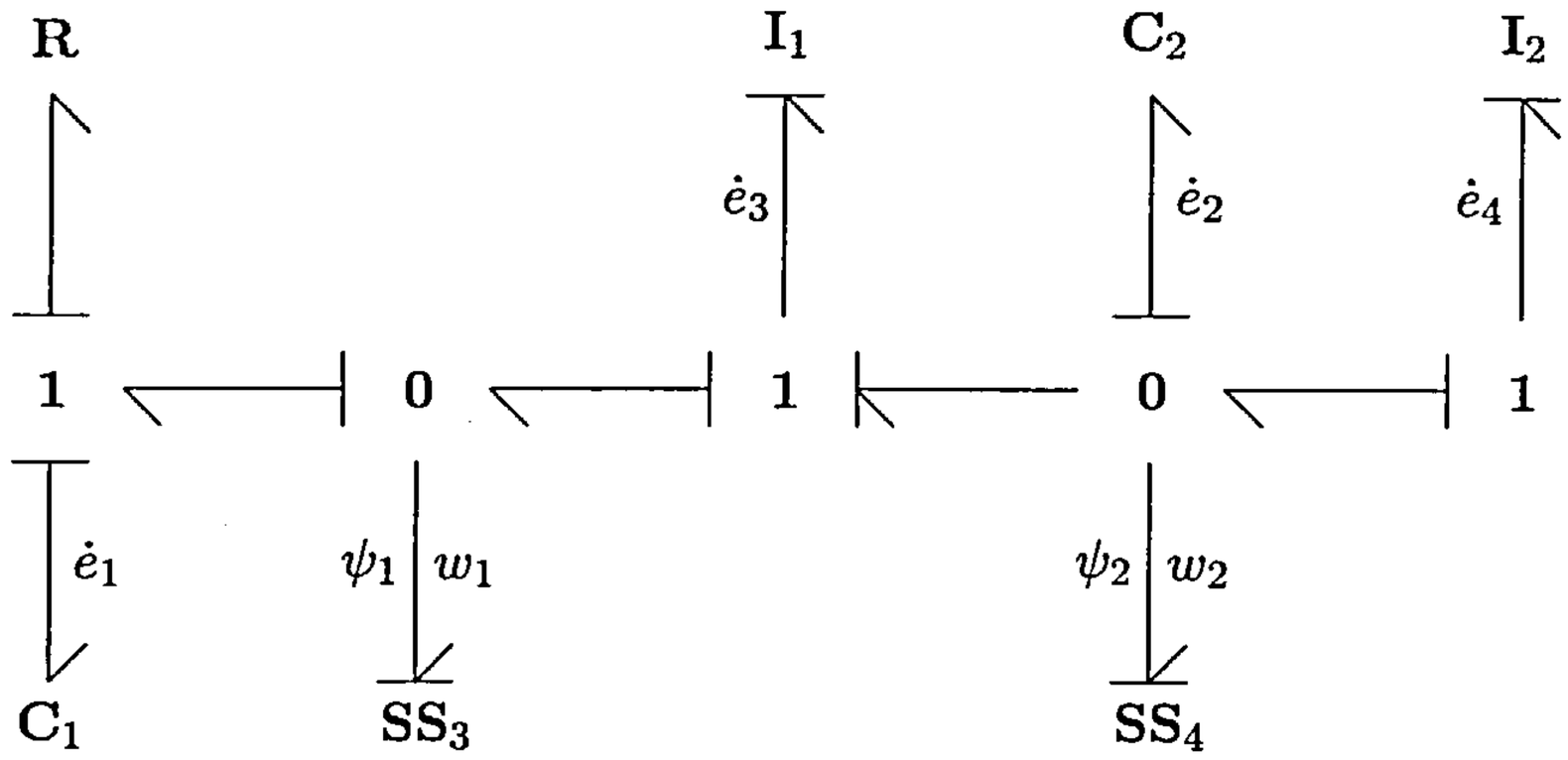

Figure 4.14.: Induced closed loop bond graph of Example 4.3.

So far it has been shown that the physical model based MMP can be defined in a manner that can be represented through bond graphs. To that end, the system is assumed to be of the form (4.3), which represents an *explicit* port–Hamiltonian system of which a subset of passive outputs are ignored. The question rises whether a class of *implicit* port–Hamiltonian systems can be used in the MMP scenario considered in this section. More precisely, can the MMP of this section be applied to the input/output configuration of the bond graphs in Figures 4.1 and 4.2 for which P and M have derivative causalities?

It is intuitively plausible that bond graph models with derivative causalities can "in principle" be used in the same MMP setup as depicted in Figure 4.1 and 4.2. That is to say that the bond graphs in Figure 4.1 and 4.2 merely depict a certain input/output configuration but do not show the bond graph topology itself, which may or may not have dependent storage elements. However, the presence of derivative causalities poses additional difficulties in regard the associated implicit dynamics of the bond graph. Furthermore, it can be argued that the closed loop bond graph representation will be more difficult to derive.

In view of the above considerations, the MMP scenario of this section requires further research on the topic of derivative causalities. It is expected that the scenario can be applied to bond graph models with derivative causalities provided the causal inverse exists and that the relative degree conditions are satisfied. However, the closed loop error dynamics can be expected not to be comparable to the explicit systems context. These issues will not be elaborated any further and a more general bond graph based MMP with dependent storage elements will considered in later sections.

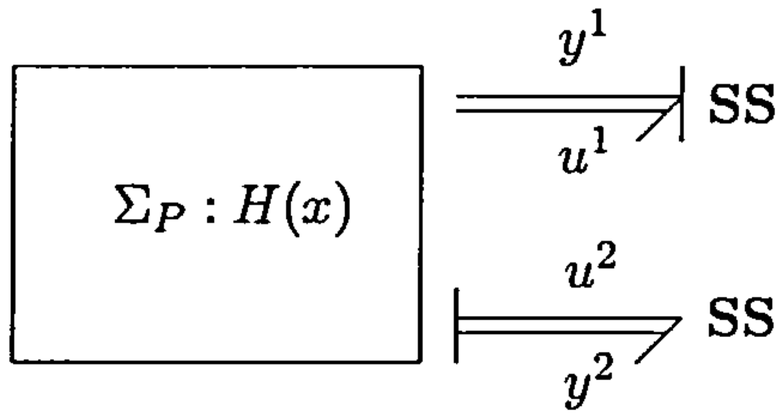

Figure 4.15.: Plant bond graph with collocated input/output pairs.

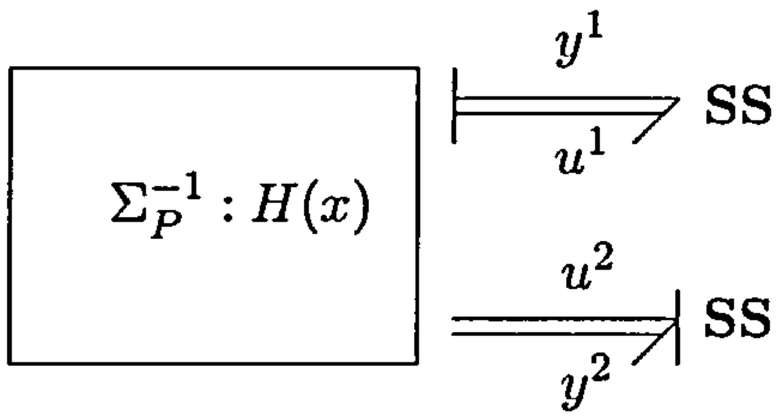

Figure 4.16.: Inverse plant bond graph.

4.3. Specification Based Inversion

In [Ngw99b], a technique called "specification based inversion" is introduced. This bond graph approach is very closely related to the bond graph based MMP design and the MMP theory considered in this chapter. Note, however, that the paper is not about controller design but addresses a (bi)causal inversion process for which certain aspects can be extended to controller design in terms of the MMP.

Specification based inversion can be outlined briefly by considering the collocated plant bond graph and its causal inverse in Figures 4.15 and 4.16. The model is equipped with a copy of the plant and has the same input/output configurations, so its bond graph need not be depicted. Causal plant inversion is used to find the control that achieves the required model input/output dynamics by imposing the constraint $y = \bar{y}$, provided the relative degree condition is satisfied. The model need not add further model dynamics, so that the control objective can be solely expressed in terms of these parametric modifications alone.

Now, for more generality, the MMP scenario in this section need not stay with the collocated case of specification based inversion in [Ngw99b], because the non–collocated case is conceptually identical to the collocated case. More precisely, the model is equipped with an exact copy of the plant and has the same input/output configuration. Figure 4.17 and 4.18 depict the bond graphs of the non–collocated MMP scenario, where $u = (u^1, u^2)$ and $y = (y^1, y^2)$. By imposing the constraint $y = \bar{y}$ it becomes possible to find the required decoupling control that solves the MMP, provided relative degree conditions on model inputs are satisfied.

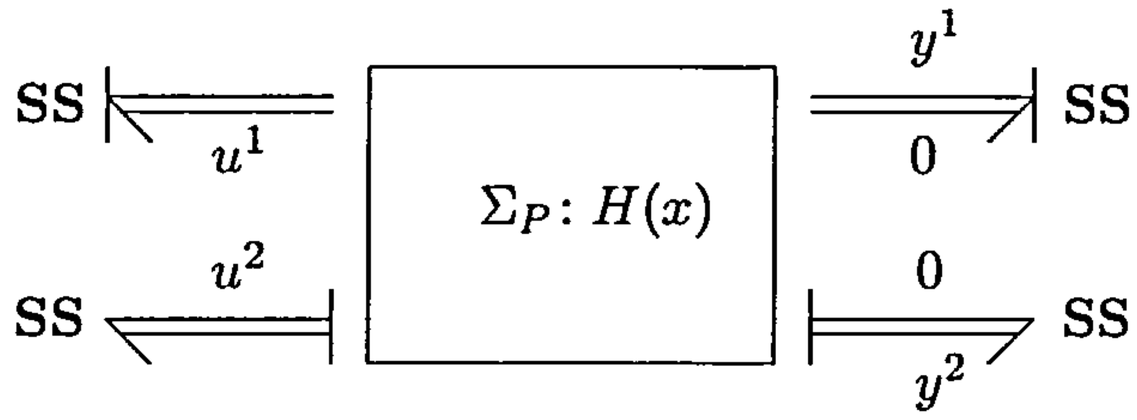

Figure 4.17.: Plant bond graph with non–collocated input/output pairs.

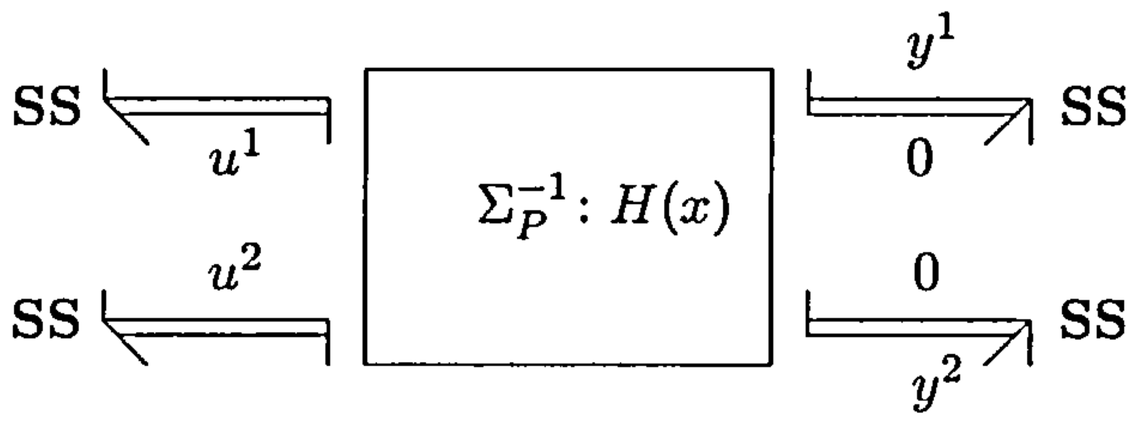

Figure 4.18.: Bicausal bond graph with non–collocated input/output pairs.

To show a possible class of dynamics suitable for specification based inversion, consider the plant P described by

$$\begin{aligned} \dot{x} &= [J(x,\mu) - R(x,\mu)]K(x,\mu) - g_j(x,\mu)u_j - q_j(x,\mu)v_j \\ w_j &= g_j^T(x,\mu)K(x,\mu), \\ y_j &= q_j^T(x,\mu)K(x,\mu), \end{aligned} \tag{4.26}$$

where $x \in \mathbb{R}^n$ and $u, y, v, w \in \mathbb{R}^m$. The k–tuple $\mu = (\mu_1, \ldots, \mu_k)$ denotes the physical parameters of the plant. Then to follow the non–collocated scenario based on Figure 4.17, for example, let the outputs w be ignored and let $v = 0$. Next consider the the model

$$\begin{aligned} \begin{bmatrix} \dot{\bar{x}}^1 \\ \dot{\bar{x}}^2 \end{bmatrix} &= \begin{bmatrix} J(\bar{x}^1,\bar{\mu}) - R(\bar{x}^1,\bar{\mu}) & -S(\bar{x}^2) \\ S^T(\bar{x}^2) & \bar{J}(\bar{x}^2) - \bar{R}(\bar{x}^2) \end{bmatrix} \begin{bmatrix} K(\bar{x}^1,\bar{\mu}) \\ \bar{K}(\bar{x}^2) \end{bmatrix} - \begin{bmatrix} g_j(\bar{x}^1,\bar{\mu}) \\ 0 \end{bmatrix} \bar{u}_j \\ \bar{y}_j &= q_j^T(\bar{x}^1,\bar{\mu})K(\bar{x}^1,\bar{\mu}), \end{aligned} \tag{4.27}$$

where $\bar{x}^1 \in \mathbb{R}^n$, $\bar{x}^2 \in \mathbb{R}^{\bar{n}}$ and $\bar{u}, \bar{w} \in \mathbb{R}^m$. The p–tuple $\bar{\mu} = (\bar{\mu}_1, \ldots, \bar{\mu}_p)$ denotes the prescribed plant parameters. Lemma 2.4 can, but need not, be invoked in this particular case.

The following example is taken from [Ngw99b] and shows the bond graph based MMP of a non–collocated system using specification based inversion.

Example 4.4. [Ngw99b] Consider the bond graph of an RC–circuit depicted in Figure 4.19. Suppose the model has been chosen to comprise an exact copy of the plant only, implying that the control objective is solely based on parametric modifications. As a result, the bond graph topology of the model is identical to the plant and need not be depicted here.

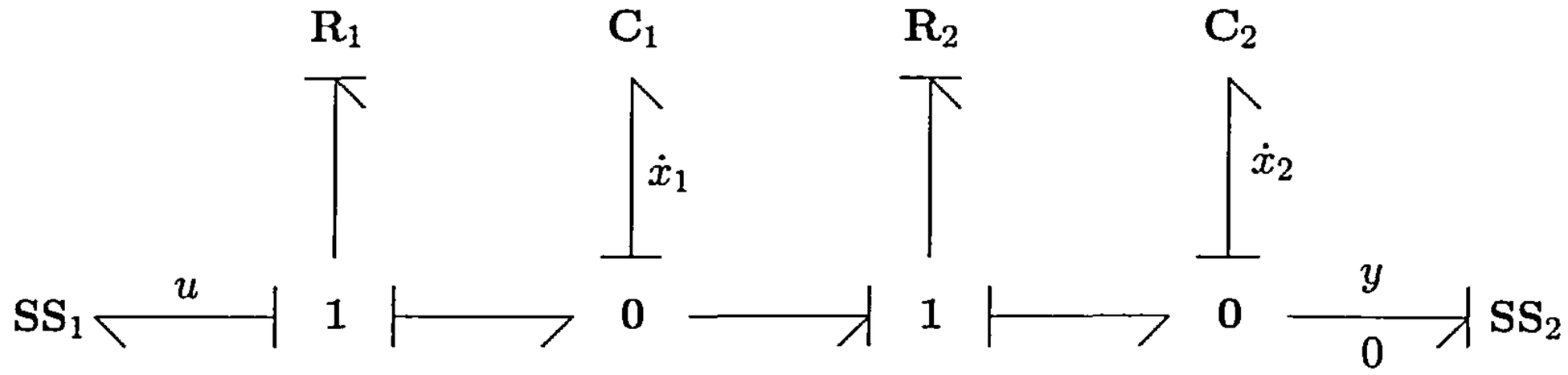

Figure 4.19.: Simple RC–circuit of Example 4.4.

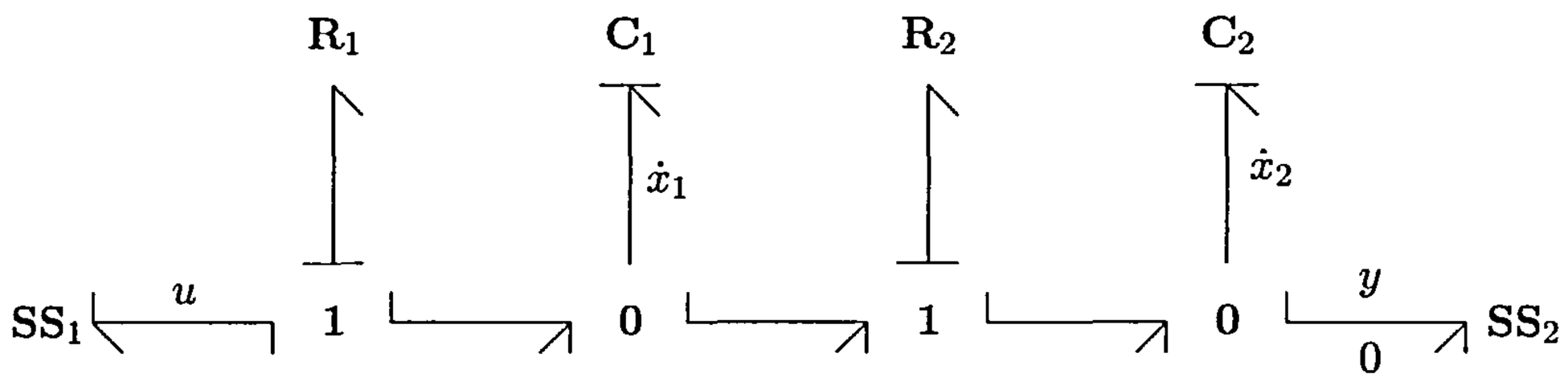

Figure 4.20.: Bicausal RC–circuit of Example 4.4.

Causal analysis of Figure 4.19 yields the system of the form

$$\begin{bmatrix} \dot{x}_1 \\ \dot{x}_2 \end{bmatrix} = \begin{bmatrix} -\frac{1}{r_1} - \frac{1}{r_2} & \frac{1}{r_2} \\ \frac{1}{r_2} & -\frac{1}{r_2} \end{bmatrix} \begin{bmatrix} \frac{1}{c_1} x_1 \\ \frac{1}{c_2} x_2 \end{bmatrix} - \begin{bmatrix} \frac{1}{r_1} \\ 0 \end{bmatrix} u \tag{4.28}$$

$$y = \frac{1}{c_2} x_2,$$

which is of the form (4.26). The passive output $w = x_1/(r_1 c_1)$ has been ignored and $v = 0$. Suppose the model is chosen with the parameters

$$\begin{bmatrix} \dot{\bar{x}}_1 \\ \dot{\bar{x}}_2 \end{bmatrix} = \begin{bmatrix} -\frac{1}{\bar{r}_1} - \frac{1}{\bar{r}_2} & \frac{1}{\bar{r}_2} \\ \frac{1}{\bar{r}_2} & -\frac{1}{\bar{r}_2} \end{bmatrix} \begin{bmatrix} \frac{1}{\bar{c}_1} \bar{x}_1 \\ \frac{1}{\bar{c}_2} \bar{x}_2 \end{bmatrix} - \begin{bmatrix} \frac{1}{\bar{r}_1} \\ 0 \end{bmatrix} \bar{u} \tag{4.29}$$

$$\bar{y} = \frac{1}{\bar{c}_2} \bar{x}_2,$$

which conforms to (4.27) with $\bar{x}^2 = 0$.

Clearly, the plant is not dynamically extended through the model M and the control objective is solely expressed in terms of parametric modifications.

The relative degree condition $r \leq \bar{r}$ is trivially satisfied and the bicausal inverse in Figure 4.20 has no causal conflict. Bicausal analysis yields the inverse of the plant of the form

$$u = -y - (c_1 r_1 + c_2 r_1 + c_2 r_2) y^{(1)} - c_1 c_2 r_1 r_2 y^{(2)} + w, \tag{4.30}$$

where w is a new control for stabilisation purposes. The decoupling control is found by imposing $y = \bar{y}$.

To show that specification based inversion is equivalent to an MMP design, the application of the constrained dynamics algorithm yields

$$Z^\star = \{(x, \bar{x}) : x - \varphi(\bar{x}) = \begin{bmatrix} x_1 \\ \\ x_2 \end{bmatrix} - \begin{bmatrix} \frac{c_1}{\bar{c}_2}\bar{x}_2 - \frac{c_1 c_2 r_2}{\bar{c}_2^2 \bar{r}_2}\bar{x}_2 + \frac{c_1 c_2 r_2}{\bar{c}_1 \bar{c}_2 \bar{r}_2}\bar{x}_1 \\ \\ \frac{c_2}{\bar{c}_2}\bar{x}_2 \end{bmatrix} = 0\}. \tag{4.31}$$

The decoupling control is then found to be

$$\begin{aligned} u = &\left(\frac{c_1 c_2 r_1 r_2}{\bar{c}_1 \bar{c}_2^2 \bar{r}_2^2} - \frac{c_2 r_1}{\bar{c}_1 \bar{c}_2 \bar{r}_2} - \frac{c_1 r_1}{\bar{c}_1 \bar{c}_2 \bar{r}_2} + \frac{c_1 c_2 r_1 r_2}{\bar{c}_1^2 \bar{c}_2 \bar{r}_2^2} - \frac{c_1 c_2 r_1 r_2}{\bar{c}_1^2 \bar{c}_2^2 \bar{r}_2^3} - \frac{c_2 r_2}{\bar{c}_1 \bar{c}_2 \bar{r}_2} + \frac{c_1 c_2 r_1 r_2}{\bar{c}_1^2 \bar{c}_2 \bar{r}_1 \bar{r}_2}\right)\bar{x}_1 \\ &+ \left(\frac{c_1 r_1}{\bar{c}_2^2 \bar{r}_2} - \frac{1}{\bar{c}_2} + \frac{c_2 r_1}{\bar{c}_2^2 \bar{r}_2} - \frac{c_1 c_2 r_1 r_2}{\bar{c}_2^3 \bar{r}_2^2} + \frac{c_2 r_2}{\bar{c}_2^2 \bar{r}_2} + \frac{c_1 c_2 r_1 r_2}{\bar{c}_1 \bar{c}_2^3 \bar{r}_2^3}\right)\bar{x}_2 \\ &+ \frac{c_1 c_2 r_1 r_2}{\bar{c}_1 \bar{c}_2 \bar{r}_1 \bar{r}_2}\bar{u} + w, \end{aligned} \tag{4.32}$$

where w is a new control. As expected, (4.32) is identical to (4.30) by substituting $y = \bar{y}$.

Stability of $Z^\star$ is addressed by defining the error $e = x - \varphi(\bar{x})$ and by writing its dynamics

$$\begin{bmatrix} \dot{e}_1 \\ \\ \dot{e}_2 \end{bmatrix} = \begin{bmatrix} -\frac{1}{r_1} - \frac{1}{r_2} & \frac{1}{r_2} \\ \frac{1}{r_2} & -\frac{1}{r_2} \end{bmatrix} \begin{bmatrix} \frac{1}{c_1}e_1 \\ \frac{1}{c_2}e_2 \end{bmatrix} - \begin{bmatrix} \frac{1}{r_1} \\ 0 \end{bmatrix} w, \tag{4.33}$$

showing that $Z^\star$ is attractive for $w = 0$. Further stabilisation is possible through the control $w = K(x - \varphi(\bar{x}))$ with some suitable gain K. Note that the closed loop has the bond graph topology of Figure 4.19. ◊

It has been shown, by means of an example, that the ideas of specification based inversion of [Ngw99b] can be extended to an MMP design. Even though the methodology has been presented through a explicit SISO system, it is readily argued that for MIMO bond graphs this MMP scenario is conceptually possible provided no causal conflicts occur. However, as argued in Section 4.2, the inclusion of dependent storage elements renders the design of the MMP more complicated with respect to the bond graph representation of the closed loop error dynamics, because the implicit dynamics is to be reduced into explicit form for analysis, thereby rendering bond graph considerations difficult. Future research could address the MIMO and implicit case in greater detail.

4.4. General Cases of Model Matching

Sections 4.2 and 4.3 presented some basic specialisations of bond graph modelling for the MMP, where it was shown that for certain MMP setups it is possible to use the bicausal approach to find the control that renders the difference $y-\bar{y}$ independent of $\bar{u}$. Furthermore, it was seen that the closed loop error dynamics allowed for a bond graph representation by means of output regulation arguments such that closed loop stabilisation could be based on passivity arguments.

Even though the previously presented MMP scenarios represent a relevant class of systems, it can be argued that their applicability can be limited due to the specialised input/output configuration. To provide more flexibility of bond graph models for the definition of the MMP, a larger class of systems that bond graphs can generate should be considered. For example, bond graph models with derivative causalities can be considered, leading to a large class of *implicit* systems. Also, less specialised input/output configurations of the plant P and model M can further enlarge the class of MMPs considerably.

Because derivative causalities often occur in a wide variety of bond graph models, it can be argued that such systems represent an important set of dynamic systems. Therefore, this section addresses bond graph models that are allowed to have storage element in derivative causality. However, in view of Theorem 2.6, the implicit systems context renders the closed loop bond graph representations of the error dynamics of limited interest. This can be explained by the fact that implicit dynamics must be reduced to explicit dynamics. Nonetheless, even though the closed loop bond graph representation of the error dynamics may not be available, the closed loop input/output dynamics remain to have a bond graph representation by construction.

As already mentioned, the following sections address a more general bond graph based MMP with no specific input/output configuration. In addition, the model M need not contain a copy of the plant, but the model will be chosen to be structurally "close" to the plant in order to satisfy the relative degree condition $r_i \leq \bar{r}_i$. Furthermore, the application of bicausal bond graphs will not be considered for system inversion purposes due to various difficulties with respect to non–standard output definitions. Also, the application of alternative causal assignment procedures to deal with derivative causalities renders the application of the (bi)causal mechanism rather difficult.

Characteristic difficulties of more general classes of bond graph models can be summarised by the following:

First, the Standard Causality Assignment Procedure (SCAP) may yield unnecessary complex dynamics due to the "automated" selection of state variables. To remedy such problems, it is possible to consider alternative causality assignment procedures, such as the Lagrangian Causality Assignment Procedure with multipliers denoted as λLCAP [Mar02]. However, it should be noted that (bi)causal bond graphs have not been developed for such alternative causal assignment procedures.

Second, it must be recognised that general bond graph models need not be feedback linearisable on the domain of interest. Therefore, if feedback linearisability is not suitable or applicable for the system at hand, one could consider the linearised MMP instead. This scenario will be demonstrated in detail later on.

Third, if non–standard input/output configurations are considered, the use of **SS** components to extract the desired output variable need not be possible without "contrived" bond graph modelling. In these cases it is readily seen that bicausal assignment becomes difficult, mainly because the bond graph does not define the output variable through the **SS** source component. As a result, such non–standard output definitions should not be modelled with bond graphs but manually appended to the derived dynamics.

4.4.1. A Class of Implicit Systems

Consider the *implicit* port–Hamiltonian plant P of the form

$$\begin{bmatrix} \dot{x}^1 \\ \dot{x}^2 \\ y \\ 0 \end{bmatrix} = \begin{bmatrix} J(x^1,\mu) - R(x^1,\mu) & 0 & -g(x^1,\mu) & -q(x^1,\mu) \\ 0 & 0 & 0 & I_{n_2} \\ g^T(x^1,\mu) & 0 & 0 & -b(x^1,\mu) \\ q^T(x^1,\mu) & -I_{n_2} & b^T(x^1,\mu) & 0 \end{bmatrix} \begin{bmatrix} K^1(x^1,\mu) \\ K^2(x^2,\mu) \\ u \\ \lambda \end{bmatrix}, \quad (4.34)$$

where $x^1 \in \mathbb{R}^{n_1}$, $x^2 \in \mathbb{R}^{n_2}$, $\lambda \in \mathbb{R}^{n_2}$ and $u, y \in \mathbb{R}^m$. Let μ be a vector of physical parameters. This type of system is typically obtained from a bond graph in which each dependent storage element is forced into *integral* causality through a Lagrange multiplier directly at the dependent storage element. Note, in particular, that the output y generally requires redefinition in order to select the proper output variable that needs to be controlled.

4.4.2. Examples

The full generality of (4.34) renders it difficult to define constructive bond graph based MMP scenarios for which, for example, bicausal bond graphs can be used and for which feedback linearisation is feasible. The approach taken here is to consider procedures similar to λLCAP found in [Mar02] in case SCAP becomes difficult. The model will be defined to be structurally "close" to the the plant such that relative degree conditions are fulfilled. In case feedback linearisation is not feasible, it will be shown that the linearised MMP can be attempted, where the bond graph definition of the plant and model remain unmodified. The following examples show instructive MMPs, but it is not attempted to present formalised procedures for implicit systems of the form (4.34).

Example 4.5. Consider a pendulum mounted on a horizontally moving, massless cart depicted in Figure 4.21. Let the Hamiltonian be given by

$$H(x) = \frac{1}{2I}x_2^2 + \frac{1}{2m}(x_3^2 + x_4^2) + mgl\sin(x_1). \tag{4.35}$$

The moment of inertia about its centre of mass G is denoted as I, the mass of the pendulum is m, the distance from the hinge to G is denoted as l. The variable $x_1 = \theta$ denotes the angular position counter clockwise from the horizontal, x_2 is the angular momentum, x_3 and x_4 are the respective vertical and horizontal momenta of G. Note that the control input u is a velocity. The bond graph representation is given in Figure 4.22 with modulations $t_1(x_1) = l\cos(x_1)$ and $t_2(x_1) = -l\sin(x_1)$. To force all elements into integral causality, Lagrange multipliers are inserted under the condition that the constraint forces λ_1 and λ_2 are to be "workless", implying that their conjugate velocities are to be nullified accordingly.

Next observe that the plant bond graph does not show a simple **SS** element that extracts the pendulum angle x_1 as a system output. In view of (4.35), the reason for doing so is that the output of the **C** element is a nonlinear function in x_1, so that the angle x_1 cannot be simply extracted by the inclusion of such **SS** element. Consequently, the bicausal approach is not readily applicable for this system due to the absence of this **SS** element. This is not believed to be a great problem, since the MMP is solved analytically once the plant and model have been defined, where the desired outputs are simply added to the plant and model definitions once the causal analysis is completed. So, bicausal assignment can add a certain convenience and systematic bond graph approach to the design, but it is not a crucial aspect of the physical model based MMP considered here.

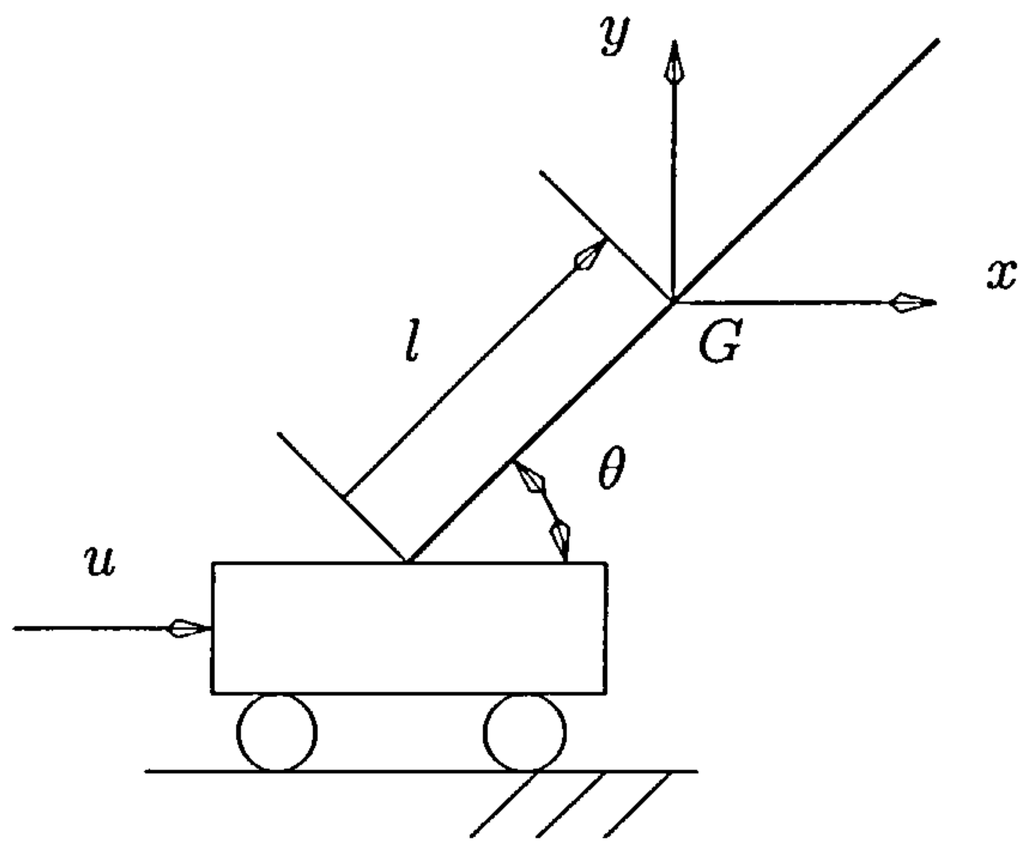

Figure 4.21.: Inverted pendulum of Example 4.5.

From Figure 4.22 it is a straightforward exercise to find the implicit port–Hamiltonian representation

$$\begin{bmatrix} \dot{x}_1 \\ \dot{x}_2 \\ \dot{x}_3 \\ \dot{x}_4 \\ y \\ 0 \\ 0 \end{bmatrix} = \begin{bmatrix} 0 & 1 & 0 & 0 & 0 & 0 & 0 \\ -1 & -r & 0 & 0 & 0 & -l\cos(x_1) & l\sin(x_1) \\ 0 & 0 & 0 & 0 & 0 & 1 & 0 \\ 0 & 0 & 0 & 0 & 0 & 0 & 1 \\ 0 & 0 & 0 & 0 & 0 & 0 & 1 \\ 0 & l\cos(x_1) & -1 & 0 & 0 & 0 & 0 \\ 0 & -l\sin(x_1) & 0 & -1 & -1 & 0 & 0 \end{bmatrix} \begin{bmatrix} mgl\cos(x_1) \\ x_2/I \\ x_3/m \\ x_4/m \\ u \\ \lambda_1 \\ \lambda_2 \end{bmatrix}, \tag{4.36}$$

where r is the friction coefficient of the hinge, and where λ_1 and λ_2 are Lagrange multipliers that are to render the dynamics tangent to the constraint manifold defined by the last two equations of (4.36). Clearly, the above system is of the form (4.34).

The *implicit* representation of the plant can be turned into an *explicit* system by eliminating the multipliers λ_1 and λ_2. Doing so yields the reduced constraint plant

$$\begin{aligned} \dot{x}_1 &= \frac{1}{I}x_2 \\ \dot{x}_2 &= -\frac{r}{I+ml^2}x_2 - \frac{mlI}{I+ml^2}(g\cos(x_1) + \sin(x_1)\dot{u}) \\ y &= x_1, \end{aligned} \tag{4.37}$$

where y has now been redefined to be the controlled angle x_1. Note that the implicit system (4.36) is readily reducible to the explicit system (4.37), but it cannot be guaranteed that the reduction of the implicit system (4.34) yields an explicit port–Hamiltonian model.

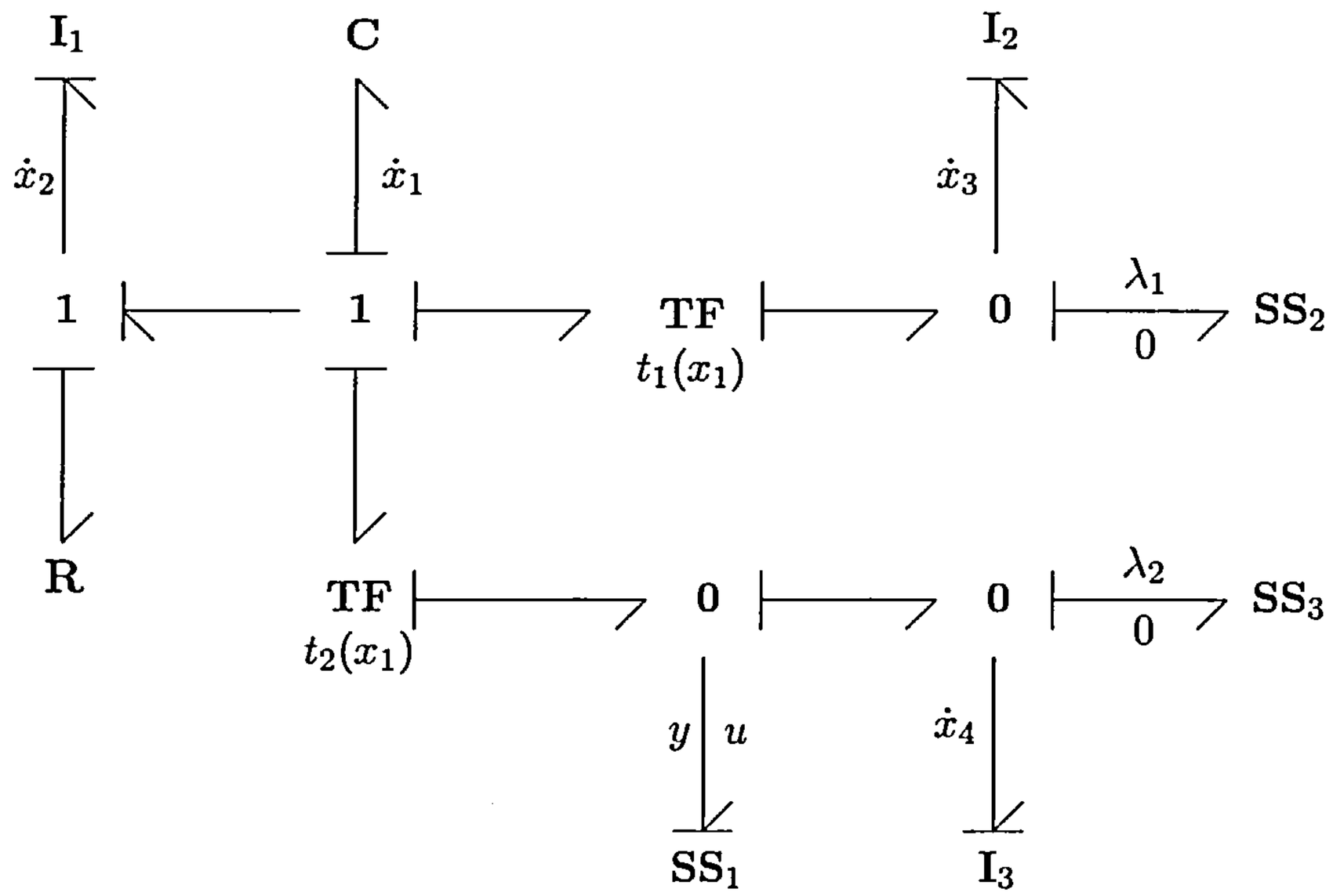

Figure 4.22.: Pendulum bond graph with λ–multipliers of Example 4.5.

The next step in the design is the definition of the control objective: stabilisation of the pendulum at the angle $x_1 = \pi/2$, which is the upright position. To this end, it is recognised that the pendulum on the moving cart is structurally "close" to a simple pendulum that pivots around a fixed point. This observation is entirely subjective but suggests a suitable model that produces angle trajectories that can be associated with the moving pendulum. The bond graph topology of the simple pendulum is depicted in Figure 4.23 and is seen to be similar to the plant, where the modulations are $\bar{t}_1(\bar{x}_1) = l\cos(\bar{x}_1)$ and $\bar{t}_2(\bar{x}_1) = -l\sin(\bar{x}_1)$. No **SS** element is used to extract an output variable since the pendulum angle $\bar{x}_1$ does not appear conveniently in the model.

Causal analysis of Figure 4.23 yields the *implicit* port–Hamiltonian system

$$\begin{bmatrix} \dot{\bar{x}}_1 \\ \dot{\bar{x}}_2 \\ \dot{\bar{x}}_3 \\ \dot{\bar{x}}_4 \\ \bar{y} \\ 0 \\ 0 \end{bmatrix} = \begin{bmatrix} 0 & 1 & 0 & 0 & 0 & 0 & 0 \\ -1 & -r & 0 & 0 & -1 & -l\cos(\bar{x}_1) & l\sin(\bar{x}_1) \\ 0 & 0 & 0 & 0 & 0 & 1 & 0 \\ 0 & 0 & 0 & 0 & 0 & 0 & 1 \\ 0 & 1 & 0 & 0 & 0 & 0 & 1 \\ 0 & l\cos(\bar{x}_1) & -1 & 0 & 0 & 0 & 0 \\ 0 & -l\sin(\bar{x}_1) & 0 & -1 & 0 & 0 & 0 \end{bmatrix} \begin{bmatrix} \bar{K}_1(\bar{x}) \\ \bar{K}_2(\bar{x}) \\ \bar{K}_3(\bar{x}) \\ \bar{K}_4(\bar{x}) \\ \bar{u} \\ \bar{\lambda}_1 \\ \bar{\lambda}_2 \end{bmatrix}, \tag{4.38}$$

where $\bar{K}^T(\bar{x}) = \mathbf{D}\bar{H}(\bar{x})$ and where $\bar{H}\colon \bar{X} \to \mathbb{R}$ is given by

$$\bar{H}(\bar{x}) = mgl\sin(\bar{x}_1) + \frac{1}{2}k(\bar{x}_1 - \frac{1}{2}\pi)^2 + \frac{1}{2I}\bar{x}_2^2 + \frac{1}{2m}(\bar{x}_3^2 + \bar{x}_4^2). \tag{4.39}$$

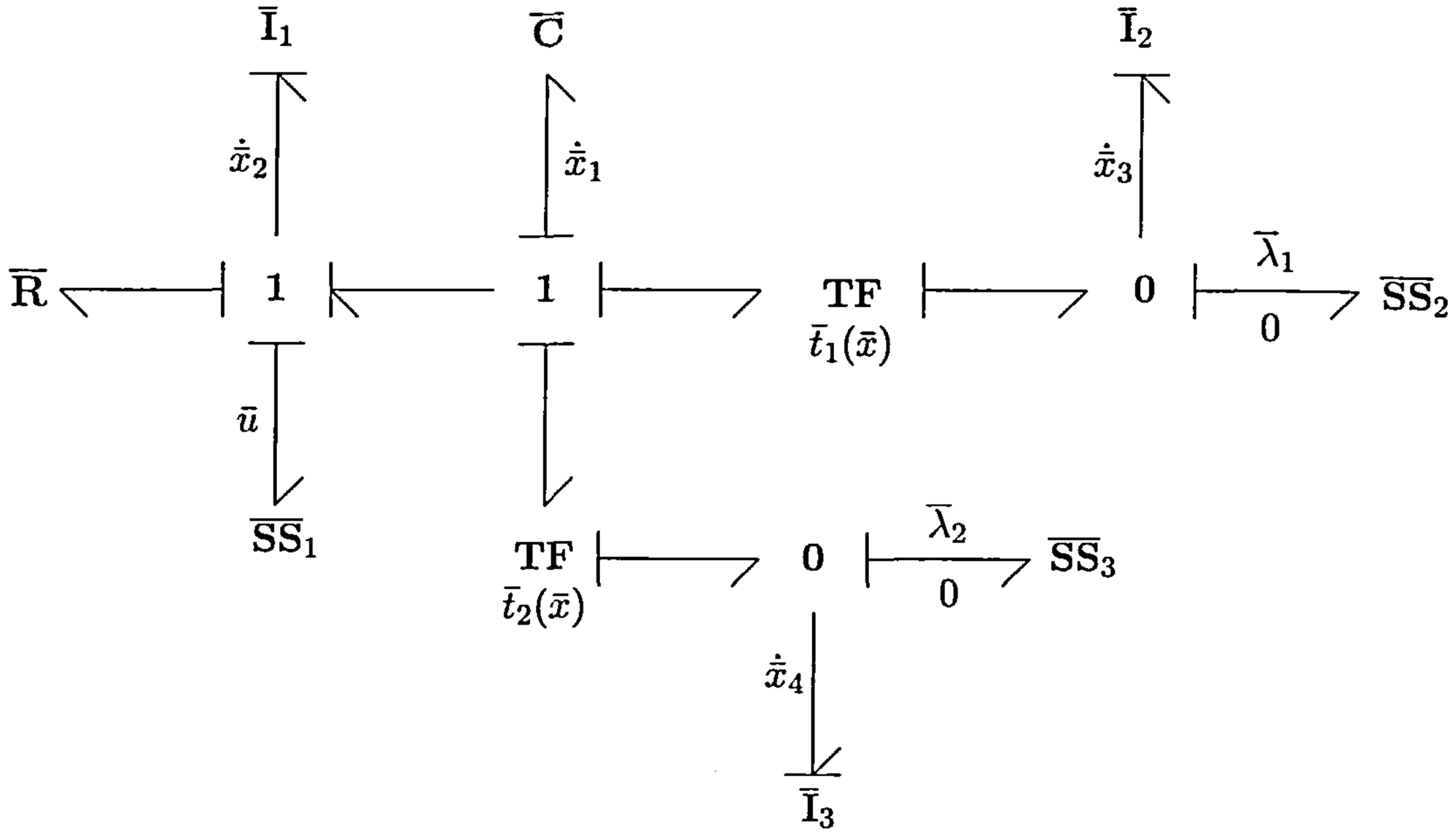

Figure 4.23.: Simple pendulum model bond graph with $\bar{\lambda}$–multipliers of Example 4.5.

The upright equilibrium position $x = (\pi/2, 0, 0, 0)$ can be rendered a global minimum by choosing $k > mgl$. This will guarantee the the simple pendulum has the upright position as an attractive equilibrium point.

Reduction of the constrained dynamics yields the model

$$\begin{aligned} \dot{\bar{x}}_1 &= \frac{1}{I}\bar{x}_2 \\ \dot{\bar{x}}_2 &= -\frac{r}{I+ml^2}\bar{x}_2 - \frac{I}{I+ml^2}(mgl\cos(\bar{x}_1) + k(x_1 - \frac{1}{2}\pi) + \bar{u}) \\ \bar{y} &= \bar{x}_1. \end{aligned} \tag{4.40}$$

Before the MMP can be addressed, observe that the absence of a relative degree for $\sin(x_1) = 0$ is an important characteristic of the plant and implies that all control authority is lost whenever the moving pendulum is in a horizontal position. Consequently, feedback linearisation is possible only for points bounded away from $x_1 = n\pi$, which implies that it is possible to asymptotically track the angle of the simple pendulum around the upright position.

On a side note, the absence of a relative degree is something that is difficult to observe from general bond graphs of arbitrary complexity and dimension, so that the structural properties of bond graph models is better facilitated through analytical means. That is to say that bond graph modelling offers a systematic procedure for obtaining the system dynamics, but standard control theory should be applied to establish the relative degree property.

Now, to render the disturbance decoupling problem simple, consider the linearising control

$$\dot{u} = -\frac{1}{mlI\sin(x_1)}[rx_2 + gmlI\cos(x_1)] - \frac{I+ml^2}{mlI\sin(x_1)}w, \tag{4.41}$$

which is defined for $x_1 \neq n\pi$ and where w is a new control. This control yields the simplest dynamics possible, being

$$\begin{aligned} \dot{x}_1 &= \frac{1}{I}x_2 \\ \dot{x}_2 &= w. \end{aligned} \tag{4.42}$$

The submanifold $Z^\star$ on which output matching occurs is simply

$$Z^\star = \{(x,\bar{x}) : x - \varphi(\bar{x}) = \begin{bmatrix} x_1 \\ x_2 \end{bmatrix} - \begin{bmatrix} \bar{x}_1 \\ \bar{x}_2 \end{bmatrix} = 0\}. \tag{4.43}$$

Then take $k_1, k_2 > 0$ and define $e = x - \varphi(\bar{x})$, so that $Z^\star$ can be made attractive with

$$\begin{aligned} w &= c(\bar{x},\bar{u}) + K[x - \varphi(\bar{x})] \\ &= -\frac{r}{I+ml^2}\bar{x}_2 - \frac{I}{I+ml^2}(mgl\cos(\bar{x}_1) + k(\bar{x}_1 - \frac{1}{2}\pi) + \bar{u}) - k_1e_1 - k_2e_2. \end{aligned} \tag{4.44}$$

◊

Some observations on behalf of the above example can be made. For instance, the inverted pendulum shows that the absence of a well–defined relative degree need not compromise the MMP objective, provided that the relative degree exists on the domain of interest. However, it is certainly conceivable that the structure of the system does not sustain a well–defined relative degree on the domain of interest, so that the MMP cannot be addressed in a manner that has been portrayed so far. The upcoming example shows that the linearised MMP can be considered if the nonlinear plant dynamics are not suitable for feedback linearisation.

Furthermore, the implicit port–Hamiltonian dynamics (4.34) shows to be a suitable representation of the inverted pendulum problem for which the elimination of the Lagrange multiplier is readily possible. On the other hand, the upcoming example shows that such implicit dynamics can yield unnecessary complex dynamics and that the Lagrangian causality assignment procedure LCAP [Mar02] is preferable instead. However, in view of such alternative causality procedures, the bicausal bond graph mechanism is of limited interest since it is mainly applied to bond graphs that are causally completed with SCAP. In fact, bicausal assignment has not yet been reported for LCAP or other alternative causality assignment procedures.

Example 4.6. Consider a sliding mass along a straight, slender rod that pivots around its non–moving centre of mass depicted in Figure 4.24. The control input u is a torque around its centre of mass. Let the plant energy function be defined as

$$H(x) = mgx_3 \sin(x_1) + \frac{1}{2I}x_2^2 + \frac{1}{2m}(x_4^2 + x_5^2), \tag{4.45}$$

where $x_1 = \theta$ and $x_3 = r$. The angular momentum is given as the coordinate x_2 and the linear momenta, denoted as x_4 and x_5, are in the x and y directions respectively. Elementary kinematic analysis based on $x = x_3\cos(x_1)$ and $y = x_3\sin(x_1)$ explains the modulations in the plant bond graph of Figure 4.25, where

$$\begin{aligned} t_1(x_1) &= \sin(x_1), & t_2(x_1) &= x_3\cos(x_1) \\ t_3(x_1) &= -x_3\sin(x_1), & t_4(x_1) &= \cos(x_1). \end{aligned} \tag{4.46}$$

Causal analysis yields the implicit port–Hamiltonian system

$$\begin{bmatrix} \dot{x}_1 \\ \dot{x}_2 \\ \dot{x}_3 \\ \dot{x}_4 \\ \dot{x}_5 \\ y \\ 0 \end{bmatrix} = \begin{bmatrix} 0 & 1 & 0 & 0 & 0 & 0 & 0 \\ -1 & 0 & t_3/t_4 & 0 & 0 & -1 & (t_1t_3 - t_2t_4)/t_4 \\ 0 & -t_3/t_4 & 0 & 1/t_4 & 0 & 0 & 0 \\ 0 & 0 & -1/t_4 & 0 & 0 & 0 & -t_1/t_4 \\ 0 & 0 & 0 & 0 & 0 & 0 & 1 \\ 0 & 1 & 0 & 0 & 0 & 0 & 0 \\ 0 & (t_2t_4 - t_1t_3)/t_4 & 0 & t_1/t_4 & -1 & 0 & 0 \end{bmatrix} \begin{bmatrix} K_1(x) \\ K_2(x) \\ K_3(x) \\ K_4(x) \\ K_5(x) \\ u \\ \lambda \end{bmatrix}. \tag{4.47}$$

The λ–multiplier has a nullified conjugate velocity, imposing the requirement that it is to be "workless". Even though the above implicit system can be reduced into explicit form systematically, the structure of (4.47) yields a model of unnecessary complexity: the horizontal momentum x_4 is a state variable while the physical structure of the system is better suited for polar coordinates.

The occasions where implicit port–Hamiltonian dynamics (4.34) yield complex reduced dynamics can sometimes be remedied by considering λLCAP instead, where multipliers are introduced if one is not able to find a minimal set of of generalised coordinates [Mar02]. Towards this end, the bond graph in Figure 4.25 is slightly modified to the bond graph in Figure 4.26, where the source elements $\mathbf{SS}_1$ and $\mathbf{SS}_2$ define the generalised coordinates.

It is important to note that λLCAP considered here reduces to LCAP since a minimal set of generalised coordinates has been found, which are $x_1 = \theta$ and $x_2 = r$, so that Lagrange multipliers are not needed.

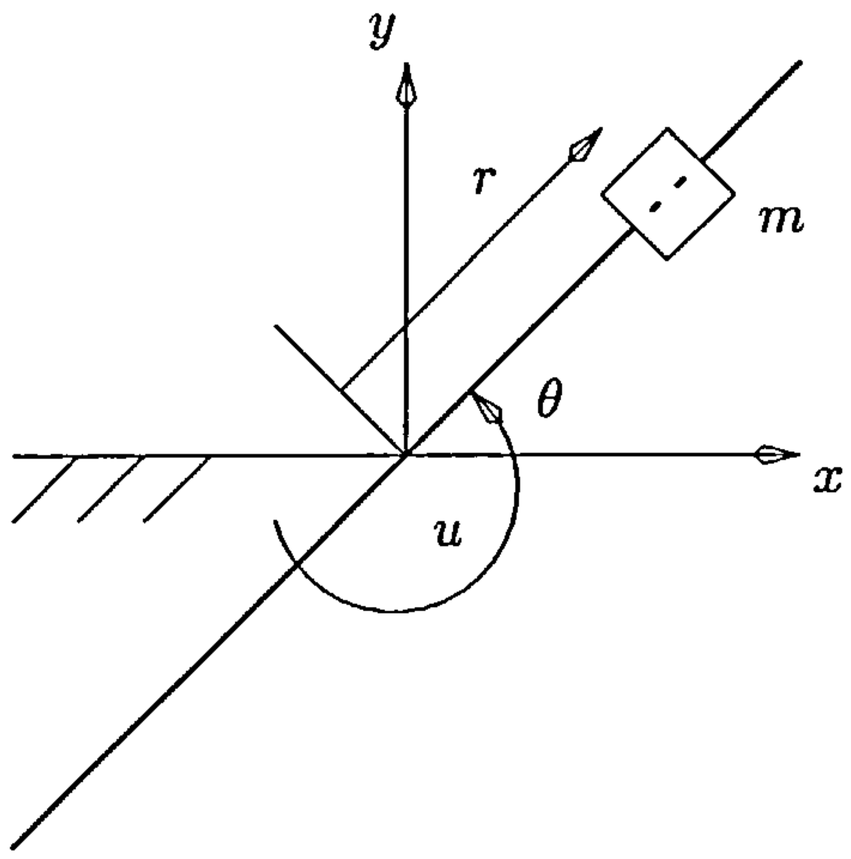

Figure 4.24.: Frictionless slider of Example 4.6.

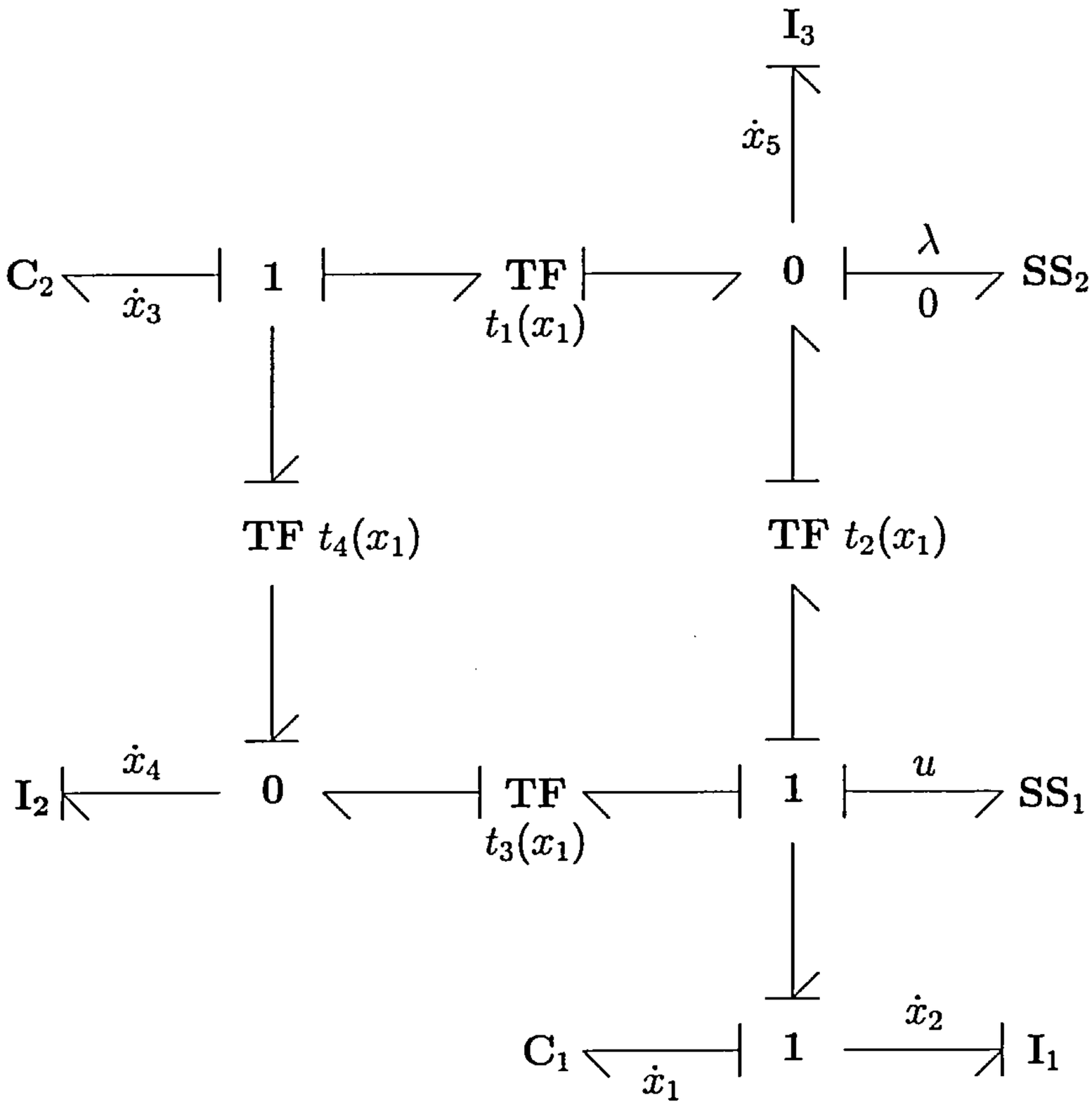

Figure 4.25.: Frictionless slider with λ–multiplier of Example 4.6.

The modulations in Figure 4.26 are defined as

$$\begin{aligned} t_1(x_1) &= \sin(x_1), & t_2(x_1) &= x_2\cos(x_1), \\ t_3(x_1) &= -x_2\sin(x_1), & t_4(x_1) &= \cos(x_1), \end{aligned} \tag{4.48}$$

which should not be confused with the modulations (4.46).

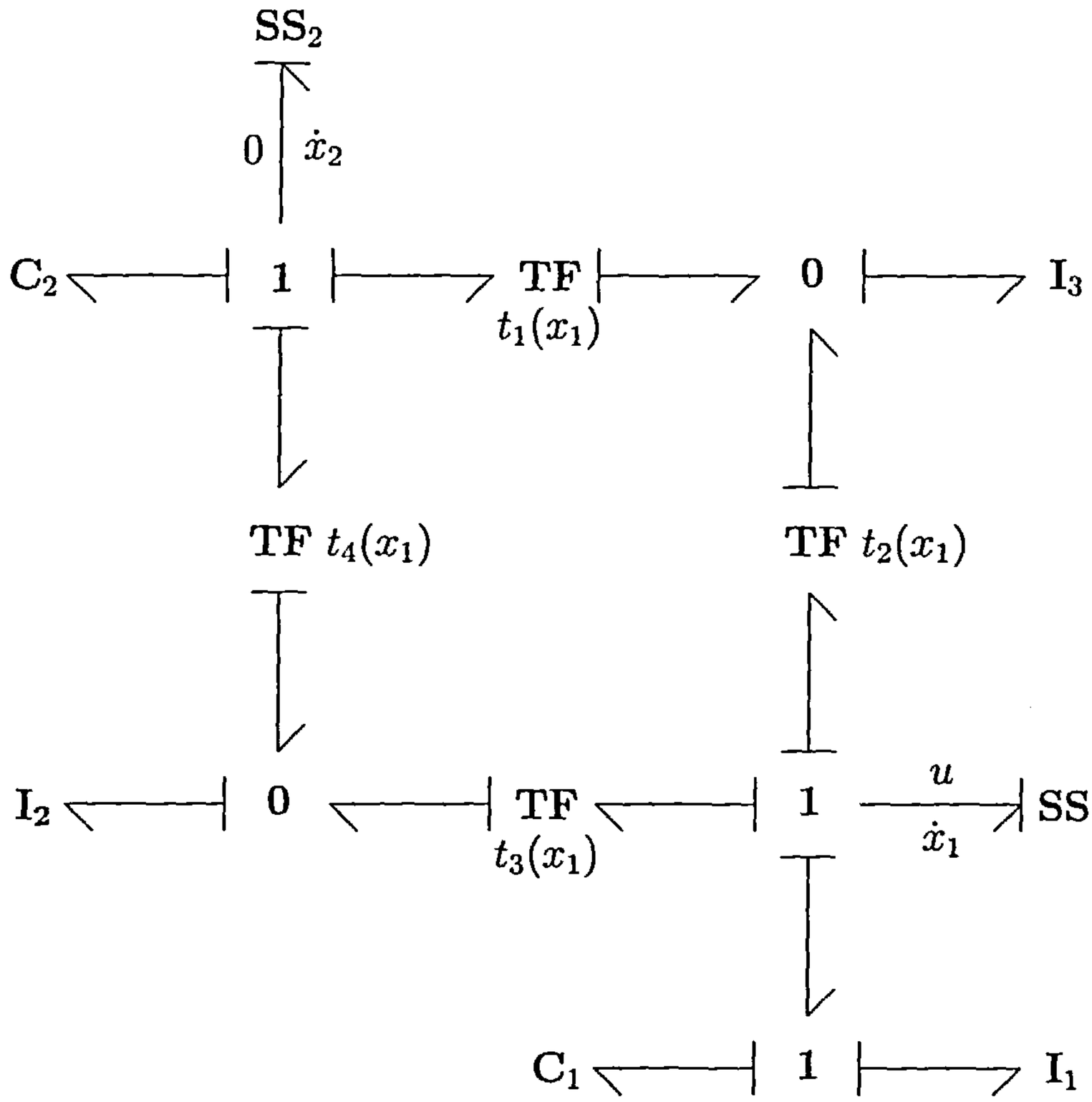

Figure 4.26.: Frictionless slider with LCAP of Example 4.6.

By applying LCAP, the equations of motions are obtained through the summation of efforts at the one–junctions to which $\mathbf{SS}_1$ and $\mathbf{SS}_2$ are connected. This yields the dynamics

$$\begin{aligned} \ddot{x}_1 &= -\frac{1}{I + mx_2^2}(2mx_2\dot{x}_2\dot{x}_1 + mgx_2\cos(x_1) + u) \\ \ddot{x}_2 &= x_2\dot{x}_1^2 - g\sin(x_1). \end{aligned} \tag{4.49}$$

By defining $z_1 = x_1$, $z_2 = \dot{x}_1$, $z_3 = x_2$ and $z_4 = \dot{x}_2$, the plant takes the first order form

$$\begin{aligned} \dot{z}_1 &= z_2 \\ \dot{z}_2 &= -\frac{1}{I + mz_3^2}(2mz_2z_3z_4 + mgz_3\cos(z_1) + u) \\ \dot{z}_3 &= z_4 \\ \dot{z}_4 &= z_3z_2^2 - g\sin(z_1) \\ y &= z_3, \end{aligned} \tag{4.50}$$

where the output $y = z_3$ has been added to incorporate the requirement that the distance of the slider with respect to the hinge point is to be controlled. On a side note, observe that it is by no means trivial how $y = z_3$ can be used in a bicausal assignment scheme for the system (4.50).

Now that the plant has been derived through LCAP, the lack of feedback linearisability of the plant is readily verified. To see this, consider

$$\begin{aligned} y^{(1)} &= z_4 \\ y^{(2)} &= z_3 z_2^2 - g\sin(z_1) \\ y^{(3)} &= z_4 z_2^2 - g\cos(z_1)z_2 + 2z_2 z_3 v, \end{aligned} \tag{4.51}$$

where $d^r y/dt^r = y^{(r)}$ and by having applied the linearising control

$$u = -2mz_2 z_3 z_4 - mgz_3\cos(z_1) - (I + mz_3^2)v. \tag{4.52}$$

Observe that the structure of the system strongly impedes feedback linearisation at the points $z_2 = z_3 = 0$, thereby rendering the tracking of prescribed trajectories around the point $z_3 = 0$ very difficult. More precisely, the condition $z_2 = 0$ implies that the angular velocity cannot be zero, which is very restrictive. In addition, the condition $z_3 = 0$ shows that the slider is at the hinge, meaning that the slider is to be positioned away from the hinge point for tracking purposes. In conclusion, the feedback linearisation of the full nonlinear case is abandoned and a linearised MMP design around the origin is considered instead.

Towards that end, let $A = \mathrm{D}_z f(0,0)$ and $B = \mathrm{D}_u f(0,0)$, where (4.50) is written as $\dot{z} = f(z,u)$ and satisfies $f(0,0) = 0$. The linear system is then written as $\dot{z} = Az + Bu$, thus

$$\begin{aligned} \dot{z}_1 &= z_2 \\ \dot{z}_2 &= -\frac{gm}{I}z_3 - \frac{1}{I}u \\ \dot{z}_3 &= z_4 \\ \dot{z}_4 &= -gz_1 \\ y &= z_3. \end{aligned} \tag{4.53}$$

Note that (A,B) is stabilisable so that Theorem 2.6 can be invoked to show that the Full Information Output Regulation Problem is solvable whenever (2.65) can be fulfilled.

Next consider the bond graph representation of M in Figure 4.27. It is now attempted to stabilise of the origin by assigning an energy function and suitable dissipation. Hence, the closed loop input/output dynamics is effectively modelled with the model bond graph.

To stabilise the origin $z = 0$, let the Hamiltonian of the model M be defined as

$$\bar{H}(\bar{x}) = mg\bar{x}_3\sin(\bar{x}_1) + \frac{1}{2}\bar{k}_1\bar{x}_1^2 + \frac{1}{2I}\bar{x}_2^2 + \frac{1}{2}\bar{k}_2\bar{x}_3^2 + \frac{1}{2m}(\bar{x}_4^2 + \bar{x}_5^2), \tag{4.54}$$

which is guaranteed to have a global minimum at $\bar{x} = 0$ for the gains $\bar{k}_1\bar{k}_2 > g^2m^2$.

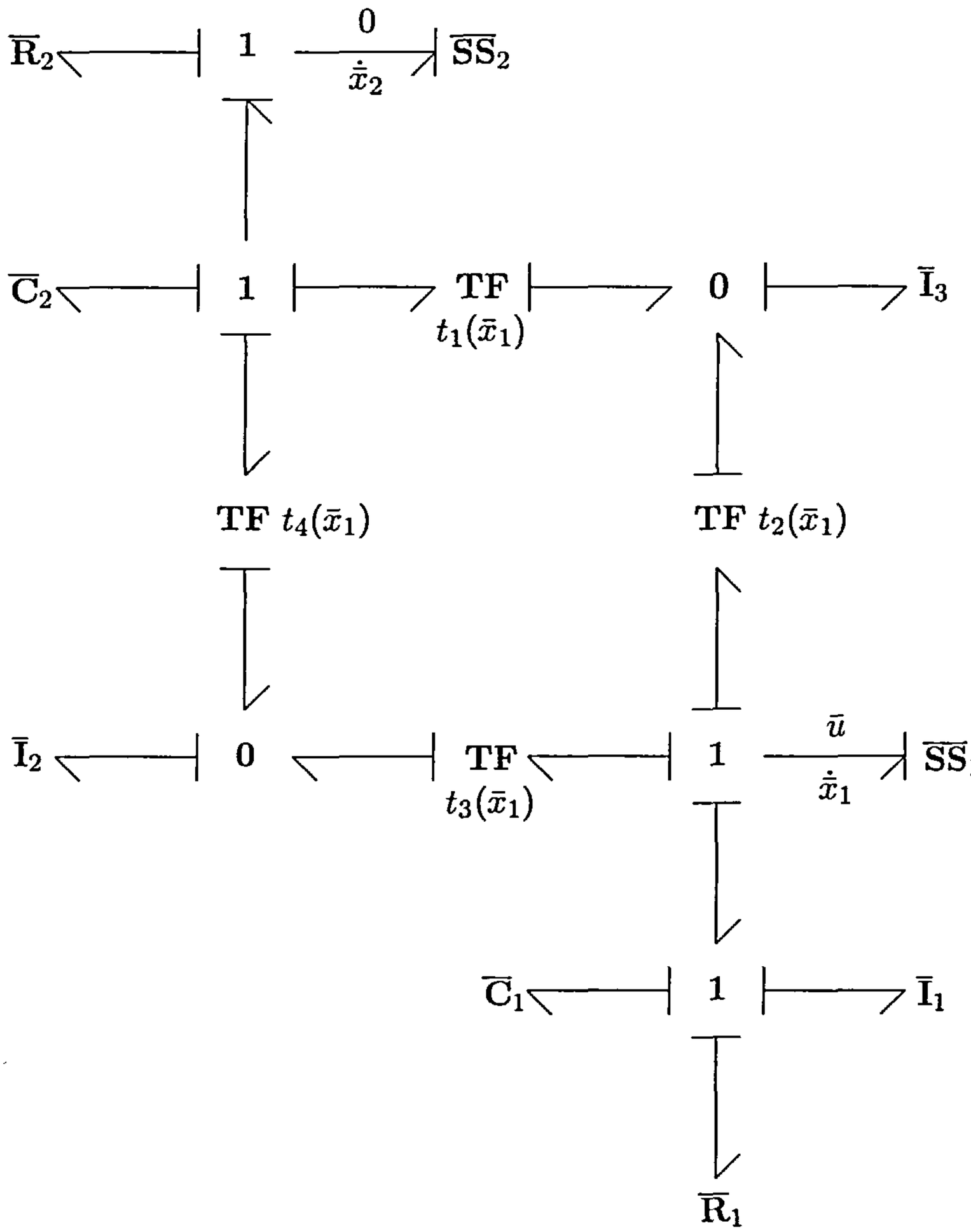

Figure 4.27.: Model slider with LCAP of Example 4.6.

By following the causal configuration of Figure 4.27 one obtains the system

$$\begin{aligned} \ddot{\bar{x}}_1 &= -\frac{1}{I+m\bar{x}_2^2}(2m\bar{x}_2\dot{\bar{x}}_1\dot{\bar{x}}_2 + mg\bar{x}_2\cos(\bar{x}_1) + \bar{k}_1\bar{x}_1 + \bar{r}_1\dot{\bar{x}}_1 + \bar{u}) \\ \ddot{\bar{x}}_2 &= \bar{x}_2\dot{\bar{x}}_1^2 - g\sin(\bar{x}_1) - \frac{\bar{k}_2}{m}\bar{x}_2 - \frac{\bar{r}_2}{m}\dot{\bar{x}}_2. \end{aligned} \tag{4.55}$$

Let $\bar{z}_1 = \bar{x}_1$, $\bar{z}_2 = \dot{\bar{x}}_1$, $\bar{z}_3 = \bar{x}_2$ and $\bar{z}_4 = \dot{\bar{x}}_2$, so that the model takes the first order form

$$\begin{aligned} \dot{\bar{z}}_1 &= \bar{z}_2 \\ \dot{\bar{z}}_2 &= -\frac{1}{I+m\bar{z}_3^2}(2m\bar{z}_2\bar{z}_3\bar{z}_4 + mg\bar{z}_3\cos(\bar{z}_1) + \bar{k}_1\bar{z}_1 + \bar{r}_1\bar{z}_2 + \bar{u}) \\ \dot{\bar{z}}_3 &= \bar{z}_4 \\ \dot{\bar{z}}_4 &= \bar{z}_3\bar{z}_2^2 - g\sin(\bar{z}_1) - \frac{\bar{k}_2}{m}\bar{z}_3 - \frac{\bar{r}_2}{m}\bar{z}_4 \\ \bar{y} &= \bar{z}_3, \end{aligned} \tag{4.56}$$

Define $\bar{A} = \mathbf{D}_{\bar{z}}\bar{f}(0,0)$ and $\bar{B} = \mathbf{D}_{\bar{u}}\bar{f}(0,0)$, where $\bar{f}(0,0) = 0$. Then $\dot{\bar{z}} = \bar{A}\bar{z} + \bar{B}\bar{u}$ and write

$$\begin{aligned}
\dot{\bar{z}}_1 &= \bar{z}_2 \\
\dot{\bar{z}}_2 &= -\frac{\bar{k}_1}{I}\bar{z}_1 - \frac{\bar{r}_1}{I}\bar{z}_2 - \frac{gm}{I}\bar{z}_3 - \frac{1}{I}\bar{u} \\
\dot{\bar{z}}_3 &= \bar{z}_4 \\
\dot{\bar{z}}_4 &= -g\bar{z}_1 - \frac{\bar{k}_2}{m}\bar{z}_3 - \frac{\bar{r}_2}{m}\bar{z}_4 \\
\bar{y} &= \bar{z}_3.
\end{aligned} \tag{4.57}$$

At this stage both the plant and model have been linearised and the linear MMP can now be addressed, where the constrained dynamics algorithm is used to find the submanifold $Z^\star$. Doing so yields

$$Z^\star = \{(z,\bar{z}) : z - \varphi(\bar{z}) = \begin{bmatrix} z_1 \\ z_2 \\ z_3 \\ z_4 \end{bmatrix} - \begin{bmatrix} \bar{z}_1 + \frac{\bar{k}_2}{mg}\bar{z}_3 + \frac{\bar{r}_2}{mg}\bar{z}_4 \\ -\frac{\bar{r}_2}{m}\bar{z}_1 + \bar{z}_2 - \frac{\bar{r}_2\bar{k}_2}{m^2 g}\bar{z}_3 + \left(\frac{\bar{k}_2}{mg} - \frac{\bar{r}_2^2}{m^2 g}\right)\bar{z}_4 \\ \bar{z}_3 \\ \bar{z}_4 \end{bmatrix} = 0\}. \tag{4.58}$$

In view of (2.65), the control $c(\bar{z},\bar{u})$ is readily found by considering the relationship

$$\mathrm{D}\varphi(\bar{z})f(\bar{z},\bar{u}) = f(\varphi(\bar{z}),u), \tag{4.59}$$

where the control $u = c(\bar{z},\bar{u}) + w$ takes the form

$$\begin{aligned}
u = \left(\bar{k}_1 + \frac{\bar{k}_2 I}{m} - \frac{\bar{r}_2^2 I}{m^2}\right)\bar{z}_1 + \left(\bar{r}_1 + \frac{\bar{r}_2 I}{m}\right)\bar{z}_2 + \left(\frac{\bar{k}_2^2 I}{gm^2} - \frac{\bar{k}_2\bar{r}_2^2 I}{gm^3}\right)\bar{z}_3 \\
+ \left(\frac{2\bar{k}_2\bar{r}_2 I}{gm^2} - \frac{\bar{r}_2^3 I}{gm^3}\right)\bar{z}_4 + \bar{u} + w.
\end{aligned} \tag{4.60}$$

Finally, the convergence of the tracking error can be assessed through the error variable $e = z - \varphi(\bar{z})$, which has the dynamics

$$\begin{aligned}
\dot{e}_1 &= e_2 \\
\dot{e}_2 &= -\frac{gm}{I}e_3 - \frac{1}{I}w \\
\dot{e}_3 &= e_4 \\
\dot{e}_4 &= -ge_1.
\end{aligned} \tag{4.61}$$

Most importantly, observe that (4.61) has the same structure as the plant (4.53). Stabilisation through spectral assignment readily solves the linear MMP for $w = K[z - \varphi(\bar{z})] = Ke$ and some suitable gain K. ◊

The inverted pendulum and frictionless slider examples have demonstrated some important characteristics and difficulties of more generalised bond graph based MMPs that can be briefly summarised as follows.

Example 4.5 shows that the model can be chosen to be structurally "close" to the plant in the implicit context, but it is believed that such model definitions are difficult to formalise because they are highly dependent on the plant. Furthermore, the bicausal approach to solve the MMP through an inversion process showed not to be possible, since the output variable was difficult to extract by means of an **SS** component. As a result, it can be argued that non–standard output definitions must be added to the plant dynamics outside the bond graph framework, thereby avoiding certain "contrived" bond graph modelling steps that would increase the complexity.

Example 4.6 touches on the issue of alternative causal assignment procedures and the solution to a linearised MMP due to the lack of feedback linearisability. It followed that the frictionless slider proved not to be particularly suitable for SCAP, but where LCAP yielded a more efficient model that simplified the MMP. The choice of the causal assignment procedure can be said to be highly dependent on the plant, so that any explicit guidelines on the selection of such procedures will not be further formalised or elaborated here. Also, the lack of feedback linearisability of the slider did lead to the linearised MMP, where the bond graph representations of the plant and model remained unaltered. Therefore, the closed loop input/output dynamics remains to have a bond graph representation as prescribed by the model even in the linearised MMP.

4.5. Concluding Remarks

This chapter showed that bond graph modelling can be used for the definition of certain physical model based MMPs. The following control theoretical concepts formed the basis of the controller design in this chapter:

1. The nonregular Dynamic Disturbance Decoupling Problem with disturbance measurement [Hui92],[Hui94].

2. The Full Information Output Regulation Problem [Isi90],[Isi95].

The explicit identification of the bond graph based MMP with the above fundamental concepts is valuable, since it formalises controller design steps that were not documented in the bond graph literature.

Because the model bond graph is based on the plant bond graph, this produces control designs that moderately alter the plant input/output dynamics. Thus, instead of a complete redefinition of plant input/output dynamics through some arbitrary model, a physical model similar to the plant can be used in the control design and to render the solvability of the MMP more likely.

The MMP for *explicit* systems can be based on the ideas of Theorem 2.6 for closed loop stabilisation purposes, where the closed loop error dynamics "inherit" the plant bond graph. The closed input/output dynamics remains to have the model bond graph representation. However, the closed loop error dynamics and its associated bond graph representation is far more difficult to find for *implicit* systems, since, depending on the method used, the reduction of implicit dynamics to explicit dynamics need not yield port–Hamiltonian dynamics. Nonetheless, the closed loop input/output dynamics for reduced implicit systems remains to have the bond graph representation of the model.

Feedback linearisation may not be feasible for certain nonlinear MMP designs, so that a linearised MMP can be considered on the domain of interest instead. The model bond graph, on the other hand, need not change for the linear model since the linearised dynamics is derived from the nonlinear bond graph dynamics.

5. Energy Shaping in Stabilisation Control

5.1. Introduction

As mentioned in Section 2.5, the notion of *feedback passivation* can be loosely referred to as the process of rendering the closed loop passive with respect to some energy function and output function through feedback [Byr91]. It can be argued that passivation techniques form a vast field in control and that they have shown to be quite successful in various (non)linear control problems. For example, the widely used backstepping approach provides a relatively systematic framework for both stabilisation and tracking control through the recursive application of feedback passivation laws [Sep97], [Isi99], [Zha98]. Other interesting examples of feedback passivation techniques are related to port–Hamiltonian systems that have appeared in authoritative works such as [Ort98], [Ort00c], [Ort02a] and [Ort02b]. These papers show that a port–Hamiltonian plant can be transformed into another port–Hamiltonian system, thereby rendering the closed loop passive by construction. Now, it should be noted that the above examples of feedback passivation belong to a small subset of control problems that can be addressed in terms of passivation theory. However, the sheer volume of literature on passivity techniques in control renders it virtually impossible to even begin to cite certain works that provide a concise overview of the topic. The reader is therefore referred to the above cited papers and references therein for further details on feedback passivation.

It is well–known that bond graph modelling is based on energy concepts [Kar00]. Indeed, the **C** and **I** elements represent energy storage, the **R** elements denotes energy dissipation, and **SS** elements represent energy supply/extraction. Bond graphs have been shown to generate a class of port–Hamiltonian systems [Gol03] but are also capable of producing the second order Euler–Lagrange (EL) dynamics through an alternative causal assignment scheme [Kar77], [Kar83], [Bre94], [Mar02]. In view of such fundamental bond graph characteristics, this chapter explores bond graph modelling in stabilisation control through feedback passivation. Some developments and ideas on energy shaping and Interconnection and Damping Assignment (IDA–PBC) [Ort00a], [Ort02b] are also considered.

This chapter is organised as follows. The first part of the chapter addresses the notion of *power balancing* from a bond graph perspective, where connections with the work presented in [Ort00a], [Ort00b] are pointed out. It will be shown that power balancing through bond graph considerations is applicable to a class of bond graphs that can produce explicit and implicit port–Hamiltonian dynamics. The particular advantage of power balancing is that a closed loop storage function need not be known beforehand. Put differently, it is often the case that some desired closed loop storage function is "guessed" for feedback passivation purposes [Ort98]. Examples of power balancing control will be presented to show that the passivation controller is solely based on bond graph junction structure considerations.

The latter part of the chapter explores bond graph modelling in Interconnection and Damping Assignment Passivity Based Control (IDA–PBC) of port–Hamiltonian systems as presented in [Ort02b]. The main feature of energy shaping and IDA–PBC is that the plant remains an explicit port–Hamiltonian system in closed loop, where the interconnection and damping structures of the system can be modified through feedback control. However, IDA–PBC designs inherently lead to a set of PDEs that are difficult to solve in general, particularly for high–dimensional systems. Even though it does not belong to the overall objective of the thesis, a proposition is presented that provides a necessary condition for these first order PDEs to be solvable at all. A detailed example shows the bond graph interpretation of a basic IDA–PBC design, where the bond graph topology is shown to aid the choice of desired closed loop interconnection and damping structures.

It is important to note that passivation techniques such as the IDA–PBC methodology cannot be addressed through bond graph considerations alone. More precisely, this chapter shows that bond graph modelling can be used to define IDA–PBC designs on a more conceptual level by means of the graphical representation of the closed loop. However, the complexity of IDA–PBC designs requires conventional analytical techniques to find the control.

This chapter is by no means exhaustive and the various developments merely present a subset of bond graph aspects in feedback passivation control. In particular, considerable analysis remains necessary for all feedback passivation designs considered here. In addition, bicausal assignment will not be used since feedback passivation designs do not have the feedback linearisation of input/output behavior as a design goal.

5.2. Stabilisation through Power Balancing

This section addresses control through power balancing, where it is shown that this control strategy can be characterised by the junction structure topology. Closed loop energy functions are shown to be almost immediately derivable when the bond graph allows for a certain decomposition. It should be noted, however, that the applicability of power balancing can be impeded by the natural dissipation of the system, which is readily identified from the junction structure.

Bond graphs do not provide any analytical information on the associated energy function; for example, it is impossible to tell whether the energy function is positive definite based on the bond graph alone. Of course, the **I** and **C** storage components distinguish between the types of energy considered, but no analytical information on the storage function is given whatsoever. As a result, aspects of bond graph modelling in any sort of energy shaping are more analytical in nature. This section, on the other hand, shows that the junction structure can provide qualitative information on attainable energy shaping whenever the closed loop is to remain passive with respect to the natural output.

The bond graph based power balancing method is a special case in which the junction structure topology provides information on the type of energy function that can be associated with feedback. Now, if the plant energy is known, and the bond graph can be decomposed into two subsystems, then it may be the case that the energy function of one subsystem is a suitable energy function for stabilisation purposes. The graphical identification of ingoing and outgoing power flows of some subsystems is shown to be crucial for the power balancing method. Various examples are presented that impart the results.

5.2.1. Introducing Power Balancing

Consider the explicit port–Hamiltonian system

$$\begin{aligned} \dot{x} &= [J(x) - R(x)]K(x) - g(x)u \\ y &= g^T(x)K(x), \end{aligned} \tag{5.1}$$

where $K^T(x) = \mathbf{D}H(x)$ for some Hamiltonian $H\colon X \to \mathbb{R}$. Next define the "shaped" Hamiltonian

$$H_s(x) = H(x) + H_a(x), \tag{5.2}$$

where $H_a\colon X \to \mathbb{R}$ is the *assigned* or *additive* Hamiltonian to be associated with the feedback law. Suppose there exists an $H_a(x)$ such that

$$\dot{H}_s(x) = \dot{H}(x) + \dot{H}_a(x) \leq -y^T(x)u + y^T(x)\alpha(x), \tag{5.3}$$

where $\alpha(x)$ is smooth. Then in view of feedback passivation it is seen that the control $u = \alpha(x) + w$ yields

$$\dot{H}_s(x) \leq -y^T(x)w. \tag{5.4}$$

Hence, the control $u = \alpha(x) + w$ renders the system feedback passive with respect to the shaped Hamiltonian $H_s(x)$.

Standard passivity theory can be invoked to assess stability, for example, if $H_s(x)$ is positive definite at the equilibrium x^e then the control $w = Sy$, with $S = S^T > 0$, asymptotically stabilises the equilibrium x^e if trajectories contained in the set $B = \{x : y(x) = 0\}$ can only be x^e [Sep97].

The following elementary example shows how a power rate of the form (5.3) can be derived by using the bond graph junction structure.

Example 5.1. Consider the bond graph in Figure 5.1, which is causally assigned with SCAP, and let the Hamiltonian $H\colon X \to \mathbb{R}$ be simply given as

$$H(x) = \frac{1}{2m_1}x_1^2 + \frac{1}{2}kx_2^2 + \frac{1}{2m_2}x_3^2. \tag{5.5}$$

By power continuity of the bond graph junction structure it must follow that

$$\sigma y = kx_2\dot{x}_2 + \frac{1}{m_2}x_3\dot{x}_3. \tag{5.6}$$

But this clearly suggests that one can choose

$$H_a(x) = \frac{c}{2}\left[x_2^2 + \frac{1}{m_2}x_3^2\right] \quad \Longrightarrow \quad \dot{H}_a(x) = c\sigma y, \tag{5.7}$$

for some gain $c > 0$. Now, since the shaped Hamiltonian is defined by (5.2), an (in)equality of the form (5.3) can be derived from Figure 5.2 by simply considering all power flows through external bonds. Doing so yields

$$\dot{H}_s(x) = -y(u - c\sigma), \tag{5.8}$$

so that the passive control is of the form $u = c\sigma + w = ckx_2 + w$, which is seen to be immediately derivable from Figure 5.1 by means of the bond signal σ.

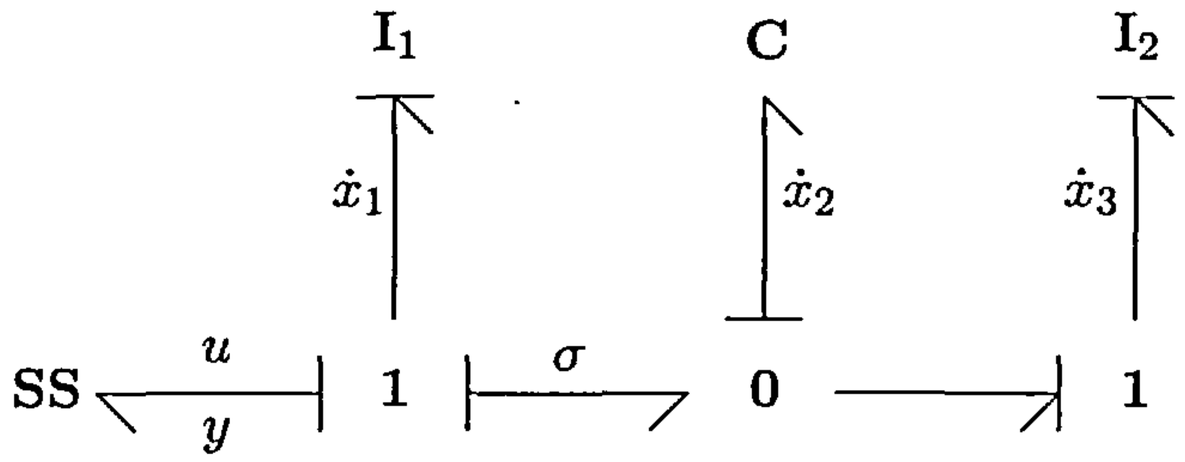

Figure 5.1.: Power flow σy for passive feedback with SCAP of Example 5.1.

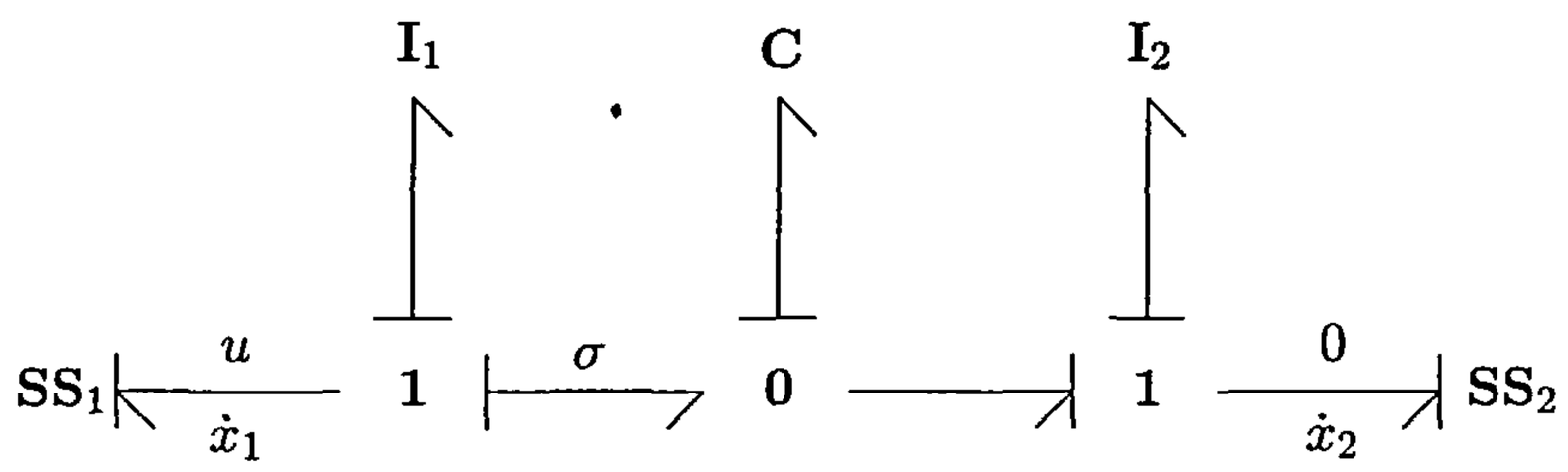

Figure 5.2.: Power flow σy for passive feedback with LCAP of Example 5.1.

The important step so far is the isolation of the bond graph subsystem associated with the **C** and $\mathbf{I}_2$, which allows for the factorisation of the form $\dot{H}_a(x) = y^T(x)\alpha(x)$.

If one prefers the Lagrangian approach in bond graph modelling, consider the bond graph causally assigned with LCAP in Figure 5.2. Note that the passive output remains conjugate to u, thus $y = \dot{x}_1$. To make the design more explicit this time, write the Lagrangian as

$$L(x, \dot{x}) = \frac{1}{2}m_1\dot{x}_1^2 + \frac{1}{2}m_2\dot{x}_2^2 - \frac{1}{2}k(x_1 - x_2)^2, \tag{5.9}$$

so that by causal analysis of Figure 5.2 one will find the simple EL–dynamics

$$\begin{aligned} \ddot{x}_1 &= -\frac{k}{m_1}(x_1 - x_2) - \frac{1}{m_1}u \\ \ddot{x}_2 &= \frac{k}{m_2}(x_1 - x_2). \end{aligned} \tag{5.10}$$

As usual, by setting $z_1 = x_1$, $z_2 = \dot{x}_1$ and $z_3 = x_2$, $z_4 = \dot{x}_2$ the system turns into the first order form

$$\begin{aligned} \dot{z}_1 &= z_2 \\ \dot{z}_2 &= -\frac{k}{m_1}(z_1 - z_3) - \frac{1}{m_1}u \\ \dot{z}_3 &= z_4 \\ \dot{z}_4 &= \frac{k}{m_2}(z_1 - z_3). \end{aligned} \tag{5.11}$$

Then if power balancing is to be applicable, the associated energy function $E(z)$ of the Lagrangian is needed and takes the form

$$E(z) = \frac{1}{2}m_1z_2^2 + \frac{1}{2}m_2z_4^2 + \frac{1}{2}k(z_1 - z_3)^2. \tag{5.12}$$

Completely analogous to (5.2), define the shaped energy as $E_s(z) = E(z) + E_a(z)$. Then, as in the SCAP case, the relevant power balance can be derived directly from the bond graph and is found to be

$$\sigma y = k(z_1 - z_3)(z_2 - z_4) + m_2 z_4 \dot{z}_4. \tag{5.13}$$

This clearly suggests to choose

$$E_a(z) = \frac{c}{2}\left[m_2 z_4^2 + k(z_1 - z_3)^2\right] \quad \Longrightarrow \quad \dot{E}_a(z) = c\sigma y, \tag{5.14}$$

which shows that the shaped associated energy must satisfy

$$\dot{E}_s(z) = -y(u - c\sigma). \tag{5.15}$$

The control is therefore $u = c\sigma + w = ck(z_1 - z_3) + w$.

It is important to note that the application of LCAP does not change the power balance method itself: Power continuity of bond graph junction structures is independent of the causality. So, this examples appears to hint at the possibility to use LCAP in cases where the bond graph would induce implicit port–Hamiltonian dynamics due to dependent storage elements. Possible applications of LCAP will be seen in a later section. ◊

Some remarks can be made on behalf of the above example. First, consider Figure 5.1 and suppose that the bond graph subsystem comprising the **C** and $\mathbf{I}_2$ elements has a resistive element connected to the 1–junction of the $\mathbf{I}_2$ element. In this scenario it is readily seen that an additional power flow associated with the resistive element will be imposed on $\dot{H}_a(x)$. Second, the storage functions associated with the $\mathbf{I}_1$, $\mathbf{I}_2$ and **C** elements are not coupled. As will be seen in the following section, the storage elements cannot be arbitrarily coupled if power balancing is to be possible.

5.2.2. Defining the Power Balance Method

Having presented an instructive example of bond graph based power balancing, a more general case of power balancing can now be considered. To that end, consider the explicit MIMO system depicted in Figure 5.3, where bond graph storage and dissipative elements are contained within the block Σ_0 but where Σ_1 has bond graph storage elements only. The Hamiltonians $H_0(x)$ and $H_1(\xi)$ denote the associated energy functions of the bond graph subsystems Σ_0 and Σ_1.

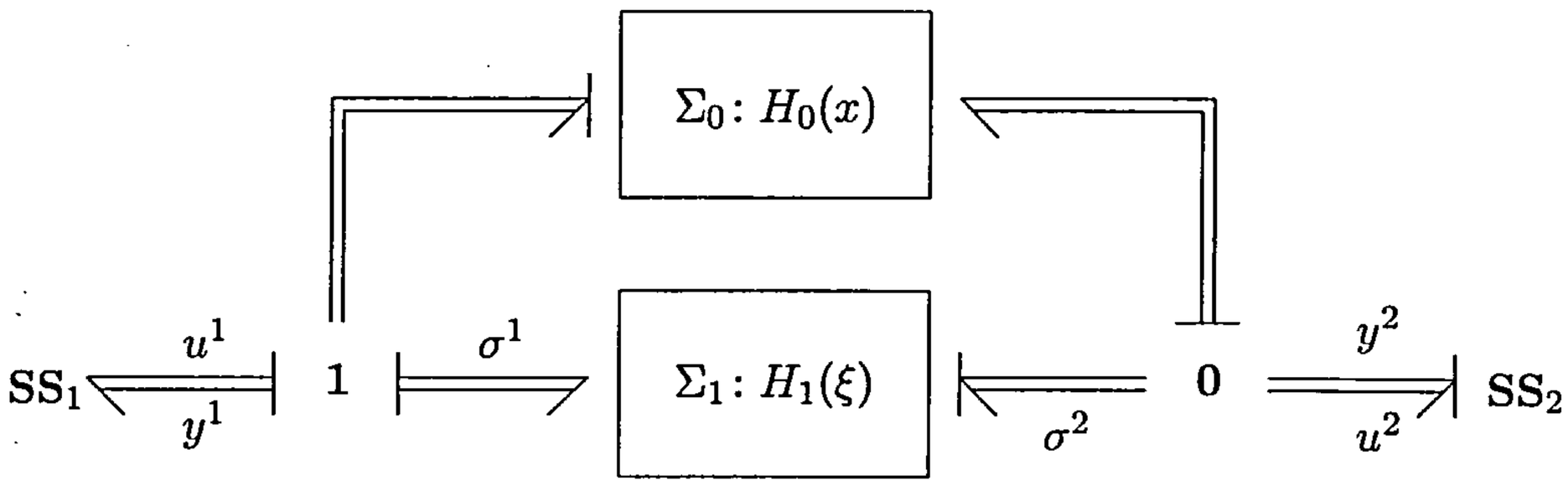

Figure 5.3.: Conceptual bond graph based power balancing with SCAP.

Now, for convenience, define $u^j = (u_1^j, \ldots, u_{n_j}^j)$, $y^j = (y_1^j, \ldots, y_{n_j}^j)$ and $\sigma^j = (\sigma_1^j, \ldots, \sigma_{n_j}^j)$ with $j \in \{1, 2\}$, and set $u = (u^1, u^2)$, $y = (y^1, y^2)$ and $\sigma = (\sigma^1, \sigma^2)$. Even though power continuity of bond graph junction structures is independent of causality, the power balance method considered here is readily defined in terms of standard causal assignment.

The point of departure is the definition of the plant Hamiltonian in Figure 5.3, given by

$$H(x, \xi) = H_0(x) + H_1(\xi). \tag{5.16}$$

Defining the plant energy in this way readily yields the relationship

$$\dot{H}_1(\xi) = y^T(x, \xi)\sigma(x, \xi), \tag{5.17}$$

where the junction structure can be modulated by all variables. As in (5.2), define the shaped Hamiltonian function $H_s(x, \xi) = H(x, \xi) + H_a(x, \xi)$, and observe that from (5.17) it follows that one can choose $H_a(x, \xi) = cH_1(\xi)$ for some $c > 0$. This yields the (in)equality

$$\dot{H}_s(x, \xi) = \dot{H}(x, \xi) + \dot{H}_a(x, \xi) \leq -y^T(x, \xi)[u - c\sigma(x, \xi)]. \tag{5.18}$$

Note that power balancing considered here assumes that the subsystems Σ_0 and Σ_1 do not have coupled Hamiltonians. Thus, the factorisation $\dot{H}_1(\xi) = y^T\sigma$ is obtained when the power flow $y^T\sigma$ is external to the system Σ_1.

Some important conditions for power balancing must be mentioned at this stage. First, suppose (x^e, ξ^e) is an admissible equilibrium that is (locally) globally asymptotically stable through the control $u = \alpha(x, \xi) + w$, where $w = Sy(x, \xi)$ and $S = S^T > 0$. Since the stabilisation problem is to regulate $y(z, \xi)$ to $y(z^e, \xi^e) = 0$ implies that $y(z^e, \xi^e)\alpha(z^e, \xi^e) = 0$. It follows that the power flow associated with the control must be zero at the equilibrium (x^e, ξ^e). The energy balancing method of [Ort00a] also mentions this particular restriction that there can be no power flow at the equilibrium.

Therefore, the above considerations show that the class of systems suitable for power balancing is limited, since various stabilisation problems exist that cannot be solved by asymptotic regulation of the natural passive output y to zero [Ort00a]. In addition, since the systems are assumed to be passive with respect to the output y and should remain so in closed loop, it must hold that the systems are (weakly) minimum phase if stabilisation is to be possible [Sep97], [Byr91]. Thus, as mentioned earlier, power balancing can address passivation problems with respect to the natural output, but the class of systems suitable for this type of control is limited.

The following example clarifies the conceptually defined MIMO power balancing as depicted in Figure 5.3.

Example 5.2. Consider the 2–input bond graph model depicted in Figure 5.4. The point of departure is to recognise that the system can be decomposed into the form as depicted in Figure 5.3. Suppose the components $\mathbf{I}_i$ and $\mathbf{C}_j$ for $i \neq j$ do not share coordinates and suppose that the plant Hamiltonian takes the form

$$H(x,\xi) = H_0(x) + H_1(\xi) = \frac{1}{2}x^T P x + \frac{1}{2}\xi^T Q \xi, \tag{5.19}$$

where $P = P^T$ and $Q = Q^T$. Straightforward causal analysis yields the dynamics

$$\begin{aligned}
\begin{bmatrix} \dot{x}_1 \\ \dot{x}_2 \\ \dot{\xi}_1 \\ \dot{\xi}_2 \end{bmatrix} &= \begin{bmatrix} 0 & 0 & -1 & 0 \\ 0 & 0 & 0 & 1 \\ 1 & 0 & 0 & -1 \\ 0 & -1 & 1 & 0 \end{bmatrix} \begin{bmatrix} p_{11}x_1 + p_{12}x_2 \\ p_{12}x_1 + p_{22}x_2 \\ q_{11}\xi_1 + q_{12}\xi_2 \\ q_{12}\xi_1 + q_{22}\xi_2 \end{bmatrix} - \begin{bmatrix} 1 & 0 \\ 0 & 1 \\ 0 & 0 \\ 0 & 0 \end{bmatrix} \begin{bmatrix} u_1 \\ u_2 \end{bmatrix} \\
\begin{bmatrix} y_1 \\ y_2 \end{bmatrix} &= \begin{bmatrix} p_{11}x_1 + p_{12}x_2 \\ p_{12}x_1 + p_{22}x_2 \end{bmatrix}.
\end{aligned} \tag{5.20}$$

By means of the junction structure in Figure 5.4 it follows that the power balancing control is given as $u_1 = c\sigma_1 + w_1$ and $u_2 = -c\sigma_2 + w_2$ for $c > 0$. This control can be verified by taking $H_a(\xi) = cH_1(\xi)$ such that the shaped energy is given as

$$H_s(x,\xi) = \frac{1}{2}x^T P x + \frac{1}{2}\xi^T [Q + cQ]\xi, \tag{5.21}$$

which satisfies $\dot{H}_s(x,\xi) = -y^T w$. Note that the power balance method does not provide a lot of room to modify the properties of the energy function by means of the gain c in this case. More precisely, since the gain is assumed to satisfy $c > 0$ shows that P and Q are to be positive definite if H_s is to be positive definite.

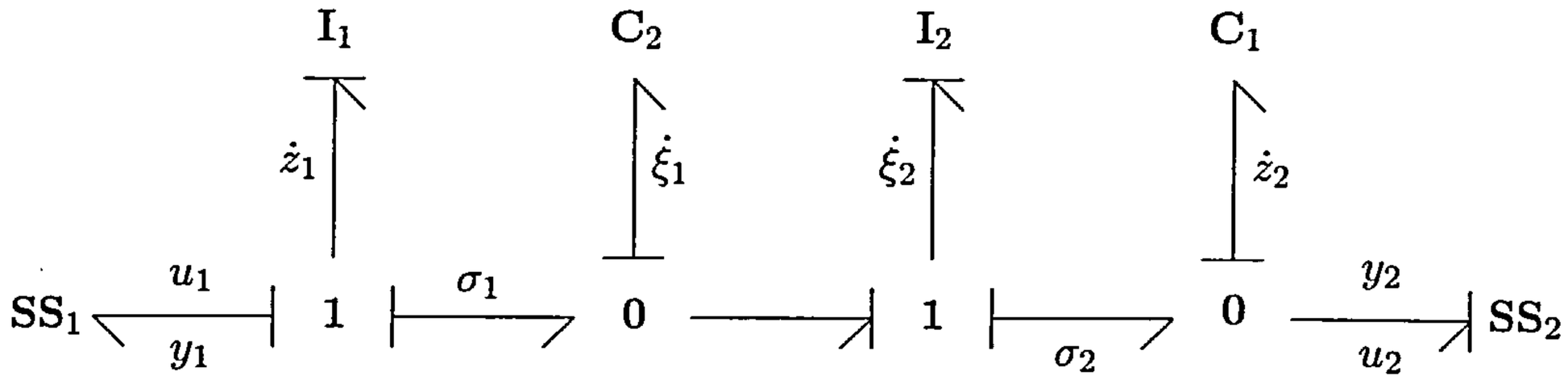

Figure 5.4.: Basic MIMO bond graph based power balancing of Example 5.2.

By assuming that P and Q are positive definite, the feedback $w = Sy$, with $S = S^T > 0$, can be used to control the asymptotic convergence. Finally, the requirement to have passivity with respect to the natural output limits the coordinate dependency of the additive energy, for it is seen that

$$\mathrm{D}H_a(x,\xi)g_j = 0 \quad \Longrightarrow \quad y = g^T K_s(x,\xi) = g^T K(x), \tag{5.22}$$

where g_j are the columns of the input matrix of (5.20). The x–coordinates can therefore not be used in the definition of H_a. ◊

Provided the system can be decomposed properly, it is seen that MIMO designs can be addressed within the power balancing framework. However, it may be difficult, if at all possible, to find the bond graph subsystems Σ_0 and Σ_1 with the added assumption that Σ_1 has no dissipation. In practice, the general way to proceed is by identifying the junctions where the control input u appears and to identify the bond signals $\sigma_j(x,\xi)$. Assuming this step can be completed, it should be checked whether the plant Hamiltonian allows for the representation of Figure 5.3, which may or may not be possible. Suppose the Hamiltonian can be written as the sum of two suitable functions, then the MIMO design can be completed provided the system is (weakly) minimum phase.

Implicit Systems: Dependent Storage Elements

Figure 5.3 is a conceptual bond graph representation that is causally assigned with SCAP. Since the interconnection of bond graph subsystems are likely to induce dependencies between various storage elements, it can be argued that not allowing dependent storage elements is rather restrictive in bond graph modelling. As a result, it is of great importance to address derivative causalities in the context of power balancing if this method is to be applicable to a larger, relevant class of systems.

It is intuitively plausible that alternative causality assignment procedures can possibly be used to deal with constraint storage elements that are manifested as derivative causalities. The insertion of Lagrange multipliers to eliminate the dependent storage elements is possible within the power balancing method. Indeed, multipliers are "workless" by definition, which implies that the associated power flow is zero such that it cannot have any contribution. However, with standard causality, the insertion of various multipliers may yield complicated dynamics since the state variables selected by SCAP may not be suitable for the problem at hand.

Even though multipliers are capable of effectively addressing certain constraint dynamics, the Lagrangian causality assignment without multipliers, denoted as LCAP, appears to be the best option for power balancing as considered here. It must be recalled, however, that LCAP is applicable if and only if a minimal set of generalised coordinates are available [Mar02]. In case this minimal set of coordinates has been found, the dependent storage elements are readily circumvented with LCAP. The second order dynamics obtained with LCAP are subsequently transformed into first order form, where the associated energy E of the Lagrangian is used as a storage function. Power balancing is achieved through the additive energy function E_a which is to be derived from the bond graph by means of the junction structure. Similar to the SCAP case, the power flow $y^T\sigma$ is found at the 1–junctions that are identified as generalised velocities.

The Lagrangian approach is quite effective in addressing the derivative causalities of bond graph models; however, the next example shows that the inequality (5.18) requires further generalisation. More precisely, as in (5.2), define the shaped energy of the Lagrangian as $E_s(z) = E(z) + E_a(z)$ and suppose there exists an additive energy $E_a(z)$ such that

$$\dot{E}_s(z) \leq -y^T p(z,u), \tag{5.23}$$

where $p(x,u)$ is smooth. Then by invoking the Implicit Function Theorem [Abr88] it is possible, in principle, to solve for a control $u = \alpha(x,w)$ such that

$$\dot{E}_s(z) \leq -y^T p(z,\alpha(z,w)) = -y^T w. \tag{5.24}$$

Thus, as per (5.23), general bond graph based power balancing can be said to address passivation problems for which a suitable factorisation with respect to the natural output can be attained by means of an additive energy function.

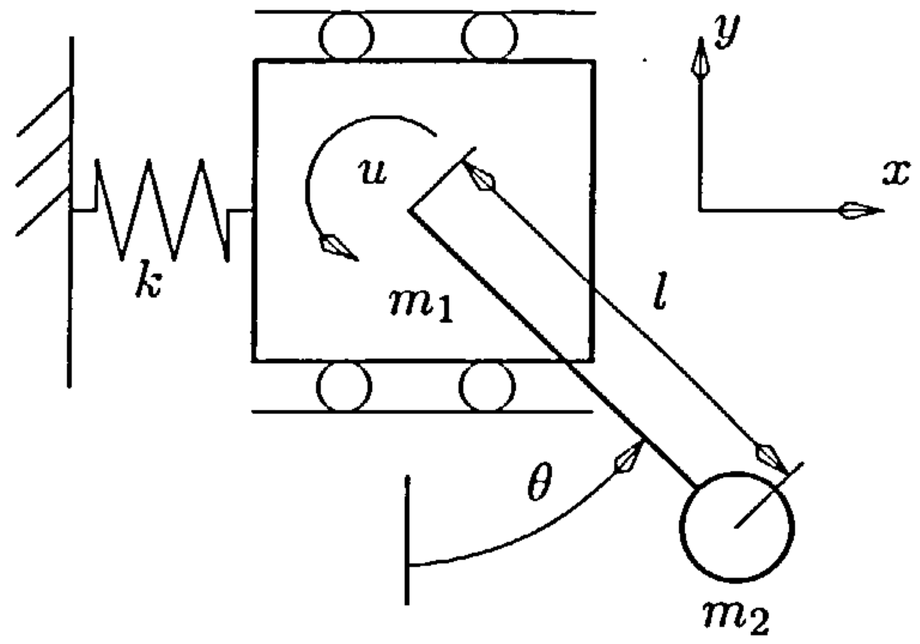

Figure 5.5.: TORA physical configuration of Example 5.3.

The following non–trivial example has been taken from [Jan96] and shows how the Lagrangian approach in bond graph modelling can be a tool in power balancing control. In particular, the additive associated energy function need not be "guessed" as such, but the junction structure hints at a candidate additive energy function.

Example 5.3. In [Jan96], the authors consider the problem of controlling the Translational Oscillations of a Rotational Actuator (TORA) as depicted in Figure 5.5; see [Wan94] for another account of the system. Now, the authors of [Jan96] present the design of various cascade and feedback passivation controllers for the TORA that are shown to stabilise the system globally. It is pointed out by [Jan96] that the passivation control designs cannot be said to be constructive since the closed loop storage function is to be "guessed" in some way. This example shows that bond graph based power balancing control can provide a way of designing a passivation controller in a relatively constructive fashion.

The structure of the TORA in Figure 5.5 consists of a platform that can oscillate without damping in a horizontal plane, thus the effect of gravity is not considered. On the platform, a rotating eccentric mass is actuated by a DC motor and its motion applies a force to the platform that can be used to control the translational oscillations, where the control input u is the torque applied to the eccentric mass to stabilise the system globally at a desired equilibrium.

Since the kinematic relations of the system will certainly induce dependent storage elements, the Lagrangian approach is considered to obtain an efficient model. It should be noted that λHCAP of [Mar02] can be applied, but the dynamics tend to become more complex. The generalised coordinates in Figure 5.5 are designated as $x_1 = x$, which represents the position of the platform, and where the pendulum angle is designated as $x_2 = \theta$.

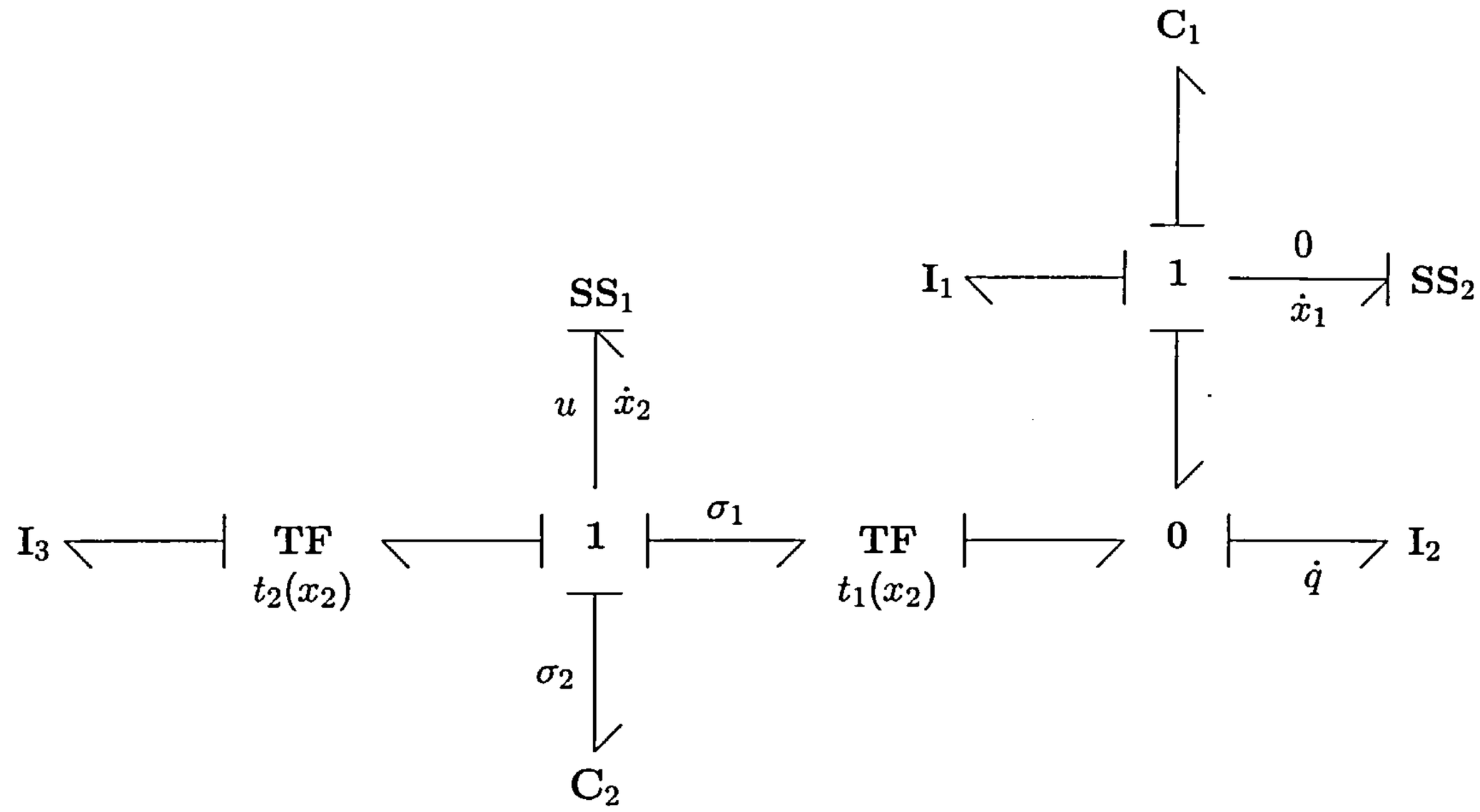

Figure 5.6.: TORA Lagrangian assigned bond graph of Example 5.3.

Figure 5.6 depicts the bond graph of the TORA with LCAP, where $t_1(x_2) = l\cos(x_2)$ and $t_2(x_2) = l\sin(x_2)$. The Lagrangian is given as the kinetic energy $T(x,\dot{x})$ minus the potential energy $V(x)$, thus

$$L(x,\dot{x}) = T(x,\dot{x}) - V(x) = \frac{1}{2}\alpha\dot{x}_1^2 + \beta\cos(x_2)\dot{x}_1\dot{x}_2 + \frac{1}{2}\gamma\dot{x}_2^2 - \frac{1}{2}kx_1^2, \tag{5.25}$$

where $\alpha = m_1 + m_2$, $\beta = m_2 l$ and $\gamma = m_2 l^2$. By following the depicted causality yields the second order equations

$$\begin{bmatrix} \alpha & \beta\cos(x_2) \\ \beta\cos(x_2) & \gamma \end{bmatrix} \begin{bmatrix} \ddot{x}_1 \\ \ddot{x}_2 \end{bmatrix} + \begin{bmatrix} -\beta\sin(x_2)\dot{x}_2^2 + kx_1 \\ u \end{bmatrix} = 0. \tag{5.26}$$

Next set $z_1 = x_1$, $z_2 = \dot{x}_1$ and $z_3 = x_2$, $z_4 = \dot{x}_2$, and write the first order dynamics

$$\begin{aligned} \dot{z}_1 &= z_2 \\ \dot{z}_2 &= -\frac{\gamma(\beta\sin(z_3)z_4^2 - kz_1)}{\beta^2\cos^2(z_3) - \alpha\gamma} - \frac{\beta\cos(z_3)}{\beta^2\cos^2(z_3) - \alpha\gamma}u \\ \dot{z}_3 &= z_4 \\ \dot{z}_4 &= \frac{\beta\cos(z_3)(\beta\sin(z_3)z_4^2 - kz_1)}{\beta^2\cos^2(z_3) - \alpha\gamma} + \frac{\alpha}{\beta^2\cos^2(z_3) - \alpha\gamma}u. \end{aligned} \tag{5.27}$$

The associated energy $E(x,\dot{x})$ in the z–coordinates takes the form

$$E(z) = \frac{1}{2}\alpha z_2^2 + \beta\cos(z_3)z_2z_4 + \frac{1}{2}\gamma z_4^2 + \frac{1}{2}kz_1^2, \tag{5.28}$$

which, as expected, is a storage function satisfying $\dot{E}(z) = -z_4u = -yu$.

In [Jan96], the first passivation controller, denoted by the authors as "P2", is chosen to be $u = cz_3 + rz_3$ for some gains $c > 0$ and $r > 0$. This control is shown to achieve global stabilisation of $z = (0,0,0,0)$. From a power balancing perspective, it is seen that this controller can be obtained by considering the power balance for $\sigma_2 y$ only, which represents the contribution of additive potential energy with respect to the angle of the pendulum. The power flow $\sigma_2 y$ implies that one can (but need not) choose the additive associated energy $E_a(z) = (c/2)z_3^2$. Even though this controller achieves stability of the origin, the authors show that the P2 controller cannot lower the settling time of x_1 beyond a certain limit. They argue that the energy can be shaped in the x_1–coordinates to improve the settling time; however, the authors do not disclose how the additive energy function is chosen to attain the x_1–dependency of the feedback passivation controller.

In view of power balancing, observe that the dependence of the controller on the x_1–coordinate can be achieved constructively by considering the power flow $\sigma_1 y$. More precisely, consider the power balance equations induced by the junction structure as

$$\begin{aligned} \sigma_1 y &= m_2 \ddot{q}\dot{q} + m_1 \ddot{x}_1 \dot{x}_1 + k x_1 \dot{x}_1 \\ \sigma_2 y &= \frac{\partial V}{\partial x_2} y, \end{aligned} \tag{5.29}$$

where $\dot{q}$ is the horizontal velocity of the mass m_2. Identifying these power flows is an important step in the design, because it becomes possible to select a candidate additive energy function yielding a factorisation in the natural output y of the form (5.23). In particular, the above power balance equations lead to the choice

$$\begin{aligned} E_a(z) &= \frac{c_1}{2}[kz_1^2 + m_2(z_2 + l\cos(z_3)z_4)^2 + m_1 z_2^2] + \frac{c_2}{2}z_3^2 \\ &= \frac{c_1}{2}[kz_1^2 + 2b\cos(z_3)z_2 z_4 + az_2^2 + cz_4^2\cos^2(z_3)] + \frac{c_2}{2}z_3^2, \end{aligned} \tag{5.30}$$

where $c_1 > 0$ and $c_2 > 0$, and where the relation $\dot{q} = z_2 + l\cos(z_3)z_4$ has been used. From the bond graph it now follows that this additive energy must satisfy

$$\dot{E}_a = z_4(\sigma_1 + \sigma_2), \tag{5.31}$$

which, in turn, implies that

$$\dot{E}_s(z) = -z_4 p(z,u). \tag{5.32}$$

By invoking implicit function arguments, it is readily seen that there exists the control $u = \alpha(z,w)$ giving

$$\dot{E}_s(z) = -z_4 p(z, \alpha(z,w)) = -z_4 w. \tag{5.33}$$

Indeed, the control satisfying (5.33) takes the form

$$u = \alpha(z,w) = \frac{1}{(\beta^2 + \beta^2 c_1 - \alpha\gamma c_1)\cos^2(z_3) - \alpha\gamma}\Big[-\beta\gamma c_1 k z_1 \cos^3(z_3) + \beta^2 c_2 z_3 \cos^2(z_3) + [\beta\gamma c_1 k z_1 + \alpha\gamma^2 c_1 z_4^2 \sin(z_3) - \beta^2\gamma c_1 z_4^2 \sin(z_3)]\cos(z_3) - \alpha\gamma c_2 z_3 + [\beta^2\cos^2(z_3) - \alpha\gamma]w\Big]. \quad (5.34)$$

The design objective to obtain the x_1–dependency has been attained with $u = \alpha(z,w)$ and the system (5.27) is feedback passive with storage function $E_s(z)$. Global asymptotic stability of $z = 0$ is achieved by the further control $w = ry$ with $r > 0$.

It is important to note that the potential energy can be arbitrary since $\sigma_2 y = (\partial V/\partial x_2)y$. Consequently, the "winding problem" as described in [Jan96] can be addressed by means of an alternative choice of potential energy, which does not compromise the factorisation (5.32).

◊

As mentioned earlier, power balancing cannot be used for systems that are not (weakly) minimum phase [Byr91]. For instance, there are occasions where a proper bond graph decomposition exists, but where the additive energy function cannot render the shaped energy function positive definite at the desired equilibrium. The following example addresses such a system.

Example 5.4. Consider the bond graph in Figure 5.7 of the frictionless slider. Since the junction structure of this system is seen to induces derivative causalities when SCAP is used, the application of LCAP is expected to yield a more efficient model.

As usual, the Lagrangian is the kinetic energy minus the potential energy and takes the form

$$L(x,\dot{x}) = \frac{1}{2}m\dot{x}_2^2 + \frac{1}{2}mx_2^2\dot{x}_1^2 + \frac{1}{2}I\dot{x}_1^2 - mgx_2\sin(x_1). \quad (5.35)$$

With $z_1 = x_1$, $z_2 = \dot{x}_1$ and $z_3 = x_2$, $z_4 = \dot{x}_2$ the associated energy $E(z)$ of the Lagrangian readily follows to be

$$E(z) = \frac{1}{2}mz_4^2 + \frac{1}{2}mz_3^2 z_2^2 + \frac{1}{2}Iz_2^2 + mgz_3\sin(z_1). \quad (5.36)$$

Set $y = \dot{x}_1$ and identify the power flow

$$\dot{E}_a = y(\sigma_1 + \sigma_2 + \sigma_3). \quad (5.37)$$

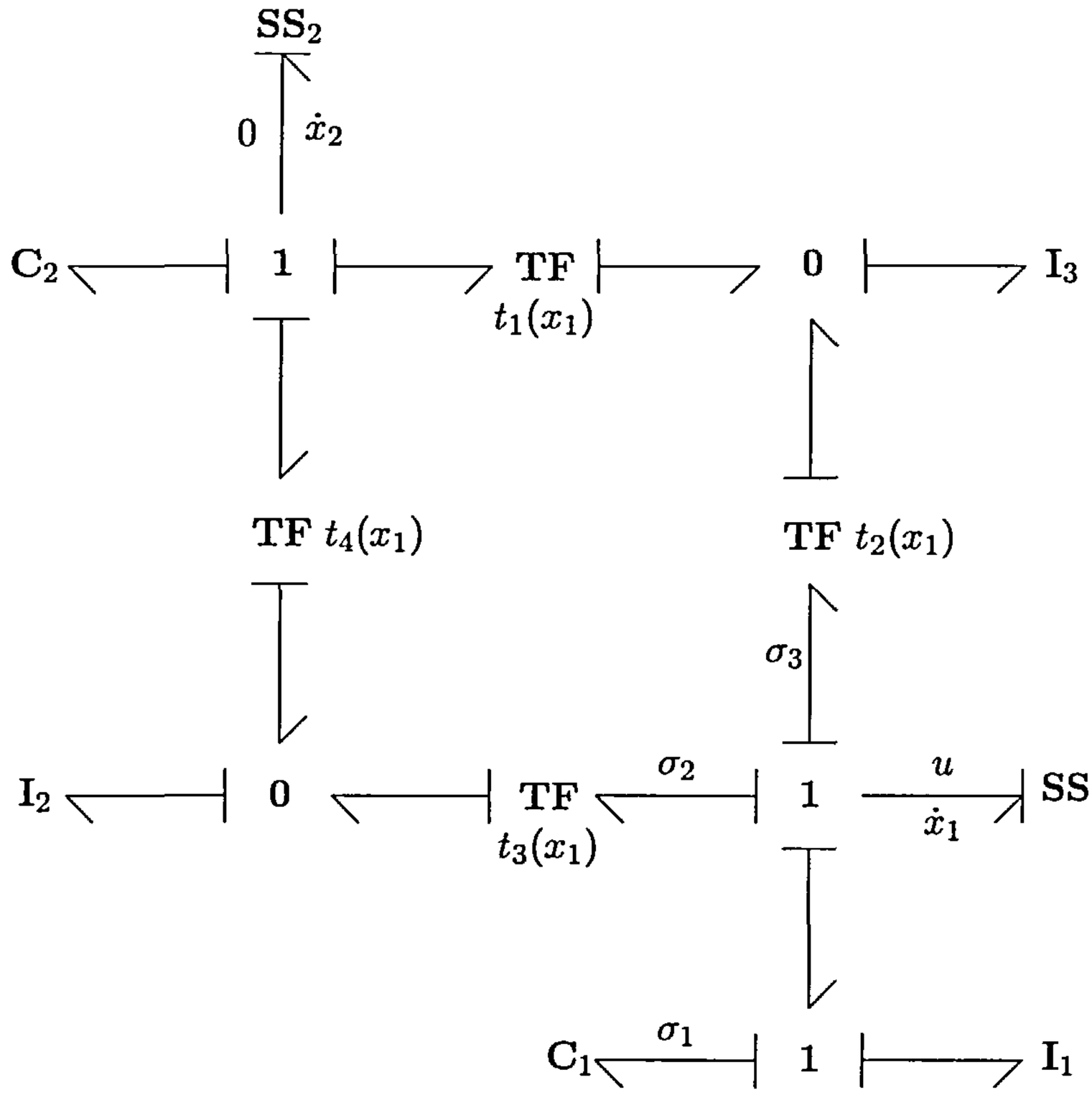

Figure 5.7.: Power balancing not applicable to slider of Example 5.4.

At this stage it must be noted that the $\mathbf{C}_1$ and $\mathbf{C}_2$ storage elements are coupled, so that the power flow $\sigma_1 y$ must be taken into account. The additive energy can be described by

$$E_a(z) = \frac{c_1}{2}\left[mz_4^2 + \frac{1}{2}mz_3^2 z_2^2 + mgz_3\sin(z_1)\right] + \frac{c_2}{2}z_1^2, \tag{5.38}$$

for some controller gains $c_1 > 0$ and $c_2 > 0$. However, it is of no use continuing the design since the shaped energy $E_s(z)$ cannot be rendered positive definite at $z = 0$. Furthermore, since the minimum phase property cannot be changed by feedback control, it is concluded that the frictionless slider cannot be stabilised by feedback passivation with respect to the natural passive output y. ◊

The above example shows that the power balancing precludes systems with unstable internal dynamics. But, as mentioned earlier, the bond graph does not provide any information on the energy function to assess internal stability. Therefore, the existence of the factorisation (5.23) does not guarantee that asymptotic stabilisation can be attained by bond graph arguments alone. Future research could address bond graph based power balancing that allows for alternative passive output factorisations for certain non–minimum phase systems.

Some Concluding Remarks

It has been shown that bond graph based power balancing can be used to obtain passivation controllers with respect to the natural output. Most importantly, the junction structure has shown to provide information on how the natural output passivity is retained when selecting the additive energy function associated with suitable power flows. This method is novel in the bond graph literature and provides a graphical means to obtain natural output passivity in closed loop. Moreover, power balancing is applicable regardless of the bond graph complexity, but the proper decomposition may be difficult to find, if possible at all.

Natural output passivation is applicable to a limited class of control problems. For example, admissible equilibria that can be stabilised are limited due to the fact that such equilibria are to be compatible with the zero output, thus $y = 0$. Furthermore, natural output passivity implies that the systems must be (weakly) minimum phase if stabilisation is to be possible. In other words, natural output passivity in closed loop requires that the internal dynamics is at least marginally stable.

Power balancing as presented here can be applied to bond graph models with dependent storage elements. For example, the Lagrangian approach has shown to circumvent the existence of dependent storage elements without compromising the power balancing method. Indeed, power continuity of the junction structure is independent of causality by definition, so any causal configuration is to satisfy power continuity by construction. In order to use LCAP, it is required that a minimal set of generalised coordinates can be found. Future research could address other causal assignment schemes in power balancing control, such as λHCAP or λLCAP, since the application of Lagrange multipliers does not require a minimal set of generalised coordinates, thereby avoiding the search for such coordinates for complex systems of interconnected bond graph submodels.

Finally, it may be of interest to see whether power balancing can be extended to include closed loop passivity with respect to different outputs, so that the class of systems suitable for bond graph based power balancing can be enlarged to include certain non–minimum phase systems. For example, the stabilisation of the frictionless slider was shown not to be possible with respect to the natural output, but by modifying the closed loop passive output this problem may be solved.

5.3. Control by Interconnection and Damping Assignment

In the previous section it has been shown that bond graph based power balancing can be used to derive an additive energy function for control purposes, and where the natural output remains the closed loop passive output. In particular, the controller design is solely based on power flow considerations, where it is important to realise that the closed loop bond graph representation does not change.

This section explores bond graph modelling aspects and interpretations of a novel technique called Interconnection and Damping Assignment Passivity Based Control (IDA–PBC) of explicit port–Hamiltonian systems as developed in [Ort02b]. The main feature of a IDA–PBC design is that the closed loop remains port–Hamiltonian with respect to some shaped energy function. But, in addition, IDA–PBC designs also consider possible modifications of the interconnection and damping structures through suitable feedback.

It will be shown that basic IDA–PBC design allow for bond graph representations, but the bond graph modelling aspects considered here are more conceptual and do not yield the solution to the PDEs associated with IDA–PBC designs. Nonetheless, it can be expected that such conceptual representations have merit and are helpful for bond graph models for which an IDA–PBC design is considered. Even though bond graph models have been identified as a class of port–Hamiltonian systems [Gol02], the aspects of bond graphs in IDA–PBC designs has hardly been addressed. This section presents an introductory account on IDA–PBC control design in terms of bond graph models.

5.3.1. Energy Shaping with Junction Structure Compatibility

The power balancing method in Section 5.2 shapes the energy of systems in way that renders the closed loop passive with respect to the natural system output. Indeed, the sole purpose of power balancing is to render the time derivative of the shaped energy non–positive. But instead of finding additive energy functions that retain passivity with respect to the natural output, it can be of interest to characterise all additive storage functions that are compatible with the original bond graph topology. This section follows the various arguments found in Section 2.6 but where interconnection and damping structure assignment is not considered at this stage. As will be seen, energy shaping that is compatible with the junction structure often leads to passivity with respect to a different output.

Following the arguments of [Ort02b] and Section 2.6, consider an *explicit* port–Hamiltonian system of the form

$$\begin{aligned} \dot{x} &= [J(x) - R(x)]K(x) - g(x)u \\ y &= g^T(x)K(x), \end{aligned} \tag{5.39}$$

where $\mathbf{D}H(x) = K^T(x)$ for some smooth Hamiltonian $H : X \to \mathbb{R}$. Define the shaped energy function

$$H_s(x) = H(x) + H_a(x), \tag{5.40}$$

where $H_a(x)$ is the additive Hamiltonian to be associated with feedback control. To that end, suppose there exists a smooth state feedback $u = \alpha(x) + v$ such that

$$[J(x) - R(x)]K_a(x) = -g(x)\alpha(x) \tag{5.41}$$

and observe that in such case the closed loop can be written as

$$\begin{aligned} \dot{x} &= [J(x) - R(x)]K_s(x) - g(x)v \\ y_s &= g^T(x)K_s(x). \end{aligned} \tag{5.42}$$

The additive function $H_a(x)$ can therefore be used, in principle, to assign some desired (local) minimum to the shaped energy $H_s(x)$, so that stabilisation is possible by rendering x^e the strict minimum. More precisely, take the standard feedback $v = Sy_s$ for $S = S^T > 0$ and define the set

$$Z = \{x \in X : K_s^T(x)[R(x) + g(x)Sg^T(x)]K_s(x) = 0\}. \tag{5.43}$$

Now, suppose $H_s(x)$ is positive definite at the desired equilibrium x^e, then by invoking a LaSalle argument [Kha92] it can be shown that asymptotic stabilisation is attained when the only trajectory contained in Z is the equilibrium x^e.

If (5.41) is to hold for all $H_a(x)$ then is must also hold that

$$g^\perp(x)[J(x) - R(x)]K_a(x) = 0, \tag{5.44}$$

where $g^\perp(x)$ is a full rank left annihilator of $g(x)$. This condition characterises the property that systems can be underactuated, which implies that the additive energy $H_a(x)$ cannot be chosen arbitrarily but is to simultaneously satisfy the set of first order PDEs (5.44). Suppose (5.44) can be solved for some $H_a(x)$, then the control is obtained with

$$-[g^T(x)g(x)]^{-1}g^T(x)[J(x) - R(x)]K_a(x) = u. \tag{5.45}$$

Even though the above energy shaping method is conceptually straightforward, the solution to (5.44) is a crucial step in the design. The following proposition provides a *necessary* condition for a set of first order PDEs to be simultaneously satisfied by one single function.

Proposition 5.1. *Let X be a smooth manifold with local coordinates $(x_1, \ldots, x_n)$ and consider the maps $F_j : T^*X \to \mathbb{R}$ with $j = 1, \ldots, m$. Suppose the function $H : X \to \mathbb{R}$ simultaneously satisfies the first order PDEs*

$$F_j(x_i, p_i) = 0, \tag{5.46}$$

with $p_i = \partial H / \partial x_i$. Then the maps F_j must then satisfy

$$\{F_i, F_j\} = 0, \tag{5.47}$$

where $\{\cdot, \cdot\}$ is the standard Poisson bracket on T^*X.

Proof. Let $F, G : T^*X \to \mathbb{R}$ and suppose $H(x_i)$ satisfies

$$F(x_i, p_i) = 0, \quad G(x_i, p_i) = 0, \tag{5.48}$$

with $p_i = \partial H / \partial x_i$. Taking partial derivatives with respect to x_i yields the relationships

$$\frac{\partial F}{\partial x_i} + \frac{\partial F}{\partial p_j}\frac{\partial p_j}{\partial x_i} = 0, \quad \frac{\partial G}{\partial x_i} + \frac{\partial G}{\partial p_j}\frac{\partial p_j}{\partial x_i} = 0. \tag{5.49}$$

Multiplying the first relation with $\partial G / \partial p_i$, the second relation with $\partial F / \partial p_i$, and subtracting the second relation from the first yields

$$\{F, G\} = \frac{\partial F}{\partial x_i}\frac{\partial G}{\partial p_i} - \frac{\partial F}{\partial p_i}\frac{\partial G}{\partial x_i} = 0. \tag{5.50}$$

□

It is interesting to note that the above proposition is merely implicitly contained in the work of [Car65] and gives a necessary condition that is to be satisfied if (5.46) is to be at all solvable for some function $H(x_i)$. Note that no explicit conditions on the solvability of (5.46) can be given [Ort02b], but Proposition 5.1 is reported here for maximum clarity.

Corollary 5.2. *In case $F_j(x, p) = F_j(0, p)$ for all j then $\{F_i, F_k\} = 0$.*

The following example shows that energy shaping as per (5.41) implies compatibility with the plant bond graph topology.

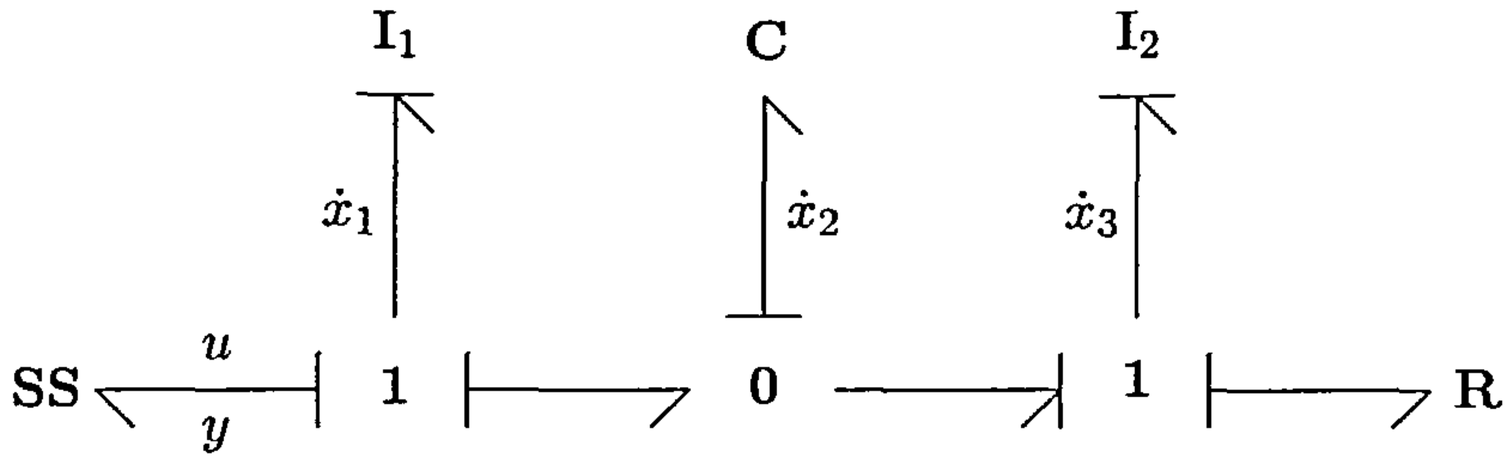

Figure 5.8.: Dissipative system of Example 5.5.

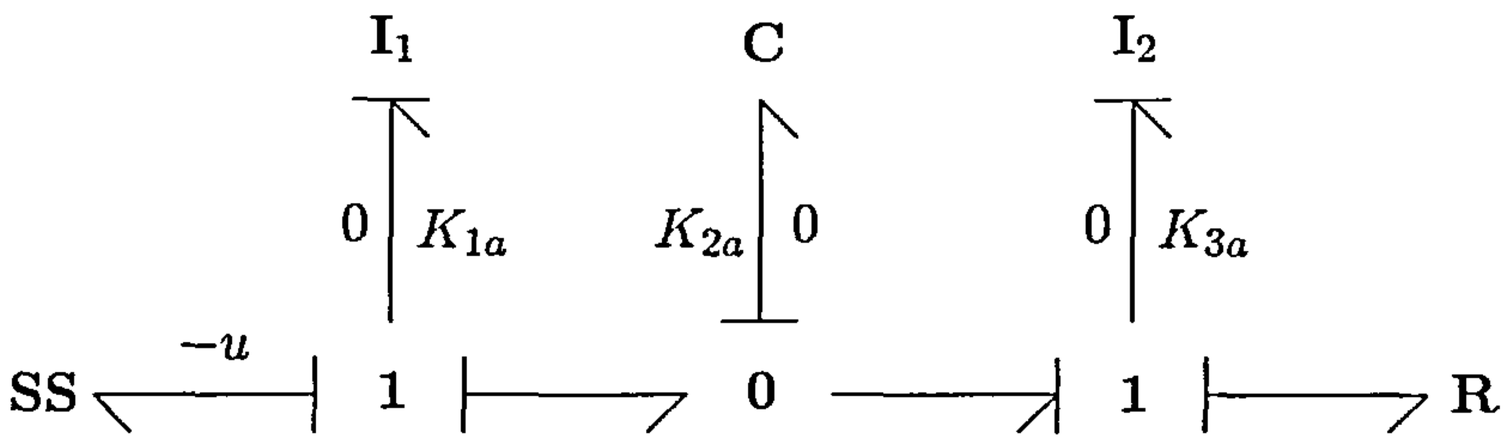

Figure 5.9.: Energy shaping compatible with bond graph topology; Example 5.5.

Example 5.5. Consider the bond graph of a dissipative system depicted Figure 5.8. For simplicity, suppose the Hamiltonian of the system is given as

$$H(x) = \frac{1}{2}x^T Q x = \frac{1}{2I_1}x_2^2 + \frac{1}{2C}x_2^2 + \frac{1}{2I_2}x_3^2, \tag{5.51}$$

where the constants I_1 and I_2 are inductances and where C is a capacitor. Causal analysis yields the simple linear dynamics

$$\begin{aligned} \begin{bmatrix} \dot{x}_1 \\ \dot{x}_2 \\ \dot{x}_3 \end{bmatrix} &= \begin{bmatrix} 0 & -1 & 0 \\ 1 & 0 & -1 \\ 0 & 1 & -r_1 \end{bmatrix} \begin{bmatrix} x_1/I_1 \\ x_2/C \\ x_3/I_2 \end{bmatrix} - \begin{bmatrix} 1 \\ 0 \\ 0 \end{bmatrix} u \\ y &= x_1/I_1, \end{aligned} \tag{5.52}$$

where $r_1 > 0$ is a resistive constant associated with the R element. The admissible equilibria of (5.52) take the form

$$x^e = (x_1^e, x_2^e, x_3^e) = (-I_1 u^e/r_1, -Cu^e, -I_2 u^e/r_1), \tag{5.53}$$

where u^e is a constant input. Then to find all additive energy functions $H_a(x)$ that are attainable through feedback, observe that the condition (5.41) can be represented as the bond graph in Figure 5.9. Thus for energy shaping to be compatible with the plant bond graph, the contribution of the additive energy is to "cancel" internally due to underactuation, which can be represented by nullifying the tangent vector $\dot{x}$ in Figure 5.9.

The PDEs to be simultaneously satisfied by $H_a(x)$ are given by (5.44) or can be derived from Figure 5.9, and doing so yields

$$\begin{aligned} \frac{\partial H_a}{\partial x_1} - \frac{\partial H_a}{\partial x_3} &= 0 \\ \frac{\partial H_a}{\partial x_2} - r_1 \frac{\partial H_a}{\partial x_3} &= 0. \end{aligned} \tag{5.54}$$

To assess whether (5.54) is at all solvable, set $p_i = \partial H_a / \partial x_i$ and define the functions $F_1(x,p) = p_1 - p_3$ and $F_2(x,p) = p_2 - r_1 p_3$, so that Corollary 5.2 can now be used to confirm that $\{F_1, F_2\} = 0$. In fact, observe that the solution to (5.54) does exist and takes the form

$$H_a(x) = \phi(x_1 + r_1 x_2 + x_3), \tag{5.55}$$

where ϕ is any differentiable function that assigns a strict minimum at x^e to the shaped energy, if possible.

For linear systems one can often consider a function $H_s(x)$ that is quadratic in $x - x^e$. To that end, define ϕ as

$$\begin{aligned} \phi(x_1 + r_1 x_2 + x_3) = \frac{1}{2} c_1 [x_1 + r_1 x_2 + x_3 - (x_1^e + r_1 x_2^e + x_3^e)]^2 \\ + \frac{1}{r_1}(x_1 + r_1 x_2 + x_2) u^e \\ + \frac{(x_1^e)^2}{2I_1} + \frac{(x_2^e)^2}{2C} + \frac{(x_3^e)^2}{2I_2}, \end{aligned} \tag{5.56}$$

where $c_1 > 0$ is a controller gain. Observe that with the above choice of ϕ it follows that the shaped Hamiltonian takes the form

$$\begin{aligned} H_s(x) &= H(x) + H_a(x) \\ &= \frac{1}{2}(x - x^e)^T \begin{bmatrix} c_1 + 1/I_1 & r_1 c_1 & c_1 \\ r_1 c_1 & r_1^2 c_1 + 1/C & r_1 c_1 \\ c_1 & r_1 c_1 & c_1 + 1/I_2 \end{bmatrix} (x - x^e). \end{aligned} \tag{5.57}$$

Finally, the control that attains the desired energy shaping is obtained from (5.45), or from the bond graph in Figure 5.9 as $u = \partial H_a / \partial x_2 + v$. Standard output feedback of the form $v = r_2 y_s$ with $r_2 > 0$ can be used to impose asymptotic convergence. ◊

As shown by the above example, energy shaping that is compatible with the junction structure induces first order PDEs by considering the summations of zero– and one–junctions. The property of underactuation can be imposed by nullifying the tangent vector $\dot{x}$.

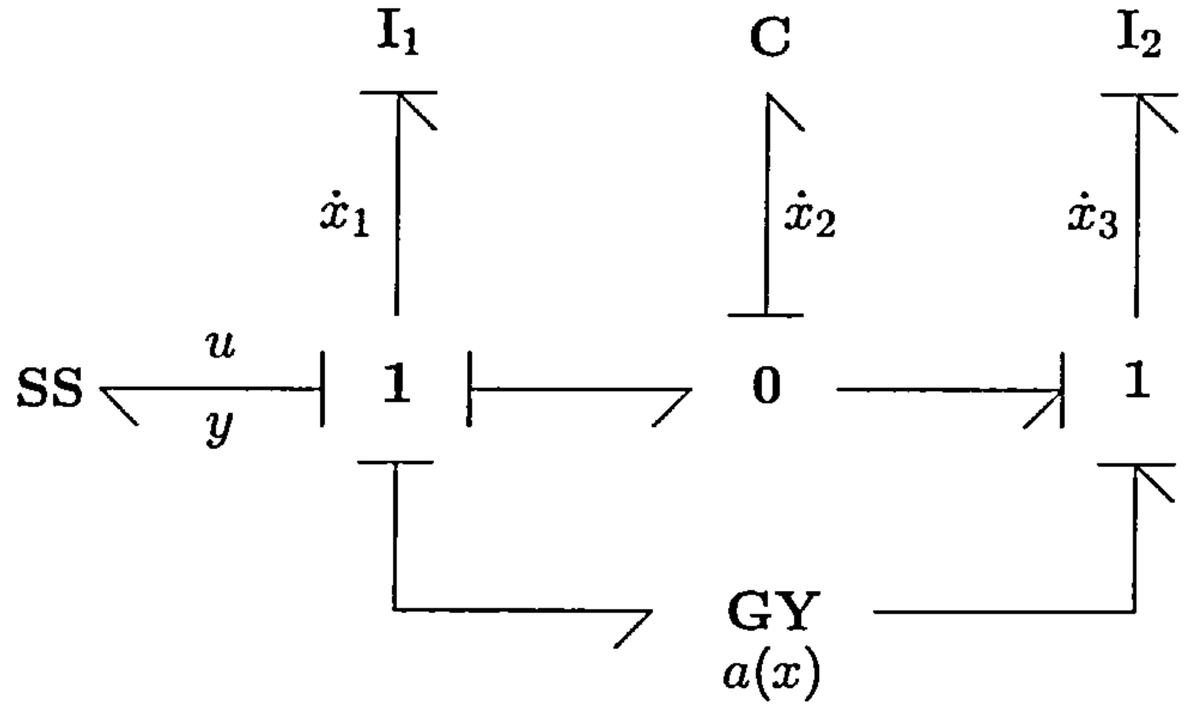

Figure 5.10.: Energy shaping impeded by modulation of Example 5.6.

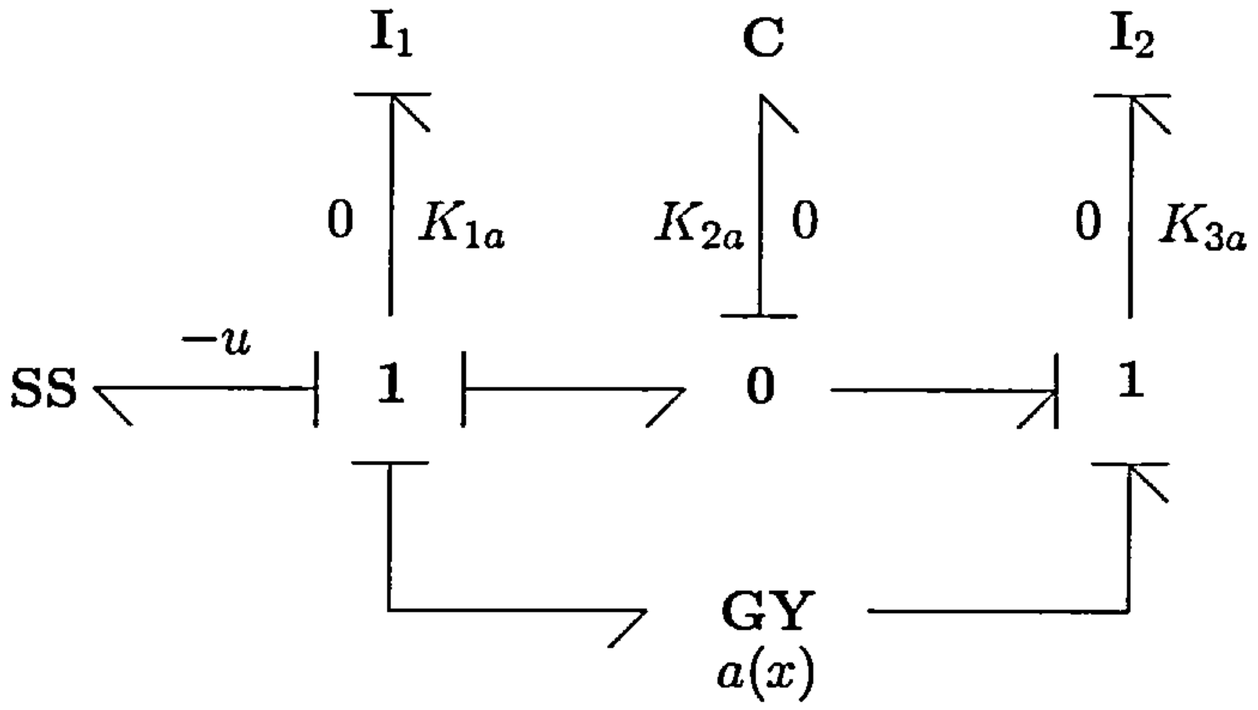

Figure 5.11.: Underactuated bond graph of Example 5.6.

In case the junction structure is smoothly modulated by x, the relation (5.47) readily provides a necessary condition for such modulations to be admissible, and this argument will also be used when interconnection and damping structures are modified through feedback control.

The following example clarifies possible problems with junction structure modulations in energy shaping.

Example 5.6. Consider the bond graph depicted in Figure 5.10, where $a(x)$ is a smooth modulation to be defined such that (5.47) is satisfied. It is not needed to evaluate (5.44) explicitly, but by following causality in Figure 5.11 it readily follows that

$$\begin{aligned} \frac{\partial H_a}{\partial x_1} - \frac{\partial H_a}{\partial x_3} &= 0 \\ a(x)\frac{\partial H_a}{\partial x_1} + \frac{\partial H_a}{\partial x_2} &= 0. \end{aligned} \tag{5.58}$$

By introducing the functions $F_1(x,p) = p_1 - p_3$ and $F_2(x,p) = a(x)p_1 + p_2$ it follows that

$$\{F_1, F_2\} = \left(\frac{\partial a}{\partial x_1} - \frac{\partial a}{\partial x_3}\right) p_1 = 0. \tag{5.59}$$

Therefore, if energy shaping is to be at all solvable for this particular example, it must hold that $a = a(x_1 + x_3)$. ◊

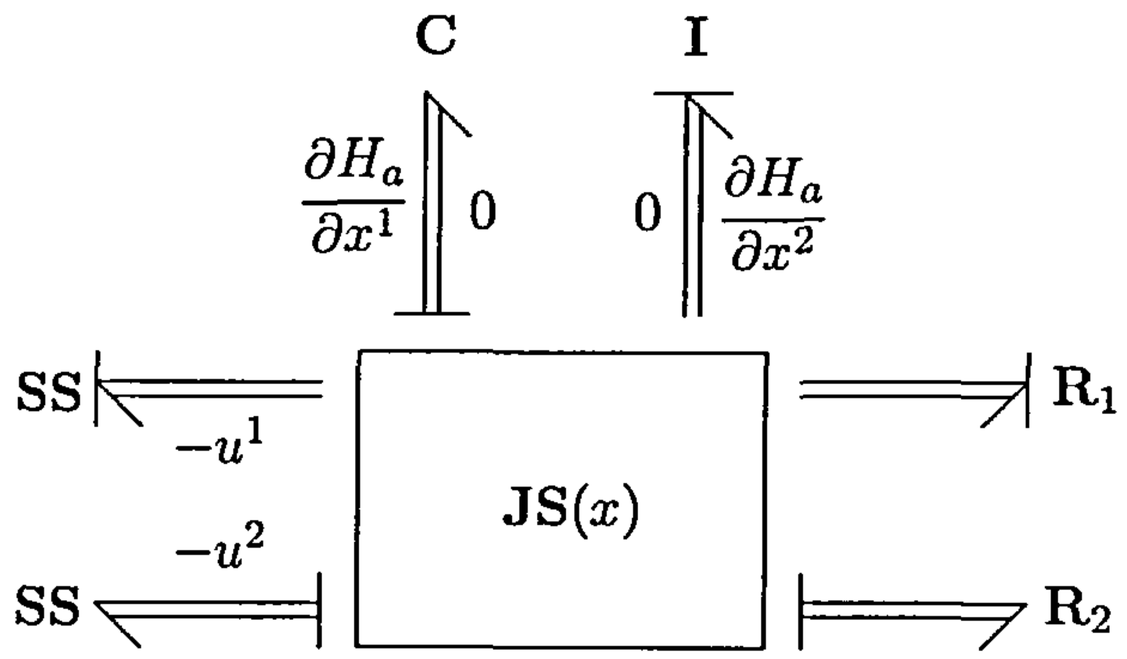

Figure 5.12.: Conceptual representation of energy shaping.

Examples 5.5 and 5.6 show that energy shaping for explicit port–Hamiltonian dynamics can be conceptually represented within the bond graph framework, but the solution is to be obtained through analytical considerations. Generalising the above examples, sole energy shaping can be conceptually depicted by Figure 5.12, where certain modulations of the junction structure JS(x) may impede energy shaping, however.

5.4. Control through Interconnection and Damping Assignment

Instead of energy shaping alone, the IDA–PBC methodology presented in Section 2.6 allows for the modification of interconnection and damping structures of *explicit* port–Hamiltonian systems through feedback control. Some instructive applications of this theory have been reported in [Ort02a] and [Ort00c]. Even though the general IDA–PBC method enlarges the class of port–Hamiltonian systems for stabilisation problems, IDA–PBC designs often lead to a set of first order PDEs that need to be solved. However, solving the associated PDEs of an IDA–PBC design need not imply that the control problem can be attained [Ort02a]. More precisely, finding a mere solution to the PDEs does not guarantee the control objective can be attained. Extensive theoretical research on the solvability of IDA–PBC type designs and the associated PDEs is still ongoing, see [Bla02] and references therein for an authoritative treatment of the topic.

The energy shaping method as described in Section 5.3.1 is completely based on [Ort02b] and is equivalent to the case for which no additive interconnection or damping structures are considered. In this section, on the other hand, mere energy shaping is complemented with possible modifications of the interconnection and damping structures through feedback.

5.4.1. Bond Graph Representations of Basic IDA–PBC Designs

This section explores basic IDA–PBC aspects from a bond graph perspective, where it is shown that IDA–PBC control can be represented through additive bond graph elements such **TF**, **GY** and **R** components. The insertion of such additive elements induces the $J_a(x)$ and $R_a(x)$ matrices of (2.77).

It must be noted that it is by no means attempted to define formal procedures and formalisations. Instead, the applicability of bond graph aspects in IDA–PBC designs is presented by means of a detailed example, which readily allows for formalisations and generalisations that can be committed to further research. The following example shows how an IDA–PBC design can be used effectively for certain stabilisation problems in which the bond graph defines the closed loop interconnection and damping structures.

Example 5.7. In [Ort01], the authors consider a magnetic levitated ball depicted in Figure 5.13. The Hamiltonian of this system is given as

$$H(x) = \frac{1}{2I(x_2)}x_1^2 + \frac{1}{2m}x_3^2 + mgx_2, \tag{5.60}$$

where x_1 is the flux linkage of the coil, and where x_2 and x_3 are the vertical displacement and momentum of the ball respectively. The inductance of the coil is given by $I(x_2) = \gamma_1/(\gamma_2 - x_2)$ for some physical constants $\gamma_1 > 0$ and $\gamma_2 > 0$. It is readily understood that this system can be modelled with a bond graph depicted in Figure 5.14, which shows a complete lack of structural interconnection between the electrical and mechanical energy domains.

The control objective is to stabilise the ball at some desired vertical position through voltage control on u. To this end, causal analysis yields the explicit port–Hamiltonian dynamics

$$\begin{bmatrix} \dot{x}_1 \\ \dot{x}_2 \\ \dot{x}_3 \end{bmatrix} = \begin{bmatrix} -r & 0 & 0 \\ 0 & 0 & 1 \\ 0 & -1 & 0 \end{bmatrix} \begin{bmatrix} x_1(\gamma_2 - x_2)/\gamma_1 \\ gm - x_1^2/(2\gamma_1) \\ x_3/m \end{bmatrix} - \begin{bmatrix} 1 \\ 0 \\ 0 \end{bmatrix} u \tag{5.61}$$

$$y = \frac{1}{\gamma_1}x_1(\gamma_2 - x_2).$$

Clearly, a set of admissible equilibria can be described by

$$x^e = (x_1^e, x_2^e, x_3^e) = \left(\sqrt{2mg\gamma_1}, \gamma_2 + \frac{1}{2r}\sqrt{\frac{2\gamma_1}{mg}}u^e, 0\right), \tag{5.62}$$

with u^e as a constant input.

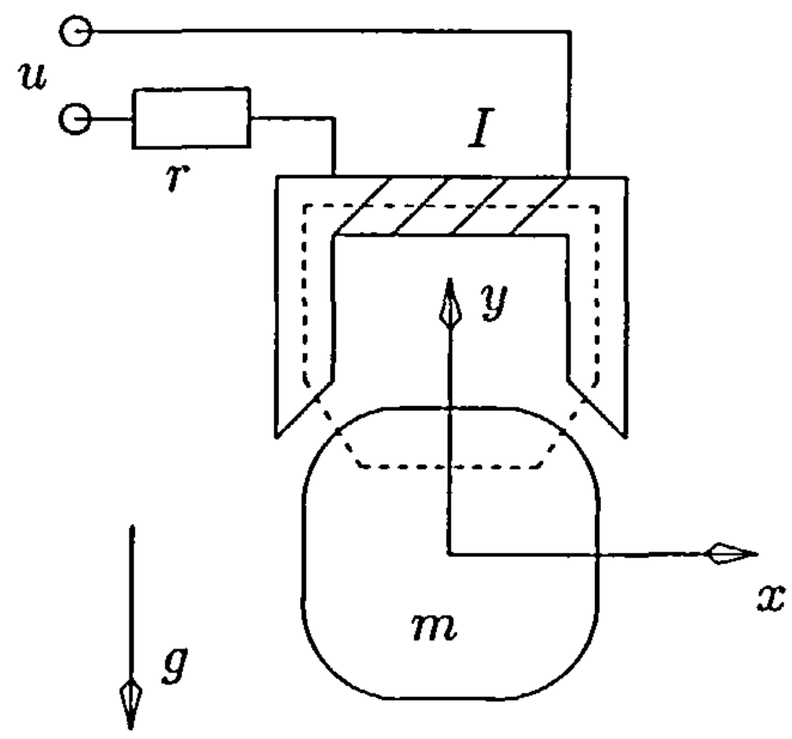

Figure 5.13.: Magnetic levitating ball of Example 5.7.

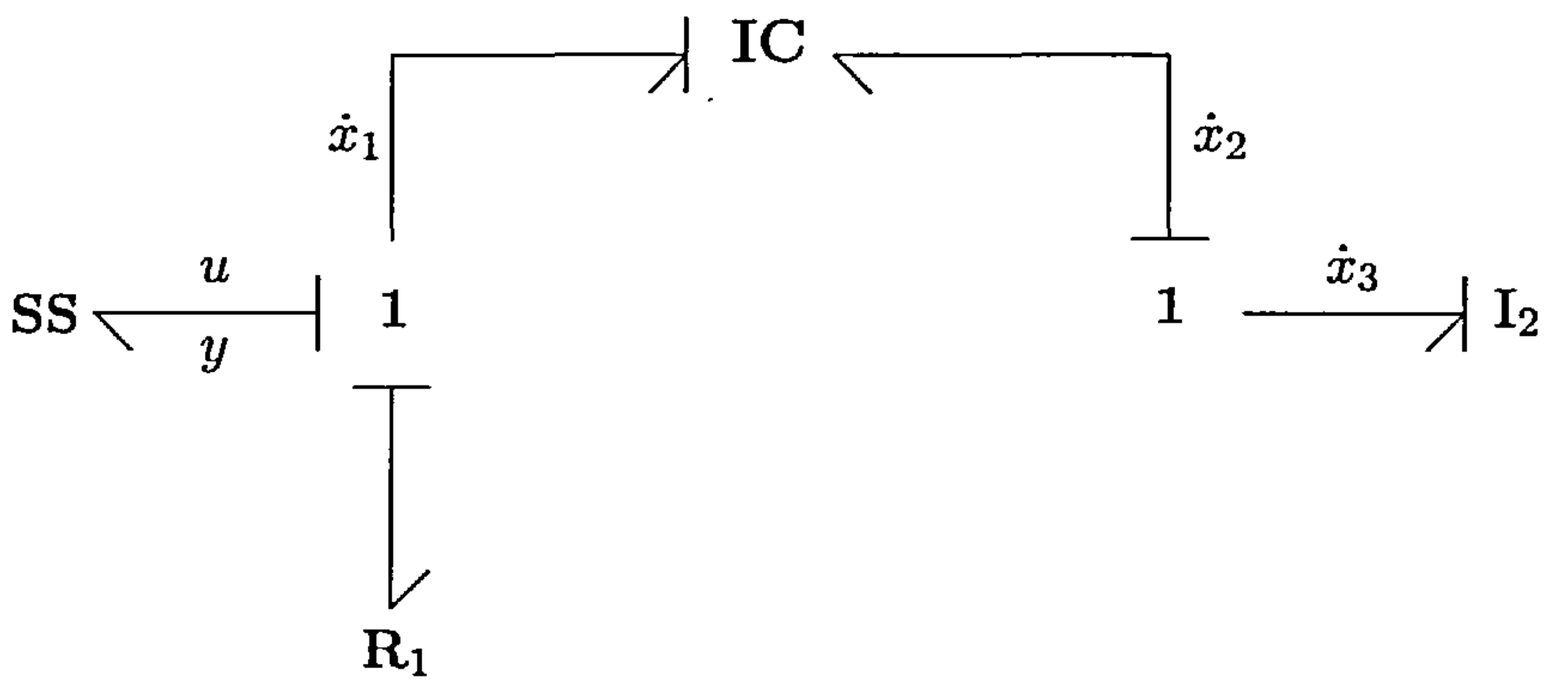

Figure 5.14.: Magnetic levitating ball bond graph of Example 5.7.

The point of departure for stabilisation is to consider mere energy shaping first, so that the additive energy is to be compatible with the bond graph topology of Figure 5.15. In case mere energy shaping is possible, it can be expected that the induced PDEs are less complex than a more general IDA–PBC design.

From (2.80), or from the bond graph in Figure 5.15, it is readily found that

$$\begin{aligned} r\frac{\partial H_a}{\partial x_1} &= u \\ \frac{\partial H_a}{\partial x_3} &= 0 \\ \frac{\partial H_a}{\partial x_2} &= 0, \end{aligned} \tag{5.63}$$

which shows that energy shaping is possible for the x_1–coordinate only. However, when the Hessian $\mathbf{D}^2 H_s(x)$ is evaluated, it becomes clear that the shaped energy $H_s(x)$ cannot be render positive definite at x^e by any function $H_a = H_a(x_1)$. Hence, it appears that an IDA–PBC design can be considered to address the stabilisation problem.

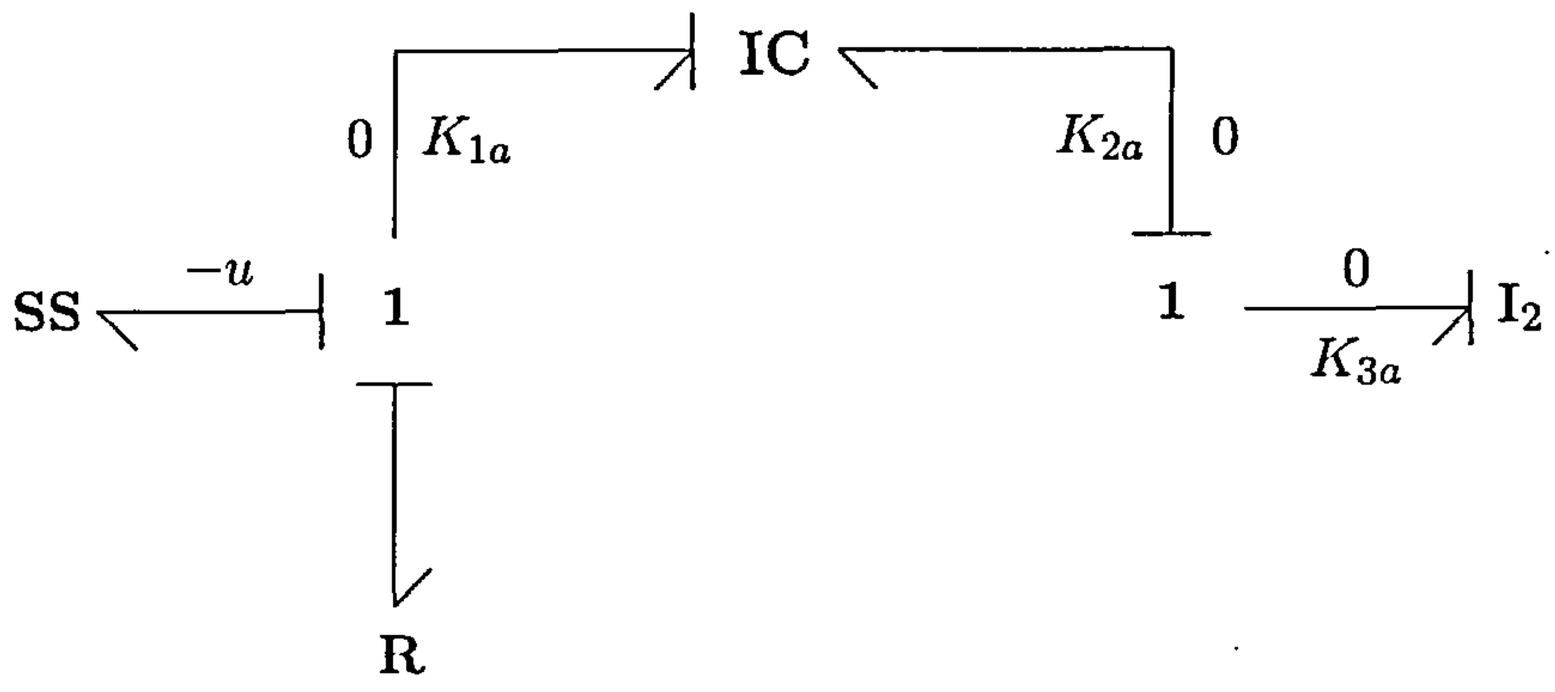

Figure 5.15.: Energy shaping compatible with bond graph topology; Example 5.7.

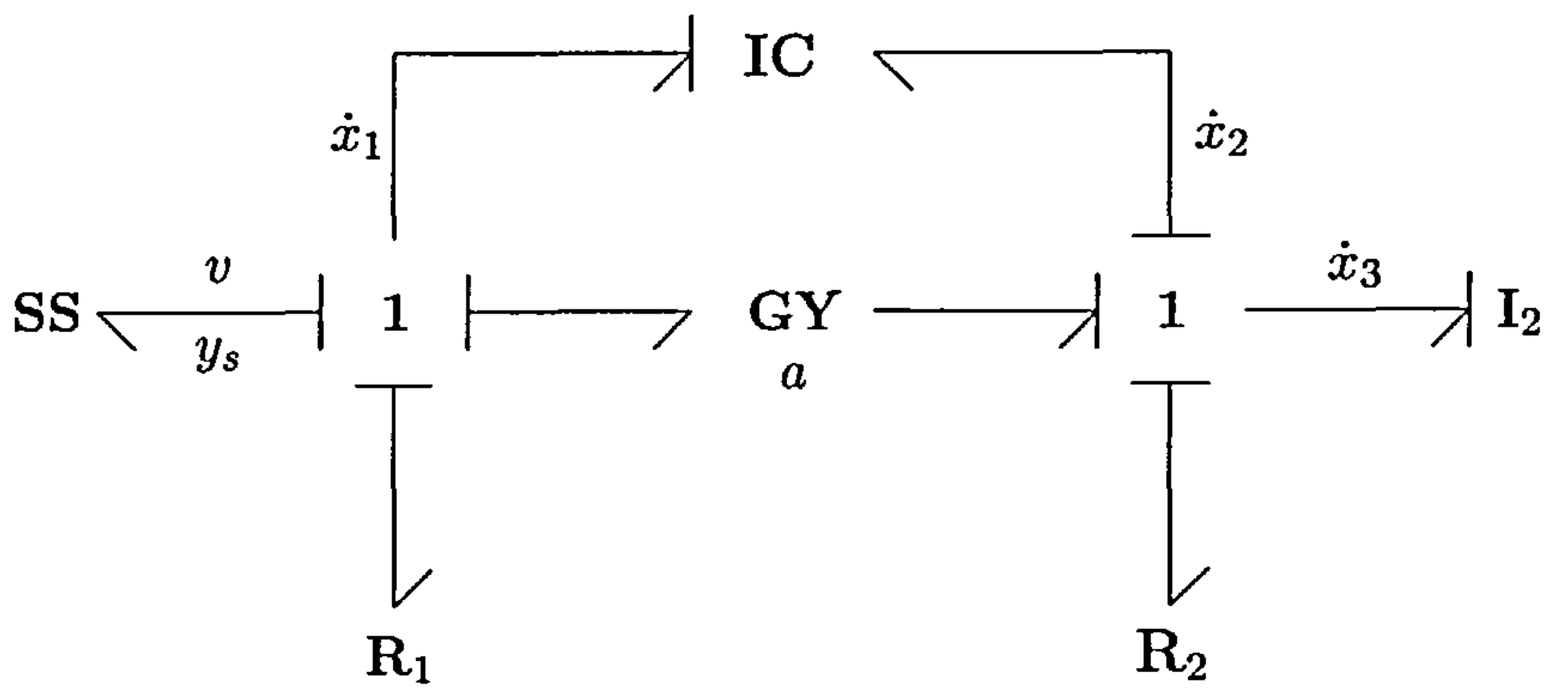

Figure 5.16.: Gyration and damping assignment; Example 5.7.

The IDA–PBC design commences by considering the plant bond graph with added gyration and damping as depicted in Figure 5.16. Observe that the gyrator and damping element $\mathbf{R}_2$ are a natural choice from a bond graph perspective: The lack of coupling is resolved through a (constant) gyrator and where linear damping in the mechanical domain may improve asymptotic convergence. Note that the resistance $\mathbf{R}_2$ is not considered in [Ort01].

At this point the IDA–PBC design is conceptually clear, but it remains to be verified whether the closed loop can be attained through feedback. To that end, take

$$J_a(x) = \begin{bmatrix} 0 & 0 & -a \\ 0 & 0 & 0 \\ a & 0 & 0 \end{bmatrix}, \quad R_a(x) = \begin{bmatrix} r_1 & 0 & 0 \\ 0 & 0 & 0 \\ 0 & 0 & r_2 \end{bmatrix}, \tag{5.64}$$

where $a > 0$, $r_1 > 0$ and $r_2 > 0$. Then by (2.80) one obtains the PDEs

$$\begin{aligned} \frac{\partial H_a}{\partial x_3} &= 0 \\ a\frac{\partial H_a}{\partial x_1} - \frac{\partial H_a}{\partial x_2} - r_2\frac{\partial H_a}{\partial x_3} - \frac{r_2}{m}x_3 + \frac{a}{\gamma_1}x_1(\gamma_2 - x_2) &= 0. \end{aligned} \tag{5.65}$$

In view of Proposition 5.1, define the functions

$$\begin{aligned} F_1(x,p) &= p_3 \\ F_2(x,p) &= ap_1 - p_2 - r_2 p_3 - \frac{r_2}{m}x_3 + \frac{a}{\gamma_1}x_1(\gamma_2 - x_2), \end{aligned} \tag{5.66}$$

from which it follows that $\{F_1, F_2\} = r_2/m$. Thus $r_2 = 0$ must hold if the current IDA–PBC setup is to be at all solvable.

Consequently, the PDEs (5.65) reduce to the single PDE

$$a\frac{\partial H_a}{\partial x_1} - \frac{\partial H_a}{\partial x_2} + \frac{ax_1(\gamma_2 - x_2)}{\gamma_1} = 0, \tag{5.67}$$

which is readily solved using the method of characteristics described in [Eva98]. To do this explicitly, define the initial data

$$\Gamma = \{(x_1, x_2, H_a) \,|\, x_1 = 0,\, x_2 = \tau,\, H_a = \phi(\tau)\}, \tag{5.68}$$

and verify that the additive energy function $H_a(x)$ takes the form

$$H_a(x) = \phi\left(\frac{1}{a}x_1 + x_2\right) - \frac{x_1^2(\gamma_2 - x_2)}{2\gamma_1} + \frac{x_1^3}{6a\gamma_1}, \tag{5.69}$$

where ϕ is an arbitrary differentiable function. It is important to note that the choice of the initial data Γ can yield solutions of variable complexity. For example, it is possible to take

$$\Gamma = \{(x_1, x_2, H_a) \,|\, x_1 = \tau,\, x_2 = 0,\, H_a = \phi(\tau)\}, \tag{5.70}$$

which would yield the additive energy

$$H_a(x) = \phi\left(x_1 + ax_2\right) + \frac{a\gamma_2}{\gamma_1}x_1x_2 + \frac{a^2\gamma_2}{2\gamma_1}x_2^2 - \frac{a}{2\gamma_1}x_1x_2^2 - \frac{a^2}{6\gamma_1}x_2^3. \tag{5.71}$$

Clearly, the simplest solution is (5.69) and seen to yield the shaped energy

$$H_s(x) = H(x) + H_a(x) = \phi\left(\frac{1}{a}x_1 + x_2\right) + \frac{1}{6a\gamma_1}x_1^3 + \frac{1}{2m}x_3^2 + mgx_2, \tag{5.72}$$

where $\phi(x_1/a + x_2)$ can be chosen to assign a strict minimum to $H_s(x)$ at x^e. For example, let ϕ be defined as

$$\phi\left(\frac{1}{a}x_1 + x_2\right) = \frac{c_1}{2}\left(\frac{1}{a}x_1 + x_2 - \frac{1}{a}x_1^e - x_2^e\right)^2 - mg\left(\frac{1}{a}x_1 + x_2 - \frac{1}{a}x_1^e - x_2^e\right), \tag{5.73}$$

so that the shaped Hamiltonian $H_s(x) = H(x) + H_a(x)$ satisfies

$$\mathrm{D}H_s(x^e) = 0. \tag{5.74}$$

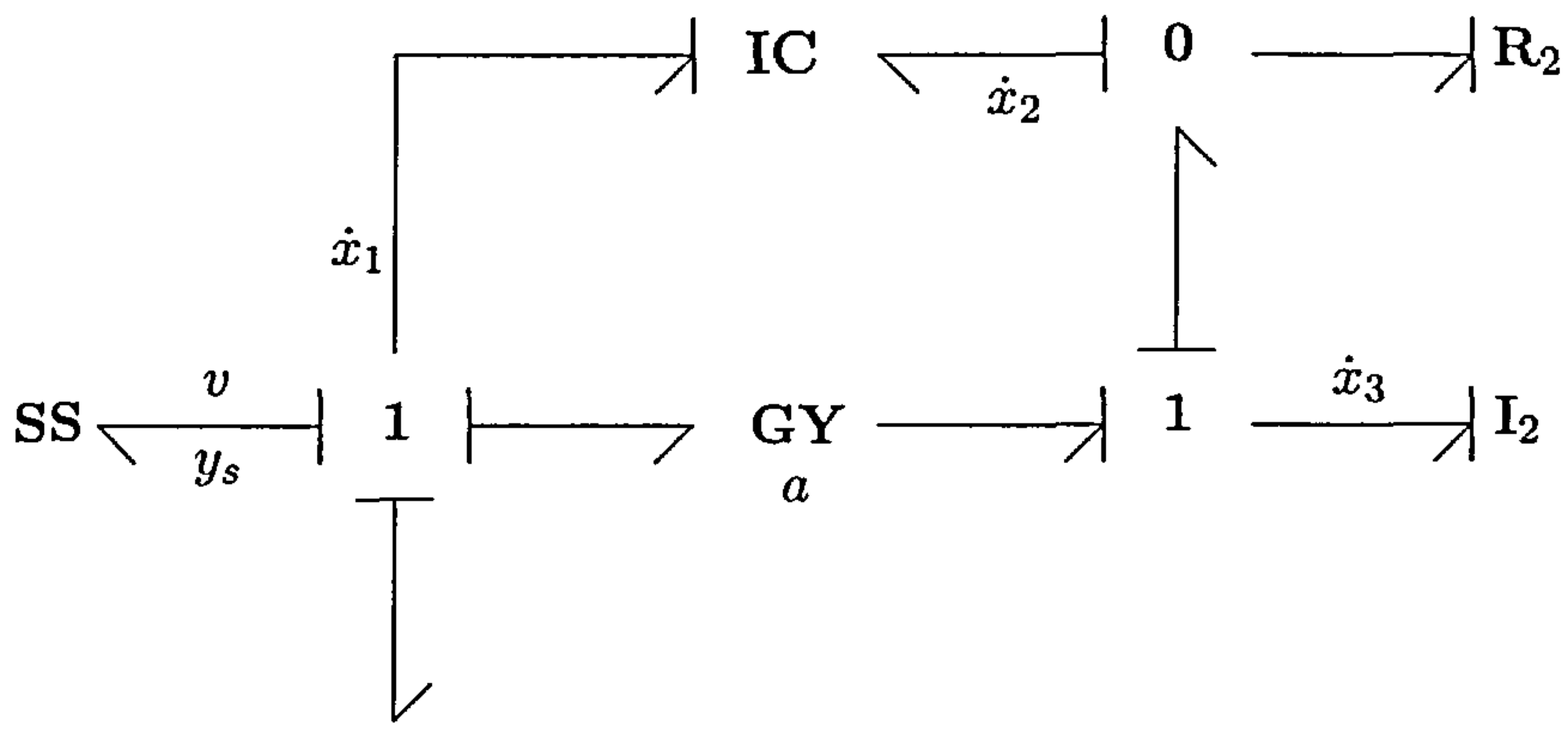

Figure 5.17.: Non–obvious additive damping; Example 5.7.

This proves the extremal assignment at x^e. Moreover, for all $c_1 > 0$, the Hessian satisfies

$$\mathrm{D}^2 H_s(x^e) = \begin{bmatrix} c_1/a^2 + x_1^e/(a\gamma_1) & c_1/a & 0 \\ c_1/a & c_1 & 0 \\ 0 & 0 & 1/m \end{bmatrix} > 0, \tag{5.75}$$

which show that x^e is a strict minimum of $H_s(x)$. Finally, the control is then found from (2.81) and takes the form

$$u = \frac{a}{m}x_3 + (r + r_1)\frac{\partial H_a}{\partial x_1} + \frac{r_1}{\gamma_1}x_1(\gamma_2 - x_2) + w. \tag{5.76}$$

Now, the IDA–PBC design shows that the bond graph in Figure 5.16 offers a relatively natural way of defining the closed loop port–Hamiltonian system. However, as mentioned before, the bond graph can only be used conceptually to represent the control objective, which may or may not be attainable. Indeed, the $\mathbf{R}_2$ in Figure 5.16 turned out not to be assignable even though its appearance is a natural choice. To further explore choices of additive damping, consider the bond graph in Figure 5.17 and observe that the $\mathbf{R}_2$ element has been moved to a 0–junction. The interconnection and damping structures are now given by

$$J_a(x) = \begin{bmatrix} 0 & 0 & -a \\ 0 & 0 & 0 \\ a & 0 & 0 \end{bmatrix}, \quad R_a(x) = \begin{bmatrix} r_1 & 0 & 0 \\ 0 & 1/r_2 & 0 \\ 0 & 0 & 0 \end{bmatrix}, \tag{5.77}$$

where $a > 0$, $r_1 > 0$ and $r_2 > 0$. The induced PDEs that need to be solved are

$$\begin{aligned} \frac{\partial H_a}{\partial x_3} - \frac{1}{r_2}\frac{\partial H_a}{\partial x_2} - \frac{gm}{r_2} + \frac{1}{2r_2\gamma_1}x_1^2 &= 0 \\ a\frac{\partial H_a}{\partial x_1} - \frac{\partial H_a}{\partial x_2} + \frac{a}{\gamma_1}x_1(\gamma_2 - x_2) &= 0. \end{aligned} \tag{5.78}$$

Invoking Proposition 5.1, define the functions

$$\begin{aligned} F_1(x,p) &= p_3 - \frac{1}{r_2}p_2 - \frac{gm}{r_2} + \frac{1}{2r_2\gamma_1}x_1^2 \\ F_2(x,p) &= ap_1 - p_2 + \frac{a}{\gamma_1}x_1(\gamma_2 - x_2), \end{aligned} \tag{5.79}$$

and observe that $\{F_1, F_2\} = 0$, implying that solutions to (5.78) may exist. The second PDE of (5.78) admits the solution (5.69), which then leads to the additive energy

$$H_a(x) = \phi\left(\frac{1}{a}x_1 + x_2 + \frac{1}{r_2}x_3\right) - \frac{x_1^2(\gamma_2 - x_2)}{2\gamma_1} + \frac{x_1^3}{6a\gamma_1} + \frac{mg}{r_2}x_3. \tag{5.80}$$

Then entirely analogue to (5.73), define ϕ to be the quadratic function

$$\begin{aligned} \phi\left(\frac{1}{a}x_1 + x_2 + \frac{1}{r_2}x_3\right) = \frac{c_1}{2}\left(\frac{1}{a}x_1 + x_2 + \frac{1}{r_2}x_3 - \frac{1}{a}x_1^e - x_2^e - \frac{1}{r_2}x_3^e\right)^2 \\ - mg\left(\frac{1}{a}x_1 + x_2 + \frac{1}{r_2}x_3 - \frac{1}{a}x_1^e - x_2^e - \frac{1}{r_2}x_3^e\right). \end{aligned} \tag{5.81}$$

It is readily verified that x^e is an extremum for $H_s(x)$, thus $\mathrm{D}H_s(x^e) = 0$, and that the Hessian satisfies $\mathrm{D}^2H_s(x^e) > 0$ for all values of $c_1 > 0$. The control now reads

$$u = (r + r_1)\frac{\partial H_a}{\partial x_1} + a\frac{\partial H_a}{\partial x_3} + \frac{a}{m}x_3 + \frac{r_1}{\gamma_1}x_1(\gamma_2 - x_2) + w. \tag{5.82}$$

◊

The above example shows an introductory deployment of bond graph representations for a basic IDA–PBC design, where the following observations can be made. First, it is seen that conceptual bond graph representations can be used to choose interconnection and damping structures. For instance, the lack of structural coupling in bond graph topological sense may hint at possible additive interconnections, such as **TF** and **GY** components. This is clearly demonstrated by Figure 5.14 in which there is no structural coupling between the electrical and mechanical domains. The insertion of a **GY** component remedies this shortage of coupling and a allows a *force* to be applied to the ball.

Second, in view of damping structures, additive damping can be based on available junctions within the bond graph, where Figure 5.16 shows that it is quite natural to place a resistive elements at the 1–junction in the mechanical domain. On the other hand, as depicted in Figure 5.17, the addition of resistive elements by explicit insertion of a new junction is certainly possible, but such choice does not immediately follow from "intuitive" bond graph arguments.

A final remark is in order, namely, it must be remembered that IDA–PBC control of [Ort02b] applies to *explicit* port–Hamiltonian dynamics, so that the associated bond graph should not induce derivative causalities. For example, the bond graph of the frictionless slider in Figure 5.7 cannot be used to represent a IDA–PBC problem in accordance with the theory of Section 2.6. As a result, bond graphs representations for IDA–PBC designs are limited to a small class of systems that do not produce derivative causalities in bond graphs.

5.5. Conclusion

The first half of the chapter introduced a novel method for bond graph based *power balancing* control, which addresses stabilisation through feedback that retains passivity with respect to the natural output. The class of systems suitable for this stabilisation technique must meet well–known detectability requirements commonly found in passive systems literature. Crucial to the power balancing method has been shown to be a proper decomposition of the plant bond graph into two subsystems with uncoupled Hamiltonians, where the subsystem having the natural outputs as system inputs is assumed to have no resistive elements. In case such bond graph decomposition can be found, it has been shown that the additive energy function can be based on the Hamiltonian associated with the subsystem that has the natural output as an input.

Power balancing as presented in this chapter can be scaled and allows for bond graphs that will either induce explicit or implicit dynamics when causally assigned with SCAP. This broad applicability can be attributed to the fact that bond graph junction structures remain power continuous regardless of the causal configuration. For example, it has been shown that the application of the Lagrangian assignment procedure circumvented derivative causalities without changing the power continuity property. In any case, however, system requirements such as detectability and internal stability remain in effect for all bond graph models, irrespective of the causal configuration.

The latter part of the chapter addressed basic bond graph interpretations of IDA–PBC designs. Unlike power balancing, the closed loop bond graph representation of an IDA–PBC design has been shown to be more conceptual in nature and does not provide a means to find the control. This can be attributed to the fact that IDA–PBC designs often lead to a set of first order PDEs that need to be solved.

Even though the bond graph aspects of IDA–PBC designs are mostly conceptual, it has been shown that the control objective can be graphically depicted, thereby increasing insight into the design to some degree. In particular, interconnection and damping structures have been shown to be represented by the insertion and modification of **GY**, **TF** and **R** components. However, the shaped interconnection and damping structures for any IDA–PBC design remains to be chosen by the designer, thereby rendering the IDA–PBC methodology quite flexible but less constructive.

6. Conclusions and Future Research

6.1. Review

This thesis presented the following control design methodologies for bond graph based control purposes: (1) Backstepping Control, (2) Model Matching Control, and (3) Energy Shaping in Stabilisation Control. Even though these topics have virtually no similarities on analytical levels, it has been shown that these methods are capable of addressing closed loop bond graph representations. More precisely, it has been argued that *open loop* bond graph modelling is well–understood, whereas *closed loop* bond graph modelling is not. Therefore, the impetus of this thesis was to collect and explore particular control design methods capable of addressing structural design goals in terms of closed loop bond graph representations. Important aspects of these structural considerations have been existing concepts of port–Hamiltonian systems in relation to bond graph models. In conclusion, this thesis has shown that the above control design methods allow for structural design goals such that associated bond graphs can be found, thereby contributing new modelling aspects in the field of physical model based control with bond graphs.

6.2. Backstepping Control

Backstepping control design has been addressed from a bond graph perspective, where the stabilising functions were defined as additive bond graph models and referred to as *virtual actuators*. Most importantly, this thesis showed that *explicit* port–Hamiltonian closed loop dynamics can be obtained through an *exact* backstepping design to ensure an associated bond graph representation. Through judiciously chosen virtual control laws, it has been shown that the plant bond graph topology can be retained such that passive stabilisation can be interpreted by means of the plant bond graph. Furthermore, the bond graph based backstepping approach readily showed to be applicable in a nonlinear context with suitable virtual control laws, thereby complementing the existing literature on the mere linear case.

Backstepping is known for its use of new coordinates that are introduced recursively at each step of the design. This thesis, on the other hand, has clarified that the bicausal inversion mechanism yields a class of exact backstepping controllers without the explicit introduction of new variables. However, these new coordinates remain necessary for the closed loop dynamics, hence for the closed loop bond graph representation. In addition, the bicausal inversion mechanism has been shown not to facilitate the further stabilisation at each step due to the absence of these new coordinates.

Most of the existing literature on bond graph based backstepping addresses single–input systems. This thesis has shown that the single–input case is readily applicable to a class of multi–input systems having the required interlaced structure for which the bond graph based backstepping can be applied. The multi–input case considered here has shown to include systems with single–input "branches", where the recursive backstepping scheme can be applied to each branch. The (bi)causal inversion mechanism has shown to be applicable to such multi–input systems.

6.3. Model Matching Control

The design of trajectory tracking controllers by means of bicausal bond graphs has previously appeared in the literature. This thesis complemented some known results by means of the Model Matching Problem (MMP) of prescribed model trajectories instead of the common framework of "arbitrary" reference trajectories. It has been shown that bond graphs can be used to define prescribed reference models, where the closed loop input/output behavior should match the input/output behavior of the prescribed model.

The main result of the bond graph based MMP has shown to be the underlying mechanism of the MMP design. Indeed, this thesis has shown that bond graph modelling for the physical model based MMP implicitly relies on the theory of dynamic disturbance decoupling and concepts of output regulation.

For certain MMP scenarios it has been shown that the "error dynamics" allows for an associated bond graph representation, so that passive stabilisation becomes possible through bond graph arguments. In particular, the error dynamics has readily been associated with center manifold considerations whereby the tracking error of state variables can be found by means of a submanifold on which output matching occurs.

On the other hand, more general MMP scenarios have been shown to merely allow for the closed loop input/output dynamics as prescribed by the model bond graph. The lack of bond graph representations for the actual error dynamics has been attributed to additional modelling difficulties, such as derivative causalities and non–preferred state variables. In order to circumvent such difficulties, reduction from implicit to explicit dynamics showed to be preferable for the MMP design. Towards that end, the Lagrangian causality assignment procedure did not yield explicit port–Hamiltonian dynamics, so that an associated bond graph representation for the error dynamics could not be found.

For certain nonlinear scenarios, the bond graph based MMP has shown *not* to be solvable by means of the feedback linearisation mechanism. As a result, the linearised MMP was attempted instead, requiring the linearisation of the plant and model dynamics about some operating point. The linearised plant retained its nonlinear bond graph representation and the prescribed linearised input/output dynamics retained its nonlinear model bond graph.

6.4. Energy Shaping in Stabilisation Control

Feedback passivation has been presented from a bond graph perspective, where the bond graph junction structures has shown to be capable of identifying feedback passive control laws with respect to the original plant output. This method has been referred to as "power balancing" and was used to derive the closed loop storage function from the junction structure instead of a predefined storage function. However, the power balancing method requires stable zero–dynamics, which is a general requirement for all feedback passivation design with respect to the original plant output. Power balancing has been shown to be suitable for multi–input bond graphs and for bond graphs having derivative causalities.

Interconnection and Damping Assignment Passivity Based Control (IDA–PBC) has been briefly shown to allow for conceptual bond graph representations. That is, bond graphs can be used to depict prescribed closed loop port–Hamiltonian dynamics by redefining the junction structure and the dissipative elements in accordance with IDA–PBC theory. The solution of IDA–PBC designs, however, is known to depend on first order partial differential equations, so that bond graph representations in IDA–PBC are applicable on conceptual level. Thus, basic IDA–PBC designs can be defined through bond graph representations, but the solutions to the design must be obtained through conventional means.

6.5. Future Research

The thesis has identified three control methods that allow for structural design goals in terms of closed loop bond graph representations. However, it is often argued that mere structural or "geometric" feedback designs often lack certain robustness margins with respect to model uncertainties. In particular, the robustness of exact backstepping and model matching controllers can be expected to be relatively low due to the linearisations performed in these designs. For example, recall that this thesis focused on *exact* backstepping, which is based on exact cancellations. Furthermore, the robustness margins of MMP designs can likewise be expected to be relatively low due to the explicit feedback linearisation of plant input/output dynamics.

Even though it can be argued that linearisation based designs are perfectly admissible in a mathematical context, real physical dynamics will generally deviate from prescribed model dynamics. As a result, controller performance often deteriorates significantly or may even cause instability in presence of model uncertainty. In view of controller commissioning and implementation, robust control of bond graph based feedback designs is the most important next step in future research. Towards that end, the significant advances of modern robust control theory for linear systems suggest that future work on bond graph based controllers should be restricted to linear systems first.

Bibliography

[Abr88] Abraham, R., J. E. Marsden. *Manifolds, Tensor Analysis, and Applications*, volume 75 of *Applied mathematical sciences*. Springer–Verlag, 2 edition, 1988.

[Bar77] Barnard, B. W., and P. D. Dransfield. Predicting response of a proposed hydraulic control system using bond graphs. *ASME Journal of Dynamics Systems, Measurement and Control*, 99(1):1–8, 1977.

[Bir90] Birkett, S. H., and P. Roe. The mathematical foundations of bond graphs – iv. matrix representations and causality. *Journal of the Franklin Institute*, 327(1):109–128, 1990.

[Bla02] Blankenstein, G., R. Ortega, and A. J. Van Der Schaft. The matching conditions of controlled lagrangians and ida–passivity based control. *International Journal of Control*, 75(9), 2002.

[Blu82] Blundell, A. *Bond Graphs for Modelling Engineering Systems*. Ellis Horwood Publishers, 1982.

[Bor00] Borutzky, W. *Bondgraphen - Eine Methodologie zur Modellierung multidisziplinrer Systeme*, volume 6 of *Fortschritte in der Simulationstechnik*. SCS European Publishing House, 2000.

[Bor04] Borutzky, W. *Bond Graphs – A Methodology for Modelling Multidisciplinary Dynamic Systems*, volume FS14 of *Frontiers in Simulation*. SCS Publishing House, San Diego, 2004.

[Bre91] Breedveld, P. Editorial: Special issue on current topics in bond graph related research. Journal of Systems and Control Engineering 328(5–6), 1991.

[Bre92a] Breedveld, P. Proposition for an unambiguous vector bond graph notation. *ASME Journal of Dynamics Systems, Measurement and Control*, 104(3):267–270, 1992.

[Bre92b] Breedveld, P., and G. Dauphin–Tanguy. *Bond Graphs for Engineers.* Elsevier Science Publisher, 1992.

[Bre95] Breedveld, P. Multibond graph elements in physical systems theory. *Journal of the Franklin Institute*, 319(1/2):1–36, 1995.

[Bre94] Breedveld, P. Multibond graph representation of Lagrangian mechanics: The elimination of the euler junction structure. In *Proceedings of the MATHMOD*, pages 24–28, 94.

[Bus98] Bush-Vishniac, I. J. *Electromechanical Sensors and Actuators.* Springer–Verlag, New York, 1998.

[BV04] Control Lab Products BV. 20–Sim. URL: http://www.20sim.com/, 2004.

[Byr91] Byrnes, C. I., A. Isidori, and J. C. Willems. Passivity, feedback equivalence, and the global stabilization of miminum phase nonlinear systems. *IEEE Transactions on Automatic Control*, 36:1228–1240, 1991.

[Car65] Carathéodory, C. *Calculus of Variations and Partial Differential Equations of the First Order.* Holden–Day series in mathematical physics. Holden–Day, 1965.

[Cel91] Cellier, F. E. *Continuous System Modeling.* Springer–Verlag, 1991.

[Dal97] Dalsmo, M., and A. J. van der Schaft. A Hamiltonian framework for interconnected physical systems. Technical report, Universiteit Twente, 1997.

[Des75] Desoer, C. A., and M. Vidyasagar. *Feedback Systems: Input–Output Properties.* Academic Press, New York, 1975.

[Dij91] Dijk, J. van, and P. Breedveld. Simulation of System Models Containing Zero–Order Causal Paths – I. Classification of Zero–Order Causal Paths. *Journal of the Franklin Institute*, 328(5/6):959–979, 1991.

[Dix74] Dixhoorn, J. van, and F. Evans. *Physical Structure in Systems Theory: Network Approaches to Engineering and Economics.* Acadamic Press, 1974.

[Dyn04] Dynasim. Dymola. URL: http://www.dynasim.se/, 2004.

[Eva98] Evans, L. C. *Partial Differential Equations*, volume 19 of *Graduate Studies in Mathematics.* American Mathematical Society, 1998.

[Gaw92] Gawthrop, P. J., and L. Smith. Causal augmentation of bond graphs with algebraic loops. *Journal of the Franklin Institute*, 329(2):291–303, 1992.

[Gaw95a] Gawthrop, P. J. Bicausal bond graphs. In *Cellier and Granda*, pages 83–88, 1995.

[Gaw95b] Gawthrop, P. J. Physical model based control: A bond graph approach. *Journal of the Franklin Institute*, 332B(3):285–305, 1995.

[Gaw96] Gawthrop, P. J., and L. Smith. *Metamodelling: Bond Graphs and Dynamic Systems.* Prentice Hall, 1996.

[Gaw00] Gawthrop, P. J. Physical interpretation of inverse dynamics using bicausal bond graphs. *Journal of the Franklin Institute*, 337:743–769, 2000.

[Gaw01] Gawthrop, P. J., D. Ballance, and D. Vink. Bond graph based control with virtual actuators. In *Simulation in Industry.* ESS, 2001.

[Gaw02] Gawthrop, P., and S. Scavarda. Editorial: Special issue on bond graphs. Proceedings of the Institution of Mechanical Engineers Part I, Journal of Systems and Control Engineering 216(1), 2002.

[Gaw03] Gawthrop, P., and D. Palmer. A bicausal bond graph representation of operational amplifiers. *Proceedings of the IMechE Part I: Journal of Systems and Control Engineering*, 217:49–58, 2003.

[Gaw04] Gawtrop, P. Bond graph based control using virtual actuators. *Proceedings of the IMechE Part I: Journal of Systems and Control Engineering*, 218:251–268, 2004.

[Gol02] Golo, G. *Interconnection Structures in Port–Based Modelling: Tools for Analyisis and Simulation.* PhD thesis, Twente University, 2002.

[Gol03] Golo G., A. J. van der Schaft, P. Breedveld, and B.M. Maschke. *Hamiltonian formulation of bond graphs*, pages 1–2. Lecture Notes for the Euro/Geoplex Summer School. Springer–Verlag, 2003.

[Hog85] Hogan, N. Impedance control: An approach to manipulation: Part i – theory. *ASME Journal of Dynamics Systems, Measurement and Control*, (1):1–7, 1985.

[Hog87] Hogan, N. Modularity and causality in physical systems modelling. *ASME Journal of Dynamics Systems, Measurement, and Control*, 109:384–391, 1987.

[Hui92] Huijberts, H. J. C. A nonregular solution of the nonlinear dynamic disturbance decoupling problem with an application to a complete solution of the nonlinear model matching problem. *SIAM Journal on Control and Optimization*, 30:336–349, 1992.

[Hui94] Huijberts, H. J. C. *Dynamic Feedback in Nonlinear Synthesis Problems.* Centrum voor Wiskunde en Informatica, 1994.

[ICB03] *International Conference on Bond Graph Modeling and Simulation (ICBGM)*, 2003.

[Isi90] Isidori, A., and C. I. Byrnes. Output regulation of nonlinear systems. In *IEEE Transactions on Automatic Control*, volume 35, pages 131–140, 1990.

[Isi95] Isidori, A. *Nonlinear Control Systems.* Springer–Verlag, 3 edition, 1995.

[Isi99] Isidori, A. *Nonlinear Control Systems II.* Springer–Verlag, London, 1999.

[Jan96] Jankovic, M., D. Fontaine, P. V. Kokotovic. TORA Example: Cascade– and passivity–based control designs. *IEEE Transactions on Control Systems Technology*, 4(3):292–297, 1996.

[Jos74] Joseph, B. J., and H. R. Martens. The method of relaxed causality in the bond graph analysis of nonlinear systems. *ASME Journal of Dynamics Systems, Measurement and Control*, 96(1):95–99, 1974.

[Jun01] Junco, S. Lyapunov second method and feedback stabilization directly on bond graphs. In *Proceedings of the ICBGM*, 2001.

[Kar77] Karnopp, D. C. Lagrange's equations for complex bond graph systems. *ASME Journal of Dynamics Systems, Measurement and Control*, 99(4):300–306, 1977.

[Kar79] Karnopp, D. C. Bond graphs in control: Physical state variables and observers. *Journal of the Franklin Institute*, 308(3):219–234, 1979.

[Kar83] Karnopp, D. C. Alternative bond graph causal patterns and equation formulatations for dynamic systems. *ASME Journal of Dynamics Systems, Measurement and Control*, 105:58–63, 1983.

[Kar92] Karnopp, D. C. An approach to derivative causality in bond graph models of mechanical systems. *Journal of the Franklin Institute*, 329(1):65–75, 1992.

[Kar00] Karnopp, D. C., D. L. Margolis., and R. C. Rosenberg. *System Dynamics: Modeling and Simulation of Mechatronic Systems.* John Wiley, 3nd edition, 2000.

[Kha92] Khalil, H. K. *Nonlinear Systems.* MacMillan, New Jersey, 2 edition, 1992.

[Kri95] Kristić, M., I. Kanellakopoulos, and P. Kokotović. *Nonlinear and Adaptive Control Design.* Wiley–Interscience, 1995.

[Lam97] Lamb, J. D., D. R. Woodall, and G. M. Asher. Bond graphs ii: Causality and singularity. *Discrete Applied Mathematics*, 73(2):143–173, 1997.

[Mai03] Maithripala, D. H. D., Berg, Jordan M., and W. P. Dayawansa. Loss of structurally stable regulation implies loss of stability. In *IEEE Transactions on Automatic Control*, volume 38, pages 483–487, 2003.

[Mar94] Marsden, J. E., and T. S. Ratiu. *Introduction to Mechanics and Symmetry*, volume 17 of *Texts in applied mathematics.* Springer–Verlag, New York, 1994.

[Mar02] Marquis–Favre, W., and S. Scavarda. Alternative causality assignment procedures in bond graphs for mechanical systems. *ASME Journal of Dynamics Systems, Measurement and Control*, 124:457–463, 2002.

[Mas92] Maschke, B. M., A. J. van der Schaft, P. C. Breedveld. An intrinsic Hamiltonian formulation of network dynamics: Non–standard Poisson structures and gyrators. *Journal of the Franklin Institute*, 329(5):923–966, 1992.

[Mas95] Maschke, B. M., A. J. van der Schaft, P. C. Breedveld. An intrinsic Hamiltonian formulation of the dynamics of LC–circuits. *IEEE Transactions on Circuits and Systems I: Fundamental Theory and Applications*, 42(2):73–82, 1995.

[MTT04] MTT. MTT: Model Transformation Tools. Online WWW Homepage. URL: http://mtt.sourceforge.net, 2004.

[Ngw96] Ngwompo, R. F., S. Scavarda, and D. Thomasset. Inversion of linear time-invariant siso systems modelled by bond graph. *Journal of the Franklin Institute*, 333B(2):157–174, 1996.

[Ngw99a] Ngwompo, R. F., and S. Scavarda. Dimensioning problems in system design using bicausal bond graphs. *Journal of Simulation Theory and Practice*, 7(5–6):577–587, 1999.

[Ngw99b] Ngwompo, R. F., F. Roger, and P. J. Gawthrop. Bond graph based simulation of nonlinear inverse systems using physical performance specifications. *Journal of the Franklin Institute*, 336:1225–1247, 1999.

[Ngw01a] Ngwompo, R. F., S. Scavarda, and D. Thomasset. Physical model–based inversion in control systems design using bond graph representation – part 1. *Proceedings of the IMechE, Part I: Journal of Systems and Control Engineering*, 215(12):95–103, 2001.

[Ngw01b] Ngwompo, R. F., S. Scavarda, and D. Thomasset. Physical model–based inversion in control systems design using bond graph representation – part 2: applications. *Proceedings of the IMechE, Part I: Journal of Systems and Control Engineering*, 215(12):105–112, 2001.

[Nij90] Nijmeijer, H., and A. J. van der Schaft. *Nonlinear Dynamical Control Systems.* Springer–Verlag, 1990.

[Ort89] Ortega, R. Passivity properties for stabilization of cascaded nonlinear systems. *Automatica*, 27:423–424, 1989.

[Ort98] Ortega, R., Loría, A., Nicklasson, and P. J., Sira-Ramírez, H. *Passivity-Based Control of Euler-Lagrange Systems.* Springer–Verlag, 1998.

[Ort00a] Ortega, R., and A. J. van der Schaft. Energy shaping revisited. In *IEEE Conference on Control Applications*, pages 123–126, 2000.

[Ort00b] Ortega, R., and I. Mareels. Energy–balancing passivity–based control. In *Proceedings of the American Control Conference*, volume 2, pages 1265–1270, 2000.

[Ort00c] Ortega, R., and M. Spong. Stabilisation of underactuated mechanical systems using interconnection and damping assignment. In *IFAC Workshop on Lagrangian and Hamiltonian Methods in Nonlinear control problems*, pages 74–79, Princeton, NJ, 2000.

[Ort01] Ortega, R., A. van der Schaft, I. Mareels, and B. Maschke. Putting energy back in control. *IEEE Control Systems Magazine*, 21(2):18–33, 2001.

[Ort02a] Ortage, R., M. Spong, F. Gómez–Estern, and G. Blankenstein. Stabilisation of a class of underactuated mechanical systems via interconnection and damping assignment. *IEEE Transactions on Automatic Control*, 47(8):1218–1233, 2002.

[Ort02b] Ortega, R., A. J. van der Schaft, and B. Maschke. Interconnection and damping assignment passivity–based control of port–controlled Hamiltonian systems. *Automatica*, 38(4):585–596, 2002.

[Pay61] Paytner, H. M. *Analysis and Design of Engineering Systems.* MIT Press, Cambridge, Massachusetts, USA, 1961.

[Rob95] Roberts, D. W., D. Ballance, and P. J. Gawthrop. Design and implementation of a bond graph observer for robot control. *Control Engineering Practise*, 3(10):1447–1457, 1995.

[Ros71] Rosenberg, R. C. State-space formulation for bond graph models of multiport systems. *ASME Journal of Dynamics Systems, Measurement and Control*, 93(1):35–40, 1971.

[Ros74] Rosenburg, L. C. *A User's Guide to ENPORT–4.* John Wiley, 1974.

[Ros87] Rosenberg, R.C. Exploiting bond graph causality in physical systems modelling. *ASME Journal of Dynamic Systems, Measurement, and Control*, 109:378–383, 1987.

[Sch96] Schaft, A. J. van der, M. Dalsmo, and B. Maschke. Mathematical structures in the network representation of energy–conserving physical systems. In *Conference on Decision and Control*, pages 201–206. IEEE, 1996.

[Sch00a] Schaft, A. J. van der. Implicit port-controlled Hamiltonian systems. *SICE*, 39:410–418, 2000.

[Sch00b] Schaft, A. J. van der. *L_2-gain and Passivity Techniques in Nonlinear Control.* Springer–Verlag, 2000.

[Sep97] Sepulchre, R., M. Janković, and P. Kokotović. *Constructive Nonlinear control.* Springer–Verlag, 1997.

[Sha91] Sharon, A., N. Hogan, and D. E. Hardt. Controller design in the physical domain. *Journal of the Franklin Institute*, 328(5/6):697–721, 1991.

[Son95] Sontag, E. D. On characterizations of the input–to–state stability property. *Systems & Control Letters*, 24:351–359, 1995.

[Str98] Stramigioli, S., B. Maschke, and A. J. van der Schaft. Passive output feedback and port interconnection. In *Proc. 4th IFAC NOLCOS*, pages 613–618, Enschede, 1998.

[Tho99] Thoma, Jean U., and O. Bouamama. *Modeling and Simulation in Thermal and Chemical Engineering : A Bond Graph Approach.* Springer Engineering, 1999.

[van94] van Dijk, J. *On the role of bond graph causality in modelling mechatronic systems.* PhD thesis, University of Twente, The Netherlands, 1994.

[Vin03] Vink, D., D. Ballance, and P. J. Gawthrop. Bond graphs in model matching control. In *Proceedings of the 4th MATHMOD*, Vienna, 2003.

[Wan94] Wan, C. J., D. S. Bernstein, and V. T. Coppola. Global stabilization of the oscillating eccentric rotor. In *Proc. 33rd IEEE Conference on Decision and Control*, pages 4024–4029, 1994.

[Wil72] Willems, J. C. Dissipative dynamical systems, parts I and II. *Archive for Rational Mechanics and Analysis*, 45:321–393, 1972.

[Yeh99] Yeh, T. Backstepping control in the physical domain. In *Proceedings of the American Control Conference*, 1999.

[Yeh01] Yeh, T. J. Controller synthesis using bond–graphs. In *Proceedings of the American Control Conference*, pages 4765–4770, Arlington, 2001.

[Yeh02] Yeh, T. J. Controller synthesis for cascade systems using bond graphs. *International Journal of Systems Science*, 33:1161–1177, 2002.

[Zha98] Zhao, J., and K. Kanellakopoulos. Flexible backstepping design for tracking and disturbance attenuation. *International Journal of Robust and Nonlinear Control*, 8:331–348, April 1998.

[Zho98] Zhou, K., and J. Doyle. *Essentials of Robust Control.* Prentice–Hall, 1998.